OSCCAR:
FUTURE OCCUPANT SAFETY FOR CRASHES IN CARS

Final virtual design of advanced passenger protection principles

Document Type	Deliverable
Document Number	D2.4
Primary Author(s)	Michael Hamacher | FKA Julian Becker | RWTH / IKA Gian Antonio D'Addetta | BOSCH Martin Östling | AUTOLIV Christian Mayer | MERCEDES Sabine Compigne | TME
Document Version / Status	3.1 | Final
Distribution Level	CO (confidential – consortium only)

Project Acronym	OSCCAR
Project Title	FUTURE OCCUPANT SAFETY FOR CRASHES IN CARS
Project Website	www.osccarproject.eu
Project Coordinator	Werner Leitgeb | VIF | werner.leitgeb@v2c2.at
Grant Agreement Number	768947
Date of latest version of Annex I against which the assessment will be made	2021-02-05
Upload by coordinator:	First submitted: 2021-12-03 Re-submitted: 2022-04-11

OSCCAR has received funding from the European Union's Horizon 2020 research and innovation programme under grant agreement No 768947.

CONTRIBUTORS

Name	Organisation	Name	Organisation
Martin Östling	Autoliv	Sabine Compigne	TME
Krystoffer Mroz	Autoliv	Shigeki Hayashi	TMC
Gian Antonio D'Addetta	Bosch	Mie Tokuyama	TMC
Maja Wolkenstein	Bosch	Hiroshi Miyazaki	TMC
Simon Dussinger	ESI	Lennart Nölle	University Stuttgart
Michael Hamacher	fka	Lotta Jakobsson	Volvo Cars
Julian Becker	ika / RWTH	Alexandros Leledakis	Volvo Cars
Genís Mensa	IDIADA	Jonas Östh	Volvo Cars
Pronoy Ghosh	MBRDI	Jens Weber	Volkswagen
Sammed Pandharkar	MBRDI	Thomas Wohllebe	Volkswagen
Atul Mishra	MBRDI	María González-García	Volkswagen
Christian Mayer	Mercedes-Benz	Michael Sprenger	ZF
Freerk Bosma	Siemens	Swen Schaub	ZF
Richard Lancashire	Siemens		

FORMAL REVIEWERS

Name	Organisation	Date
Steffen Peldschus	LMU Munich	2021-02-13
Daniel Schmidt	Bosch	2021-02-09

DOCUMENT HISTORY

Revision	Date	Author / Organisation	Description
1	2021-01-20	Hamacher / FKA	First overall draft
2	2021-01-28	Hamacher / FKA	Draft for internal review
3	2021-02-26	Hamacher / FKA	Final version
3.1	2022-03-25	Hamacher / FKA	Updates after EU Review

TABLE OF CONTENTS

LIST OF FIGURES

LIST OF TABLES

ABBREVIATIONS AND DEFINITIONS

Term	Definition
ACR	Active Control Retractor
AD	Automated Driving
ADAC	German Automobile Club
AEB	Autonomous Emergency Braking
AHBM	Active Human Body Model
AHM	Active Human Model
AIS	Abbreviated Injury Scale
ASIS	Anterior Superior Iliac Spine
ATD	Anthropomorphic Testing Device
AV	Autonomous Vehicle
BLL	Belt Load Limiter
CLT	Crash Locking Tongue
CNIS	China National Institute of Standardization
COG	Centre of Gravity
CORA	Correlation and Analysis Method
CSDM	Cumulative Strain Damage Measure
DoE / DOE	Design of Experiments
DOF	Degrees of Freedom
ECU	Electronic Control Unit
EMG	Electromyography
ERR	Electrical Reversible Restraint
Euro NCAP	European New Car Assessment Programme
FEM	Finite Element Method
FF	Full Frontal
FW	Full Width
FWRB	Full Width Rigid Barrier
HAV	Highly Automated Vehicle
HBM	Human Body Model
IP	Instrument Panel
MSB	Motorised Seat Belt
MTU	Muscle-Tendon-Unit
NFR	Number of Fractured Ribs
NHTSA	National Highway Traffic Safety Administration
LL	Load Limiter
LTAP	Left Turn Across Path
LTAP-OD	Left Turn Across Path - Opposite Direction
OHA	Over-Head Airbag
PDOF	Principal Direction of Force

Term	Definition
PMHS	Post Mortem Human Subjects
PP	Protection Principle
PPT	Pre-Pretensioner (generic)
SCP	Straight Crossing Path
SOTA	State of the Art
TCRDL	Toyota Central R&D Labs
THOR	Test Device for Human Occupant Restraint
THUMS	Total Human Model for Safety
TMC	Toyota Motor Corporation
TTF	Time to fire
TUC	THUMS User Community
USNCAP	United States New Car Assessment Program
UVA	University of Virginia
VPS	Virtual Performance Solution
VCP	Visual-Crash PAM
WG	Working Group
WP	Work Package
WorldSID	Worldwide Harmonized Side Impact Dummy
YO	Years Old

Although this deliverable is of official confidentiality level CO, the OSCCAR General Assembly unanimously decided to make its contents publicly available. You can find it in its complete form on the OSCCAR webpage (https://www.osccarproject.eu/media/deliverables/) for your reference.

1 EXECUTIVE SUMMARY

This report presents the investigation of different advanced passenger protection principles for highly- and fully-automated vehicles within the framework of corresponding simulation studies, guided by predetermined research questions. In total six protection principles have been defined for different seating positions and occupant postures related to automated driving. Both an adaptation of the restraint systems towards these new boundary conditions and a repositioning of the occupant into a conventional seating configuration and / or seat position prior to a crash are considered. For each protection principle a working group has been established in order to investigate the functionality as well as the expected adequate occupant restraint effects for potential future applications. By the use of human body models (HBMs) the occupant kinematic boundary conditions and the related injury mechanism for selected test cases are analysed. This also includes the identification of appropriate evaluation criteria and possible HBM limitations as well as necessary improvements. Different levels of automation, occupant characteristics, postures, etc. as well as pre-crash activation and adaptation are considered, depending on the protection principle.

Protection Principle 1 addresses an occupant who is sitting in a slightly rotated position (pointing away from the driving direction). If a crash is unavoidable, the seat is actively rotated into the crash direction during the pre-crash phase. Protection Principle 2 is similar but here the seat rotation is caused due to the inertia of seat and occupant by an active release of the seat, i.e. no actuator is needed to rotate the seat. For both principles, the influence of a pre-rotated seat on occupant safety and kinematics in both the pre-crash and in-crash phase is analysed.

The focus of Protection Principle 3 is on a reclined occupant position and the challenges for the restraint system and the testing devices associated with such a configuration. It is investigated how to avoid submarining and if no submarining occurs how to reduce loadings on pelvis and lumbar spine. Furthermore, specific challenges related to obesity or seat-integrated countermeasures are analysed by simulations with HBMs. The working group also encompasses research questions related to the influence of sitting postures in a wider context than reclined seating only.

Protection Principle 4 is based on a living room interior configuration with upright occupant position, i.e. the occupants are sitting forward and rearward, facing each other. In case of a crash a so-called Mushroom Airbag is inflated from the vehicle roof, filling up the space between the occupants in order to reduce loadings to head and neck and to avoid interactions between them. Beside the protection potential of the Mushroom Airbag in frontal (oblique) collisions, it is investigated whether a single volume airbag is capable to fill the space between the occupants.

Protection Principle 5 comprises an active seat for different reclined seating configurations. Prior to the crash, the seat back is actively raised to bring the occupant from a reclined into a “normal” upright sitting posture. At the same time, the seat base allows a longitudinal displacement which offers additional space for deceleration and energy absorption. The main research questions are related to an appropriate and safe implementation of an active repositioning, adapted to the restraint systems, e.g. regarding submarining and accelerations in the repositioning phase.

Finally, Protection Principle 6 addresses occupant restraint with regard to a side crash in a future interior without centre console. Considering different restraint system layouts as well as seat side supports it is investigated how to limit the excursion of the far-side occupant (opposite side to the one that is struck) in order to provide protection from a collision between two rear-seated occupants.

Keywords: automated driving, occupant restraint, protection principles, seating position, occupant repositioning, human body model, test case

2 BACKGROUND AND OBJECTIVES

Work package 2 (WP2) of the OSCCAR project deals with the conception and investigation of advanced occupant protection principles (PP) for high and fully automated vehicles. Since future interiors will offer more degrees of freedom for passengers, e.g. rotated or reclined seating positions, the conventional restraint components like belts or airbags have to be adapted towards these new boundary conditions or even new restraint principles have to be developed. This might also include a safe repositioning of the occupant into a conventional seating configuration prior to a crash in order to overcome problems caused by rotated or reclined configurations.

The main objective of WP2 is to define and further elaborate several advanced occupant protection principles addressing different future seating configurations and vehicle automation levels respectively. Different hardware test series have been performed in order to gain data for the validation of the respective simulation models and to demonstrate the functionality of selected protection principles. However, these hardware tests are not part of this deliverable and will be illustrated in deliverable D2.5 [1].

2.1 Background

As a first step in WP2, a methodology has been developed in order to structure and define combinations of aspects relevant for occupant protection evaluation in future passenger cars, which is described in deliverable D2.1 [2]. The methodology is created based on a three-dimensional matrix structure, the so-called Test Case Matrix, and some pre-processes. A Test Case thereby contains specifications regarding occupant use cases (seating configurations, sitting postures, etc.), individual human variations (for example age and size) as well as future crash configurations (impact point, impact angle and impact velocity) (WP1, [6] [28]). A literature study and two user studies have been performed on preferred seat rotation angles and sitting postures in future cars in order to provide input with regard to the developed methodology.

For the virtual investigation of advanced occupant protection principles, respective simulation models have been generated or adapted from already existing baseline model setups (deliverable D2.2 [3]). These generic models represent possible future interior concepts. In order to cover the complex occupant use cases of the Test Case Matrix on the one hand and the physical availability on the other hand, a distinction had to be made between purely virtual and physically available model components. Based on the selected components, several vehicle automation-specific working models have been created: A “Generic Interior Model” addressing automated driving levels 1-3, a “Living Room Interior Model” addressing automated driving levels 4 & 5 and a so-called “Homologation System Model” as an environment which is even further generic and serves as a demonstrator test case within OSCCAR in terms of virtual testing and homologation. The focus of this demonstrator test case is on a reclined seating position and the challenges for the restraint system as well as the testing devices associated with such a configuration, not only on a virtual, but also on a physical level. It is directly connected to the work in WP4 and WP5.

As a basis for the ideation of advanced occupant protection principles, a safety deficiency study has been conducted, focussing on safety issues related to seating configurations (e.g. the number, location and occupancy of the seats), interior features, seat positions (e.g. adjustment of the seat, such as the backrest and seat pan angle, and possible additional support structures as leg supports) and sitting postures in future vehicles. The actual step in defining and selecting advanced occupant protection principles took place in an ideation workshop with involvement of almost all OSCCAR partners (deliverable D2.3 [4]). Finally, five protection principles were selected for further

investigation, dealing with rotated seats, reclined seating positions as well as an advanced airbag design for a “living room” configuration (occupants facing each other). Respective working groups (WG) were defined for this purpose, led by different partners. In the course of the work, it was decided to define an additional sixth protection principle and to establish a corresponding working group in order to also address future occupant restraint with regard to a side crash. Figure 1 gives a general overview of the respective protection principles investigated in WP2.

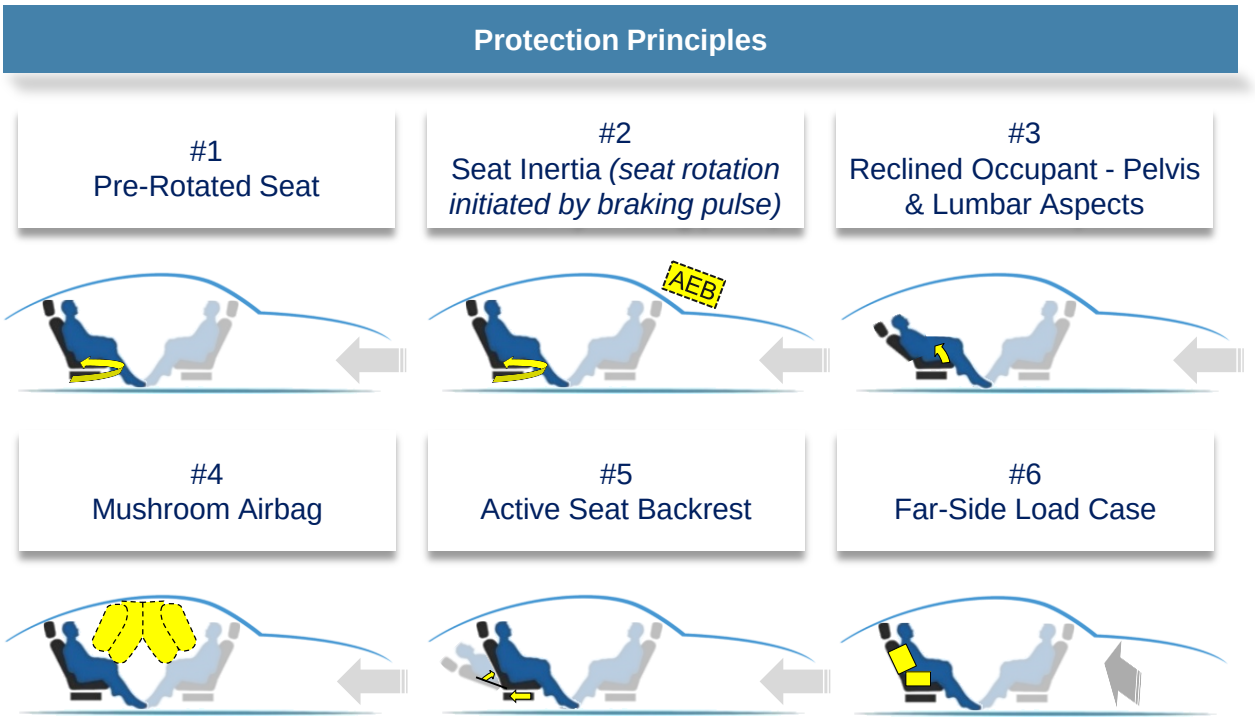

Figure 1 Protection principles investigated in WP2

The studies carried out by the various working groups have been guided by predetermined research questions and are described within Chapter 3 of this deliverable. A list of the abbreviations and definitions used in this context can be found at the beginning of this report.

In addition to this, further research activities related to WP2 have been conducted by OSCCAR China. The OSCCAR China team has received funding from the Chinese Ministry of Science and Technology and operates independently but in regular exchange with the European colleagues. One study by OSCCAR China investigates the possible benefits of a uniform occupant restraint where the loads are ideally applied and distributed to individual segments of the body. Another study deals with the conceptual design of seat-based restraint devices. The results of these studies will be published by OSCCAR China and are not part of this deliverable.

2.2 Objectives

With the overall OSCCAR objective of developing a novel, simulation-based approach to safeguard occupants involved in future vehicle accidents, this report serves the purpose to describe the virtual conception and investigation of several advanced occupant protection principles for sitting positions and postures related to automated driving.

Regarding the studies conducted by the different working groups in order to analyse the selected protection principles, the considered test cases cover accident scenarios defined in WP1 as well as different levels of automation, occupant characteristics, postures, etc. Both pre-crash activation and

adaptation as well as in-crash protection are included. Furthermore, advanced models and methods with respect to occupant modelling and injury risk evaluation from WP3 are used where applicable. The extensive use of human body models (HBMs) within the different studies allows aspects like occupant variety and omnidirectional occupant loading to be considered and conclusions to be drawn for HBM application in novel use cases.

The working groups develop a virtual design of the respective protection principles, allowing a general proof of functionality and effectiveness with regard to the investigated environments. The demonstration of selected protection principles by corresponding hardware tests is another WP2-related objective, but this is the subject of deliverable D2.5 [1].

3 DESCRIPTION OF WORK

The work done by the respective working groups is described in the following sub-chapters, with a separate sub-chapter for each of the six protection principles. Each sub-chapter ends with a conclusion specific to the protection principles. Finally, Chapter 4 draws an overall conclusion for Chapter 3, comparing the results of the working groups.

3.1 Protection Principle 1 - Pre-Rotated Seat

The overall objective of Protection Principle 1 (PP1) is to evaluate pre-crash induced protection principles for passengers on a rotated seat. The corresponding working group consists of Bosch, ESI, ika, Mercedes, Siemens, Uni Stuttgart, Volkswagen, ZF and is led by Bosch.

3.1.1 Motivation and Background

In the transition period from conventional to autonomous driving, passengers will benefit from an increased spatial freedom along with potential changes in interior and seating design. Configurations with rotating seats may allow a higher degree of communication between passengers. These new rotated seating positions will pose novel challenges for current restraint systems. The pre-rotated seat configuration and the related Protection Principle 1 resulted from the OSCCAR ideation workshop held in April 2019 and reported in deliverable D2.3 [4] (Chapter 2.1). The ideation process was prepared and organised in a seven-step procedure. The relevant occupant use cases from deliverable D2.1 [2] and accident scenarios reported in D1.2 [5] were selected and used as input in order to generate ideas for advanced protection principles. In the case of the accident scenarios this includes a description of the crash as well as pre-crash phase in the form of acceleration pulses, i.e. including the relevant crash pulses created by VSI TU Graz and reported in deliverable D1.3 [6]. The PP1 studies investigate in- and outward rotated seats prior to frontal and oblique vehicle crashes and focus on the effects of turning seats back to a more beneficial situation before the crash takes place and main interaction with the restraint system(s) commences. A literature study revealed only few relevant sources on rotated seats and related protection principles and involvement of HBMs.

The general procedure for analysis and assessment of Protection Principle 1 follows the path as in the analysis of other protection principles reported in this deliverable. It will start with the identification of adequate research questions, followed by definition of suitable evaluation criteria and HBMs to be used in PP1 studies. The functionality assessment and evaluation of expected occupant restraint effects will lead to a discussion of protection principle efficiency and HBM limitations.

Recent studies have investigated different seat rotation angles in combination with different impact directions. The main issues were observed when the seat was not facing in the direction of the crash. Physical test results have been presented in references [7], [8] and [9] using a THOR-M and a Hybrid-III dummy to investigate the reproducibility and to assess the effects of seat rotation or different pulse directions. References [10], [11] and [12] presented results using human body models for similar investigations. All these studies focused on the interaction between occupant and belt system. Interactions with airbag systems and interior structures were mostly excluded. One finding was, that for shoulder belts an inward seat rotation in frontal crash cases could lead to unfavourable belt to neck contact for high rotation angles, which showed increased Neck Injury Criteria (Nij) [9] and Neck Moment (My) [10] values. Apart from complex cervical spine loadings, neck to belt contact can cause a blunt carotid artery injury, which can lead to serious consequences for the patient [13]. In [7] and [12] possible seat-integrated countermeasures are discussed, to ensure safety under all potential rotation angles. Lateral seat support structures and head restraint enlargement, as well as

seat-integrated belt systems (see [8], [9]), were introduced to restrain the occupant on a rotated seat in all impact directions. Active seat rotation is discussed in [11].

The reviewed literature sources showed possible safety deficiencies in rotated seating positions. Several countermeasures were already discussed in recent studies. When it comes to active countermeasures, like rotation of the seat and occupant into a more beneficial position prior to a crash, available literature is limited. With respect to a lack of validated occupant models for pure rotational loading conditions, these scenarios need to be further investigated.

3.1.2 Research questions

One of the key purposes within OSCCAR is to investigate new protection principles in selected Demonstrator Test Cases. According to the definitions in deliverable D2.1 [2] this comprises new Occupant Use Cases in combination with relevant Crash Configurations. Essential ingredients for every research project are the identification of adequate research questions as well as the alignment of the project or study results with these research questions. This approach creates impulses for both quantitative and qualitative research and pushes the community to improve knowledge.

In the case of OSCCAR, the overall research question addresses mainly the understanding whether the available tools (especially HBMs) are capable to represent a modelling and assessment tool for occupant safety in future HAVs, and what refinements are needed in order to capture important interactions enabling development of protection. The focus for the protection principle analyses reported in this deliverable lies on occupant safety and functional issues, but limitations of current HBMs are relevant as well. In the case of Protection Principle 1, pre-rotated seat, the following two main research questions were identified during the process of ideation and forming of the working group:

- What influence on occupant kinematics and occupant safety does a pre-crash rotated seat have?
- Does the active pre-crash rotation of the occupant lead to additional (minor) injury risks and how can this injury be assessed?

3.1.3 Simulation studies

Generally, the tasks were subdivided into pre- and main studies. Goal of the pre-studies, carried out by Bosch using the Active Human Model (AHM) in Simcenter Madymo (further referred to as Madymo), was an assessment of the pre-crash phase. In particular, rotation characteristics like initial seat rotation, seat rotation timing, seat rotation velocity, and seat rotation axis were analysed and settings for the main studies were defined. Thus, the outcome was used by different partners (Bosch, ika, Mercedes, Volkswagen) to carry out their main studies with focus on pre- and in-crash phase. Background for this procedure is the low numerical effort of Simcenter Madymo AHM in combination with a long simulation duration of the pre-crash phase. In contrast to that, Finite-Element HBMs such as THUMS offer better injury representation due to a higher detail level for the crash phase.

In Chapter 3.1.3.1 the involved simulation models and relevant boundary conditions and settings are described followed by a short wrap-up of the theory on soft tissue injuries in Chapter 3.1.3.2. The results of the Protection Principle 1 pre-studies are reported in Chapters 3.1.3.3 and 3.1.3.4. Afterwards, the results of the main studies with focus on the highway case scenario are reported in Chapters 3.1.3.5 and 3.1.3.6. A comparison of the application of different HBMs for the harmonised highway case is summarised in Chapter 3.1.3.7. Main studies on the urban scenario are the focus of Chapters 3.1.3.8, 3.1.3.9 and 3.1.3.10.

3.1.3.1 Simulation models and boundary conditions for all studies

The general working principle of this Protection Principle, a pre-crash rotation of the seat along the z-axis (vertical axis), is sketched in Figure 2: the occupant on a rotated seat is repositioned into a close-to-standard frontal facing position prior to an unavoidable collision of the HAV. A seat rotation curve characterised by a spline interpolation is used to represent the pre-crash motion of the seat actuator. It allows for a plausible kinematic behaviour of the seat without jerk motion. Typical rotation characteristics and timing of the implemented seat rotation are visualised in Figure 3.

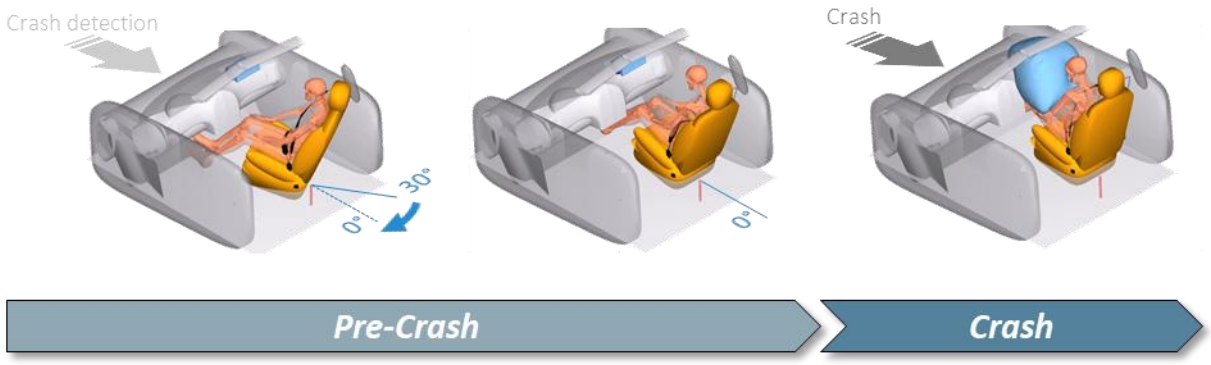

Figure 2 Working principle of Protection Principle 1

The simulation studies carried out by the members of the working group on Protection Principle 1, aim to give an insight into the occupant's kinematic behaviour by use of four different HBMs: THUMS TUC-VW AHM, A-THUMS-D 3.3.6 (pre-crash), THUMS-TUC-LSDYNA (crash), and Simcenter Madymo AHM v3.1. Furthermore, the generic interior models created for OSCCAR to study potential protection principles, which are reported in deliverable D2.2 [3], are used. The aligned environment is created in the three different simulation codes VPS, LS-Dyna and Simcenter Madymo and contains state-of-the-art restraint systems, a seat, an instrument panel and a passenger. The different interior models are highly parameterised in order to study parameter variation effects in a design of experiment (DoE) study and optimisation.

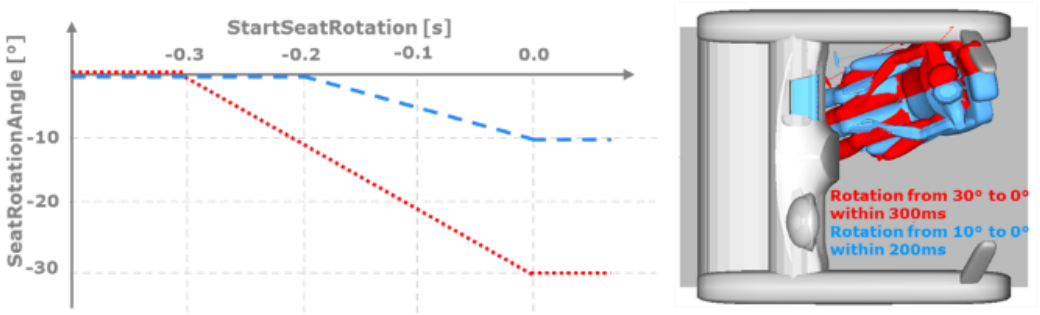

Figure 3 Two examples for seat rotation curves

Overall, a large set of simulations has been carried out within the main studies. An overview of relevant information on the highway scenario, models and seat-related settings is listed in Table 1 and settings and information for the urban scenario are listed in Table 2.

Partner	Volkswagen	Mercedes	ika/fka	Bosch
Chapter	3.1.3.6 & 3.1.3.7	3.1.3.5 & 3.1.3.7	3.1.3.4	3.1.3.3 & 3.1.3.7
Crash scenario	highway	highway	highway	highway
Crash pulse	generic FF40	generic FF40	Madymo generic USNCAP FF 56	Madymo generic USNCAP FF56
Braking	yes	yes	yes / no	yes / no
Braking pulse	generic	generic	Madymo	Madymo
Position of seat as per D2.1	2	1,2,3,4	2	2
Interior model	generic	generic	generic	generic
Simulation code	VPS	LS-Dyna	Madymo	Madymo
HBM	THUMS TUC-VW AHM	A-THUMS-D336, THUMS-TUC	Simcenter Madymo AHM	Simcenter Madymo AHM
Active HBM	yes	yes	yes	yes
Initial seat rotation	30°	0° to 30°	-30°	0° to 30°
Target angle	0°	0°, PDOF	0°	0°, PDOF
Position rotation axis	H-point THUMS middle of seat (y)	H-point THUMS	H-point AHM	H-point AHM
Seat activation	-300 ms	-350 ms	-350 ms – -50 ms	-400 ms – -50 ms
Belt anchorage	seat integrated	seat integrated	seat integrated	seat integrated

Table 1 Simulation matrix for Protection Principle 1 highway case

Partner	Mercedes	Bosch	ZF
Chapter	3.1.3.8	3.1.3.9	3.1.3.10
Crash scenario	urban	urban	urban
Crash pulse	SCP06	generic SCP06/04/02	gener. USNCAP FF 56, SCP06
Braking	yes	no	yes
Braking pulse	generic	-	Madymo
Position of seat as per D2.1	1,2,3,4	2	3, 4
Interior model	generic	generic	generic
Simulation code	LS-Dyna	Madymo	Madymo
HBM	A-THUMS-D336, THUMS-TUC	Simcenter Madymo AHM	Simcenter Madymo AHM
Active HBM	yes	yes	yes
Initial seat rotation	0° to 80°	-90° to 0°	30°
Target angle	PDOF	PDOF	0°
Position rotation axis	H-point THUMS	H-point AHM	H-point AHM
Seat activation	-350 ms	-	-200 ms
Belt anchorage	seat integrated	seat integrated	seat integrated

Table 2 Simulation matrix for Protection Principle 1 urban case

In the following sections, the specific settings for each model/code will be described by the used simulation code.

Simcenter Madymo (Bosch, ika, ZF)

The pre-studies made use of the Madymo generic multibody interior model that was created for OSCCAR. The model contains (generic) state-of-the-art restraint systems, a seat and a passenger (see Figure 4), which is represented with the Simcenter Madymo AHM v3.1. Figure 4 also illustrates the acceleration-based motion that is used in the presented study, a 1 g automated emergency braking (AEB) manoeuvre followed by a crash (US NCAP Full Width Rigid Wall 56 km/h crash pulse). This model is described in detail in deliverable D2.2 [3].

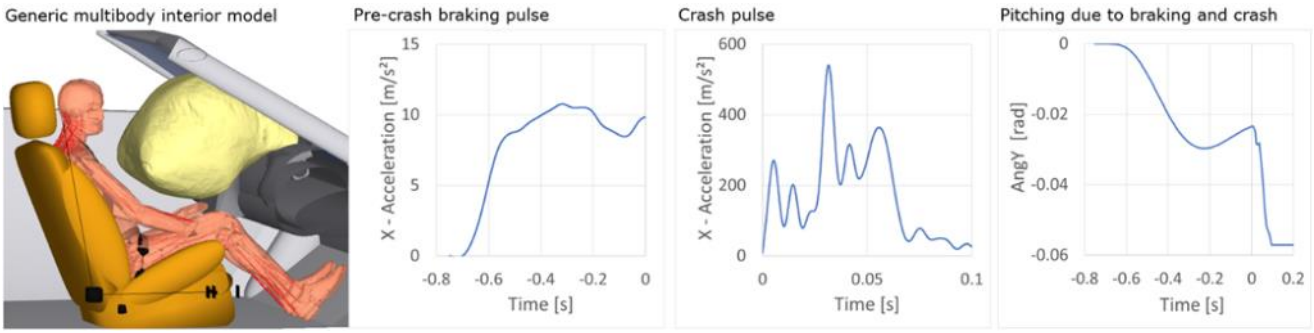

Figure 4 Generic Simcenter Madymo multibody interior model and pulses

In pre-studies carried out by Bosch the kinematic behaviour of the occupant was analysed, i.e. the trajectories of the different body parts, as well as further kinematic variables like accelerations. In order to simplify the analysis and to discriminate the rotation trajectory of occupants' body parts with respect to the seat, additional relative measures were introduced - see Figure 5, left. In particular, outputs for the relative head angle β1, relative shoulder angle β2, relative pelvis angle β3 and relative knee angle β4 have been defined.

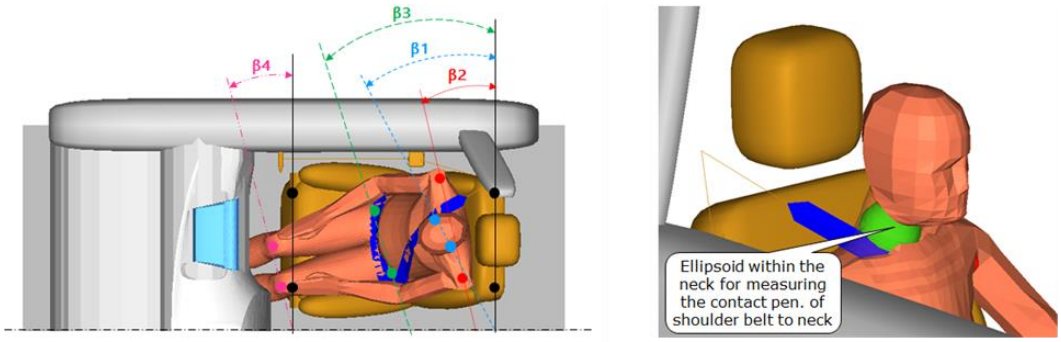

Figure 5 Definition of relative angles between occupant/seat (left) and belt neck contact (right)

A crucial effect during the pre-crash rotation of the seated occupant is the seat belt-to-neck interaction. To facilitate the analysis, a measuring "tool" was included into the Madymo HBM's neck. A spherical ellipsoid surface, see Figure 5, right, was attached to the C7 body of the neck and an additional contact with negligible contact stiffness between shoulder belt and ellipsoid was introduced. The ellipsoid surface is completely inside the outer element surface of the HBM neck and therefore does not produce any HBM surface change. The ellipsoid surface only enables measurement of the local penetration of the belt into the neck surface, which is allowed by the force-penetration contact definition.

VPS (Volkswagen)

The translation of the generic interior from LS-Dyna to VPS incorporates the work flow as described in [3] in Chapter 4.4.2 and can be subdivided in the following steps:

1. Automatic conversion of most definitions with VCP's built-in converter tool
2. Manual correction of various entities converted by tool such as PYVAR parameters blocks, variables, TRSFM cards, contact parameters, rigid body definitions
3. Material validation VPS versus LS-Dyna based on single element tests:
    a. For load conditions uniaxial tension, compression, simple shear and pure shear
    b. With loading and unloading
    c. With various loading velocities
4. Validation on component and full model level for passenger airbag, seat and belt with pretensioner

In the following, the validation of the passenger airbag is described exemplarily. For validation on component level the airbag, windscreen and dashboard have been isolated. During inflation the airbag is impacted with a rigid cylinder. Four different combinations of cylinder mass and velocity have been utilised to represent different load conditions. Important results for comparison between codes are airbag mass, inflow mass, outflow mass, volume, pressure, temperature, active surface and contact force between impactor and airbag. Figure 6 shows results for a load condition impactor mass of 45 kg and a velocity of 6 m/s (green: LS-Dyna, red: VPS).

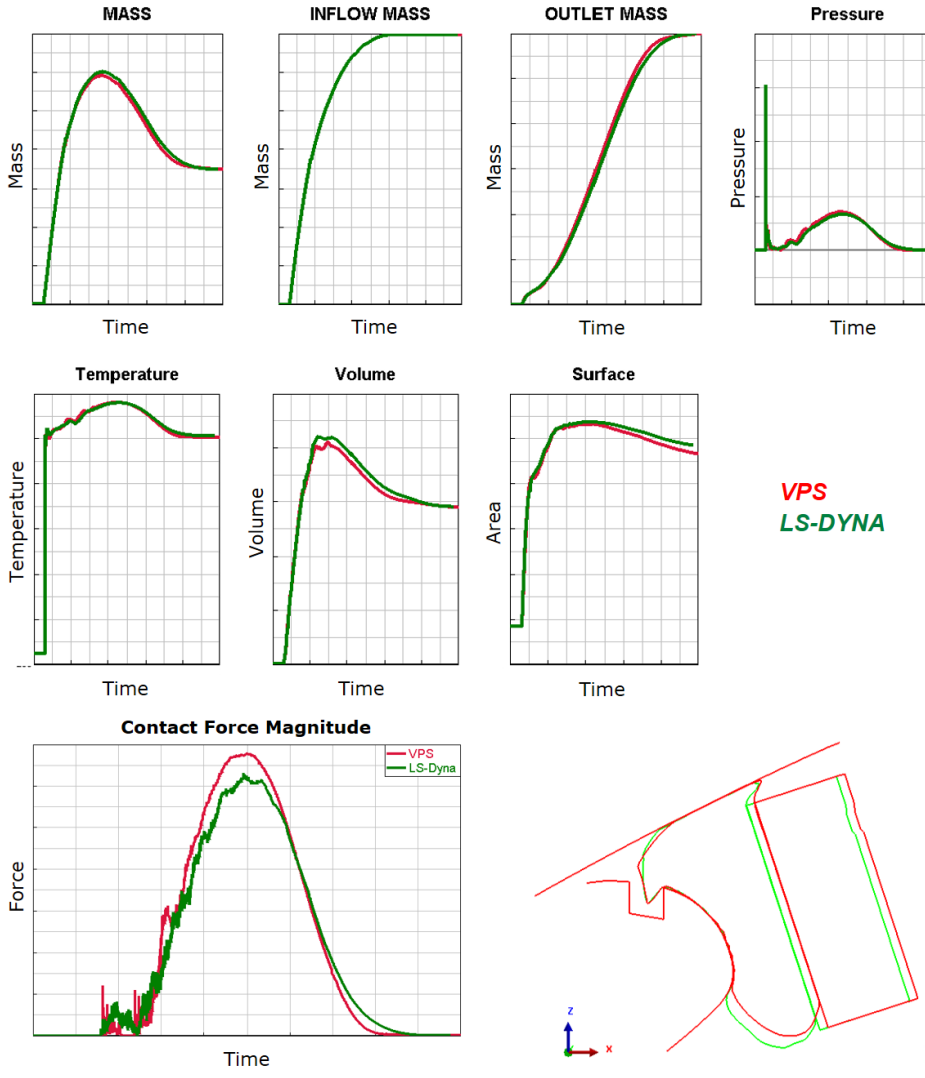

Figure 6 Result curves for airbag on component level - deformation state at 150 ms

In order to be able to investigate the planned protection principle combined with additional countermeasures, the belt system included in the generic model was replaced with an internal Volkswagen belt system. This belt system model enables more variations of the parameters.

An overview of the adjustable belt parameter is shown in Table 3. Only the marked parameters were used in the Volkswagen DOE study for Protection Principle 1.

Belt Component	Buckle	Anchor	Retractor
Pre-Pretensioner		X	X
Pretensioner	not used	not used	X
Load Limiter		not used	X
Locking Tongue	X		

Table 3 Belt system used by Volkswagen

The belt locking tongue was included in all Protection Principle 1 simulations of Volkswagen. The retractor load limiter was set to 2.1 kN in all simulations.

Some further modifications of the generic interior model were required to be able to use it in this study. First of all, the parametric rotation mechanism characteristic was integrated into the seat. Additionally, the contacts to the centre console and to the side structure were deactivated to be able to rotate the seat with the occupant.

The active HBM used by Volkswagen is the THUMS TUC-VW AHBM which represents a 50th percentile male. This model is based on the version THUMS TUC 2019 in VPS code, which is a passive HBM. The initial upgrade towards an active HBM carried out at Volkswagen is described in detail in [57], [58] and [59]. Since then, the model has been continuously updated with the latest THUMS TUC [60] versions, though keeping necessary modifications concerning passive properties, e.g. soft tissue materials, for the active model. In addition, controller updates to further improve the active HBM with respect to numerical stability and robustness, usability and run time efficiency were implemented. The THUMS TUC-VW AHBM applied to the studies in WP2 is based on the validation mentioned in [57] and [58]. However, a further validation was carried out in parallel, which is reported in [63].

The active HBM was used in both the pre- and in-crash phases. However, the muscle control was deactivated during the in-crash phase.

The pre-positioning of the Volkswagen HBM was performed using the PIPER tool [61]. The final positioning onto the seat was done by applying gravity forces to the HBM, as it can be seen in Figure 7.

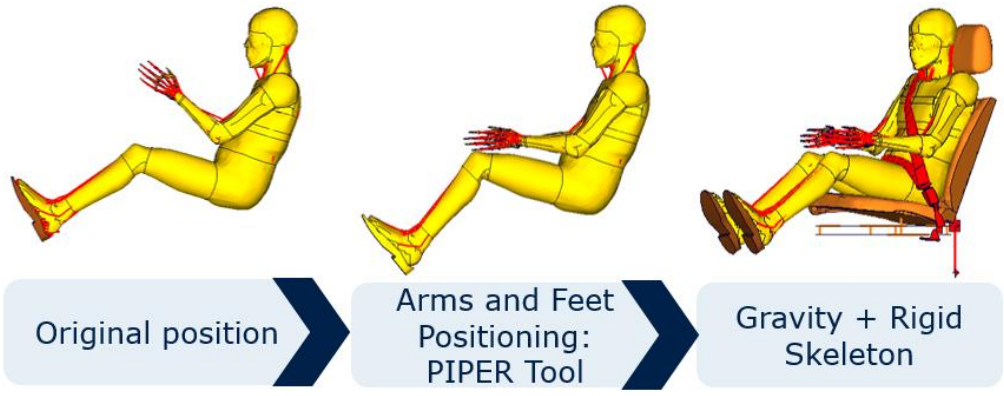

Figure 7 Positioning process

Focus of the study carried out by Volkswagen was a so-called highway scenario defined in WP1. Therefore, in all simulations the generic acceleration-based crash pulse for a full-frontal impact with 40 km/h was used, relevant for the highway scenario and proposed by WP1 (see Chapter 3.1.3.7). This crash pulse was combined with a pre-crash braking pulse also recommended by WP1.

LS-Dyna (Mercedes)

Environment and boundary condition description for the Highway Pilot scenario

The assessment of Protection Principle 1 involves simulation of both pre-crash and in-crash phase. An integrated safety tool chain as described in [14] was used with A-THUMS-D 3.3.6 (Active HBM developed at Mercedes-Benz) in the pre-crash phase to simulate occupant kinematics in the presence of muscle activity, along with THUMS-TUC 2020 HBM in the in-crash phase. Simulations were conducted in LS-Dyna.

Overview of restraint systems and environment

a) **Seat** – The seat model used was developed as a part of the OM4IS Phase 2 Project funded by PDB and executed at TU Graz and VIF (COMET Program). This was further improved in the PRECOONI project (funded by Daimler, Volkswagen, Porsche and ZF) and executed at TU Graz and VIF (COMET Program). The seat model has been described in detail in Chapter 3.1.2 of OSCCAR deliverable D2.2 [3].

   In the current study, the seat was modified by including side bolsters in the cushion region in order to better represent an automotive seat and to provide lateral support during the pre-crash rotation to a standard position (Figure 8 c).

b) **Seatbelt** – The generic restraint system (deliverable D2.2 [3], Chapter 3.3) was used with the following modifications:

   i. D-Ring positioning - The restraint system was modified to represent a seat integrated system. The D-ring was positioned to suit a seat-integrated D-ring location and was constrained to the seat.

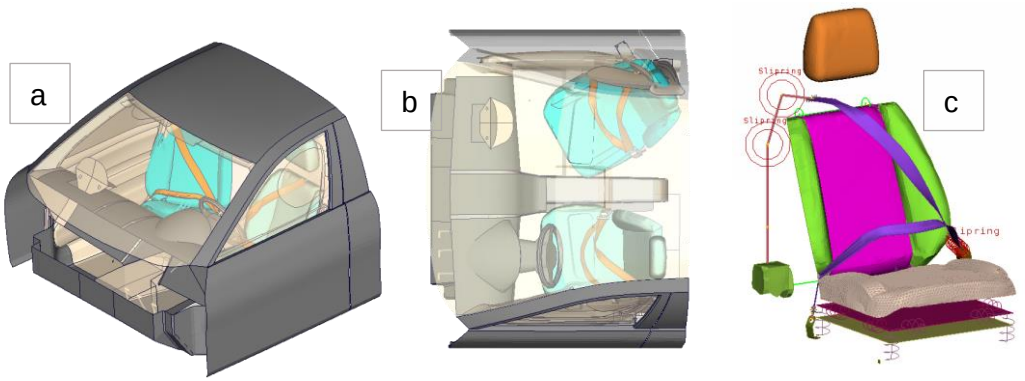

Figure 8 a), b) OSCCAR generic level 3 environment, front-side & top view, respectively. c) OSCCAR generic seat with added cushion bolsters & integrated seatbelt system

   ii. Pre-Pretensioner integration - A reversible pretensioning in the pre-crash phase commonly referred to as Pre-Pretensioning (PPT) was modelled to remove belt slack and to improve the coupling of the occupant to the seat in the pre-crash phase. The modelling of the PPT was done using LS-Dyna *ELEMENT_PRETENSIONER assigned with a generic load curve suitably representing force characteristics of a PPT (Figure 9).

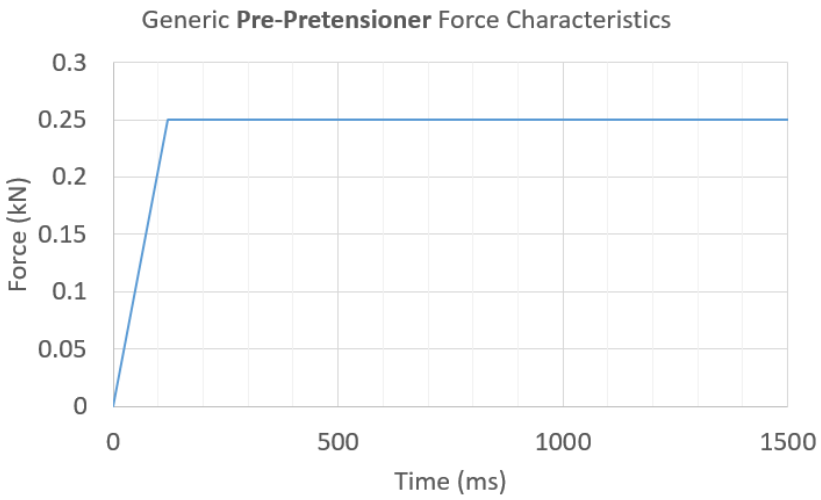

Figure 9 Generic Pre-Pretensioner force characteristics (peak force = 250 N)

c) **Airbag** – The passenger airbag model described in Deliverable D2.2 [3] (Chapter 3.3) was used. The airbag was moved by 12 mm in outboard direction of the vehicle to better align the airbag centreline with the seat centreline and to improve the occupant-airbag interaction.

d) **Environment** – The OSCCAR generic vehicle environment illustrated in Chapter 3.3 of deliverable D2.2 [3] was considered. The centre tunnel was removed to accommodate the legs in inward rotated position. The IP surface in the original Generic Interior Model has been defined with rigid material but for the current study the region of the IP contacting the HBM knees was converted to a deformable material with stiff plastic structural properties in order to avoid contact instabilities. The PPT force was kept at 250 N, the PT force was 2.5 kN. The other boundary conditions were defined as described in Chapter 3.1.3.1.

e) **HBM Positioning** – HBMs positioned in most ergonomic position using RAMSIS tool [15].

Environment description for the Urban Scenario

The robocab environment is a conference sort of seating configuration with occupants facing each other for urban scenarios. In this context, a 50th percentile male standard occupant is positioned in the robocab environment, facing rearward. The SCP06 (Straight Crossing Path) pulse developed in WP1 is used for the evaluation with a principal direction of force (PDOF) of ~70° (Figure 10).

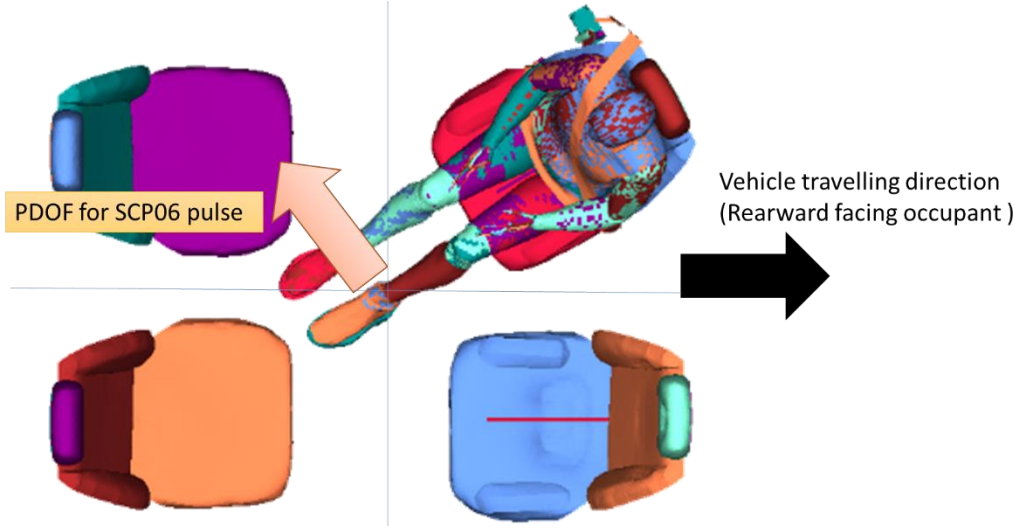

Figure 10 Robocab occupant seating configuration

The vehicle environment used in this study was slightly adapted. The floor was extended sideward to ensure that the feet stay in contact with the vehicle during the occupant motion. The arrangement of the seat and the distances were derived based on the cockpit size of existing public transport vehicles in the market. Unlike the highway pilot configuration, here a passive HBM (THUMS-D SUFEHN) is used in both pre-crash and in-crash phase. Table 4 illustrates the parameters and system description for the vehicle environment.

Parameters	System Description
Crash scenario	Urban
Crash pulse	Generic SCP06
Braking	Yes
Braking pulse	Generic
Position of seat according to D2.1	2
Interior model	Generic
Simulation code	LS-Dyna
HBM	THUMS-D with SUFEHN
Active HBM	No
Initial seat rotation	80°
Target angle	PDOF
Position rotation axis	H-point THUMS-D
Seat activation	-350 ms
Belt anchor point	Seat integrated

Table 4 Parameters & system description for the vehicle environment in the Urban Scenario

Simulation matrix

Two simulations were conducted for the benefit assessment of the protection principle as defined in Table 5.

Case	Description
Baseline (Case 1)	Seat and occupant in relaxed position in 30° inward rotated position with SCP06 pulse applied with the front passenger facing rearward and a pre-crash braking pulse of 500 ms.
Pre-Rotated seat (Case 2)	Seat and occupant in 30° inward rotated position. Seat rotates back to 0˚ position in pre-crash phase to ~80° outward aligning with the principal direction of force of the SCP06 pulse, considering a pre-crash braking pulse of 500 ms.

Table 5 Case description

3.1.3.2 Theory on soft tissue injuries

Many injury criteria for different parts of the human body have been defined and are currently used for the evaluation of occupant safety in car crash scenarios [16]. Even though significant efforts in this field have been made, accident-related injuries of the muscle-tendon-unit (MTU) have not yet been taken into consideration [17]. Therefore, three distinct injury thresholds for the tendon as well as the passive and the activated skeletal muscle were defined based on biomechanical data found in literature (see Table 6). The tendon injury threshold values were related to strain while those of the muscle were defined as a percentage of the tensile force needed to pull the muscle to failure (F_{tf}). To account for the different activity levels of the muscle, injury threshold values were linearly interpolated between the passive and active muscle injury thresholds depending on the muscle activity. A more detailed description of these MTU injury criteria can be found in the OSCCAR deliverable D3.3 and the short communication by Nölle et al.[18].

Type of Injury	Tendon	Passive Muscle	Active Muscle
Minor Injury	2% strain	30% F_{tf}	70% F_{tf}
Major Injury	5% strain	80% F_{tf}	90% F_{tf}
Rupture	10% strain	100% F_{tf}	100% F_{tf}
References	[19]	[20],[21]	[22]

Table 6 Injury thresholds of tendon, passive & active muscle

This novel method is applied in separate studies by Bosch (see Chapter 3.1.3.3), Volkswagen (see Chapter 3.1.3.6) and Mercedes (see Chapter 3.1.3.8). The results are reported in the according chapters.

3.1.3.3 Pre-study on inwards rotated seat

The overall motivation for Protection Principle 1 is to ensure occupant safety by rotating the seat along the z-axis during the pre-crash phase, i.e. from an initial seat position e.g. inwards rotated seat by 30° to a “safer” seat position, e.g. 0° in a full frontal crash. In this pre-study by Bosch the influence of the seat rotation velocity (seat base angle and start of seat rotation) on occupant kinematics and also the interaction with the restraint system is analysed.

First question to be answered was what would happen if the occupant remains in the rotated seat position, e.g. 30° inwards, and the dedicated protection principle of rotating the seat is not applied. Therefore, an initial DoE study was conducted where the occupant is rotated to an inwards sitting position between 1° and 30° prior to the crash with and without pre-crash braking, followed by an USNCAP crash with 56 km/h (Appendix 1.2). Afterwards, the interaction of the shoulder belt to the neck during the crash phase has been analysed. A variation of the seat base angle from 1° to 30° creates two curves for the effective contact measure as shown in Figure 11.

No contact is visible in any case during the pre-crash phase. The picture changes in the in-crash phase. Without pre-crash braking, no contact is visible between 0° and 13°, while with a braking action this region is between 0° and 7°. As a result, no pre-crash seat rotation would be needed in the defined angle regions with respect to the neck injury predictor. The overall belt to neck contact is lower, particularly for higher initial seat rotation angles (> 20°), for cases with pre-crash braking compared to those without. It is presumed that pre-crash braking allows for a better coupling of the occupant to the vehicle in the crash situation.

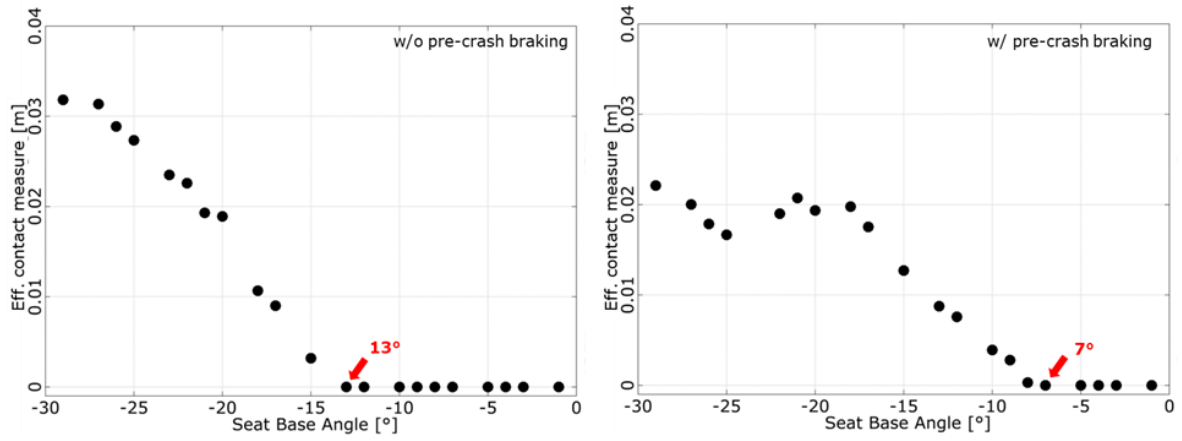

Figure 11 In-crash shoulder belt to neck interaction without AEB (left) and with AEB (right)

Results of the first DoE indicate that from a certain inwards seat rotation, here 7°/13°, additional measures must be taken into account to ensure occupant safety with respect to shoulder belt-to-neck interaction. Thus, in the next step a DoE simulation was defined where the occupant is rotated from an initial inwards seat rotation between 1° and 30° to the standard seating position (0°) during the pre-crash phase. Additionally, the start of the seat rotation was varied from -0.4 s to -0.05 s whereas the end of the seat rotation is always at T = 0 ms (start of the in-crash phase).

The variation of seat-base angle (around z-axis) and start time of the seat rotation in the pre-crash phase creates a response surface for the relative β-angles (see subsection 3.1.3.1), as shown in Figure 12, where the x-axis represents the initial seat-base-rotation-angle from -30° to 0° while the y-axis represents the start time of the seat rotation in seconds from -0.4 s to -0.05 s. The black dots represent the corresponding simulation conditions, while the colouring defines the differential angle from 0° to -20°.

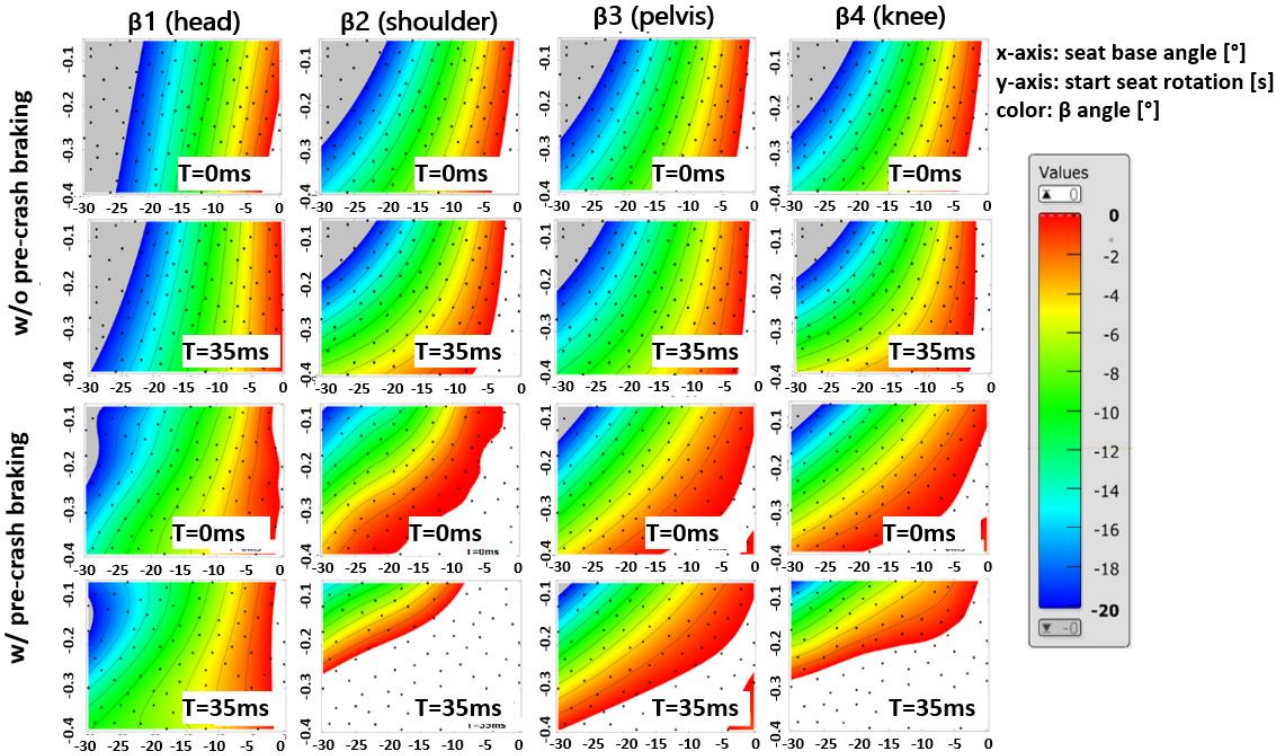

Figure 12 Relative occupant/seat rotation angle in [°]. Without AEB (top), with AEB (bottom)

White-coloured areas within the diagram represent values above the upper limit, grey areas represent values below the lower limit. The upper part of the figure represents a situation in which no AEB is applied, while the lower part shows the results where the braking action is included. The effect of the protection principle on the occupant position relative to the seat is investigated at the time of the crash (T = 0 ms) and at T = 35 ms, just before the occupant contacts the passenger airbag. The pre-crash braking has a favourable effect on the occupant repositioning due to the better coupling of the occupant to the restraint system, i.e. the values are lower in this case (red colour) and thus the occupant follows the seat rotation more closely than without braking. In cases with a high relative angle (blue), the occupant follows the seat rotation with delay, i.e. the faster the seat rotation, the more delayed the occupant movement. The relative head angle β1 shows less influence of the rotation compared to the other angles, even for lower rotation velocities. This means that the head movement is delayed with respect to the rest of the body and therefore shows higher relative angles.

The analysis of the occupant body accelerations in the pre-crash phase shows that pre-crash braking yields higher overall resultant accelerations compared to a situation without any braking. Without braking, only the effect of the seat rotation is seen. However, the resultant accelerations are on a low level overall and reach values of up to 6 g for the fastest seat rotation. Furthermore, the interaction between shoulder belt and neck has been analysed for the same seat-base angle and seat rotation start time parameters. In Figure 13 the colour represents the interaction between shoulder belt and neck in meters for given parameters, left for the case without AEB and right with AEB. Furthermore, Figure 13 displays the in-crash belt to neck contact in meters as function of the initial seat-base angle in degrees and the seat rotation start time in seconds. The grey colour represents a value of zero (negative values caused by response surface smoothing method). Similar to the case with static initial seat rotations, no contact is visible during the pre-crash phase and the braking action has a favourable effect on the contact. The effect of a higher shoulder belt-to-neck contact with increasing rotation velocities is envisioned, for example, by comparing simulation SIM43 (slow seat rotation) to SIM78 (fast seat rotation). Based on the shoulder belt-to-neck interaction a function could be generated where for larger initial seat rotation angles an earlier start of the seat rotation is required than for the smaller initial angle.

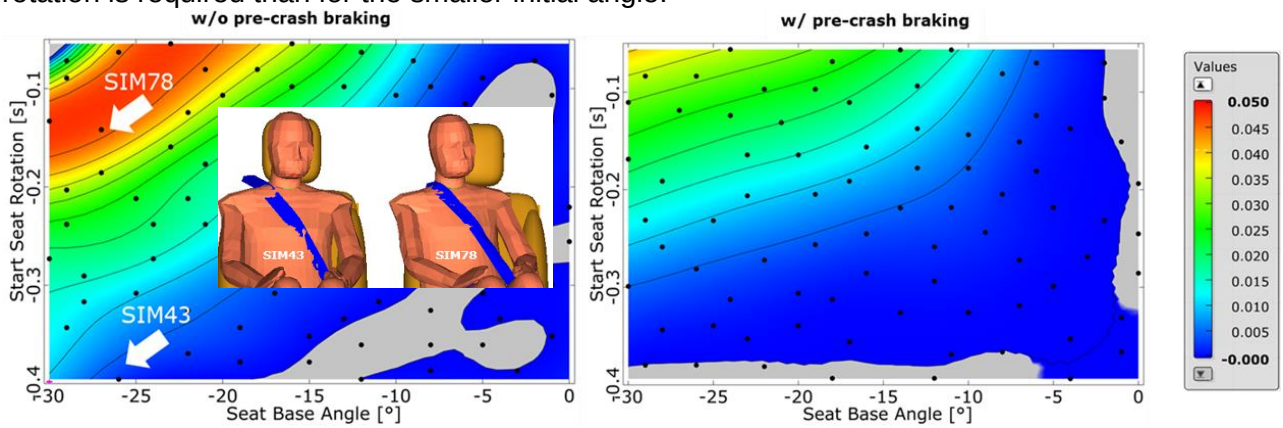

Figure 13 In-crash belt to neck contact. Without AEB (left) and with AEB (right)

Considering simulation studies with static (seat remains in rotated position and PP1 is not applied) and dynamic seat rotations, i.e. the seat is not rotated back to the 0° position but to that in Figure 11 (0° to 7°/13°), a later start of the pre-crash rotation is feasible. In the case of SIM43, for example, the rotation velocity is 65°/s. If the occupant needs only to be rotated from -26° to -13° and the same rotation velocity of 65°/s is applied, the rotation action can be started 200 ms before the crash instead of 400 ms. This would allow for a later detection and less ambitious requirements for the pre-crash detection system.

In a third simulation series, the seat rotation velocity was kept constant, but the starting time was varied. Thus, situations arose where the seat rotation was completed before the crash began, e.g. for case m400 starting at -400 ms and ending -200 ms before the crash starts. The rotation duration for 30° was fixed to 200 ms (equals 150°/s) and the starting time varied from -400 ms to -200 ms. Only cases without pre-crash braking were analysed. The focus was on kinematic values, like relative angles βi, and resultant accelerations. The relative angles βi were measured at T = 0 ms and compared with the maximum values during the pre-crash phase. Figure 14 shows that the maximum relative angles are independent of the starting time of the rotation. Here, the maximum angle during the pre-crash phase is shown in dark grey and the angle at T = 0 ms is shown in light grey. With the chosen rotation velocity of 150°/s, a rather large angular difference between occupant and seat may appear during the pre-crash action. Occupant inertial effects have a beneficial impact on the relative angle at T = 0 ms, even if the rotation was stopped 200 ms before the crash. The relative angles at start of the in-crash phase at T = 0 ms scale with the starting time of the rotation.

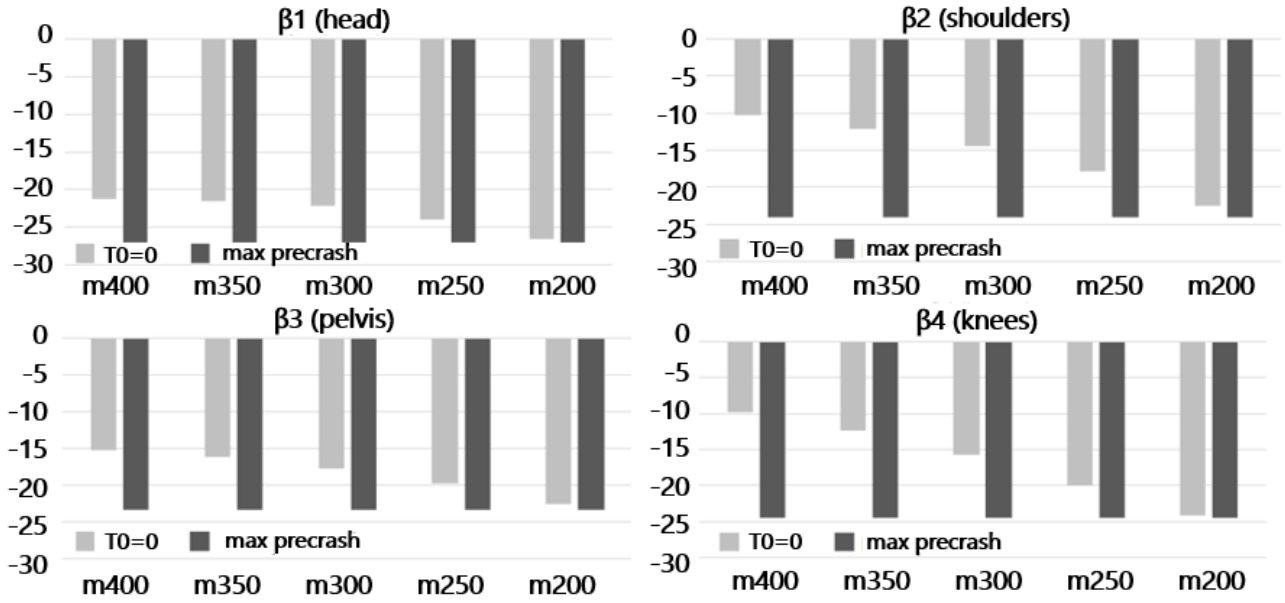

Figure 14 Relative occupant to seat rotation angles [°]

The later the rotation starts, the higher the absolute relative angle values at T = 0 ms and the less time the occupant has to reach the final direction of 0°, facing fully forward. This effect is also seen in the βi vs. time diagram in Figure 15. Relative angles for shoulder and knee are affected more strongly by the inertial effect than those for the pelvis and head. The results show that the chosen rotation velocity is rather high, and one can expect lower effects and better occupant guidance for lower rotation velocities.

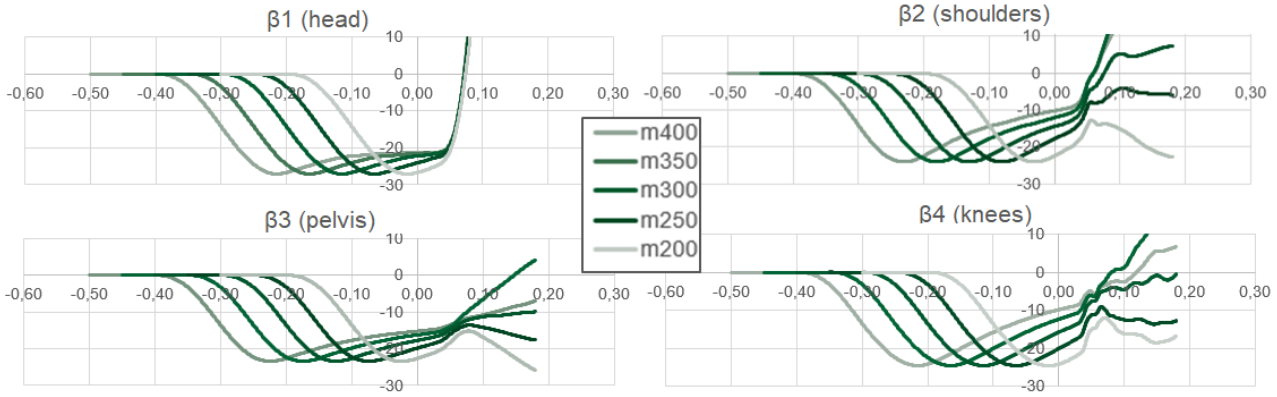

Figure 15 Relative occupant to seat rotation angles [°]

As the evaluation of the body accelerations in the pre-crash phase in Figure 16 (top) illustrates, the maximum accelerations are overall at a very low level and show no significant correlation. Accelerations in the crash phase in Figure 16 (low) also do not show any distinctive features and may indicate that the starting point of the seat rotation action (for the given high velocity) has a low impact on the occupant body load.

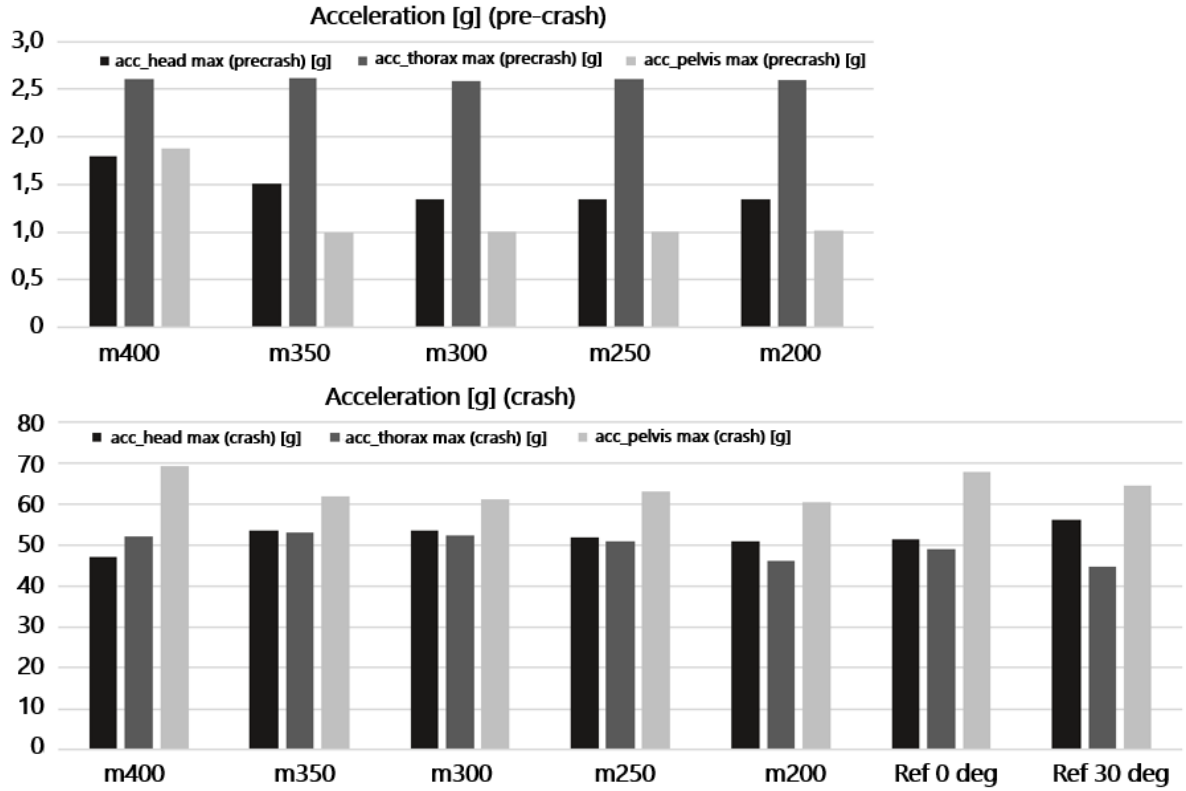

Figure 16 Head, thorax, pelvis acc. [g] for pre- /in-crash phases with diff. rotation start times

In this study only the rotation from an inwards rotated position (e.g. 30°) to the standard position (0°), where the occupant is rotated into the shoulder belt, was analysed. As a final result of this study, a rotation velocity of approximately 85°/s (rotation of 30° within 0.35 s) is recommended for cases without pre-crash braking. With pre-crash braking and considering the effect of shoulder belt to neck interaction, higher rotation velocities can be considered, e.g. 120°/s (rotation of 30° within 0.25 s). Further analysis is needed to identify whether the recommended velocities can also be applied if the occupant is rotated out of the shoulder belt (e.g. outwards rotated, -30° to 0°), since in this case the shoulder belt could slip off the shoulder.

In a final simulation study the method for the evaluation of potential muscle injury risks, described in Chapter 3.1.3.2, was applied to Madymo data. For the assessment of the method, the same simulation settings were used as in the comparison study described in Chapter 3.1.3.7. In the following description, the application for one specific muscle (Semispinalis Capitis L T3Sk, compare Table 7) will be shown and afterwards all muscles in the AHM Madymo model will be considered.

First the tensile force F_{tf} needed to pull the muscle to failure must be calculated based on the muscle's maximum isometric force.

$$\boldsymbol{F_{tf} = 3.32 * F_{max}}$$

In the next step, the threshold forces for the passive and active muscle, for the three injury severity levels can be calculated based on F_{tf}. In Table 7 the threshold forces for the semispinalis Capitis L T3Sk muscles are shown.

Type of Injury	Passive Muscle	Active Muscle
Minor Injury	30%F_{tf} = 62.8 N	70%F_{tf} = 146.4 N
Major Injury	80%F_{tf} = 167.3N	90%F_{tf} = 188.2 N
Rupture	100%F_{tf} = 209.2 N	100%F_{tf} = 209.2 N

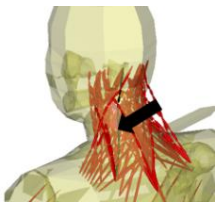

Table 7 Threshold forces for passive & active Semispinalis Capitis L T3Sk muscle

A prerequisite for the application of the model is that the considered muscle must be in tension. In Figure 17 in the left graph the normalised length of the semispinals capitis muscle is shown and an increase is visible from -0.2 s. The middle graph of the same figure shows the muscle activity over time. The activity curve and the calculated thresholds for the passive and active muscle are given in Figure 17, right side.

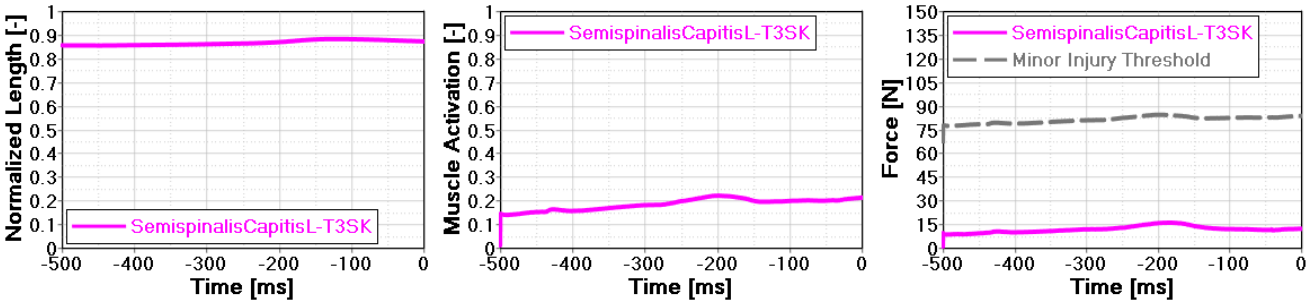

Figure 17 Normalised length (left), muscle activity (middle) and result. force (right)

The muscle threshold force can be calculated with the following formula

$$\boldsymbol{F_{thres}(a) = F_{thres,pa} + a(F_{thres,ac} - F_{thres,pa})}$$

where **F_{thres}** is the muscle threshold force [N]

$F_{thres,ac}$ is the active muscle injury threshold [N]

$F_{thres,pa}$ is the passive muscle injury threshold [N]

a is the activity level of the muscle 0…1

The calculated threshold curve for minor injury is displayed in Figure 17 in the rightmost graph (grey dashed curve). The muscle resultant force is then compared to this calculated threshold. As displayed in Figure 17, the measured force is much smaller than the threshold. In order to check the model, the above described procedure has been applied to all muscles. For better visibility and comparability of all muscles only the maximum resultant force and maximum threshold force of each curve have been analysed and displayed in Figure 18. In the graph, only muscles with resultant forces higher than 2 N are displayed.

Figure 18 Evaluation of all AHM muscles for minor injury based on seat rotation velocity

The evaluation of the Madymo results shows that in this particular case no minor injuries occur. Since the proposed method by Uni Stuttgart in Chapter 3.1.3.2 highly depends on the muscle modelling and settings in the HBM, the statement quoted above is only valid for the current maturity of the model and muscle modelling as well as related injury criteria.

3.1.3.4 Pre-study on outwards rotated seat

Within this study related to PP1 performed by ika and fka, a pre-crash seat rotation into the principal direction of force for an outwards rotated seat is investigated. From the perspective of belt to occupant interaction, a similar situation can be created, when an inboard belt routing is applied to an inwardly-rotated occupant to whom a pre-crash seat rotation is applied. The outward seat rotation was generally rated positive in one of OSCCARs User Studies [2] and motivated the following study.

The objective of this study is to show the effect of the seat rotation direction (from an outwards to a standard seating position) on the repositioning of an occupant prior to a frontal crash. The focus of the study lies on the effect of different seat rotation velocities on the interaction between occupant and restraint systems (belt system and passenger airbag). The benefits of a pre-crash activated motorised seat belt (MSB) are discussed within this context.

Method

The multi-body simulation study was conducted within the generic OSCCAR Madymo interior model, using a Madymo Simcenter AHM v3.1 model with head and neck muscle activation. The occupant is simulated in the passenger position facing 30° outwards in the initial situation (see Figure 19 left). During the pre-crash the occupant is rotated into a forward-facing position. The repositioning curve is modelled as a spline interpolation function, generating smooth rotational-velocity transitions at the beginning and at the end of repositioning. A state of the art three-point outboard-routed belt system and a passenger airbag were used in the study.

To measure the interaction between occupant and belt during the repositioning, especially for cases in which the belt slips off the shoulder, an indicator was introduced and modelled as a spherical body attached to the AHM shoulder (see Figure 19 right). The outer surface of the spherical body touches the centre of the humerus joint. Contact penetration between the spherical body as well as the

inwards and the outward shoulder belt nodes can be measured, indicating at what time the belt passes the humerus joint.

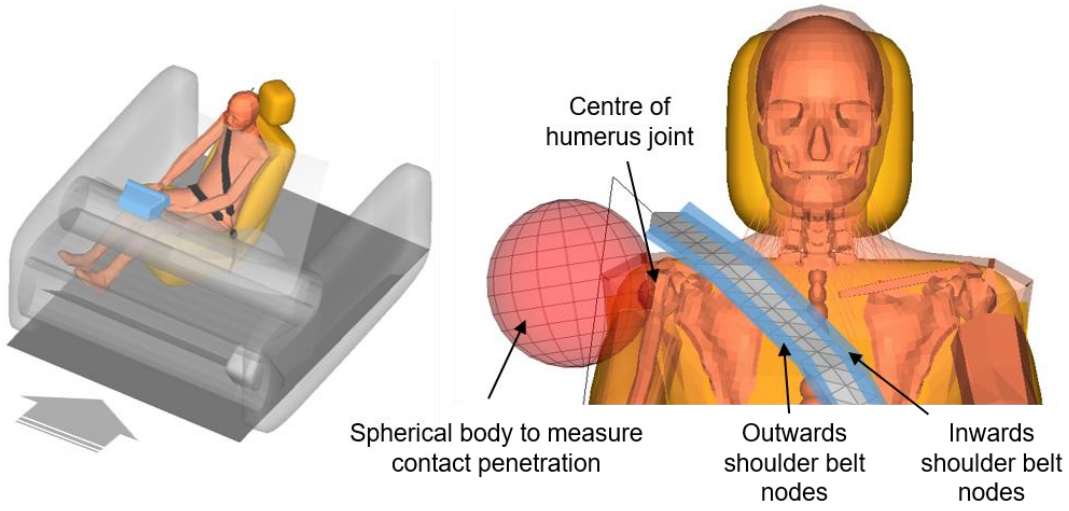

Figure 19 Outwards seat rotation in model envir. (left), shoulder belt slip-off indicator (right)

Within the study, the Madymo generic USNCAP FF 56 km/h crash pulse was simulated with- and without AEB being applied prior to the crash. The rotation start time was varied from 350 ms to 50 ms before the crash, resulting in an average seat rotation velocity of 600°/s to 86°/s (30° in 50 ms and 30° in 350 ms). In a second study, an MSB applying 250 N of retractor tensioning force at the start of the repositioning was added to the simulation setup.

Results

For a static 30°-outwardly rotated seat, belt slippage was observed during the full frontal crash. Due to the rotated occupant position, the occupant does not contact the passenger airbag in the centre (see Figure 21 red and blue curve). When the seat and integrated belt system are rotated prior to the crash, the belt slippage can be avoided in some cases. The occupant follows the seat rotation and a more centred airbag contact can be achieved. The effectiveness of repositioning depends on the seat rotation velocity. As shown in Figure 20, with high rotational velocities, the belt also tends to slip off the shoulder already during the seat rotation.

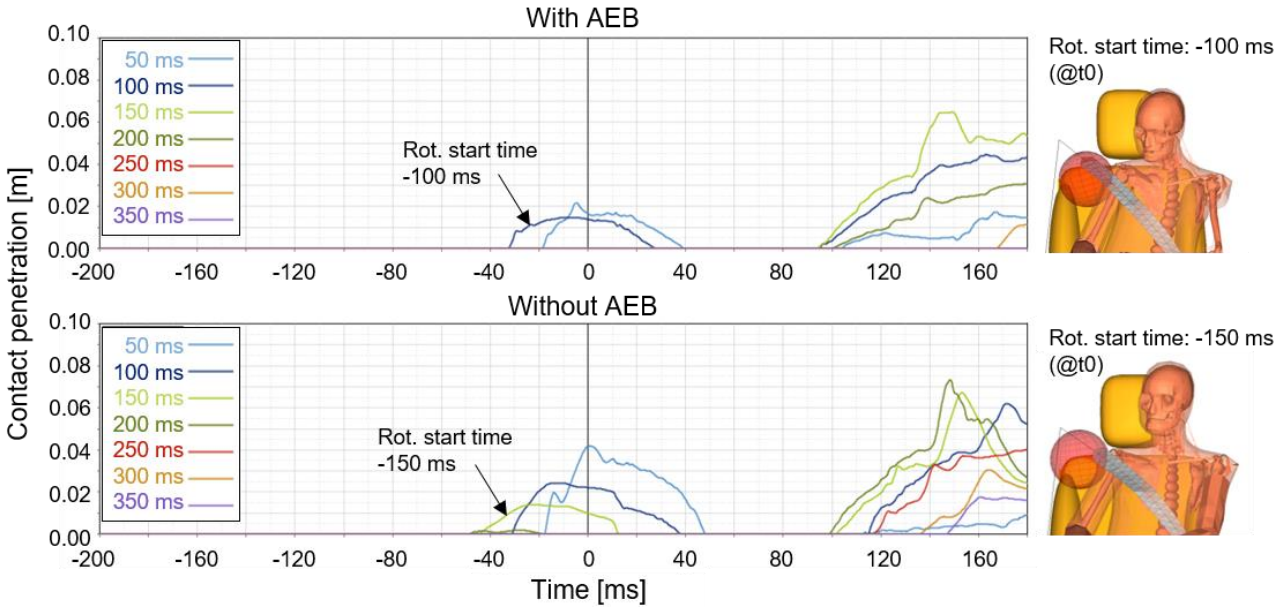

Figure 20 Contact penetration of inward shoulder belt nodes with slip-off indicator

For cases where AEB is applied the belt slips off during the repositioning for rotation start times of 100 ms before the crash (velocity 300°/s), and without AEB for rotation start times of 150 ms before the crash (velocity 200°/s). Lower rotational velocities show no belt slippage in the pre-crash phase. Exemplarily for these two rotation velocities, the occupant position at the start of the crash (at t0) is shown in Figure 20, highlighting the belt position relative to the shoulder and the slip-off indicator. Even though the contact penetration decreases during the first 40 ms of the crash phase, an effect can be seen when assessing the trajectory of the occupant during the crash. For the cases where the belt slipped off the shoulder during repositioning, the head slides off the passenger airbag.

AEB reduces the belt slippage tendency in pre-crash, due to the inertia-based forward displacement of the occupant, which leads to a better coupling between shoulder belt and occupant.

The effect of a pre-crash activated MSB is illustrated in Figure 21 for an exemplary simulation, where the seat rotation is activated 100 ms before the crash and belt slippage was observed in the initial simulation setup, without MSB.

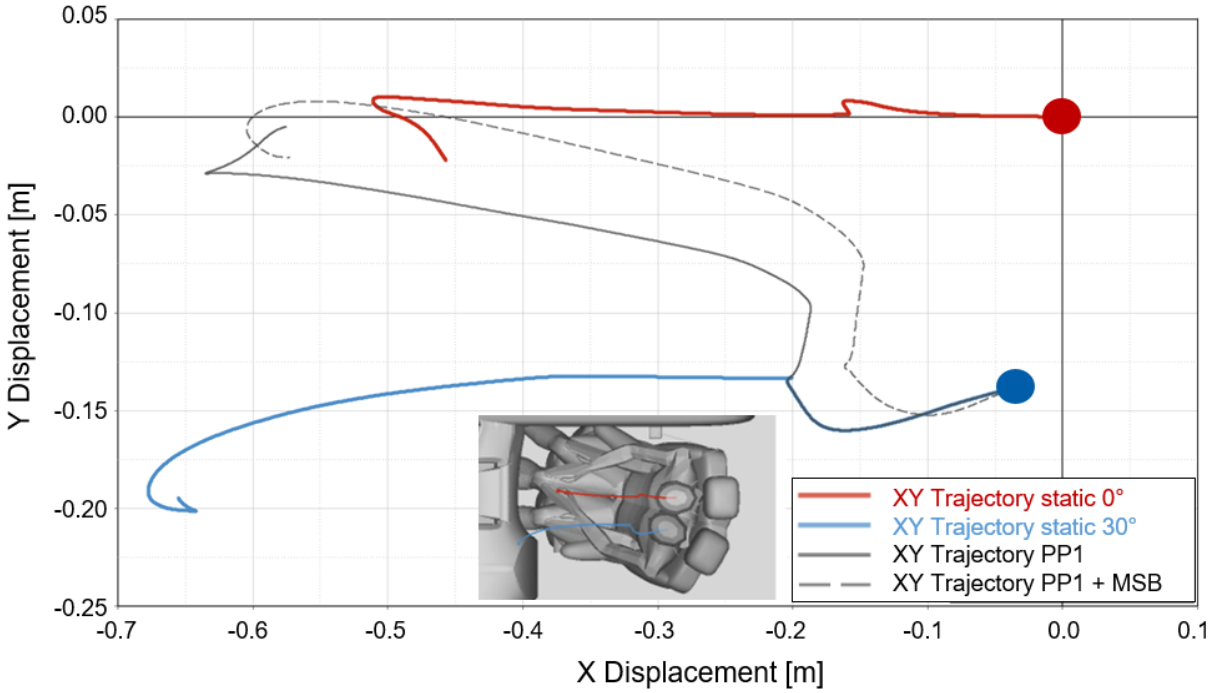

Figure 21 Effect of MSB on occupant trajectory (X-Y section), with AEB

The MSB could not prevent the belt from slipping during the rotation, but generates a better coupling between occupant and belt, leading to less movement of the occupant out of the belt and less forward excursion. In comparison to the baseline simulations for a 30° rotated (blue) and a 0° fixed (red) seating position, it can be seen that the MSB brings the movement of the occupant closer to a standard seating position, leading to a more centralised airbag interaction during the crash.

3.1.3.5 Benefit assessment of pre-rotated seat to non-rotated seat

Three simulations were conducted for the benefit assessment of the protection principle as defined in the simulation matrix below. All the cases had a 500 ms pre-crash phase with 1 g braking applied (see Table 8).

Case	Description
Baseline (Case 1)	Seat and occupant in standard position

No Seat Rotation (Case 2)	Seat and occupant in 30° inwardly-rotated position but no pre-crash rotation of seat to standard position
Pre-Rotated seat (Case 3)	Seat and occupant in 30° inwardly-rotated position. Seat rotates back to 0° position in pre-crash phase (rotation speed = 85.7°/s)

Table 8 Case description

Results

The occupant kinematics in all three cases are illustrated in Table 9. A more detailed overview, containing more time steps, is given in Table 34 of Appendix 1.3. The final state of the A-THUMS_D 3.3.6 model at the end of the pre-crash phase (t = 500 ms) shows a comparable upper body position between Case 1 and Case 3, although the leg position is different in the two cases. As expected, the position at the end of the pre-crash phase in Case 2 is very different from the other two cases.

Compared to the baseline (Case 1), the crash phase kinematics of Case 2 show a poor occupant-airbag interaction and a higher seatbelt loading on the neck. The occupant kinematics in Case 3 appear similar to Case 1 in terms of interaction with airbag and seatbelt owing to the similar upper body position at the end of the pre-crash phase.

Time (ms)	Case 1	Case 2	Case 3
-500	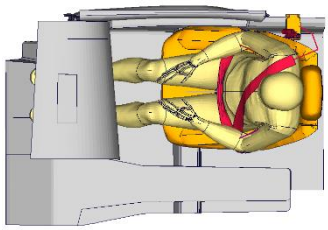	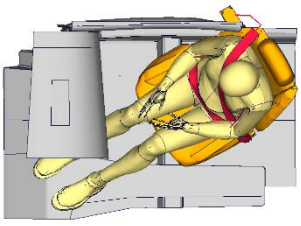	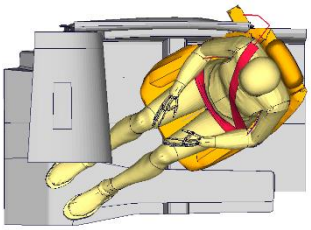
-200	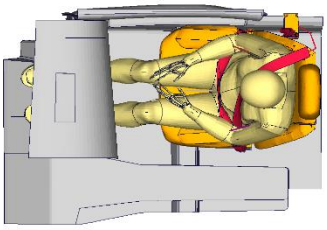	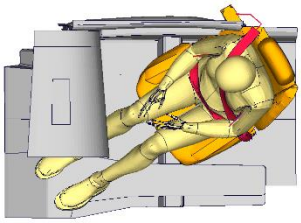	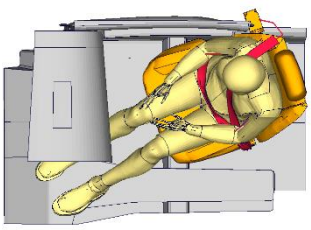
0	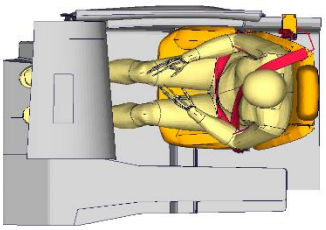	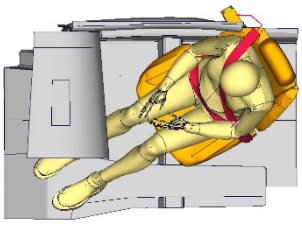	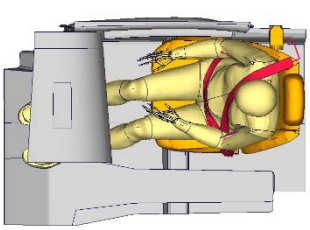
	end of pre-crash phase		
0	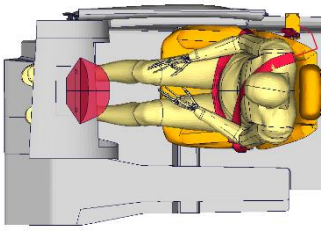	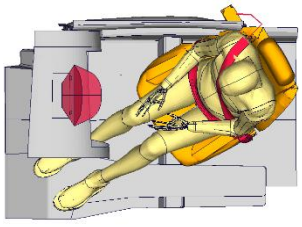	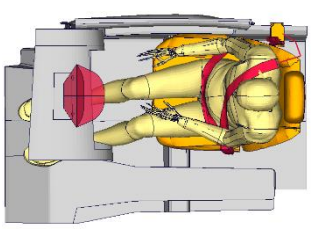
	data transferred to THUMS-TUC HBM		

20	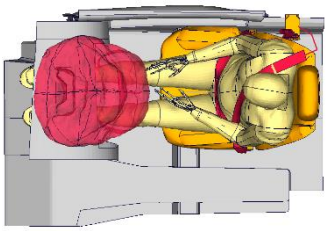	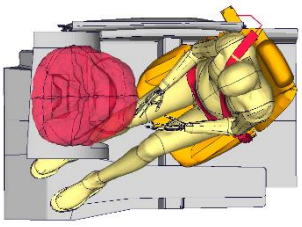	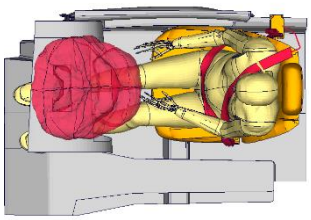
100	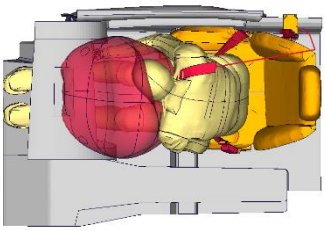	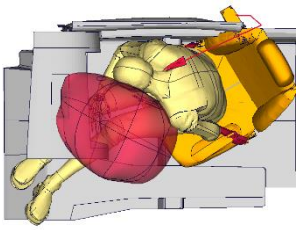	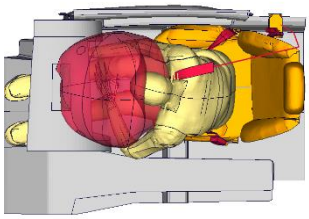
160	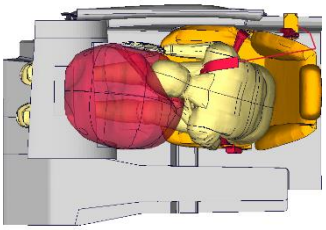	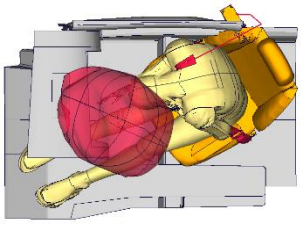	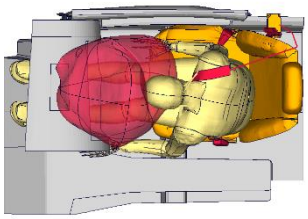
180	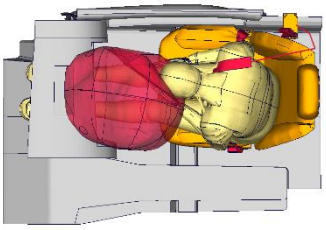	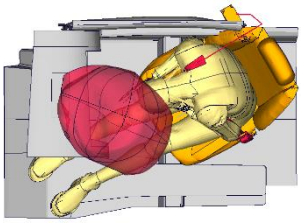	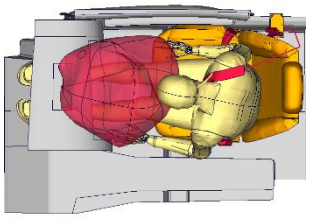

Table 9 Occupant kinematics for Case 1, 2 & 3

Injury-risk related post-processing

1) Neck Injuries

The peak extension force in the neck was registered to be 0.5 kN in Case 1 (compare Figure 22, left graph) and increased up to 1.26 kN in Case 2 as the airbag offered no support to the head because of the HBM sliding around its side. In Case 3 the neck extension force reduced to 0.44 kN owing to an improved airbag interaction even compared to the baseline case. The improved interaction with the airbag, and hence the better restraint system performance, leads to a significant reduction in neck forces as compared to the values registered without having the pre-crash seat rotation.

In addition to extension forces in the neck, the contact force between seatbelt and neck was monitored (compare Figure 22, right graph). The peak seatbelt to neck contact force in Case 1 is 0.19 kN which increases to 1.04 kN in Case 2 due to a HBM movement in the direction of the pretensioned (hence taut) seatbelt. This loading of the neck due to an interaction with the seatbelt can be potentially hazardous. In Case 3, the kinematics change and the seatbelt does not directly load the HBM neck and the contact force registered in the simulation is 0.3 kN, which indicates a reduced loading of the neck by the seatbelt and a reduced injury risk.

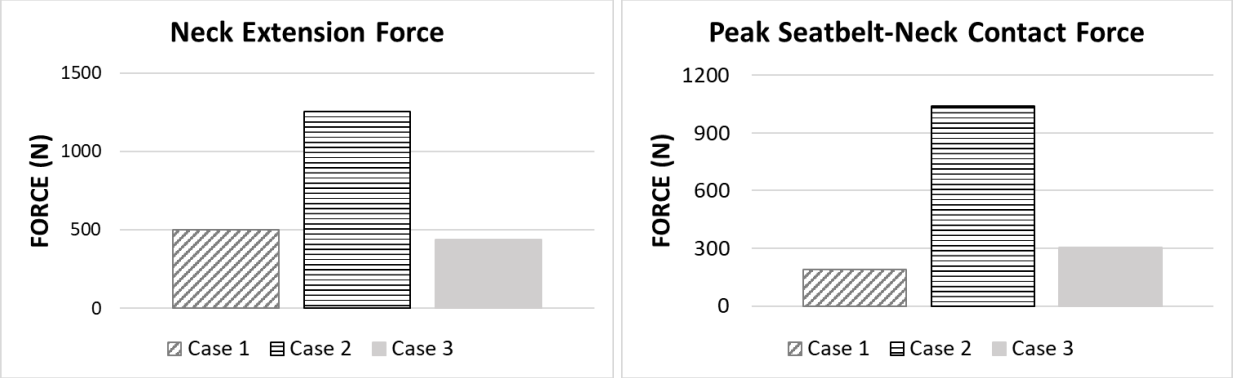

Figure 22 Peak neck extension forces & peak seatbelt-neck contact forces

2) Thorax

The rib fracture risk was evaluated as per Forman *et al.* [43] using the Dynasaur tool. Multiple fractured ribs were recorded in all three cases. The probability of 4 or more fractured ribs was 97% for Case 1 and 100% for the other two cases.

The number of fractured ribs in Case 3 is higher than in Case 1 due to more fractured ribs on the left side of the ribcage. This effect could be explained by small changes in kinematics seen between Case 1 and 3. For example, the arm stayed between the occupant's thighs and torso in Case1 and moved away from the body in Case 3, leading to more loading of the lower left ribs in the latter (compare Figure 23). An optimisation of the restraint systems could reduce the rib fracture risk in both Cases 1 and 3.

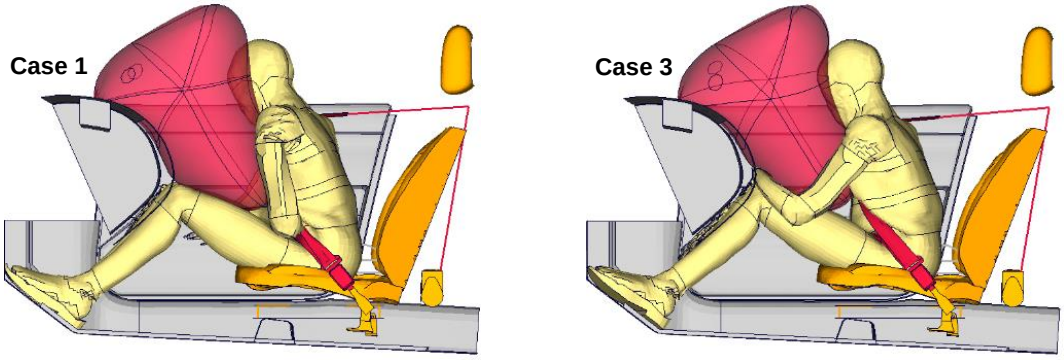

Figure 23 Difference in arm kinematics between Case 1 & Case 3 (t = 580 ms)

3) Head

An AIS4+ risk was monitored based on the Cumulative Strain Damage Measure (CSDM) [67]. But no risk of an AIS4+ head injury was recorded in any of the cases. This further underlines the need of criteria for evaluating lower severity head injuries in the future.

4) Muscle Injuries

The strain-based muscle injury criterion has been defined in Chapter 3.1.3.2. The injury risk was monitored for selected muscles registering high axial forces in the simulation. The axial forces in the muscles were well below the threshold for minor injury risk, which was the case for all of the load cases. The active pre-crash seat rotation is thus not expected to be critical for the muscles of the occupant.

The build-up of the axial muscle forces and a comparison with the minor injury threshold for selected neck muscles is presented in Figure 24. The muscle forces increase as the muscle activity, controlled by [65], builds up in the course of the simulation.

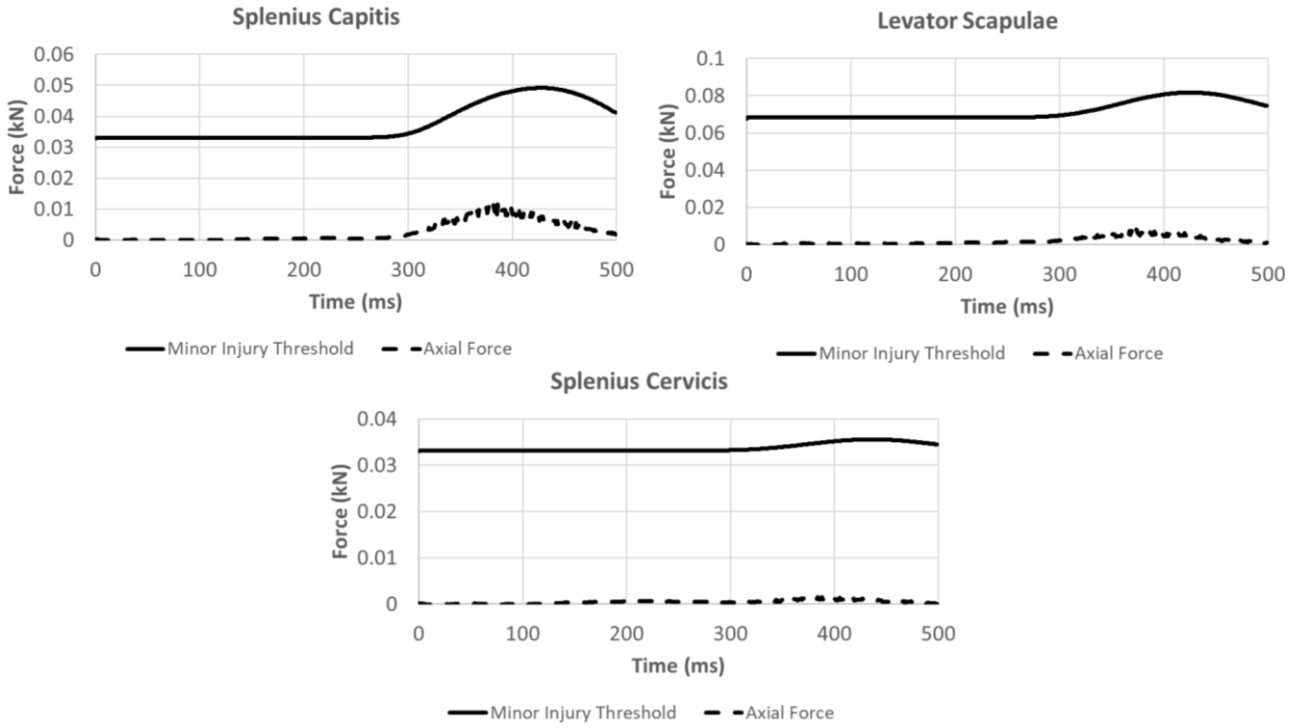

Figure 24 Muscle forces with minor injury thresholds in Case 3 for selected neck muscles

3.1.3.6 Study on pre-rotated seat considering different countermeasures

In this study performed by Volkswagen, the objective related to the research questions was to analyse the influence of additional countermeasures combined with Protection Principle 1 (PP1), the pre-rotated seat. The intention of these additional countermeasures was to improve the coupling of the occupant with the seat during the seat rotation.

The simulations in this study were carried out in the VPS code using the simulation model described in Chapter 3.1.3.1. In this chapter also more details regarding the used pre-crash and crash pulse can be found. In all simulations a pre-crash pulse was used, assuming that in all cases where the pre-rotated seat can be activated, pre-crash braking will also be triggered. The effect of the different additional countermeasures was compared using the same combination of pre-crash and in-crash pulse in all simulations.

The main parameter settings of the pre-rotated seat have been taken from the pre-study performed by Bosch and previously presented in Chapter 3.1.3.3. The initial inward seat-rotation angle was 30°. The location of the rotation axis around the z-axis was under the H-point of the HBM and in the middle of the seat pan in y-direction. The seat rotation characteristic was also taken as recommended by Bosch (Figure 3). The seat rotation activation time was set to 300 ms prior to the imminent impact.

The overall time line used in all Volkswagen simulations including all triggering points (time to fire - TTF) of the active measures is shown in Figure 25.

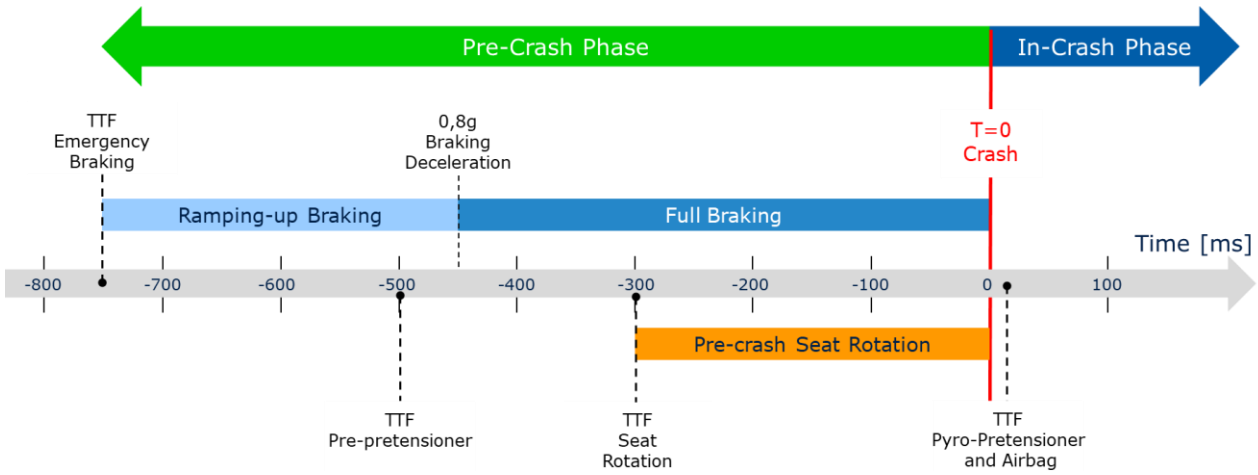

Figure 25 Overall simulation time line used in Protection Principle 1 study

First of all, a baseline simulation was performed with the seat in a fully forward-oriented position (0°). The baseline simulation also included the pre-crash phase with the braking pulse and the pre-pretensioning of the shoulder belt. In the next step, the seat was rotated by -30° around the z-axis in inboard direction. In all other simulations, different countermeasures were added to Protection Principle 1 with the aim to improve the coupling of the occupant to the seat rotation (Figure 26).

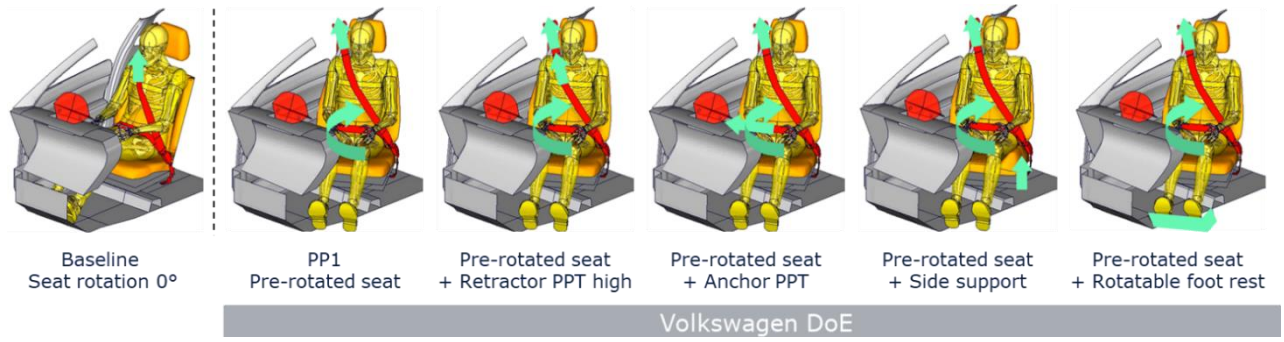

Figure 26 Countermeasures evaluated and compared in the Volkswagen DoE

In all simulations a generic retractor pre-pretensioner with a low force was used to tighten the shoulder belt with 250 N in the pre-crash phase. As first additional countermeasure, a high-performance generic retractor pre-pretensioner was combined with PP1, able to tighten the shoulder belt with 500 N. The second countermeasure was a second generic pre-pretensioner located at the anchor point of the seat belt, able to tighten the lap belt with 250 N if activated. The third countermeasure was a seat pan side support of approx. 100 mm height. The last analysed countermeasure was a rotatable footrest connected to the seat and therefore rotating with the same rotation characteristic as the seat. As an overview, all analysed additional countermeasures are shown in Table 10 with the used parameter settings.

Countermeasure	Parameter settings - Var0	Parameter settings - Var1
Retractor PPT (pre-pretensioner)	Low: 250 N	High: 500 N
Anchor PPT (pre-pretensioner)	0 N	250 N
Side support	0 mm	~100 mm
Rotatable foot rest	No	Yes

Table 10 Parameter settings of the investigated countermeasures

The simulation study considered not only the potential benefit of each single countermeasure, but also all possible combinations of the different countermeasures. This approach led to a full DOE matrix with a total of 16 simulations and all were performed within this study.

The analysis of the simulation results was split into two parts. In the first part only the pre-crash phase was evaluated and in the second part the in-crash phase was evaluated and compared to the baseline simulation with the seat in the 0° position.

To evaluate the benefit of each single countermeasure, the results of the four DOE runs with one single countermeasure added are presented here first and compared to the results with the pre-rotated seat alone. Additionally, the DOE run with all investigated countermeasures included, here named “pre-rotated seat + all countermeasures”, is presented in the comparison of the results.

Evaluation of the pre-crash phase

Related to the research questions mentioned in Chapter 3.1.2, the evaluation of the pre-crash phase was focussed on the occupant kinematics and potential minor injuries caused by the seat rotation.

The kinematic evaluation was done in the same way as by other PP1 partners. The aim of the seat rotation was to reach the same occupant position relative to the seat after the pre-crash phase (t_0 = 0 ms) as in the baseline simulation without any seat rotation. Therefore, the relative angles between selected body parts of the occupant and the forward oriented seat at the time t_0 were used as evaluation criteria. The definition of the used angles is shown in Figure 5.

In the baseline simulation a pre-crash braking pulse was provided, therefore the occupant position in this simulation has also slightly changed during the pre-crash phase. To consider this, all angles shown in Figure 27 are the relative angles at t_0 between the baseline occupant and the occupant in the corresponding DOE run.

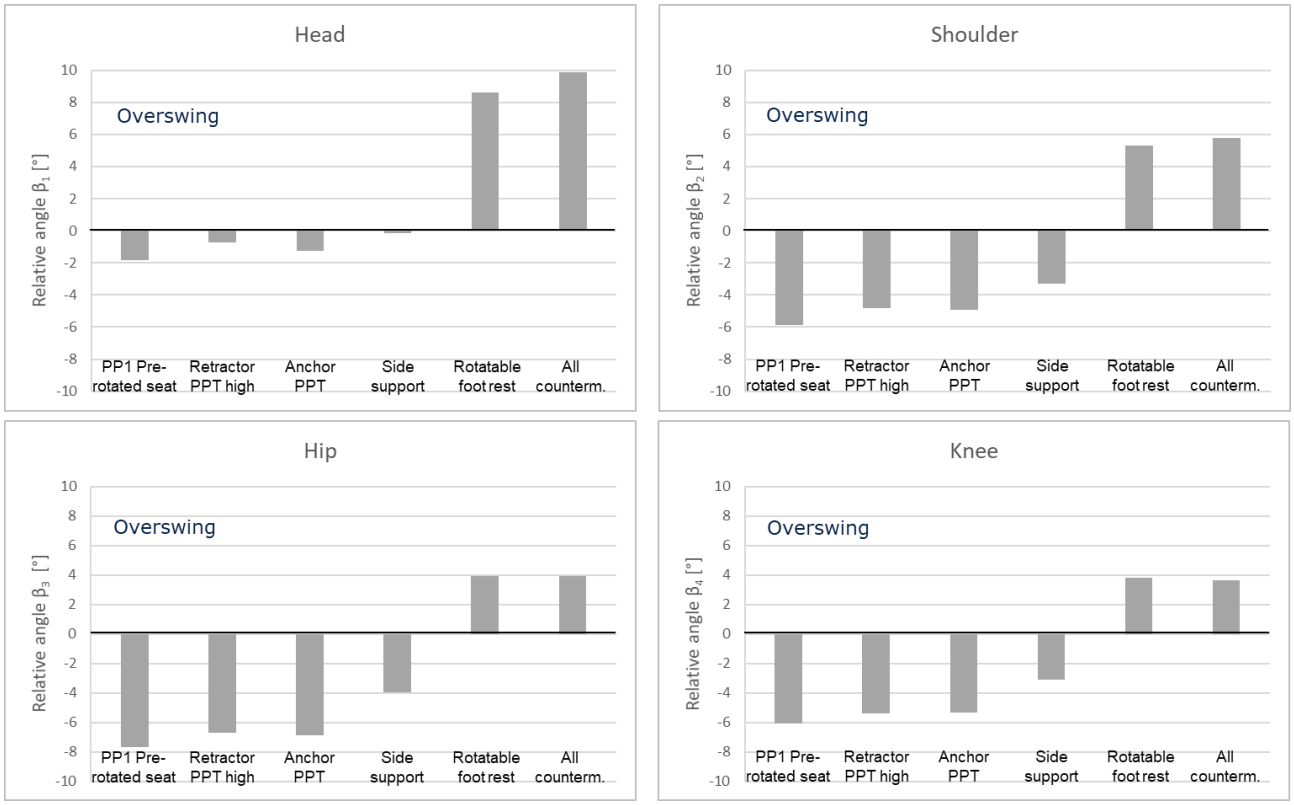

Figure 27 Relative angles between baseline and DoE occupants for selected body parts at t_0

With PP1 only, the deviations in the occupant position were up to -8°, meaning that the occupant was still slightly rotated inwards at t_0. The lowest deviations in the overall occupant position were received with the higher seat pan side support. The position of the baseline occupant was not completely reached at time t_0, but the differences were overall lower than -4° and thereby below the differences of the occupant with the pre-rotated seat alone (see Figure 28). The simulations including the rotatable foot rest were resulting in an over-swinging of the occupant due to a too good coupling of the whole occupant, including the legs, to the seat rotation. All other countermeasures led to similar results with minor improvements compared to PP1 only. It must be mentioned here, that the occupant positions considered in Figure 27 and Figure 28 were taken at the time t_0. This does not mean, that the occupant motion has already stopped at that time. In all simulations the occupant rotated further during the beginning of the in-crash phase.

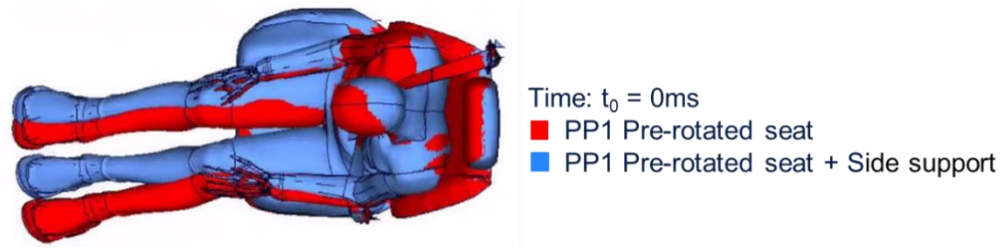

Figure 28 Occupant position at t0 = 0 ms for PP1 and PP1+Side support

The second evaluation criterion in the pre-crash phase was focused on minor injuries possibly caused during the repositioning of the occupant by the seat rotation. For this evaluation the approach by University Stuttgart was used (Chapter 3.1.3.2).

The neck muscles included in the THUMS TUC-VW AHBM were evaluated. In this deliverable the two muscles with the highest activation levels are reported, namely the Longus and Semispinalis Capitis. All the neck axial muscle forces lie below their corresponding thresholds. Therefore, no minor injuries are expected during the pre-crash phase. However, it is important to point out that the THUMS TUC-VW AHBM has been validated against volunteer test data, under frontal and lateral accelerations, only in terms of kinematics and not of either EMG recordings nor muscle forces. In Figure 29 it can be seen that the muscle forces reach comparable values among the different versions studied. Furthermore, in Figure 29 the a) Longus and b) Semispinalis Capitis location are shown on the right side [62].

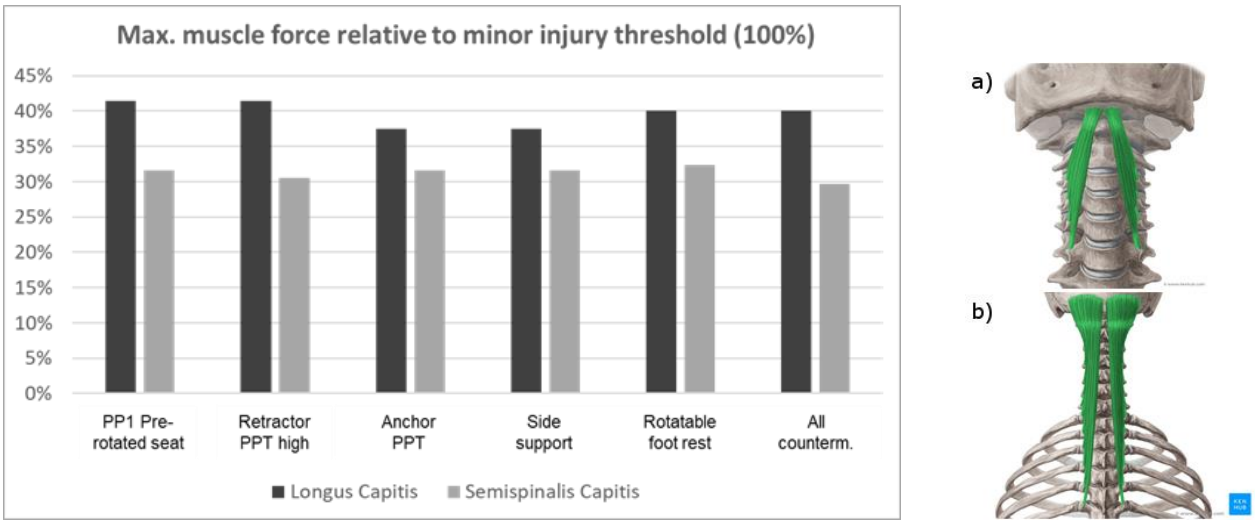

Figure 29 Maximum muscle forces of the Longus & Semispinalis Capitis with respect to their corresponding minor injury thresholds

Evaluation of the in-crash phase

The evaluation of the in-crash phase was focused on the head and thorax loadings. In Table 11 the kinematics of the considered simulation runs are shown at different time steps.

At the time step T = 50 ms the occupant's head makes first contact with the airbag. In the baseline simulation the head contacts the centre of the airbag. In all simulations with the pre-rotated seat the contact point of the head to the airbag is shifted to the right of the airbag centreline. The main reason for this is that with the pre-rotated seat, the occupants rotate further in the first milliseconds of the in-crash phase. This also results in a higher z-rotation of the head compared to the baseline. Especially in the two simulations where the rotatable footrest is included, also the whole thorax was more rotated around the z-axis at T = 50 ms. The occupant positions in the ride down phase are shown for the time step T = 75 ms.

The maximum forward displacement in all simulations was reached at approx. T = 100 ms, before the rebound phase started. The positions of the occupants in the top view are very similar. For all occupants a high head z-rotation was observed. This was probably caused by the generic airbag used, which was not developed or adapted for this specific use case.

Settings	T = 50 ms	T = 75 ms	T = 100 ms
Baseline	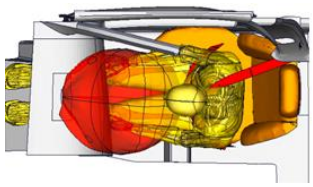	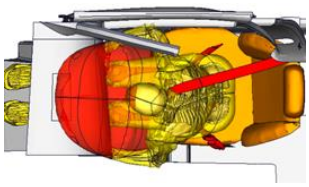	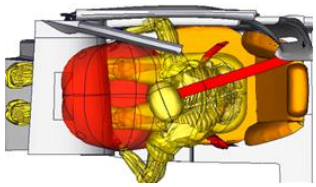
PP1 Pre-rotated seat	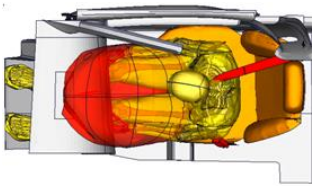	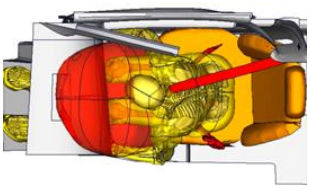	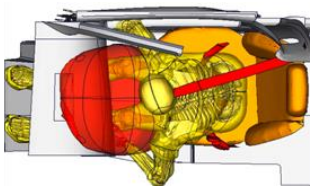
Retractor PPT high	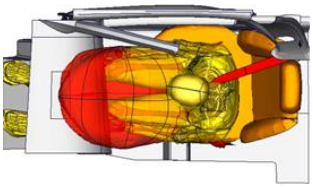	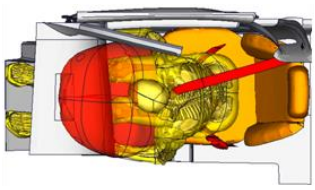	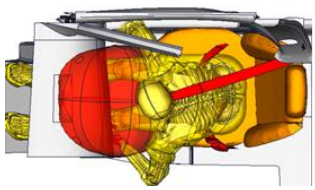
Anchor PPT	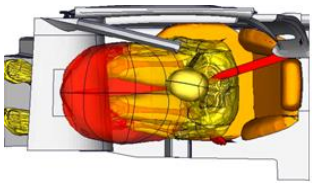	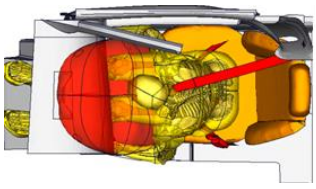	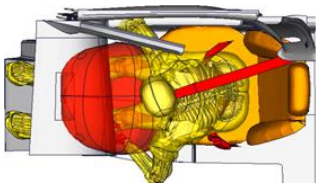
Side support	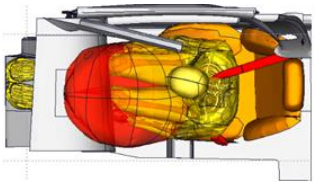	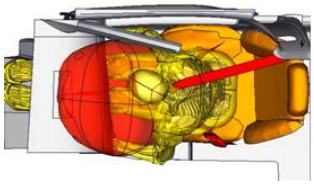	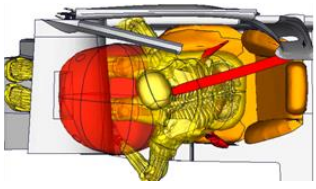

Rotatable foot rest	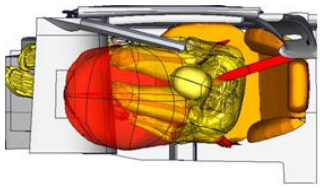	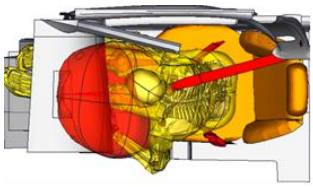	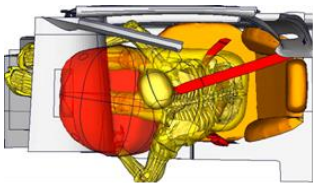
All counterm.	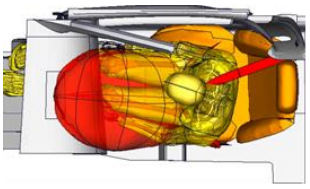	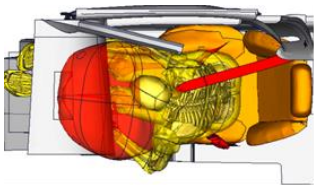	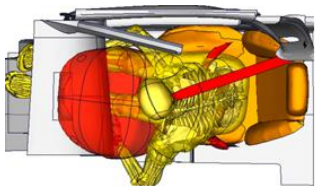

Table 11 Occupant kinematics at three different time steps of the crash phase

Some selected occupant loadings for the head and thorax region are shown in Figure 30.

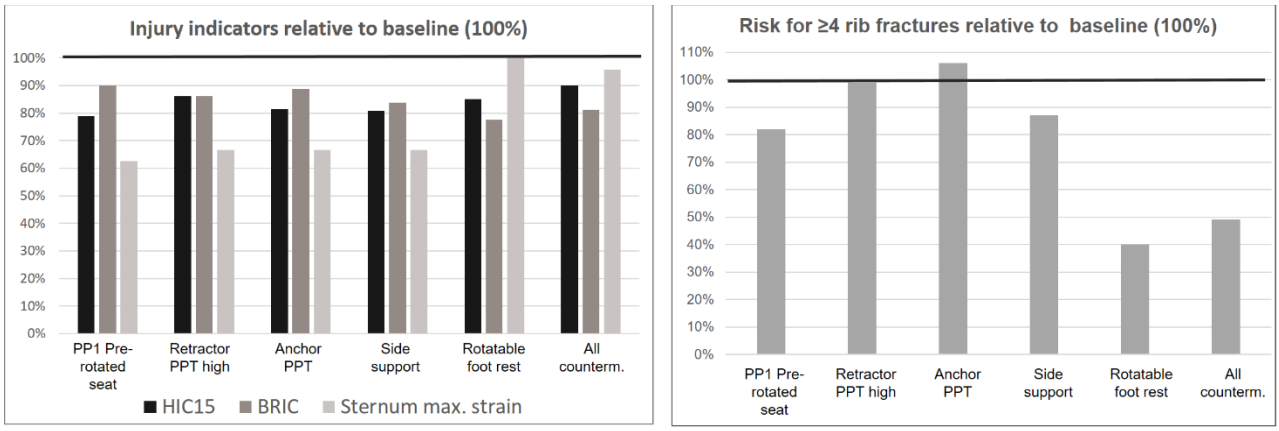

Figure 30 Occupant loadings with pre-rotated seat compared to the baseline simulation

With the pre-rotated seat, the evaluated occupant loadings were below the baseline, mainly due to the different occupant interaction between seat belt and thorax as well as between head and airbag. The HIC and BRIC values in the DOE variations are on a similar level, varying in a range of 5-10%.

A larger difference was observed for the maximum strains on the sternum. The values for the pre-rotated seat versions are a result of the changed shoulder belt routing along the thorax during the rotation. In the baseline, the sternum is loaded more in the middle part, leading to higher bending loads (Figure 31). With the pre-rotated seat, the shoulder belt loads the upper edge of the sternum more. Due to the larger z-rotation of the thorax in the simulations with the footrest included, the occupant rotates more into the shoulder belt. This results in higher loadings of the upper part of the sternum compared to the other DOE simulations with PP1.

In Figure 30 in the right diagram the rib fracture risk AIS3+ relative to the baseline is shown. The calculation was done using the method proposed in WP3 and is based on [43]. For the injury risk calculation an age of 45 years was selected.

In all DOE simulations with the pre-rotated seat the rib fracture risk is below or equal to the baseline. The reduced risk values are a result of the changed belt routing over the thorax (sternum + ribs). In the simulations with the footrest included, the lowest rib fracture risks were observed due to the changed shoulder belt routing and the stronger loading of the sternum.

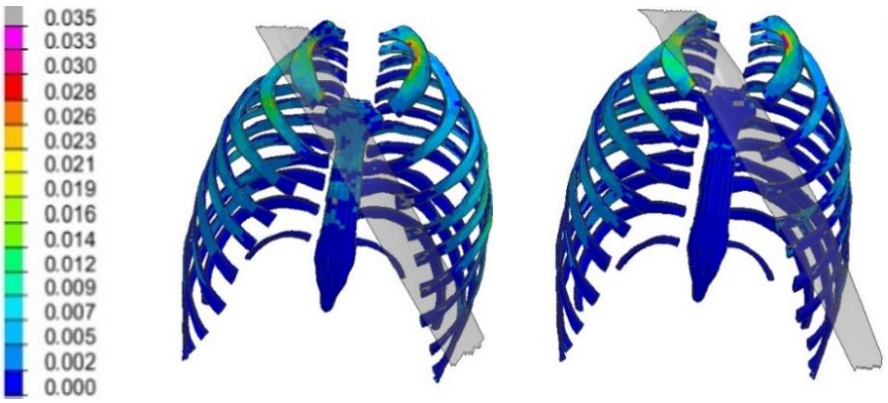

Figure 31 First principle strains & shoulder belt position for baseline (left) & with pre-rotated seat (right) at 75 ms

In conclusion, the positive effect of Protection Principle 1 (pre-rotated seat) can be further improved by adding seat- or belt-related countermeasures. A good overall system approach with balanced occupant loadings is the pre-rotated seat combined with the side support at the seat pan.

In this study no indications for minor muscle injuries were observed caused by the repositioning of the occupant during the pre-crash phase.

3.1.3.7 Qualitative comparison study for a highway crash scenario

In the initiation phase of the Protection Principle 1 working group, a simulation matrix was elaborated which contains the studies of each partner to be performed in WP2 Task 2.3 (Appendix 1.1). Volkswagen, Mercedes and Bosch performed different simulations within their main studies focusing on the highway scenario. In addition to this planned work, the working group decided to conduct a qualitative comparison study in order to identify similarities and differences with the different HBMs. As a remark; this comparison is carried out as an addition to the work which will be done and reported within WP4 on the Homologation Test Case.

For the comparison study one dedicated case out of each partner's highway scenario was chosen. The crash configuration consists of a pre-crash braking (compare Figure 32, left) which starts at -0.5 s followed by a full frontal crash with 40 km/h (compare Figure 32, middle and right).

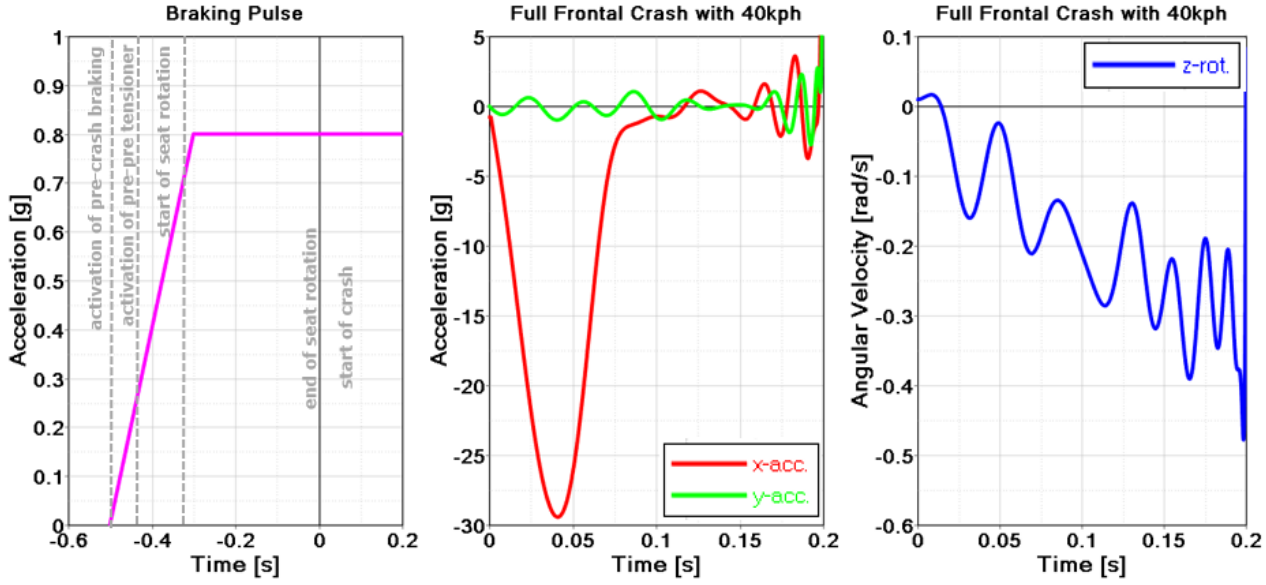

Figure 32 Pre-crash braking curve (left). USNCAP crash pulse with 40 km/h (middle, right)

According to the seat-specific settings reported as outcome of the Bosch pre-study in Chapter 3.1.3.3 the passenger is rotated by 30° inwards and will be rotated towards 0° with a rotation velocity of approx. 85°/s (start of the seat rotation at -0.35s prior to the crash). A detailed list of further parameters has been aligned among the partners Volkswagen, Mercedes and Bosch, shown in a matrix in Appendix 1.1. Besides the parameters which have been aligned between the partners, a few settings and boundary conditions have not been aligned, including:

- Settling of the HBM (position of head, leg, arm)
- Activity of neck (AHM)
- Belt routing
- Position of belt anchor point at seat (D-ring)
- Seat side structure (ability to restrain side movement of occupant)
- Friction between occupant and seat
- Airbag shape

Table 12 and Table 13 show the results of the performed study by each partner. Table 12 shows the side view of the three models with the top line at start of the pre-crash braking (-0.5 s), the middle line at the end of the seat rotation and start of the in-crash phase and the bottom line during the crash at 0.1 s. Table 13 shows the top view for the same three models at same simulation times.

Time (s)	Volkswagen	Mercedes	Bosch
-0.5		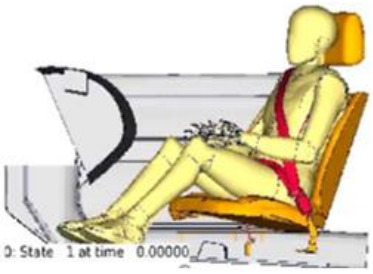	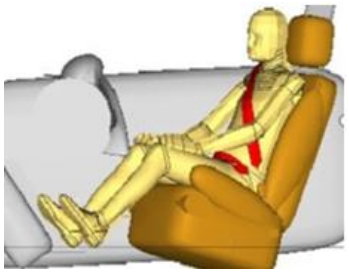
0.0		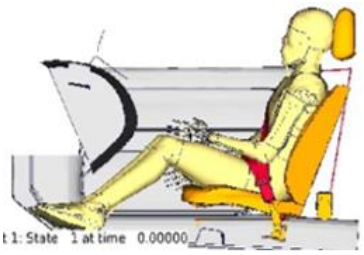	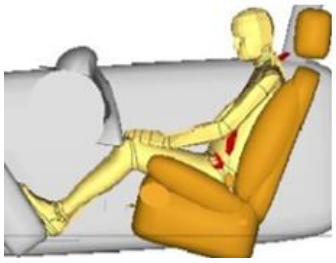
0.1		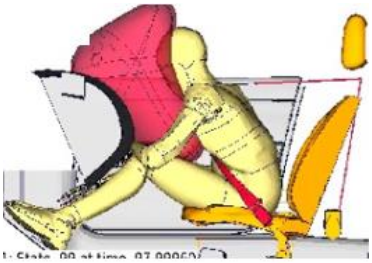	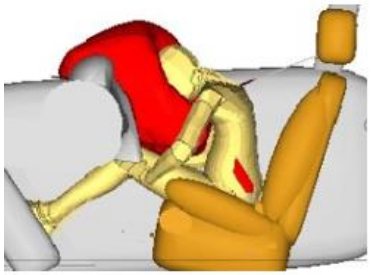

Table 12 Comparison of occupant motion - side view

In comparison to the start position (-0.5 s), at the end of the pre-crash phase, the head of the VPS and the Madymo model are tilted forward whereas the head of the LS-Dyna model is still upright and in contact with the head rest (compare Table 12, upper and middle line). Probable reason for this

effect is the different representation of the head-neck part within the different HBMs including the active muscle representation.

In general, the Madymo AHM seems to follow the seat rotation more closely than the FE-models which can be seen on the basis of the leg position at the end of the seat rotation. Possible reasons could be the higher seat side structure in the Madymo seat model which could cause a better coupling between occupant and seat (compare Table 13, upper and middle line) but also the friction between seat and occupant. Nevertheless, at the start of the crash all three models have reached a position where the relative rotation between seat and occupant is very low.

During the in-crash phase the Madymo model has earlier contact with the airbag than the two THUMS models. The contact time with the airbag varies between the models due to different initial head positions at the start of the crash, as already outlined above. The occupant motion at 0.1s after the start of crash shows that the upper body of the Volkswagen and Mercedes THUMS models have a higher forward displacement than the Madymo model. Since the anchor point of the belt to the seat (D-ring) is different in the three models the restraining load on the upper body by the shoulder belt might be different as well (angle of shoulder belt to upper body is different). Due to the different shape of the passenger airbag, the upper body and the head of the THUMS models are aligned whereas in Madymo the upper body and neck is tilted. The reason for this difference could be the contact area between passenger airbag and chest of the occupant due to the different airbag shape, i.e. this shape is different in the Madymo model. The position of the shoulder belt at 0.1 s (compare Table 13, lower line) is closer to the neck in the FE-models and the head in the Volkswagen model is twisted along the z-axis, which causes almost a side contact between head and passenger airbag.

Time (s)	Volkswagen	Mercedes	Bosch
-0.5	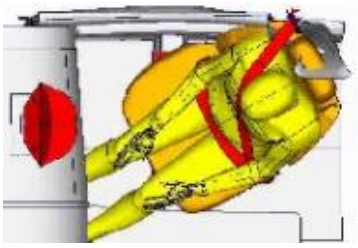	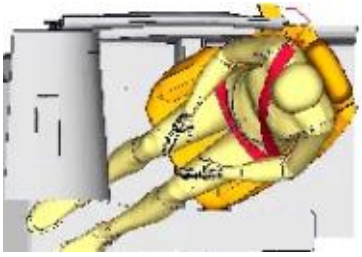	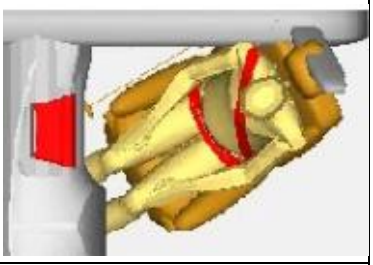
0.0	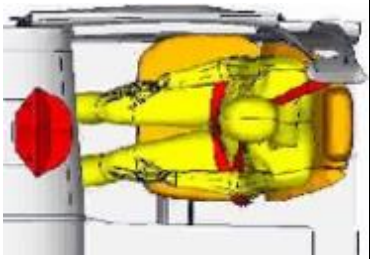	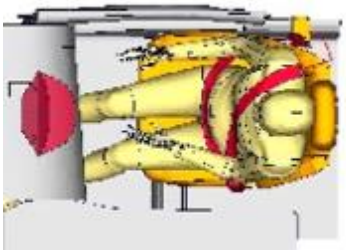	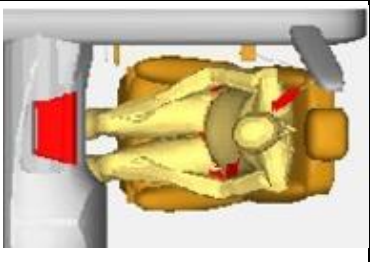
0.1	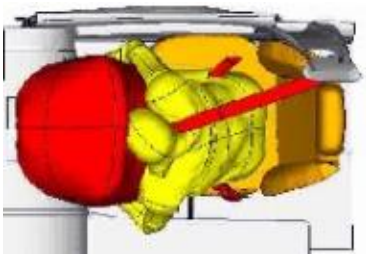	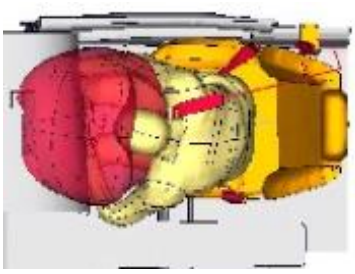	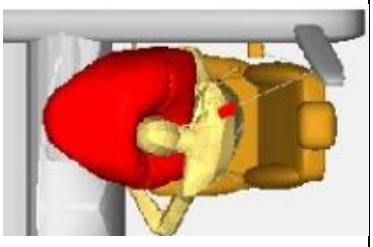

Table 13 Comparison of occupant motion - top view

Besides the qualitative 3D motion comparison, the occupant position at landmarks headCOG, C7, T8, ASIS R+L have also been compared. Thereby the models have been aligned at C7. The three

models are equally positioned and oriented at landmark C7, while the other landmarks displace accordingly, see Figure 33.

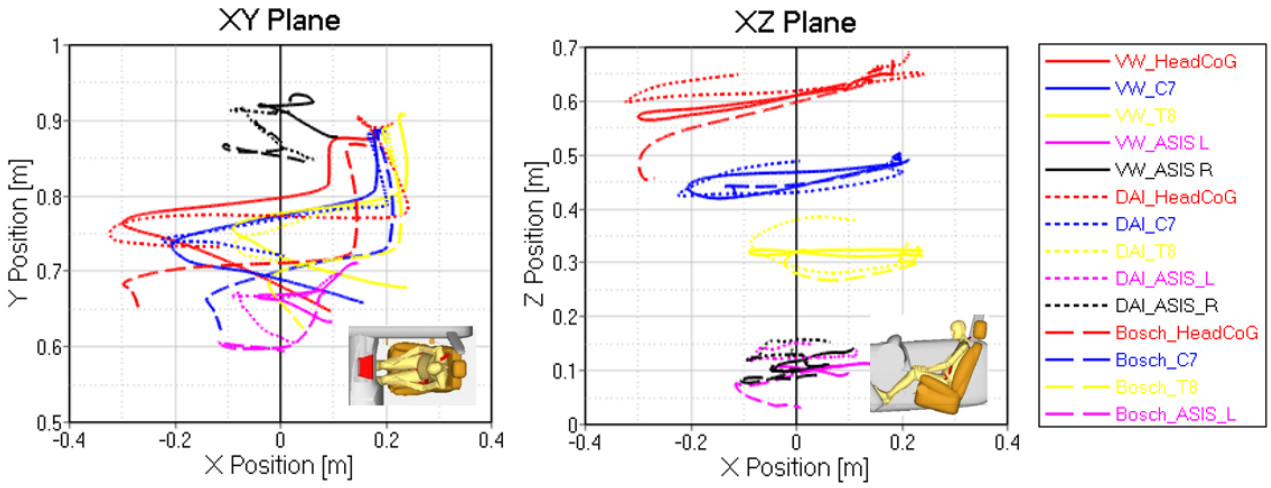

Figure 33 Position of key landmarks Head, C7, T8, ASIS L+R in xy (left)- and xz-plane (right)

As already visible in the animation data in Table 12 and Table 13, the y-positions of headCOG, C7 and T8 differ during the pre-crash phase, where the LS-Dyna and VPS models are more aligned than the Madymo model. The further downwards the landmark (z-direction) the smaller the difference in y-position between LS-Dyna and VPS. The forward displacement of the Madymo AH

M at C7 and T8 is smaller than for the FE-models. This was also visible in the animation data.

As summary, the VPS and LS-Dyna models are more aligned to each other than to the Madymo model. This seems to be a reasonable result since the interior model, the restraint model and also the HBM are more related to each other than the Madymo model is. Despite the different codes, occupant models and partly different model settings, the comparison of the simulation results shows an acceptable agreement. These findings increase the confidence in the models and thus in the simulation results. Differences in the three models can be perceived as a possible variation of restraint systems and occupants, i.e. as a representation of a set of population and restraints.

3.1.3.8 Benefit assessment of pre-rotated seat in rearward facing case

The robocab configuration evaluated in this study provides the opportunity to explore the benefit of a pre-rotated seating configuration for a scenario where the occupant is facing rearward. The objective is to understand the influence of pre-crash rotation of the seat on occupant kinematics and explore the possibility of whether seats can serve as a restraint system. Case 1 shows the baseline study without any pre-crash rotation whereas Case 2 represents the pre-crash rotation of the seat towards the principal direction of force with respect to the SCP06 crash configuration. Occupant kinematics for both cases are reported in Table 14.

Time [ms]	Case 1	Case 2
-500	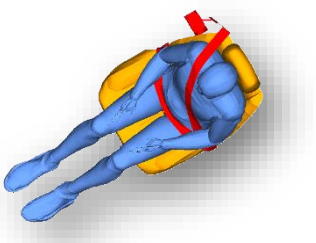	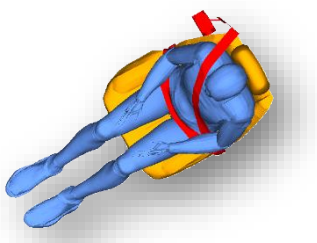

0	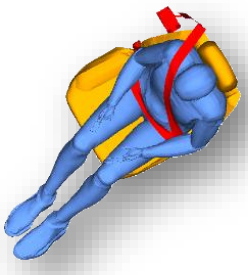	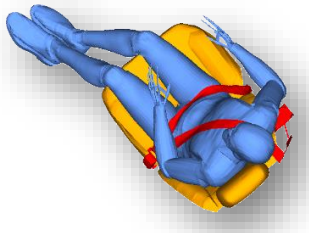
	end of pre-crash phase	
60	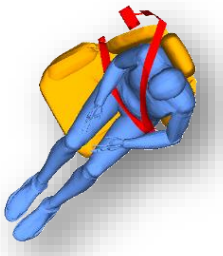	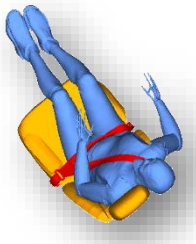
100	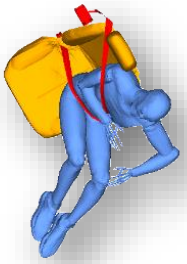	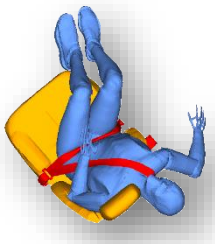

Table 14 Occupant kinematics for Case 1 and 2

A more detailed overview, containing more time steps, is given in Table 35 of Appendix 1.3. The occupant kinematics are completely different in both non-rotated and rotated configuration. The non-rotated seat configuration is predominantly a side crash loading scenario. The rotated seat configuration comes closer to a rear crash loading for the occupant, as was originally intended with this principle. However, a “standard support” by the back and the head rest is not given to the thorax and head due to the sideward movement of the occupant (occupant rotation lagging behind seat rotation) respectively and some more pre-crash time is required to reposition the occupant.

Injury Risk Evaluation

1. Head: The risk for head respectively brain injury (DAI - Diffuse Axonal Injury) is evaluated with the SUFEHM IRA tool and illustrated in Figure 34 and Figure 35. Due to the fact that there is no head contact with the surrounding parts, a low injury risk is observed in both cases.

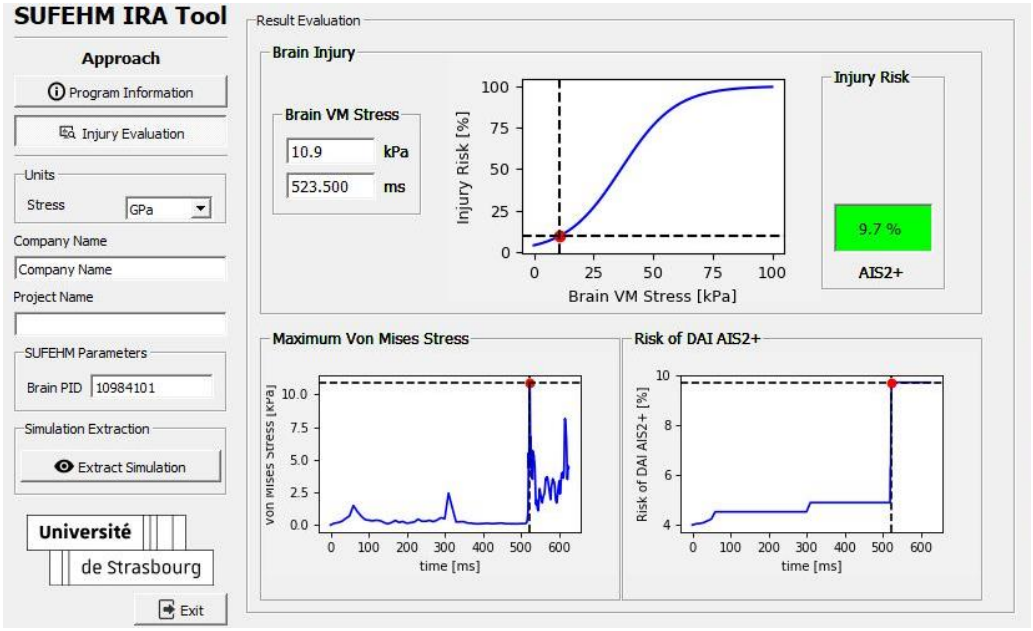

Figure 34 Case 1: Head injury risk (9.7%)

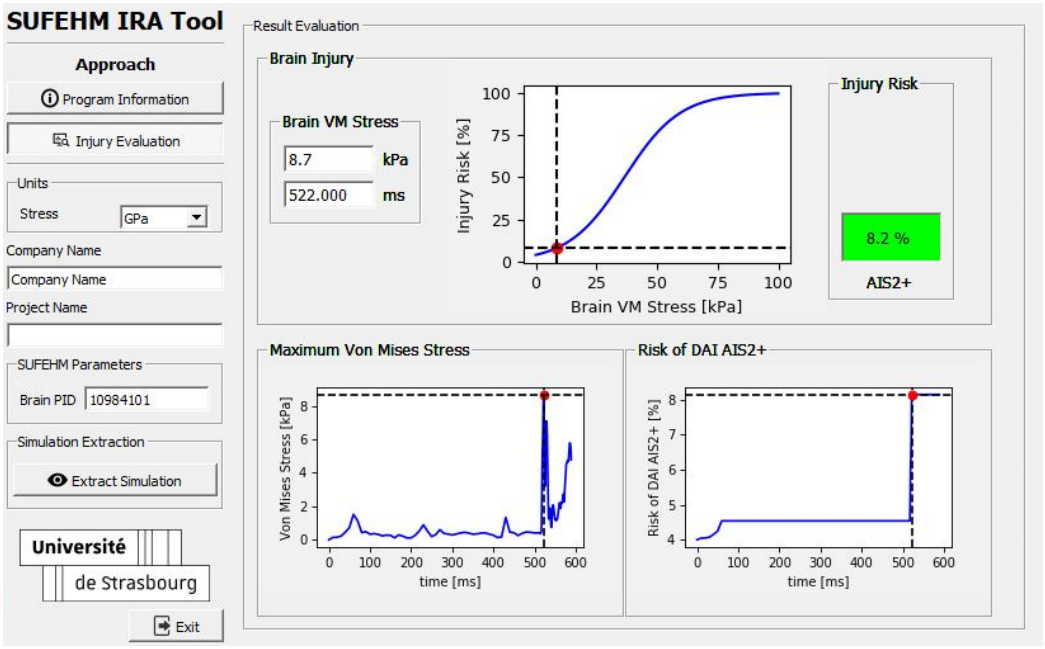

Figure 35 Case 2: Head injury risk (8.2%)

2. Neck Injury: The neck injury risk is illustrated in Figure 36 and was developed in WP3 by University of Strasbourg. A high risk of whiplash injury (force based as well as moment based) is predicted for both configurations, without and with rotation. Neck shear forces are observed to increase significantly after 18 ms from the crash pulse onset due to ramping of the thorax on the seat back, leading the neck to experience a momentary jerk due to contact with the headrest. However, it is observed that rotation of the seat does not offer any benefit to the neck complex as the head grazes away and support provided by the headrest is lost in both cases. Nevertheless, from the kinematics of case 2 one can draw the conclusion that with slightly improved seat and headrest design, support for head and neck is possible.

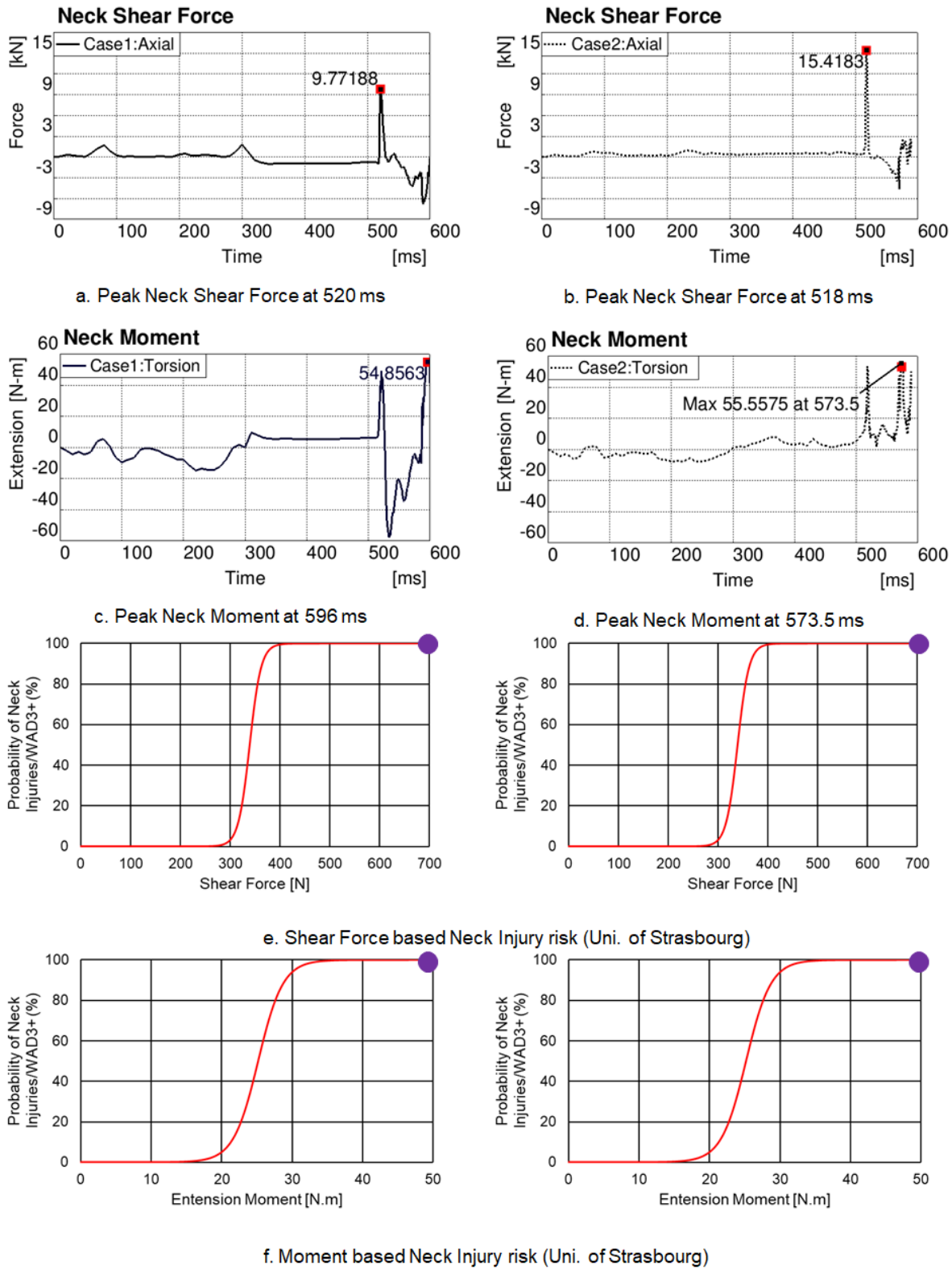

Figure 36 Neck injury risk

3. Thorax: Rib fracture risk is evaluated as per reference [43] using the Dynasaur tool. Multiple fractured ribs were recorded in both cases and illustrated in Figure 37 for different AIS levels. The number of fractured ribs for the non-rotated case are lower than for the rotated seat configuration. The rib fracture risk arises due to the contact of the thoracic region with the backrest structure, due to complete compression of the backrest foam of the generic seat.

The rib fracture risk is higher in the rotated seat configuration due to a higher engagement of the thorax with the backrest.

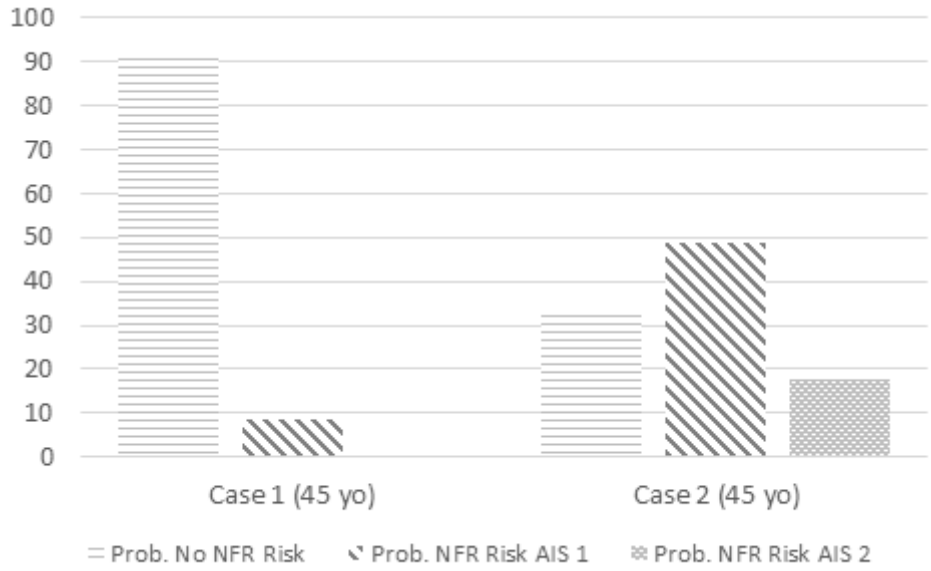

Figure 37 Rib fracture risk

In summary, the benefit of a rotated seat is not clearly established for the SCP06 collision scenario and rearward facing occupants. However, the seat design currently is one of the major limitations of this study. As already discussed above, a more realistic seat structure and raised side bolsters at backrest and head rest would definitely improve the effectiveness of an occupant rotation towards PDOF respectively of such a protection principle.

3.1.3.9 Seat rotation in oblique crash scenario

In the documentation of Bosch's pre-study on the pre-crash rotation of the seat in Chapter 3.1.3.3 the seat rotation from an initial inwardly-rotated seat towards a standard seating position of 0°, followed by a full frontal crash has been analysed. The aim of the pre-study was to rotate the occupant in a full-frontal crash towards the principal direction of force (PDOF), which also matches the driving direction. In oblique crash situations a rotation toward the standard seat position may not be the most favourable option. Therefore, another study has been carried out by Bosch where the effect is investigated for the case that the occupant is rotated towards the direction where the restraint systems like belt and passenger airbag have their best restraining efficiency.

As outcome from prospective accident research analyses reported in deliverable D1.1 [28], a high share of urban cases where the PDOF does not match the driving direction, may still occur with HAVs in intersection scenarios. What does this mean for Protection Principle 1? What would a strategy look like in an oblique crash scenario where the vehicle acceleration is equally high in the x- and y-directions, and thus the PDOF does not match the driving direction?

For the following simulation study, the "straight crossing path" no. 6 (SCP06) crash pulse has been applied and the Simcenter Madymo AHM was used. It was reported in deliverable D1.3 [6] and is also shown in Figure 38. The characteristic of this pulse is a high deceleration in x- as well as y-direction (Figure 38, middle) which also results in a significant vehicle rotation (angular velocity) around the z-axis (Figure 38, right). The key idea of this study is to rotate the occupant from an initial seating position of 0° towards an unknown angle which would match the PDOF of the SCP06 crash as shown in Figure 38 (left).

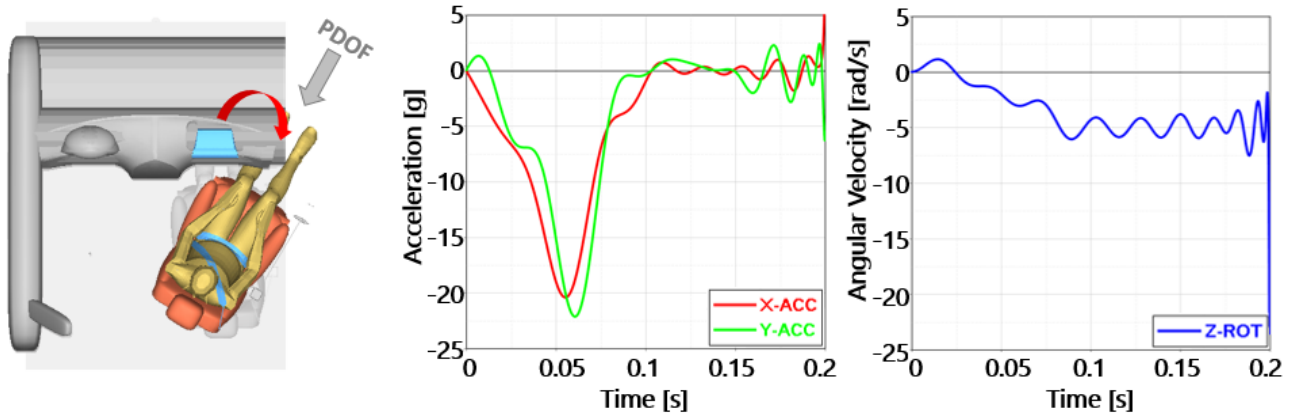

Figure 38 Occupant rotation from initial standard seating position of 0° to PDOF

As outcome of Chapter 3.1.3.3 an optimal rotation velocity (for coupling of the occupant to the seat rotation while minimising the seat belt to neck risk) is known. Thus, this effect on the occupant is assumed to be known and only the in-crash phase will be considered in this study. The occupant will be rotated prior to the crash to a certain angle of 1° to 90° from the standard position. Furthermore, the assumption has been made that the occupant seat position and vehicle interior could provide enough space such that a seat rotation (e.g. 90°) becomes possible. Therefore, the contacts between the occupant and the door, the IP structure and the passenger airbag are deactivated. The remaining applicable restraint system in the crash phase is the 3-point belt which is triggered at T = 10 ms after the crash starts and is applied for all seat rotation angles between 1° and 90°.

As an example in Table 15, the occupant motion for rotation angles of 17°, 37° and 53° at two different points in time during the in-crash phase (0.07s and 0.14s) are displayed.

Time (s)	Design 2 Seat Angle 17°	Design 28 Seat Angle 37°	Design 7 Seat Angle 53°
0.07	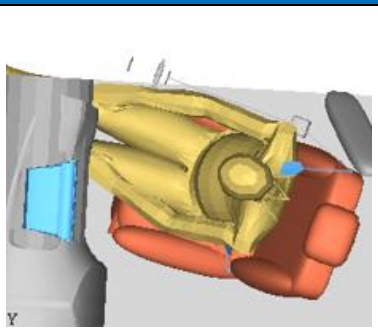	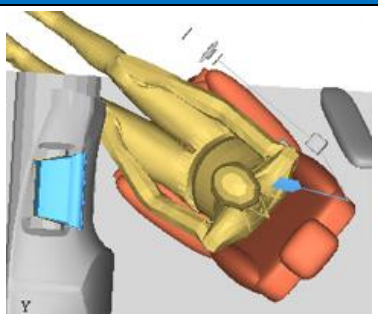	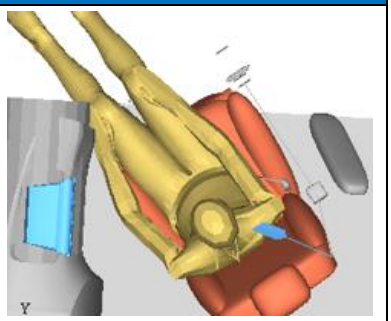
0.14	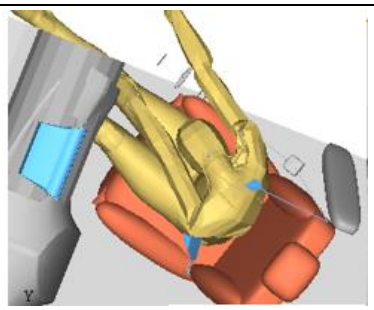	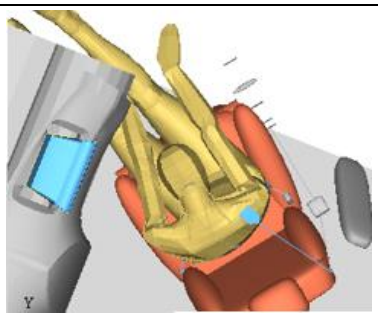	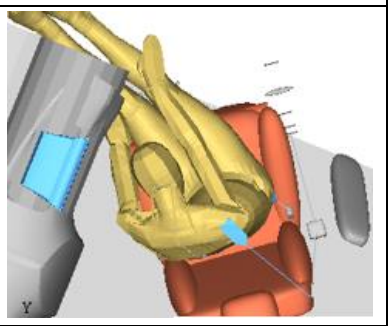

Table 15 Occupant motion in a SCP crash configuration for three different initial rotation angles

For the evaluation of the “correct” angle (should correspond to the angle of PDOF) towards which the seat should be rotated in case of the SCP06 crash, one should first compare whether the occupant is aligned with the seat structure and thus the occupant experiences a frontal loading. In case of the seat rotation by 17° (Table 15, left) it is visible that the occupant pelvis area pushes against the seat structure on the side facing the crash direction. Also, a significant interaction between the shoulder belt and the neck occurs which is especially visible at 0.14s of the crash. These observations suggest that the rotation angle of 17° is too low and that the occupant must be rotated further than 17°.

If the seat is rotated by 53° (Table 15, right) the occupant is pushing against the seat side structure on the opposite side. It is also visible that the shoulder belt is slipping off the shoulder. That would mean the rotation by 53° is too high. The perfect choice in this case is a rotation angle of 37°. Here the occupant is ideally aligned with the seat (occupant is moving parallel to the seat). Thus, no contact with the seat side structure occurs which results in a fully frontal loading of the occupant and the seat belt can restrain the occupant in an optimal manner.

Results of the first DoE in Figure 39 for a seat rotation angle from 1° to 90° (seat base angle) indicate that from a certain outwards rotation onwards for example 35° the head, thorax and pelvis resultant acceleration can significantly be reduced. The bar chart in Figure 39 (right) shows the possible acceleration reduction for head, thorax and pelvis when 1° and 37° seat rotation is compared. From this chart it becomes clear that a reduction of pelvis acceleration of approximately 30% is feasible, if a 37° instead of 1° seat rotation is considered. The reason for such a high reduction of pelvis acceleration might be the avoidance of contact between pelvis and upper legs with the seat side structure.

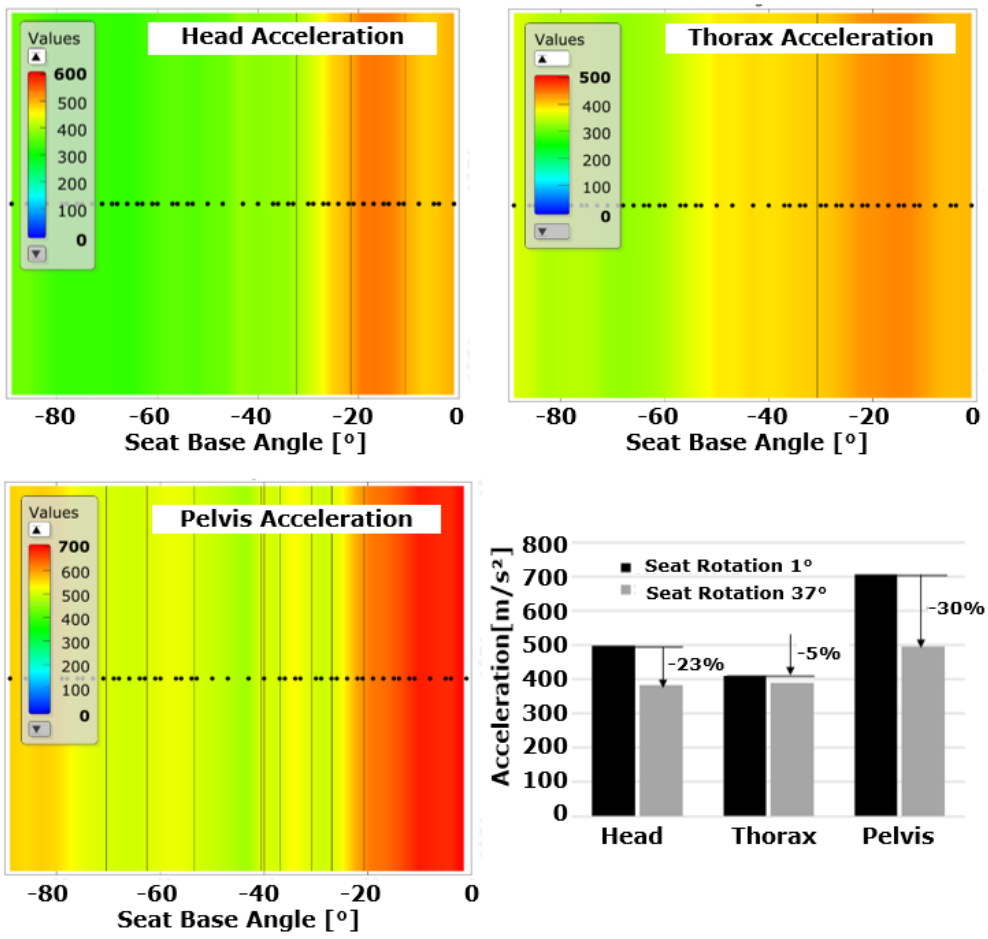

Figure 39 Resultant acceleration for head, thorax & pelvis for rotation angles between 1° to 90°

Furthermore, the interaction between shoulder belt and neck can be reduced or avoided if the seat is rotated further than 35°, compare Figure 40. As defined in the methodological introduction a measuring tool representing a dedicated injury predictor was introduced to detect the local penetration of the belt into the neck surface in [m]. In this case, the 35° angle corresponds to the lower limit from which onwards no neck interaction with the belt would occur. The upper limit for the seat rotation angle is defined through the effect when the shoulder belt slips off the shoulder as indicated in Table 15 for the seat rotation angle of 53°. Since there is no quantitative measure for the belt slipping off the shoulder, the graphs in Figure 39 and Figure 40 show only the lower limit.

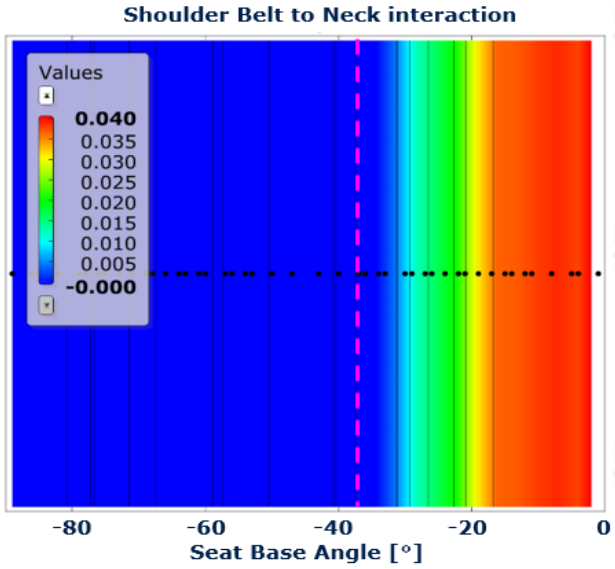

Figure 40 Shoulder belt to neck interaction when occupant is rotated towards PDOF

In deliverable D1.1 [28], collisions between two cars at an intersection were analysed in detail. Three relevant intersection scenarios were identified and characterised by different parameters like velocity, impact angle etc.: Straight Crossing Path (SCP), Left Turn Across Path - Lateral Direction (LTAP-LD) and Left Turn Across Path - Opposite Direction (LTAP-OD). Three different SCP pulses SCP02, SCP04 and SCP06 were selected for further application. In the first DoE, only the SCP06 crash pulse (pulse with highest lateral acceleration contribution) was analysed and focus was on the seat rotation angle towards the PDOF. Two additional velocity configurations have been outlined for the straight crossing path crash configuration in this study: SCP02 with 74 km/h / 33 km/h (Host/Opponent) and SCP04 with 37 km/h / 68 km/h (Host/Opponent), see Figure 41 left and middle graph. So, how significant is the change of the seat rotation angle towards which the seat should be rotated, if the crash configuration remains the same but not the crash velocity?

In the second DoE the seat rotation angle was again varied from 1° to 90° but, in addition to the first DoE, for all three reported SCP crash pulses. The graph in Figure 41 (right) shows the belt to neck interaction for the crash pulses SCP02 / 04 / 06 in relation to the seat rotation angle from 1° to 90°. The figure illustrates that with a lower limit for the seat rotation angle (seat rotation should be higher than the lower limit) and depending on the crash velocity the “correct” angle for the seat rotation also changes, e.g. for SCP04 the seat rotation angle must be higher than 40° and for SCP02 higher than 20°. The SCP06 is somewhere between SCP02 and SCP04.

From the pre-study results reported in Chapter 3.1.3.3 it is known that an angular deviation from the PDOF by 7°/13° for the case with and without pre-crash braking is possible without decreasing the level of occupant safety. The mentioned angular deviation represents the delta between effective PDOF vs. achieved seat rotation during pre-crash phase. Overall, for the SCP crash pulses this means there is not a single “correct” and stable PDOF angle to be applied, but rather a range of

optimal angles towards which the seat and thus the occupant should be rotated. This range of angles is limited by a lower angle which indicates the shoulder belt-to-neck interaction, and an upper angle which leads to belt slipping off the shoulder.

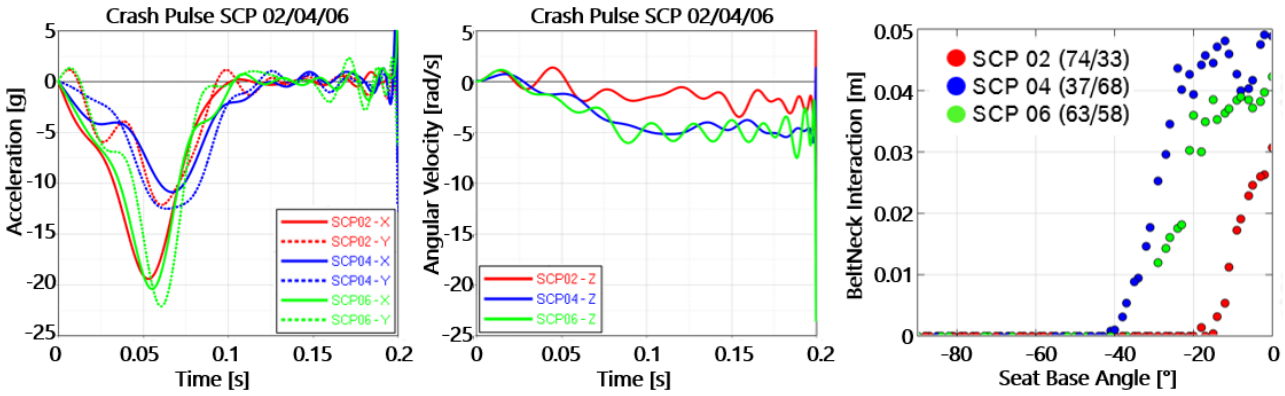

Figure 41 Vehicle acceleration pulse SCP02 / 04 / 06 & shoulder belt to neck interaction

Although the target angle for the seat rotation is not a single number but rather a range, the question is: What are the relevant impact factors for this range? It can be assumed that future HAV vehicles will have a set of environmental sensing equipment to scan the situation in front, behind and to the side of the vehicle. For example, it is expected that camera, radar and LIDAR-based systems will be on-board to enable a safe SAE L4 driving mode. A typical pre-crash restraint actuation logic would imply that based on the sensor equipment of the dedicated HAV the PDOF must be estimated during the pre-crash phase and accommodated, e.g. the seat or passive safety ECU to activate the seat rotation during the pre-crash phase.

In this chapter, only the seat rotation towards the PDOF with the occupant facing forward in the direction of the crash has been analysed. An additional strategy could be to rotate the occupant away from the crash so that the occupant is pushed into the seat, effectively and primarily using the seat as restraint system. However, in this case the seat structure and setup must be optimised adequately. Whether the occupant is rotated towards the crash or away from the crash mainly depends on how much time during the pre-crash phase is available (including sensor setup, performance, latencies, etc.), which of the two positions could be reached faster and of course the available space within the vehicle.

3.1.3.10 Pre-pretensioning effects during pre-crash rotation

This study performed at ZF is based on the pre-study from Bosch as described in Chapter 3.1.3.3. This implies that interior definitions, especially the initial seat rotation angle, the seat rotation velocity and the location of the pivot as well as other mechanical model parameters like friction values, contact definitions and belt routing have been used accordingly. For this study occupant positions 3 and 4 are used, see deliverable D2.1 [2]. As the second seat row is further away from the IP, no steering wheel or airbag are considered.

Focus and research question

This study focuses on the electric seatbelt pre-pretensioner (PPT) attached to the retractor. This is a reversible intervention, i.e. the belt force is low enough to not harm the occupant and in case no crash will happen the webbing can be released again. This device can be activated during pre-crash phase, if reasonable evidence is given for a critical impact (crash) to come. Reasonable evidence in this context means that the criticality or confidence level for triggering the reversible PPT shall be

lower than the one for triggering the seat rotation. Hence, the triggering of both elements can be seen as independent for this study.

The Madymo model used for the pre-study reported in Chapter 3.1.3.3 includes a generic PPT definition. This generic model uses a simplified force-over-time characteristic with constant force, independent of the environment or reaction force. The real PPT technology is based on an electric drive unit (motor and gear box) coupled with the seat belt retractor. This mechatronic unit has to be seen as dynamical system of masses, springs and dampers, which will experience significant oscillations during highly dynamic actuation in pre-crash or crash. Therefore, a more realistic model should include the main physical effects like inertia of the moving masses, internal friction and the webbing on spool effect, to mention a few. Furthermore, realistic applications in vehicles need to respect limitations in motor torque / force for given electrical power limits.

For this study, a more realistic model representing real products widely used in today's vehicles globally is introduced. The parameters for this model have been derived from the ZF Active Control Retractor (ACR) as one representative product in the market. This ACR model includes all above-mentioned physical effects. Using the ACR model and comparing it with the generic PPT of the Madymo base model allows investigation of a more realistic approach on the pre-crash activated pre-pretensioning feature to analyse effectiveness and limitations in the application for the pre-crash seat rotation. No PPT activation is added as a reference configuration.

Parameter variation

For this study, reversible pre-pretensioning was only considered at the retractor. The triggering time and the power output (i.e. belt force) of the ACR model were varied and compared to the generic PPT definition identified as working best in the pre-study, see Chapter 3.1.3.3. Furthermore, two crash pulses (generic full-frontal and SCP06, see Figure 42) are used in this study to analyse the impact of different pre-pretensioning characteristics on the restraint function and HBM values. An overview of the simulation model set-up can be found in Table 16.

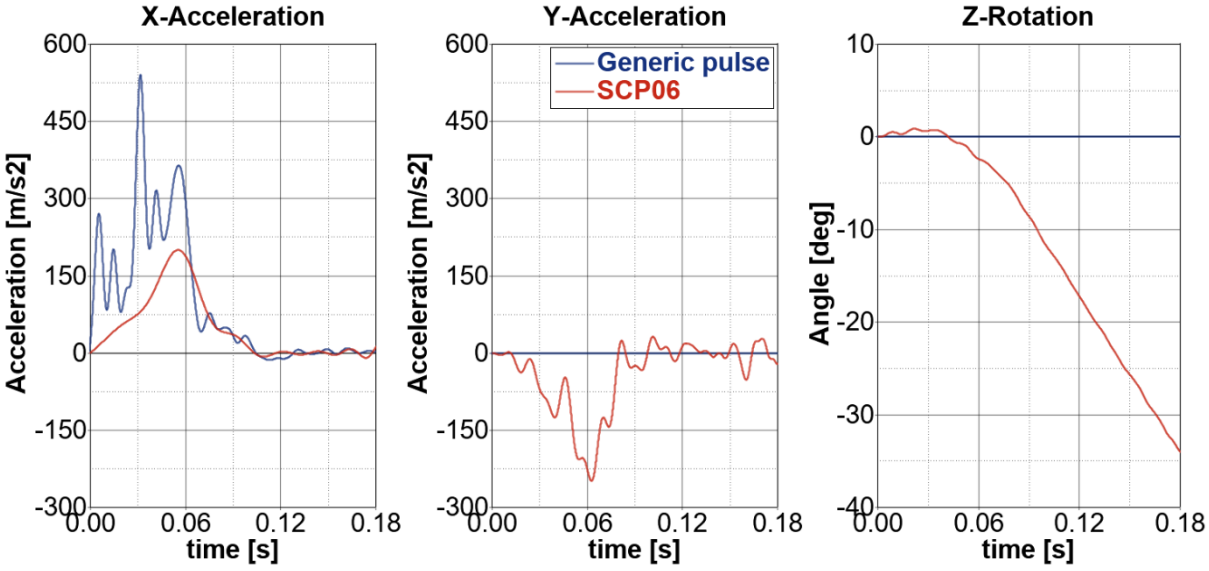

Figure 42 Acceleration of the generic full-frontal (blue) & SCP06 (red) crash pulses

Parameter	PP1
Occupant position	P3, P4
Pre-crash pulse **Crash pulse**	Figure 4 Madymo's generic 56 FF, SCP06

Initial z-seat orientation **Z-seat rotation** **Z-seat rotation start** **Seat rotation velocity**	30° Prescribed motion -200 ms See Figure 4
Initial seatback rotation **Seatback rotation velocity**	20° -
Occupant model type **Excitation**	AHM v3.1 Soft
Airbag	None
Pre-pretensioning at retractor **Seat belt system type**	None / gen. PPT / ACR Fully seat integrated
Retractor pyro pretensioner TTF	10 ms
Load limiter type **Shoulder force**	Constant 3 kN
Anchor pyro pretensioner **Anchor pyro pretensioner TTF**	None -
Buckle pyro pretensioner **Buckle pyro pretensioner TTF**	None -
Generic PPT TTF **ACR TTF**	200 ms -500, -400, -300 ms
Generic PPT belt force **ACR belt force**	250 N 175, 250, 425 N
Simulation solver	Madymo 7.8
OSCCAR model	Generic interior

Table 16 Simulation model set-up

Results

The results section is divided into three parts. The first compares the influence of the generic PPT to the more realistic ACR and no pre-pretensioning as reference for a given crash pulse. The second compares the pre-pretensioning effect for different pulses. The third part investigates how different power limits and hence belt force levels of the ACR influence the pre-crash rotation motion.

1. The generic PPT definition results in a belt force of 250 N, see Figure 9. The pre-study concluded that it is recommended to trigger the generic PPT at the same time as the beginning of the rotation of the seat at -200 ms, see dark red in Figure 43 left. The ACR model includes physical effects like internal friction and inertia and therefore shows some delay after triggering, before a relevant belt force can be experienced at the webbing outside the retractor, see blue lines in Figure 43 left.

   In this system environment, the belt pull-in starts ~100 ms after triggering. Therefore, in order to achieve similar effects, the ACR needs to be activated at -300 ms to achieve the same negative belt outlet (means belt pull-in) as the generic PPT triggered at -200 ms, see Figure 43 right. Belt force and belt outlet are measured just above the retractor.

   Analysing the belt force curves of generic PPT and ACR in more detail, the model follows exactly on the prescribed force characteristics given for the generic PPT whereas the ACR curves describe an oscillating system. After triggering significant internal inertia and film spool, the retractor has to be accelerated, before the webbing outside the retractor can experience a force. After initial acceleration of the inertia and after reaching the peak torque

of the motor the masses continue to move and further increase tension on the webbing, a kind of “overshoot” can be observed. Webbing elasticity allows continued belt pull-in even when the force drops below 250 N. The oscillation settles down on a level of 250 N, before at around -50 ms the seat has reached its final position and therefore the occupant continues moving relative to the seat due to inertia. Diagrams in Figure 43 are taken from simulations for positions P4, i.e. continued occupant movement after the seat has stopped rotation releases belt tension and therefore belt force for the ACR drops below 250 N after -50 ms.

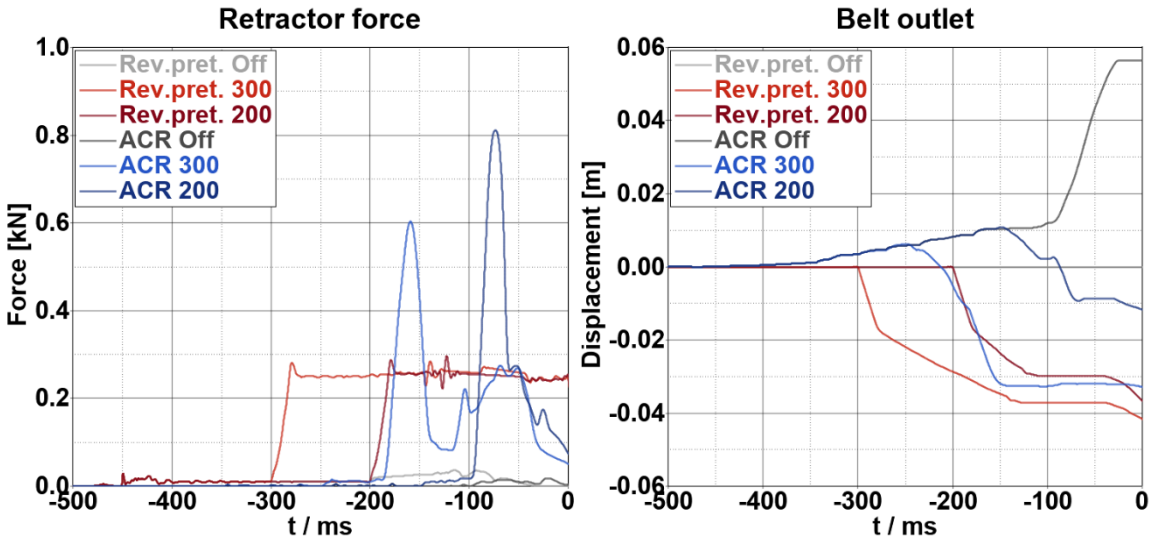

Figure 43 No-PPT (grey), PPT (red) & ACR (blue), belt force (left) and belt outlet over time

Using -300 ms for the ACR and -200 ms for the generic PPT and a nominal belt force of 250 N, both pre-pretensioners support the pre-crash rotation in the same way. The best improvement for the occupant-seat coupling effect is achieved for the shoulder and knee movement, as characterized by the relative angles introduced in Figure 5. Figure 44 shows the resulting relative shoulder angles β2 for the different pre-pretensioning parameters.

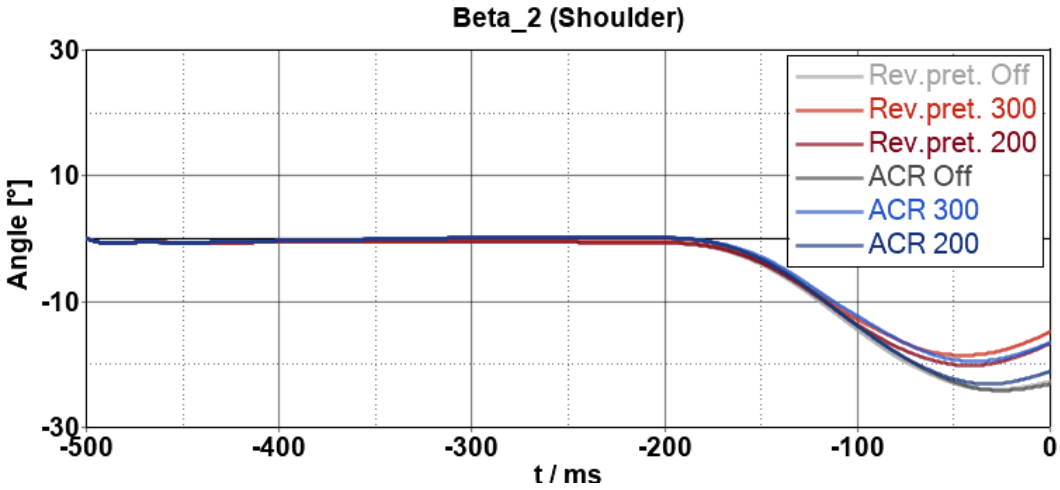

Figure 44 Relative shoulder angles β2 for different pre-pretensioners

For ACR triggered at -300 ms (light blue), a similar behaviour can be achieved as with generic PPT triggered at -200 ms (light red). But also, the pelvis-seat coupling can be

improved. Figure 45 shows the occupant position at t0 for no pre-pretensioner (grey) compared to PPT / ACR (gold).

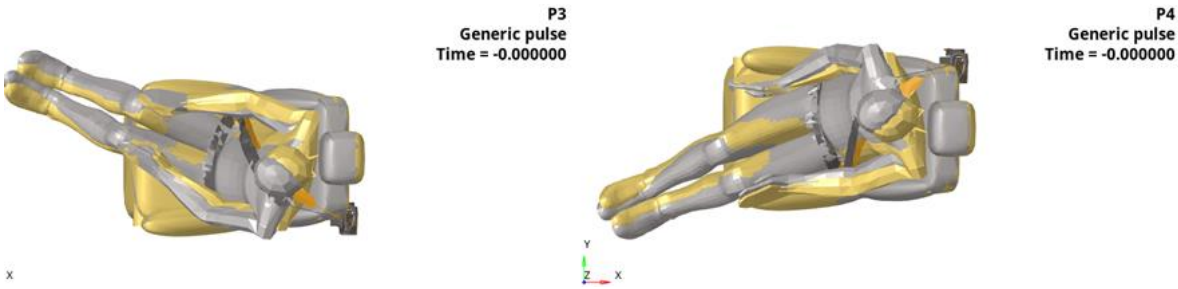

Figure 45 Occupant position at t0 for no pre-pretensioning (grey) compared to PPT / ACR (gold) for P3 (left) and P4 (right)

In the pre-crash phase, not more than 2 g accelerations are caused by combining active seat rotation, seat belt pre-pretensioning and pre-braking. This low acceleration value is in-line with other studies in this report and is considered to be of minor injury risk. However, for some simulation runs numerical effects during the settling phase of the occupant in the very early stage of the simulation were observed causing high acceleration peaks, see Figure 46. Those peaks have no physical meaning as they are numerically induced noise.

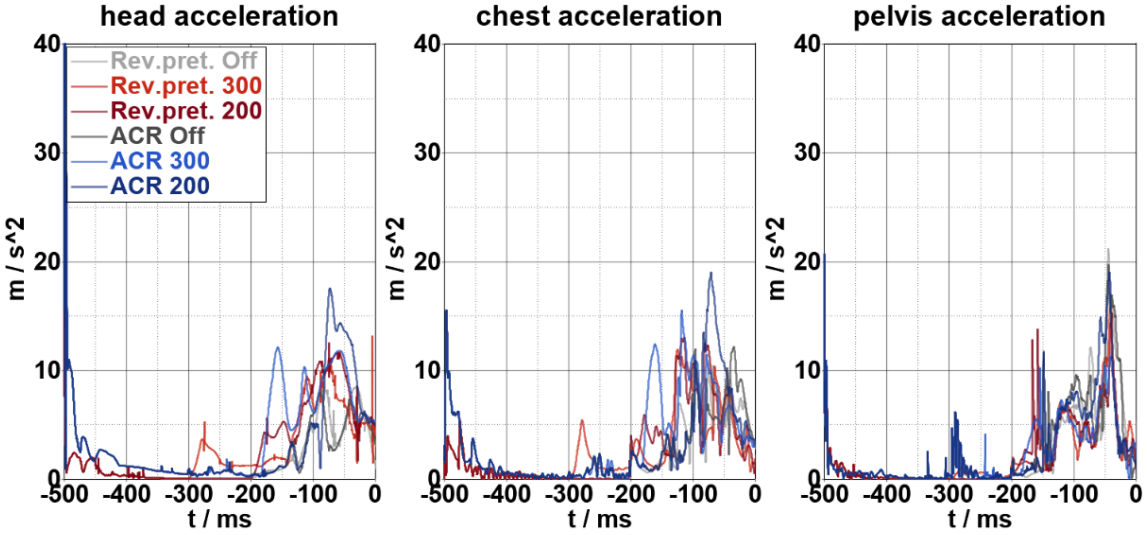

Figure 46 Resultant occupant accelerations during pre-crash seat rotation

When the ACR is triggered earlier than -300 ms, only minor additional gains can be achieved. This result confirms similar findings from the pre-study at Bosch, where TTF for the generic PPT was varied.

2. As can be seen in Figure 42, the two crash pulses are very different. The generic 56 km/h full-frontal pulse has very high x-component accelerations which result in a large forward displacement of the occupant. As there is no airbag in this conceptual restraint system study for rear seat occupants, the restraint function is not adequate for this high pulse. The resulting occupant accelerations are very high, and the kinematics do not look acceptable, see Figure 47, top row. To achieve adequate restraint performance an airbag solution would have to be added which was not part of this PP1. However, comparing the occupant kinematics with and without pre-pretensioning, less forward displacement for the head and upper body can be observed for the pre-pretensioning activation. This is a clear signal that

this additional seat belt technology can improve occupant restraint performance for pre-crash rotated seats, especially for more demanding crash pulses.

In case of SCP06, the occupant is pushed / rotated further into the seat which results in an intrinsically improved seat-occupant coupling. The x-component of the pulse is much weaker. Hence, the load case is less critical than the full-frontal pulse. It can be observed that for this lower pulse the effect of pre-pretensioning is significantly higher, especially in the leg / pelvis area. However, both cases with and without pre-pretensioning show acceptable low occupant accelerations for this moderate crash pulse.

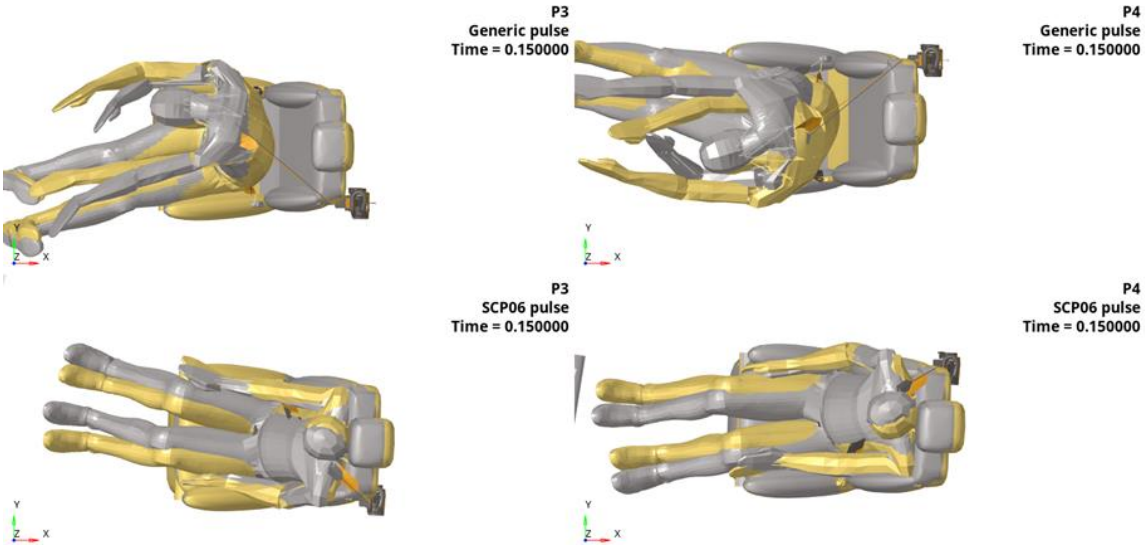

Figure 47 Occupant displacement at 150 ms for generic pulse (top) & SCP06 pulse (bottom), P3 (left) & P4 (right), no pre-pretensioning (grey) & PPT / ACR (gold)

3. Finally, the influence of a power limitation in the car which limits the maximum belt force for the ACR has been investigated. Higher power has two main effects: Firstly, it accelerates the initial motor turnings and hence can reduce the delay due to internal friction and inertia effects. Secondly, more power also increases the maximum belt force that can be achieved with electrical reversible seat belt pre-pretensioning. Comparing different input power parameters (see Table 16), higher power leads to improved β2 angles for the shoulder, see Figure 48.

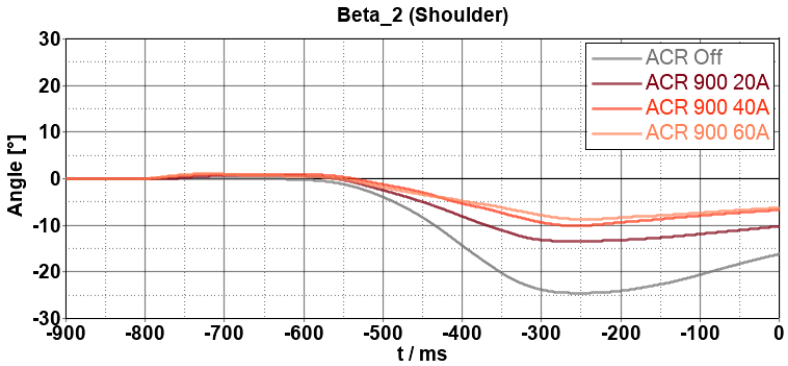

Figure 48 Relative shoulder angle β2 for different ACR power limits

Analyzing the date in more detail it can be concluded that the first effect (timing) is more relevant to the occupant coupling during the pre-crash seat rotation than higher nominal force. Increasing the power by 50% can reduce the initial time delay by almost 30%, i.e. 70-

80 ms earlier triggering for the ACR with 50% more power would be enough to achieve similar results compared to the generic PPT. Changing the final belt forces in the range from 175 N to 425 N only without changing the motor acceleration does not show significant effects. All these force levels are high enough to generate sufficient occupant-seat contact for the pre-crash seat rotation.

Discussion

To better understand the pre-pretensioning effect for PP1 a more realistic pre-pretensioner was introduced. This ACR model is based on existing production hardware in the automotive market. Considering more physical effects, this ACR model shows some initial delay after triggering before a significant belt force can be experienced outside of the retractor. Comparing the more realistic ACR model with the generic PPT model, very comparable results can be achieved if the activation time is adapted, i.e. 100 ms earlier. This finally confirms all findings in this report using the generic PPT. However, the activation time for a more realistic pre-pretensioner must be 100 ms earlier, which can be easily achieved in practical application since this is a reversible actuator.

Comparing pre-pretensioning for 30 ° inboard rotated occupants applying different crash pulses after the pre-crash seat rotation, it was observed that a seat belt-only restraint system cannot provide adequate protection for rear seat occupants in high crash pulses. Further restraint components must be included for those cases, e.g. airbags for rear seat occupants, which was not focus of this PP1 study. However, even for high crash pulses the effectiveness of pre-pretensioning in supporting the pre-crash seat rotation could be demonstrated leading to less forward displacement for head and upper body, due to better occupant position at t0.

Finally, investigating application-relevant power limitations for the electrical pre-pretensioner, a clear effect could be observed: more power leads to higher accelerations in the motor and hence reduced time delay on reaching effective belt forces after triggering. This timing effect reduces the necessary earlier activation for the ACR, which reduces the demand on the pre-crash sensing equipment. Resulting belt forces have not shown a significant effect for the analysed cases.

3.1.4 Conclusion

OSCCAR’s overall research question addresses whether the available HBMs are capable of representing the challenges of new interiors, and what refinements are needed in order to capture important interactions enabling the development of protection principles. In the case of Protection Principle 1 the main research questions refer to the influence on the occupant kinematics and occupant safety of a pre-crash rotated seat, whether the active pre-crash rotation of the occupant leads to additional minor injury risks and how this injury risk can be assessed. With the principle of pre-rotated seats, the occupant could be repositioned from an actual seating position to a position which is considered to be safer based on the crash configuration and available restraint systems. In all Protection Principle 1 (PP1) studies the “principal direction of force” (PDOF) is considered as the preferable direction towards which the seat should be rotated if possible.

Baseline studies performed by partners have shown that if the occupant remains in the original (rotated) position the resulting injury risk of the occupant may increase. The in-depth studies by the partners reveal the challenges of pre-rotated seats in view of occupant injury assessment (if applicable) and chances of rotating the seat prior to the crash. Depending on the belt anchor point position (seat integrated left or right) a high interaction intensity between the seat belt and occupant was identified (compare Chapters 3.1.3.3, 3.1.3.5) leading also to higher neck forces (compare Chapter 3.1.3.5) as well as the belt slipping from the shoulder (compare Chapter 3.1.3.4). Furthermore, if the occupant remains in a rotated position (not in direction of PDOF) additional injuries could arise due to the interaction between occupants and e.g. seat buckle, seat back

(compare Chapter 3.1.3.8) or seat side support (compare Chapter 3.1.3.9). During the in-crash phase the occupant may fail to contact the airbag in the centre portion (compare Chapters 3.1.3.4, 3.1.3.5) which is comparable to an out of position situation. However, the results from Chapter 3.1.3.3 suggest that a certain deviation (7 ° with parallel AEB activation and 13 ° w/o AEB) of the seat rotation from the optimum PDOF based seat rotation is tolerable and may not lead to additional injuries (statement only valid for inwards seat rotation). This finding is in agreement with a recent frontal ATD (Anthropomorphic Testing Device) based ADAC study [11], where a seat rotation deviation of ±15 ° is suggested as tolerable in a full frontal crash with 40 km/h without causing additional occupant injury risks.

For seat rotations with deviations higher than 15 ° from the PDOF additional countermeasures must be taken. From Chapter 3.1.3.3 to 3.1.3.10 the pre-rotated seat has been analysed for different seating and crash configurations to identify the significant parameters with respect to PP1 and its influence on the occupant kinematics and injury.

The main studies with focus on the highway case scenario were reported in Chapters 3.1.3.5, 3.1.3.6 and 3.1.3.7. Main studies on the urban scenario were documented in Chapters 3.1.3.8, 3.1.3.9 and 3.1.3.10.

Highway Cases

In the highway case (full frontal crash) the occupant is always rotated to the standard seating position of 0° where the airbag and belt have their best restraining efficiency. The rotation velocity of the seat has a major effect on the occupant rotation relative to the seat. If the occupant is rotated towards the belt, seat rotation velocities of < 85 °/s (without pre-crash braking) and <120 °/s (with pre-crash braking) should be applied with respect to belt-to-neck interaction during the in-crash phase (compare the pre-study results in Chapter 3.1.3.3). In the pre-crash phase belt to neck interaction was not visible in any of the studies, although the position of the belt on the shoulder changes during pre-crash action. If the occupant is rotated out of the belt (compare the pre-study results in Chapter 3.1.3.4) velocities <200 °/s (without AEB pre-crash action) and <300°/s (with AEB) can be applied to avoid the belt slipping from the shoulder during the pre-crash phase. However, during the in-crash phase the slipping of the belt cannot fully be avoided, even if the slowest seat rotation velocity is applied and realistic belt-to-occupant friction representation is applied. Results of studies in Chapter 3.1.3.3 and 3.1.3.6 have shown that occupant inertia can be used to further position / rotate the occupant. This applies even though the rotation of the seat has already stopped at start of the in-crash phase at T = 0 ms. However, a contradictory effect may arise, i.e. the occupant is rotated further than the desired position (beyond final seat position) during the in-crash phase.

In Chapter 3.1.3.6 it was shown that a higher (in z-direction) seat side support structure increases and thus improves the coupling between seat and occupant. This may yield smaller relative rotation between seat and occupant. Additional foot support as described in Chapter 3.1.3.6 may cause an over rotation of the occupant and thus should not be considered in PP1. The activation of belt pretensioning during the pre-crash phase with forces up to 250 N (compare Chapters 3.1.3.4, 3.1.3.5, 3.1.3.6, 3.1.3.10) also improves the coupling between occupant and seat. Further increase of the pretensioning force beyond 250 N leads to rather small improvements. If the generic OSCCAR belt model is considered, activation of the pre-pretensioning at the start of repositioning is sufficient. However, if a more “realistic” system is used, an activation of 100 ms prior to the start of repositioning is necessary (compare Chapter 3.1.3.10).

If the parameters for the seat rotation are chosen appropriately the principle of rotating back a pre-rotated seat has the potential to reduce the occupant loading compared to the baseline situation (seat remains in rotated position inwards / outwards) in the in-crash phase. In this case the interaction with the belt can be reduced, the neck forces can be lowered and finally the head injury level can be kept at the same level. Nevertheless, the rotation of the seat leads to different occupant kinematics,

e.g. arm position (compare Chapter 3.1.3.5), and also to different belt routing. In case of the inwards rotated seat the belt is positioned higher at the thorax (after repositioning) and yields lower sternum loading but a higher rib fracture risk (compare Chapters 3.1.3.5, 3.1.3.6). The analysis of muscle injury risks during the pre-crash phase, based on the method developed by University of Stuttgart (compare Chapter 3.1.3.2), predicts no injuries at all. However, the reported method is still under development; it is highly dependent on the used muscle parameter and settings and thus only valid for the current modelling of the HBM muscles.

The comparison of different simulation codes and models for a dedicated highway use case scenario emphasises the applicability of the HBMs. Despite the different codes, occupant models and partly different model settings, the comparison of the simulation results showed an acceptable agreement. Thereby, the VPS and LS-Dyna models are more aligned than the Madymo model. Coming back to the research questions, the influence on the occupant kinematics and occupant safety through a pre-crash rotated seat could be analysed qualitatively well with the given HBMs. These findings increase the confidence in the models and thus in the simulation results. Whether the active pre-crash rotation of the occupant leads to additional minor injury risks needs to be analysed in more depth. The method for analysing muscle injuries during the pre-crash phase represents a good starting point. Further work on how the HBM settings and muscle representation influence the minor injury assessment is addressed in other research projects.

Urban Case

In the urban case, the occupant is rotated towards the PDOF, which in the given OSCCAR use cases does not match the driving direction. Studies in Chapter 3.1.3.8 and 3.1.3.9 show that depending on the seating configuration, two different seat rotation strategies can be applied: either with the occupant facing forward or rearward with respect to the PDOF. In the forward-facing case, the belt acts as primary restraint system, while in the rearward facing case the seat acts as primary restraining device.

In the forward-facing situation, i.e. in an oblique crash (SCP06), a rotation towards the PDOF generally decreases the occupant loads for head, thorax and pelvis (compare Chapter 3.1.3.9). The results for the rearward-facing case emphasise that the current seat shape and structure is not adequate to reduce the occupant loads sufficiently (compare Chapter 3.1.3.8). Furthermore, the kinematic data for this case shows that the occupants cannot properly follow the seat rotation since they are rotated against the PDOF. In this case, the vehicle deceleration pulls the lower leg towards the PDOF (against rotation direction) and thus the legs do not follow the seat rotation. However, a redesign of the seat including a rotating footrest as shown in Chapter 3.1.3.6, in combination with a pre-crash seat rotation, shows the potential to increase the level of occupant safety.

This study has shown that the leg rotation (around the z-axis) or the lack of it (if rotated against the braking / crash direction) has an influence on the rotation capability of the entire occupant. Thus, it can be assumed that different leg positions, e.g. crossed leg, could also influence the repositioning of the occupant. A variation of the crash velocity for the SCP crash case (compare Chapter 3.1.3.9) shows that the angle of PDOF towards which the occupant should be rotated changes and thus must be considered for the PP1 principle. It can be summarised that systems that aim to capture the functionality of Protection Principle 1, i.e. to rotate the seat prior to a crash to a more beneficial situation, may have a very beneficial effect on occupant safety in new interiors. In particular, for SAE L4 and L5 vehicles seats rotated by 10°, 15° or even 30° may become reality. It could be shown that HBMs will allow to create and assess pre-crash safety systems for future accidents. It is worth mentioning that these results are very helpful in designing pre-crash functions and the according logic within the safety control units of future vehicles, as well as creating an according layout of the safety system itself. Furthermore, these findings are very helpful for a requirement elicitation of electric drives for the pre-crash actuation of seats in new interiors.

Coming back to the research questions: the influence on the occupant kinematics and occupant safety through a pre-crash rotated seat could be analysed qualitatively well with the given HBMs. Whether the active pre-crash rotation of the occupant leads to additional minor injury risks was not analysed for the urban use case. However, further research is needed. Varying the occupants, i.e. variation in size, weight as well as gender dependent effects, needs to be considered. A further effect that was not considered here are different seating postures. A general limitation is the implemented restraint systems, e.g. airbag and seat belt. Generic models are used that were created for a typical L0 / L1 / L2 vehicle with a “classical” seat position and without consideration of a rotating seat. In future studies airbag models shall be used that are better adapted to the use case of a pre-crash rotating seat, e.g. offering a wider central region. The trigger time of the pre-crash system was not in focus here. However, this will play an important role in advance development studies. In particular, the impact of delayed triggering of the pre-crash actions is of interest.

3.2 Protection Principle 2 - Pre-Rotated Seat - Seat Inertia

This chapter summarises the results related to Protection Principle 2 (PP2), which were generated by ika and fka, supplemented by work from ZF (effects of seat belt pre-pretensioning). Some of the presented results and ideas were already documented and published in an earlier project state in the proceedings of the IRCOBI conference 2020 (see [26] for additional information).

3.2.1 Motivation and Background

PP2 addresses a rotated seating position in an automated driving vehicle, causing the occupant to face sideways (see Figure 49). This seating position could be introduced for better communication and relaxed seating in conventional interiors as well as spacious interior configurations of future vehicles.

Within rotated seating positions, the conventional restraint system which is developed for forward facing seating positions might not generate sufficient measures to safeguard the occupant during the crash. Due to the inwards rotated seat, neck-to-belt contact (outboard belt routing) increases during the crash phase in frontal crash scenarios [9] [10]. The unfavourable belt-to-neck interaction can increase the risk for blunt carotid artery injuries [27]. The interaction with the frontal airbag can also be difficult when the occupant is exposed to a crash in this unconventional seating position. A centralised airbag impact might no longer be a given when the occupant is sitting in a rotated position at the start of the crash. Therefore, a repositioning of the occupant to a conventional, forward facing position could be a beneficial measure in terms of occupant safety aspects.

Based on the outcomes of the ideation workshop, documented in Deliverable D2.3 “Selection of viable advanced passenger protection principles for further investigation” [4], PP2 describes an inertia based seat rotation prior to an unavoidable crash. The seat rotation and the associated occupant repositioning is only based on the inertia of the system, which is induced by pre-crash autonomous emergency braking (AEB) (see Figure 49). If a crash situation is detected, AEB is applied to the vehicle. When the occupant is sitting in a rotated seating position, facing away from the impact direction, the system, consisting of occupant and seat is released and can freely move around a previously-defined rotation axis. When the seat is rotated to a standard position the rotation axis will be locked, ensuring a state-of-the-art seating position and occupant interaction with the restraint systems.

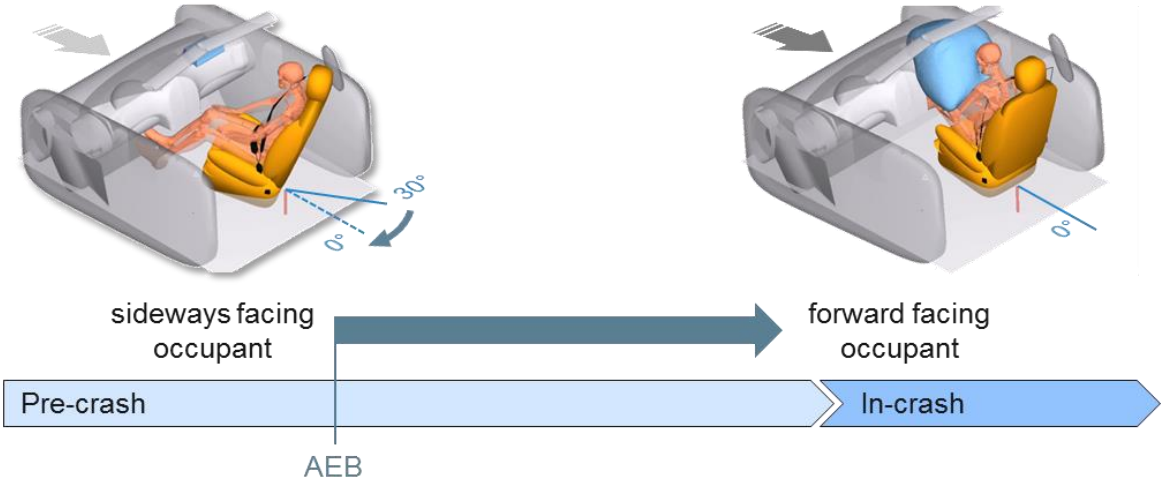

Figure 49 General mechanism & timing of Protection Principle 2 within passenger use case

3.2.2 Research Questions

Two main research questions were defined in terms of PP2. The first one is addressing the overall functionality of an inertia-based repositioning mechanism, whereas the second question refers to the effect on the occupant kinematics and safety during the pre-crash phase and at the time of the crash.

I. Can a pre-crash manoeuvre (AEB) be used to reposition the occupant and seat only due to inertia?

II. How does an inertia-driven rotation of the seat affect occupant position, loading and safety?

3.2.3 Simulation Studies

Within this section, the simulation studies of PP2 are presented. The documentation starts with a definition of boundary conditions and a description of the simulation model. These specifications apply to all presented studies in this chapter.

3.2.3.1 Boundary conditions and simulation model

The following simulation studies are investigating a standard interior model with an inwardly rotated passenger seat. The maximum rotation angle of the seat was limited to 30° from a package perspective. A frontal impact scenario is considered for the investigated use case and it is assumed that AEB always acts before the crash.

The simulations are performed using the multi-body solver Simcenter Madymo. The applied model is based on the OSCCAR Generic Interior Model (see [3] for a detailed description of the model). Only the frontal passenger as 50th-percentile male is investigated in the studies, which is represented by the Simcenter Madymo AHM v3.1. The mass of the occupant is 75.3 kg and the centre of gravity (COG), relative to a local coordinate system referenced to the seat's H-point, is measured at x = -0.0442 m and y = 0.0 m (see Figure 50). The passenger seat mass measures 31.4 kg, representing an average seat of a conventional vehicle. The COG of the seat is placed at x = 0.0752 m and y = 0.0 m relative to the local coordinate system in the H-point (see Figure 50).

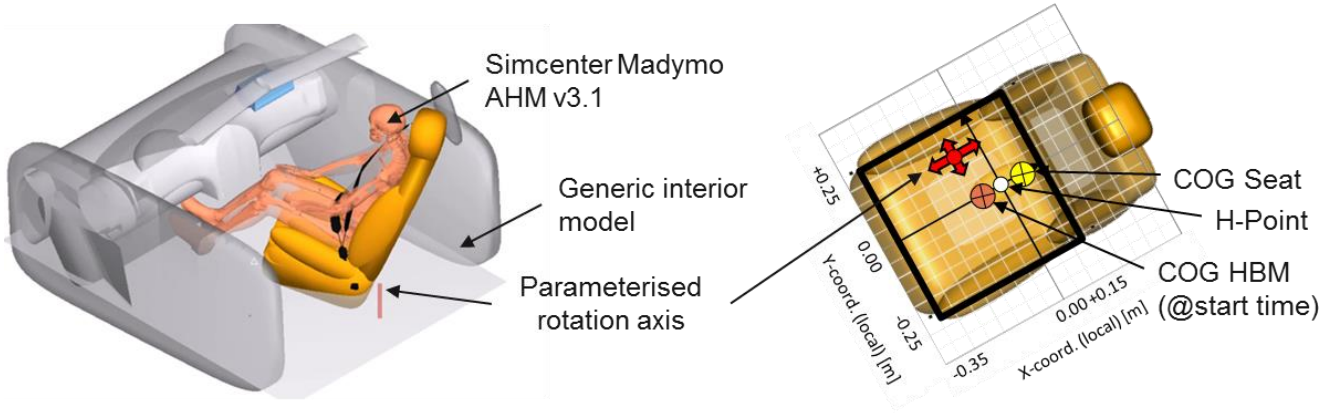

Figure 50 Simcenter Madymo generic interior model and definition of rotation axis & the system's centre of gravities

The applied model includes a restraint system, consisting of a passenger airbag (triggered 10 ms after the crash) and a three-point belt system. To ensure belt restraint during the seat rotation, the

belt system was modelled seat-integrated. The belt system includes a retractor load limiter, limiting the belt force to 2100 N, and a retractor pre-tensioner, which tensions the belt 10 ms after the crash with a load of 2500 N.

The default static and dynamic friction values in the model are set to 0.3 for the contacts between occupant and seat as well as occupant (shoes) and floor. For the contacts between occupant and airbag as well as occupant and seat belt, a friction coefficient of 0.2 is set.

To allow a rotation of the seat during the pre-crash phase, a mechanism to unlock and lock the seat z-rotation was introduced into the simulation model within the seat base joint. Locking and unlocking is defined via time and angular switches in Simcenter Madymo. Simultaneously with the start of the AEB application, the seat rotation axis is unlocked, and the start of seat rotation is initiated. When the seat has rotated to the final position (defined as 0° rotation angle, representing a standard, forward-facing seat orientation), the seat rotation ends and the rotation axis is locked (see Figure 51). The position of the rotation joint is parameterised and can be varied within the X-Y-plane of the seat base area (local y-coordinate: ±0.25 m and x-coordinate: -0.35 m to 0.15 m relative to the H-point of the seat) to investigate the effect of different rotation axis positions (see rotation axis representation in red in Figure 50).

The AEB pulse applied in the following studies was modelled as generic curve, starting at a maximum time of 1 s before the crash (see Figure 51). The corresponding acceleration level is ranging from 0.3 g to 0.8 g. The range of AEB levels represents different levels of brake force, from partial to full braking. Before the defined acceleration level is reached, a ramping function of 35 m/s³ is applied (according to the AEB definition in [11]). The curve presented in Figure 51 is transformed by spline interpolation in the simulation model, to ensure smooth transitions in the beginning and end of the ramping section.

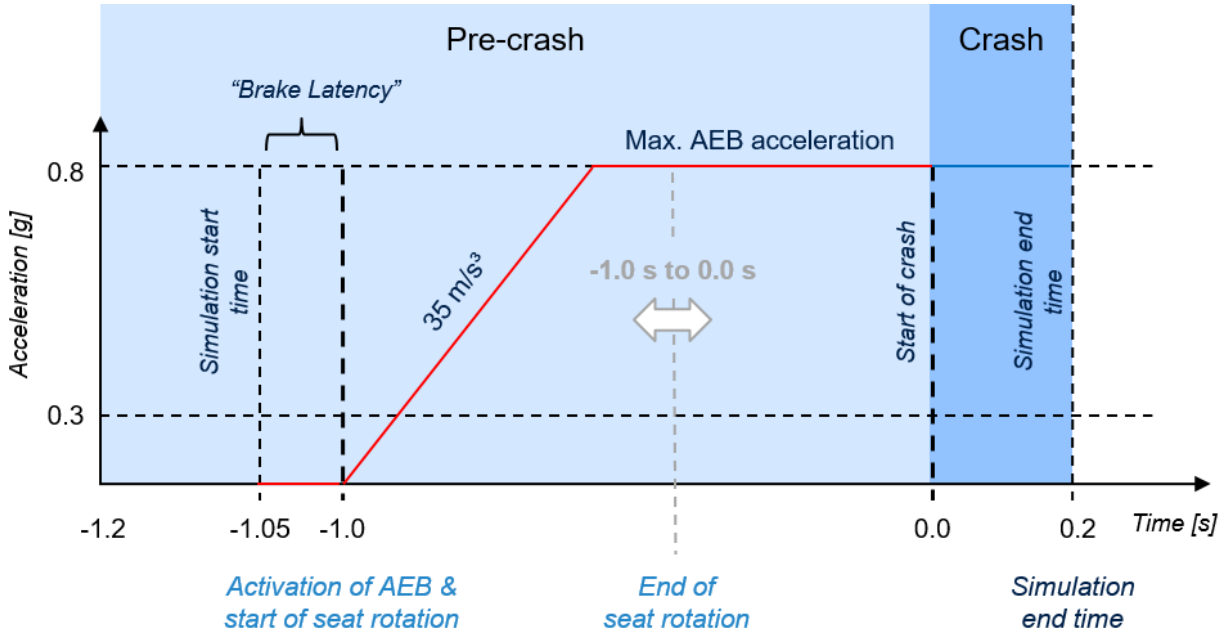

Figure 51 Definition of AEB pulse curve & timing of PP2 related seat rotation

3.2.3.2 Functionality and limitations of inertia-based repositioning

Within this section a study on the effects of different rotation axis positions as well as two AEB acceleration levels is presented. The objective of the study is to identify general limitations of PP2 and to give a first, broad overview on the application range of the principle.

Method

The rotation of the seat is caused by the mass inertia of the seat and the occupant under a braking acceleration. The rotation direction and velocity is generally defined by:

- **Position of rotation axis**
- Direction and **level of brake acceleration**
- Position of COG and mass of the occupant
- Position of COG and mass of the seat system
- Initial rotation angle of the seat
- Friction between system boundaries

In this first study the effects of the position of the rotation axis and the level of brake acceleration with respect to the necessary time frame to rotate the occupant from a rotated to a standard seating position before the crash are investigated. The direction of the AEB acceleration is assumed to be one-dimensional frontal (left and right wheels with the same brake force) and no steering during the brake / pre-crash phase. Dipping due to the vehicle front suspension is also neglected. The generic brake pulse is defined according to Figure 51. The position and mass of the occupant and the seat system are set according to the definitions in Chapter 3.2.3.1. Initially the passenger seat is rotated 30° inwards. Friction values are set to default values (see Chapter 3.2.3.1). The simulation model which was applied in this study is described in Chapter 3.2.3.1.

The x- and y-position of the rotation axis is varied within the seat base as it was defined in Figure 50 (right). The coordinates of the rotation axis are varied with a step size of 0.05 m, whereas the acceleration level of the AEB pulse is varied only on two levels (0.3 g and 0.8 g). A full factorial sampling was chosen to set up the study, creating a number of 242 simulation runs. The simulation results are displayed in colour plots using a radial basis function for approximation.

Study 1: (full factorial sampling)	
X-axis position (relative to H-point) [m]	-0.35 … 0.15 (delta = 0.05)
Y-axis position (relative to H-point) [m]	-0.25 … 0.25 (delta = 0.05)
Max. AEB acceleration [g]	0.3 | 0.8

Table 17 Study parameters & parameter step size (full factorial sampling)

Results

The occupant kinematics during the pre-crash repositioning are shown for two example simulation runs in Table 18. For both AEB levels, partial- (blue, 0.3 g) and full-braking (red, 0.8 g), the simulation steps are displayed in a 100 ms step size. The exemplary results are shown for a rotation axis position of x = 0.15 m and y = 0.25 m relative to the H-point. This axis has the highest average rotation velocity of all investigated rotation axis positions under the defined boundary conditions of the simulation study as well as the environment and is herein after referred to as R1.

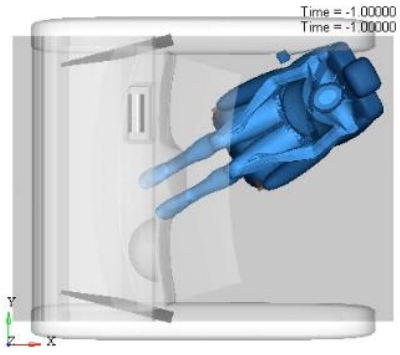 -1000 ms	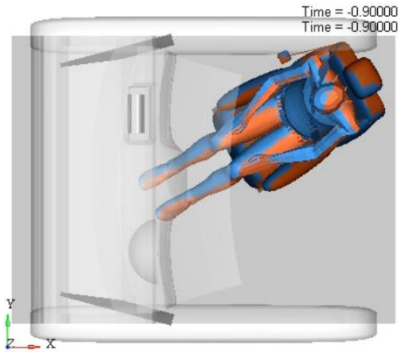 -900 ms	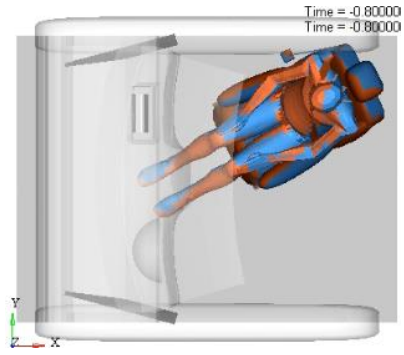 -800 ms
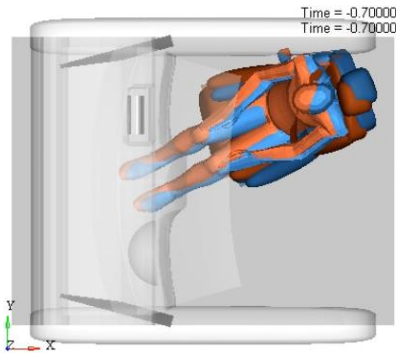 -700 ms	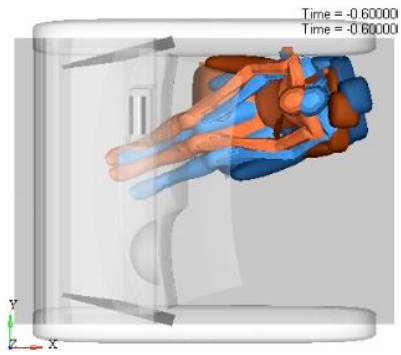 -600 ms	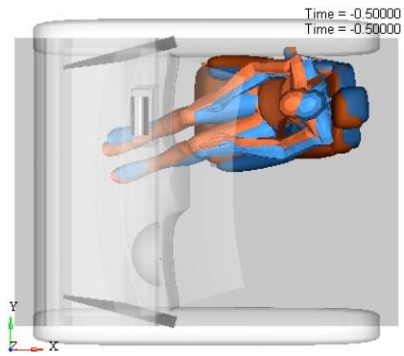 -500 ms
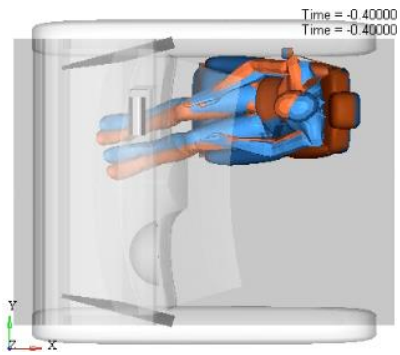 -400 ms	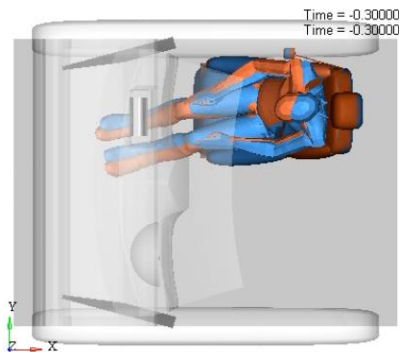 -300 ms	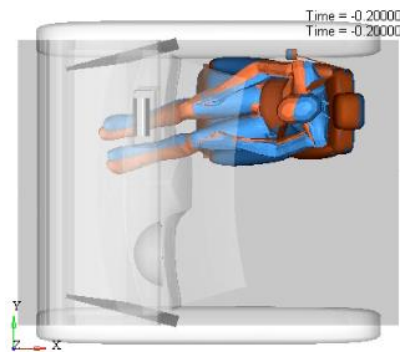 -200 ms
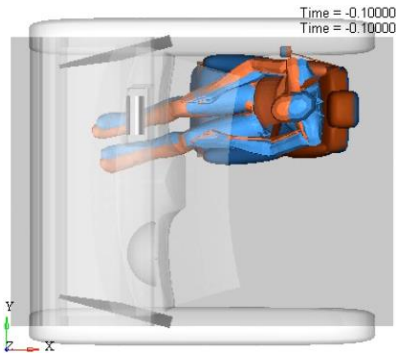 -100 ms	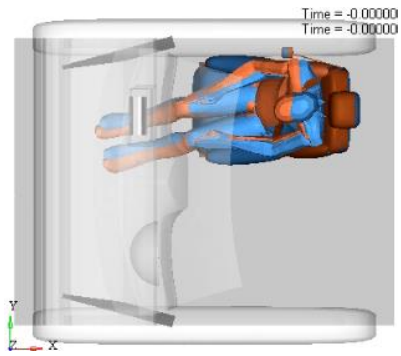 0 ms (start time of crash)	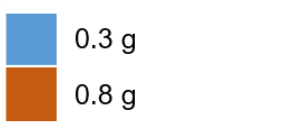 Max. AEB acceleration 0.3 g 0.8 g

Table 18 Occupant kinematics for R1 (blue: max. AEB acc. = 0.3 g; red: max. AEB acc. = 0.8 g)

In Table 18 the difference between the two investigated AEB levels can be seen exemplarily for R1. Differences in the occupant kinematics can be observed in the feet and the head position, which is due to the higher rotation velocity and the higher inertia of the head in the 0.8 g acceleration run. The higher AEB level leads to a higher forward head excursion during the repositioning, whereas the feet are rotated faster, but end up at a less rotated posture at the end of repositioning for the 0.8 g run. The final occupant positions of the 0.3 g and the 0.8 g run are reached at different simulation times and the position changes only marginally after the final position (0°) of the seat is reached. With 0.3 g acceleration level, the 0° position is reached at a simulation time of -450 ms and for 0.8 g the position is reached at -615 ms, leading to required rotation times of 550 ms and 385 ms measured from the beginning of the AEB application.

The measured rotation times for all investigated rotation axis positions are displayed in Figure 53 (0.3 g) and Figure 52 (0.8 g). The coordinates show results for different positions of the rotation axis in the X-Y-plane base area of the seat (see H-point at x = 0 m and y = 0 m). Only results that reach the 0° position within a 1200 ms time frame are shown in the two colour plots.

For a brake acceleration of 0.3 g, the time to rotate an occupant under the given boundary conditions ranges from 550 ms to 912 ms. The average rotational velocities for the 30° rotation are calculated at between 54.5 °/s and 32.9 °/s. The time to rotate an occupant from a 30° inwardly-rotated seat to a 0° seat orientation ranges from 385 ms to 901 ms when a brake acceleration of 0.8 g is applied (see Figure 53), leading to a range of average rotational velocities of 77.9 °/s to 33.3 °/s for the investigated positions of the rotation axis. The shortest rotation times (also the highest average rotational velocities) are measured at positions with the biggest distance to the system's COG (see Figure 52 and Figure 53), as large distances of the system mass to the rotation point increase the momentum of rotation.

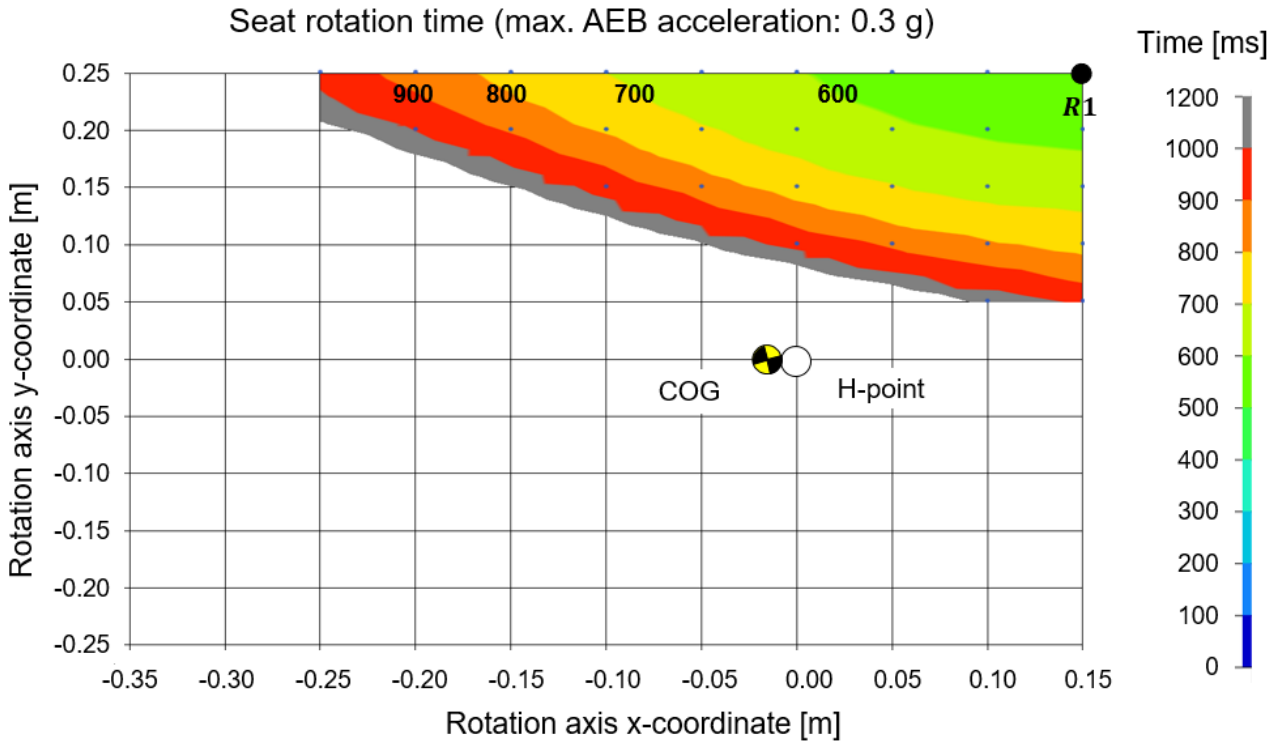

Figure 52 Rotation time (delta seat angle = 30°) for different rotation axis positions for 0.3 g AEB acceleration (fitting quality: R^2 = 0.99)

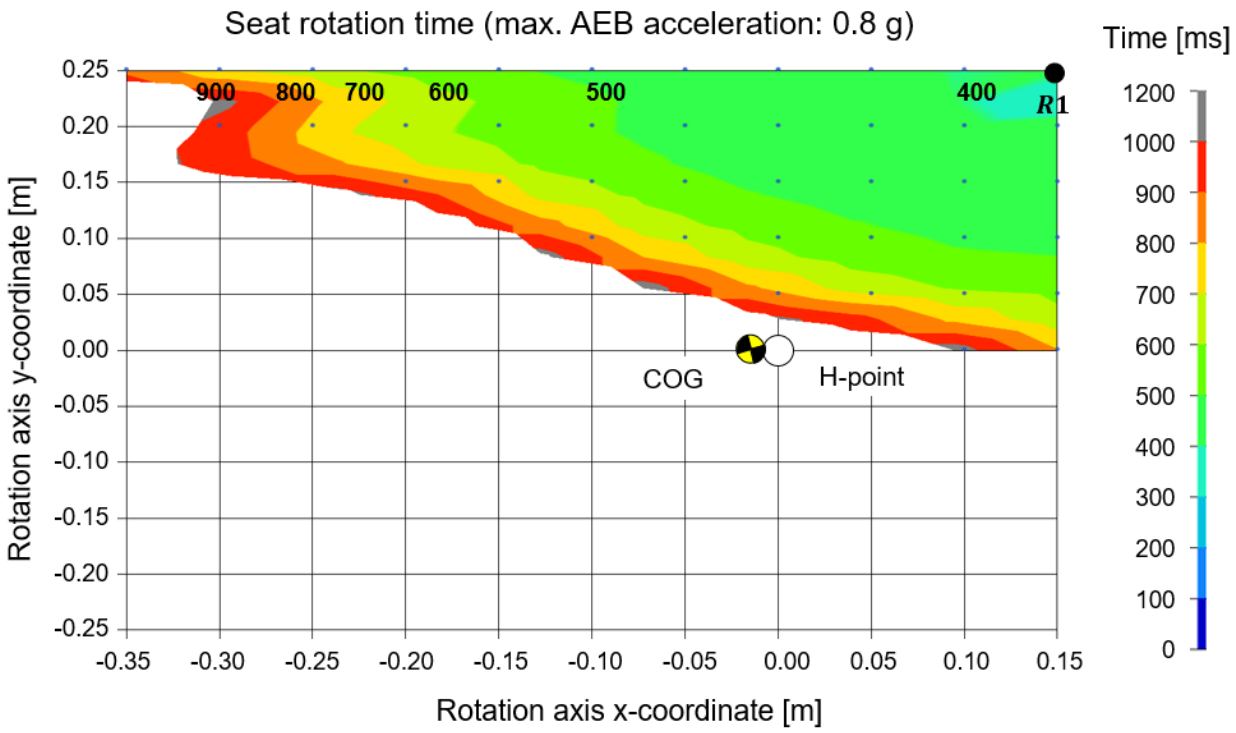

Figure 53 Rotation time (delta seat angle = 30°) for different rotation axis positions for 0.8 g AEB acceleration (fitting quality: R^2 = 0.95)

Discussion

Within this study, it was shown that an AEB based pre-crash rotation of a passenger seat is possible with different positions of the rotation axis. It may be noted that all results are limited to the investigated simulation environment and model settings.

The necessary time frames to rotate an initially 30° rotated seat to a “standard” rotation angle of 0° by inertia (AEB based) were identified for two AEB acceleration levels (0.3 g and 0.8 g). For full braking cases, the minimum required time frame for rotation is 385 ms. For partial braking cases, the minimum required time frame for rotation is 550 ms. Crash detection would be necessary at least within these time frames to rotate the seat during the pre-crash phase from a 30° rotated to a standard seat position. The position of the rotation axis and the level of AEB define the functionality of the principle and therefore limit the application range. A comparison of the colour surfaces of the two acceleration levels reveals a larger surface of the 0.8 g colour plot, showing that more rotation axis positions can be used with a higher AEB level.

The highest average rotation velocity that was generated by a 0.8 g brake acceleration of the seat was measured at 77.9 °/s. Compared to [11], where a vehicle seat is actively rotated during the pre-crash phase (all injury criteria are well below thresholds for a rotation velocity of 225 °/s), it can be assumed that the rotation itself will not harm the occupant in any way. In any case the difference in rotation velocity affects the final position of the occupant after repositioning; this needs further investigation, as a different occupant position at the beginning of the crash could affect the interaction between occupant and restraint system during the in-crash phase.

3.2.3.3 Effects of inertia-based seat rotation on the occupant repositioning

Within this study the effect of several AEB levels, friction, human body model muscle activation and a pre-crash belt tensioner on the rotation time of PP2 and the relative angle between occupant and

seat is investigated. The objective of the study is to highlight the effect of the investigated parameters on the functionality of the principle and the effectiveness of repositioning for one specific rotation axis position.

Method

The study parameters of the following investigations are presented in Table 19. Apart from the study-related parameter settings, all definitions and simulation model specifications within the study are according to Chapter 3.1.3.1.

For this study, a fixed rotation axis position R1 (x = 0.15 m, y = 0.25 m) is sampled with different parameters. The variation of friction coefficients is done in the contact definition for static as well as dynamic contact friction settings of the respective parts of the simulation model. For the applied occupant model, two different levels of muscle activation are simulated, aware (braced) and unaware (relaxed). The settings are chosen according to reference [29] for the activated spine and neck model. Optionally, a generic pre-pretensioner (PPT), which applies 250 N to the belt during the pre-crash phase, is triggered. The system is triggered at the start of braking.

Study 2: (R1 sampled with parameters)	
Rotation axis position [m]	R1 (x = 0.15 m, y = 0.25 m)
Max. AEB acceleration [g]	0.3 … **0.8** (delta = 0.05)
Friction floor-occupant [coeff.]	0.01 | **0.3** | 0.5
Friction occupant-Seat [coeff.]	0.1 | **0.3** | 0.5
Muscle activation [-]	**aware (braced)** | unaware (relaxed)
Belt pre-pretensioner load [N]	**0 (inactive)** | 250 (active)

Table 19 Study parameters & step size (R1 sampled with different parameter settings, default values in bold)

To measure the effectiveness of repositioning, the relative angles between occupant and seat are tracked during the simulation runs. The angles for head, shoulders, pelvis and knees are defined according to PP1 and Chapter 3.1.3.1.

Results

In the previous chapter the effect of two AEB levels (partial and full) on the rotation time for several rotation axis positions was investigated (see Chapter 3.2.3.2). To create a full picture for one exemplary rotation axis position (R1), the range between partial (0.3 g) and full braking (0.8 g) is covered with a first simulation setup. In Figure 54, the rotation times and the associated average rotation velocities are displayed. The curves confirm the observed trend from the previous chapter: the higher the brake acceleration, the lower the rotation time to rotate from the 30° inwards rotated seat position to a standard position (0°).

The effect of different AEB levels on the occupant repositioning is displayed in Figure 55 for partial and full braking. The relative angles are measured at the end of the seat rotation, which differs for the two AEB levels, as displayed in Figure 55 (left). A negative angle describes an inwards rotation of the occupant relative to the seat. For high negative relative rotation angles, the repositioning was

not sufficient and the occupant stayed in its initial position (30° rotation). These cases indicate a low coupling between occupant and seat, leading to a rotation of the seat without rotating the occupant.

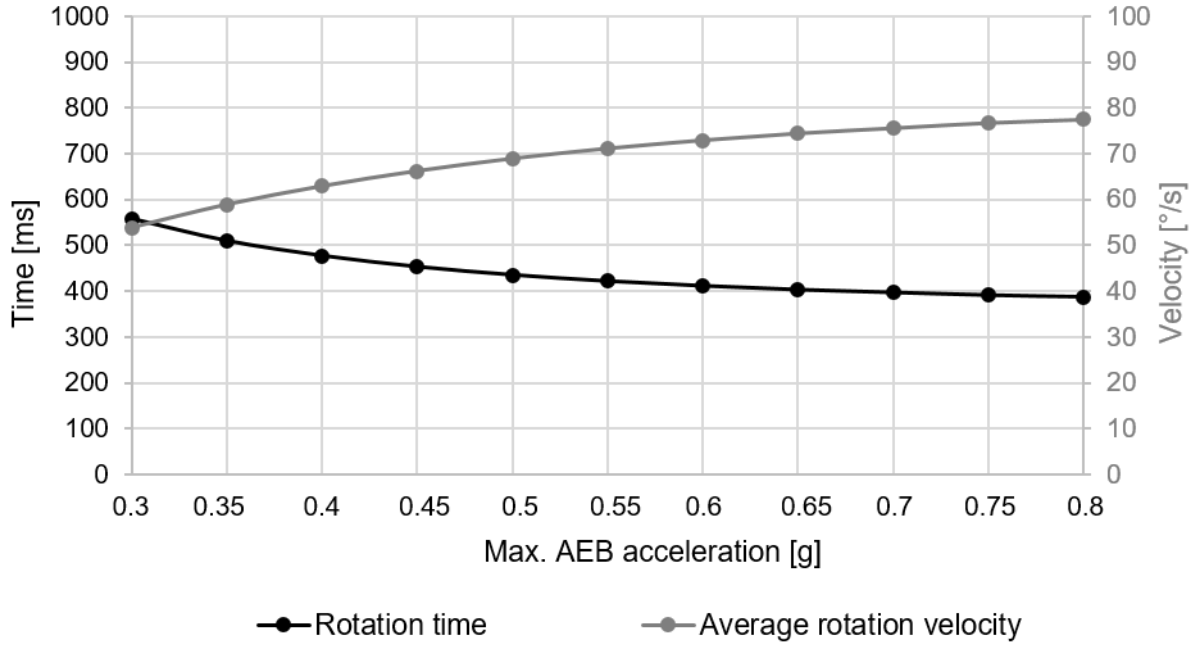

Figure 54 Rotation time curve as function of max. AEB acceleration for R1 (x=0.15 m, y=0.25 m)

The relative angles between occupant and seat increase with an increase of acceleration level. The shoulders and knees especially show the highest differences in angle between the 0.3 g and 0.8 g acceleration level. For both levels, the head shows the highest relative rotation angle, the pelvis comes second.

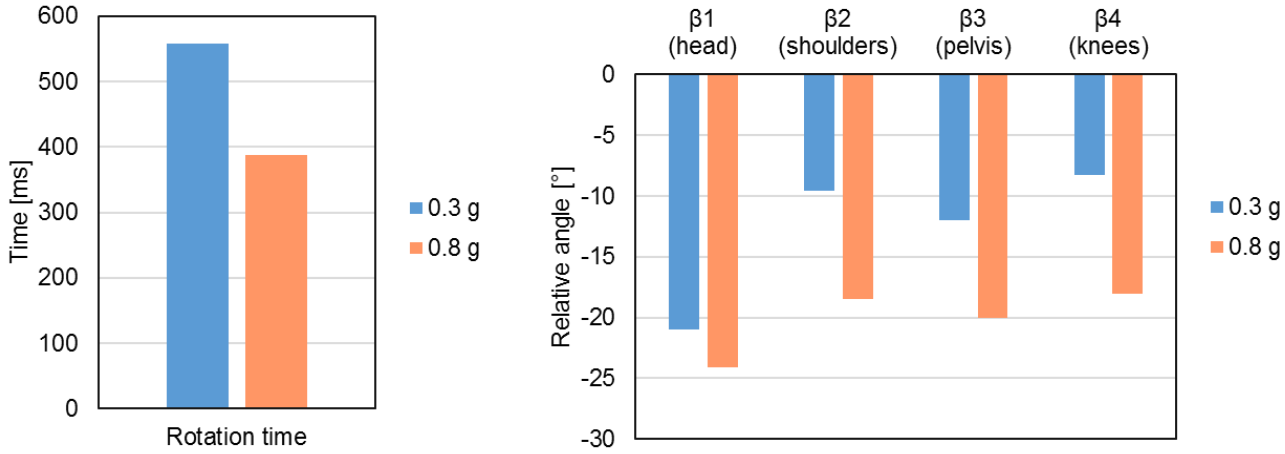

Figure 55 Effect of AEB level (0.3 g & 0.8 g) on the relative angle between occupant & seat at the end of rotation time (for R1)

Figure 56 and Figure 57 show the effect of friction on the functionality of PP2 and the occupant repositioning. In Figure 56, the friction between the shoes of the occupant and the vehicle floor is simulated as 0.01, 0.3 and 0.5. The 0.01 friction value should display the effect of lifted feet, which are almost not in contact with the floor, and that of 0.5 high friction shoes. The default value from the original simulation model was set to 0.3.

The effect of the floor friction on the rotation time is only marginal. A similar image can be observed for the relative angles of the occupant. An increase of floor friction leads to a minor increase of the relative angles of head, shoulders, pelvis and knees.

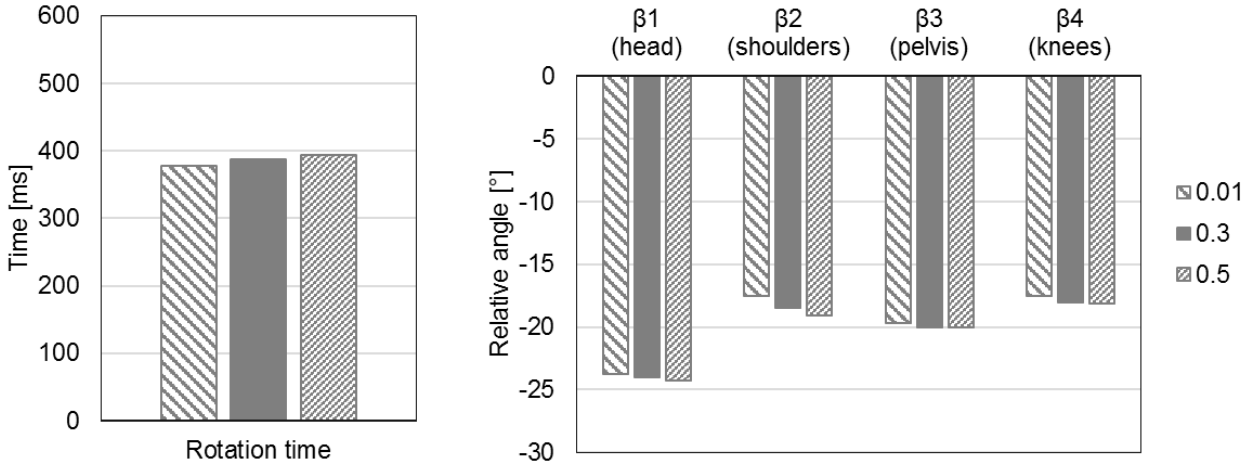

Figure 56 Effect of friction between occupant & floor on the rotation time & relative angles between occupant & seat at the end of rotation time (for R1)

The results of a friction variation between occupant and seat (coefficient 0.1, 0.3 and 0.5) also show a minor effect on the rotation time. The rotation time increases slightly with an increase of friction, whereas the relative angles between occupant and seat are affected more drastically. The body regions which are in contact with the seat, show particularly lower relative angles with an increase of friction. The head also shows a reduction of relative angle for an increase of friction.

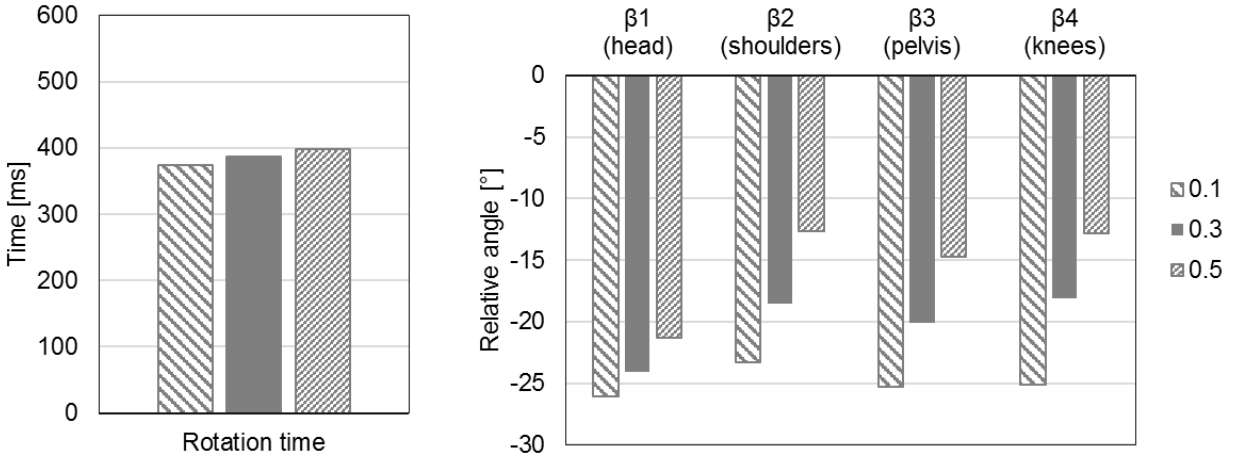

Figure 57 Effect of friction between occupant & seat on the rotation time & relative angles between occupant & seat at the end of rotation time (for R1)

Figure 58 shows the effect of two different Active Human Model (AHM) muscle activation settings on the rotation time and the relative angles between occupant and seat. The rotation time is not affected by the muscle activation level of the occupant, but especially the upper body part shows a high response on the activity setting. A decrease of the head and shoulder angle with a reduction of the awareness level (lower muscle activity) can be observed. The higher the muscle activity, the more the occupant remains in his starting position. The muscle activation setting affects the neck and spine of the occupant due to the previously defined model activity settings, explaining the higher response of the upper body parts.

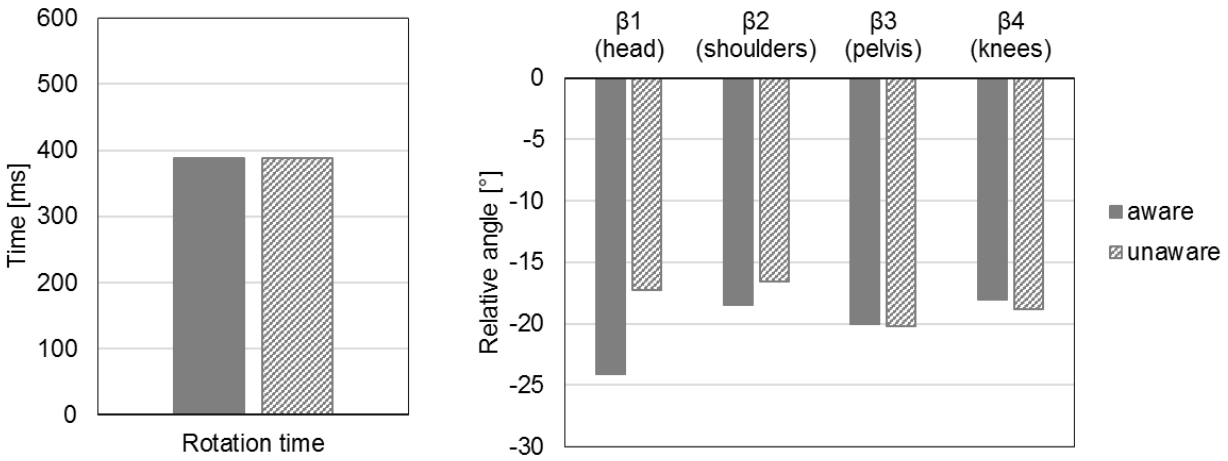

Figure 58 Effect of AHM muscle activation settings on the rotation time & relative angles between occupant & seat at the end of rotation time (for R1)

Within Figure 59, the effect of the generic pre-pretensioner (PPT) is shown. The effect on the rotation time is rather marginal, whereas the effect on the relative angles becomes more obvious. All relative angles between occupant and seat decrease, when the belt is tensioned with 250 N at the start of the AEB. The highest effect can be observed on the shoulders of the occupant, where contact to the shoulder belt increases when the belt is tensioned at the retractor.

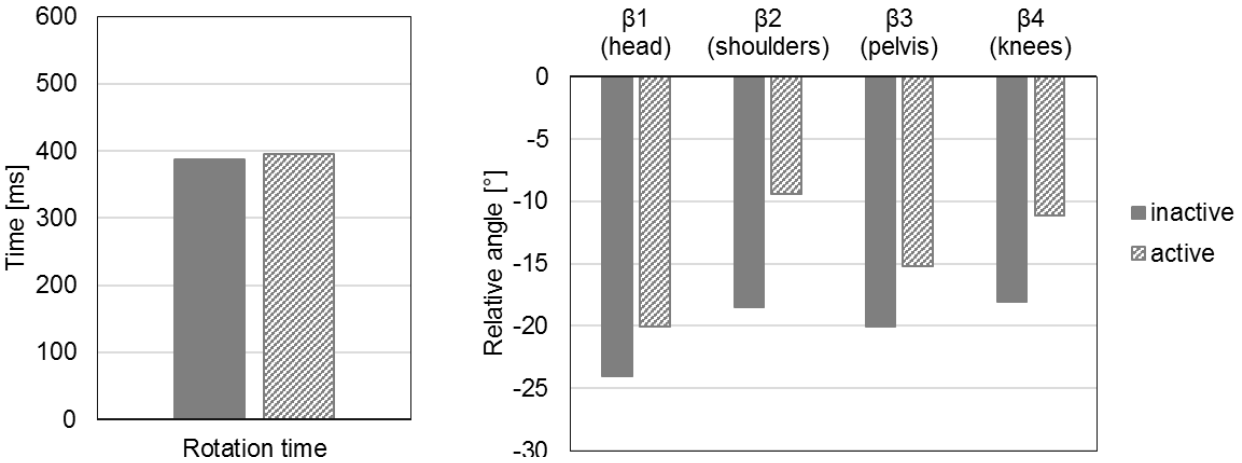

Figure 59 Effect of PPT activation on the rotation time & relative angles between occupant & seat at the end of rotation time (for R1)

Discussion

In this study it was shown that the relative angles between occupant and seat increase with an increase of acceleration level, whereas the shoulders and knees show the highest differences in angle. For both investigated acceleration levels (0.3 g and 0.8 g), the head shows the highest relative rotation angle, the pelvis comes second. When PP2 is applied in a pre-crash situation a trade-off between a short rotation time and sufficient repositioning of the occupant might occur.

The friction between occupant and floor as well as occupant and seat has a marginal effect (< 5% relative to the default setting) on the time required to rotate from 30° to 0°, whereas an increased occupant to seat friction supports the repositioning effect, especially for the shoulders / thorax.

An increase of the muscle activity level decreases the repositioning effect for the upper body. For the rotation time no effect of the AHM muscle activity was observed.

The PPT (250 N at the time of PP2 and AEB application) has a positive effect on the repositioning, especially the shoulders. It can function as coupling support which might be useful to be applied together with PP2. Furthermore, a foot support, a 4-point belt system or an increase of the seat friction could be introduced to reduce the relative angles for acceleration levels and rotation axis positions that provide a short rotation time.

3.2.3.4 Effects of seat belt pre-pretensioning

ZF's contribution is based on the results of ika / fka's pre-study, see Chapter 3.2.3.2. This implies that interior boundary conditions, especially the initial seat rotation angle and the location of the pivot, are selected such that the protection principle works, i.e. the seat rotates by inertia only and the rotation direction turns the seat back towards 0°. Furthermore, similarly as in PP1, the initial seating position, the seat integrated belt concept and all other mechanical properties like friction values, contact definitions and belt routing are taken over from the pre-study in Chapter 3.2.3.2. In this study, again only occupant position P2 (front passenger) is investigated, assuming no interaction with the instrument panel or airbags. Reversible pre-pretensioning during the pre-crash phase as well as pyrotechnical pretensioning during the in-crash phase were only considered at the retractor position.

Parameter variation

An overview of the simulation model set-up and parameter variation can be found in Table 20. The pre-crash braking pulse used is shown in Figure 4, while in-crash pulses are used as in the corresponding PP1 study in Chapter 3.1.3.10, see Figure 42: The blue curves show the generic and 1-dimensional 56 km/h full frontal crash pulse, and the red curves show the 50 km/h SCP06 pulse reflecting an urban oblique car-to-car crash.

Parameter	PP2
Occupant position according to D2.1 [2]	P2
Pre-crash pulse **Crash pulse**	Figure 4 Madymo's generic 56 km/h FF, SCP06
Initial z-seat orientation **Z-seat rotation** **Z-seat rotation start** **Seat rotation velocity**	30° Prescribed motion seat inertia -750 ms -
Initial seatback rotation **Seatback rotation velocity**	20° -
Occupant model type **Excitation**	AHM v3.1 Soft
Airbag	None
Pre-pretensioning at retractor **Seat belt system type**	None / generic PPT / ACR Fully seat integrated
Retractor pyro pretensioner TTF	10 ms
Load limiter type **Shoulder force**	Constant 3 kN
Anchor pyro pretensioner **Anchor pyro pretensioner TTF**	None -
Buckle pyro pretensioner **Buckle pyro pretensioner TTF**	None -
Generic PPT TTF **ACR TTF**	-200 ms -500, -400, -300 ms

Generic PPT belt force **ACR belt force**	250 N 175, 250, 425 N
Simulation solver	Madymo 7.8
OSCCAR model	Generic Interior

Table 20 Simulation model set-up

Focus and research question

This study is focusing on the impact of pre-pretensioning during seat rotation for improved seat to occupant coupling. Similarly to the study for PP1, see Chapter 3.1.3.10, a more realistic pre-pretensioning model based on ZF's Active Control Retractor (ACR) is introduced compared to the simplified generic pre-pretensioner (PPT) included in the baseline models. The parameters ACR activation time, pre-pretensioning power and two different crash pulses are considered within this investigation to see the impact of the more realistic ACR model on the occupant movement and restraint system function.

Results

To investigate the effect of different ACR pre-pretensioning parameters three simulation loops were conducted. Firstly, the influence of the ACR activation time was investigated, secondly the further improvement potential for higher electrical power limits was analysed, and finally the effect of using the ACR during the pre-crash seat rotation on the final occupant restraint function in the in-crash phase was simulated using two different crash pulses.

1. Comparing the results without and with pre-pretensioning (with a belt force of 250 N) in varying activation times during the pre-crash phase, it can be seen that earlier ACR activation can improve seat to occupant coupling to some extent, see Figure 60 showing the relative shoulder angle β2. For no pre-pretensioning the biggest angle of ~25° can be observed. Using an ACR activation time of -500 ms, which is much later than the start of the seat rotation, this can be only slightly reduced by ~3°. Moving the ACR activation time to -750 ms shows a bigger improvement of ~12°, almost reducing the angle to halve. However, shifting the activation time to -900 ms does show almost no additional effect during the pre-crash phase compared to -750 ms. This can easily be understood since seat rotation starts approximately at -750 ms, so an activation much before that time makes no difference.

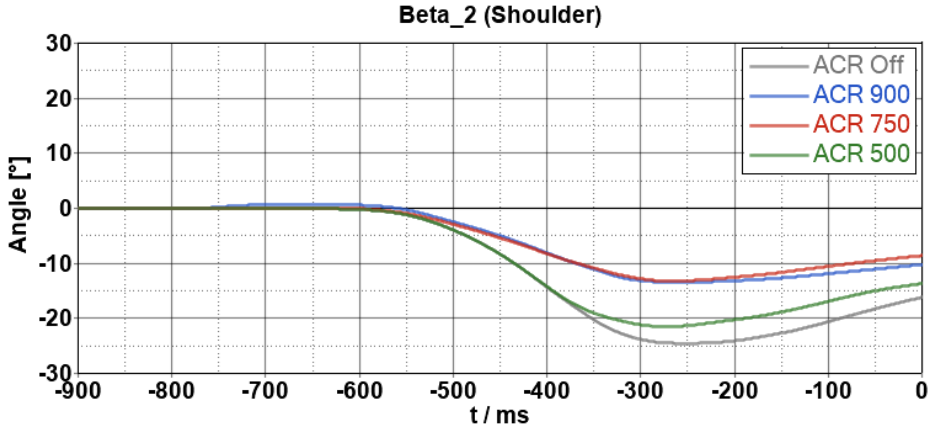

Figure 60 Relative shoulder angle β2 for different ACR activation times [ms]

2. Starting from the early activation time of -900 ms, further improved seat to occupant coupling can be achieved by using more electrical power. Figure 61 shows further reduction

on the shoulder angle β2 to 10° for doubling electrical power and belt force. However, further power increase shows only a minor effect, because all belt slack is already eliminated, and further belt pull-in could only be obtained through unwanted deformation of seat and / or occupant soft tissue.

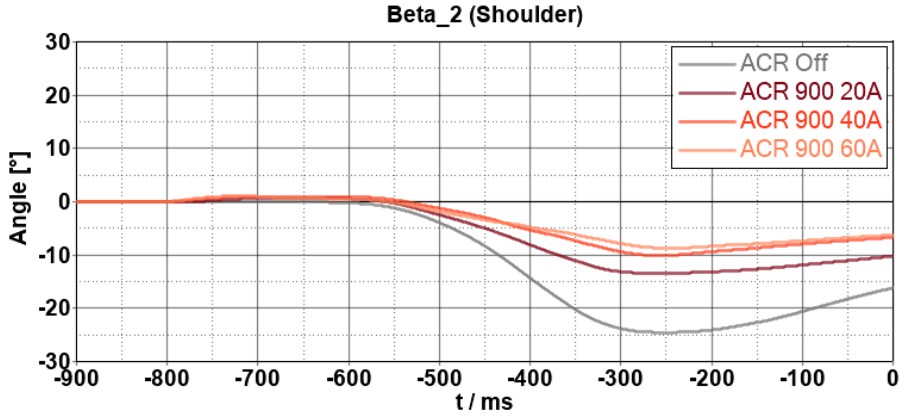

Figure 61 Relative shoulder angle β2 for different ACR power limits

3. As already seen in the corresponding study for PP1 (Chapter 3.1.3.10), the two investigated crash pulses are very different: While the SCP06 pulse is not causing a large occupant displacement, the generic full-frontal pulse is much harder and leads to a high forward displacement, see Figure 62. However, as observed in the PP1 study, an application of a realistic pre-pretensioning can improve the restraint function due to a better coupling of the pelvis area, resulting in improved kinematics and an improved restraint system performance.

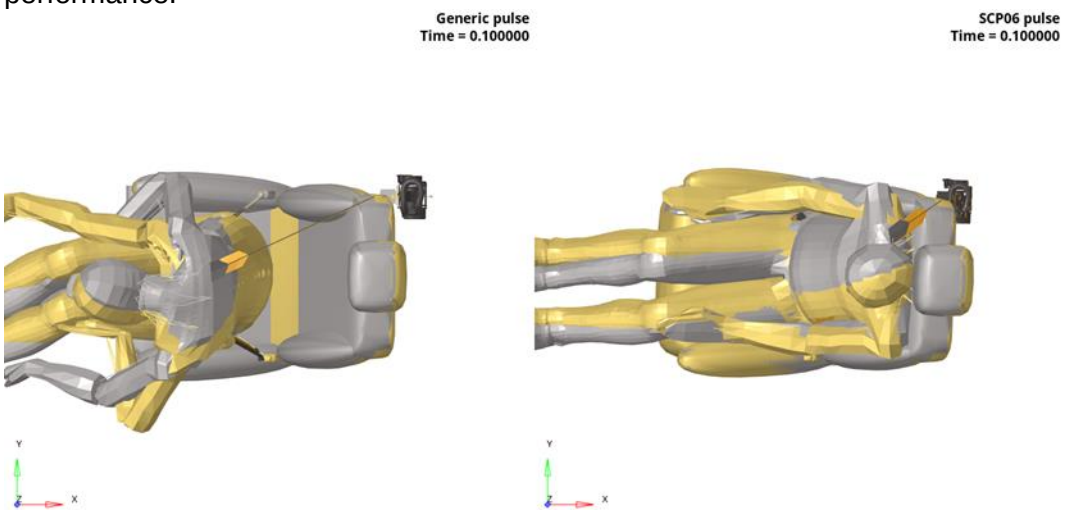

Figure 62 Occupant displacement at 100 ms for generic FF pulse (left) & SCP06 pulse (right), no pre-pretensioning (grey) & ACR (gold)

Discussion

Since the PP1 study in Chapter 3.1.3.10 showed that the generic PPT and a more realistic pre-pretensioner model (ACR) lead to comparable results, no further distinction was made between the two models in this investigation, so that only the ACR model was considered. Taking into account the main physical effects of real products in the market demonstrates positive effects on the seat to occupant coupling during seat rotation with respect to PP2. This improved coupling can be observed for all body regions and, in the case of the pelvic area, can finally also improve the restraint function

in the following crash. All findings confirm the results from the corresponding PP1 study and also underline the findings of the previous PP2 simulation studies.

3.2.4 Conclusion

Coming back to the initially-stated research questions in Chapter 3.2.2, it was found in the three simulation studies that an AEB-based repositioning of the occupant and seat can be achieved within the simulated environment. Based on the position of the rotation axis and the angle of initial seat rotation, the principle shows different performance. It should be noted that all results are limited to the investigated simulation environment and model settings.

The highest average rotation velocity that was generated by a 0.8 g brake acceleration of the seat was measured at 77.9 °/s, rotating the seat from 30° to 0° in 385 ms. This result was generated with the most outward and rearward rotation axis position within the seat base (x = 0.15 m, y = 0.25 m relative to the H-point). Seat rotation angles above 30° were not investigated in this study.

With respect to a safe and successful repositioning of the occupant, it was found that the head shows the highest relative angle for all brake levels and rotation axis positions, with the pelvis coming second. A close-to-standard position rotated occupant, ensuring the functionality of a state-of-the-art restraint system during the in-crash phase, was the objective of the pre-crash repositioning. The unrestrained body parts are especially challenging to rotate and control during the seat rotation phase. The relative angles between seat and occupant increase for all body regions with an increase of the brake coefficient and the associated reduction of rotation time (= increase of average rotation velocity).

Several parameters were investigated with respect to their effect on PP2. The friction between occupant and floor as well as occupant and seat have a marginal effect on the time required to rotate from 30° to 0°. An increased occupant to seat friction supports the repositioning effect, especially for the shoulders. A higher muscle activity level (higher awareness of the occupant) decreases the repositioning effect for the upper body, whereas the rotation of the seat is not affected by the AHM muscle activity setting. The repositioning effect was measured as relative angles between seat and occupant. Additional to the rotation of the seat, a PPT can support the repositioning of the occupant. It was found that a generic PPT with 250 N belt tensioning triggered at the time of unlocking the seat lowers the relative rotation between occupant and seat significantly, especially for the shoulders. Further detailed investigations on pre-pretensioning introducing a more realistic ACR model confirmed the general positive effect. With optimised ACR parameters an even better seat to occupant coupling could be achieved compared to the generic PPT. Depending on the crash pulse, an increased seat to occupant coupling leads to a better re-positioning of the occupant an thus improves the restraint function in the in-crash phase.

3.3 Protection Principle 3 - Reclined occupant: Pelvis & lumbar aspects

The overall objective of this working group is to evaluate how different HBMs respond to a number of countermeasures (i.e. protection principles), to the risk of submarining and, if no submarining occurs, to increased loading to the pelvis and lumbar spine in the reclined seating position. In addition, one of the studies investigated the influence of sitting postures on HBM responses.

3.3.1 Motivation and Background

The protection principles used in the investigation focus mainly on seat pan or seat belt-integrated protection principles, addressing the risk of submarining. If no submarining occurs, the focus is on evaluation of the influences of loading to the pelvis and lumbar spine for occupants in reclined seating position. The evaluated use cases were identified based on the OSCCAR deliverable D2.1 “Test Case Matrix and selecting Demonstrator Test Cases” [2]. The target vehicle is a L4 / L5 vehicle with model year 2030 operating in urban areas. With this, the remaining crossing intersection crashes determined in deliverable D1.3 [6] (see also [47]) have been used in combination with more generic full frontal pulses. The occupant use case that is mainly used is a seat with neither frontal airbags nor knee bolster, being representative of the rear seat in a living room seating configuration. The selections were motivated by the importance of evaluating how HBMs could be used to assess occupant protection principles in frontal and frontal oblique crashes, in the reclined seating position in interiors without knee bolsters. Figure 63 shows how this area of focus was identified and selected in deliverable D2.3 [4].

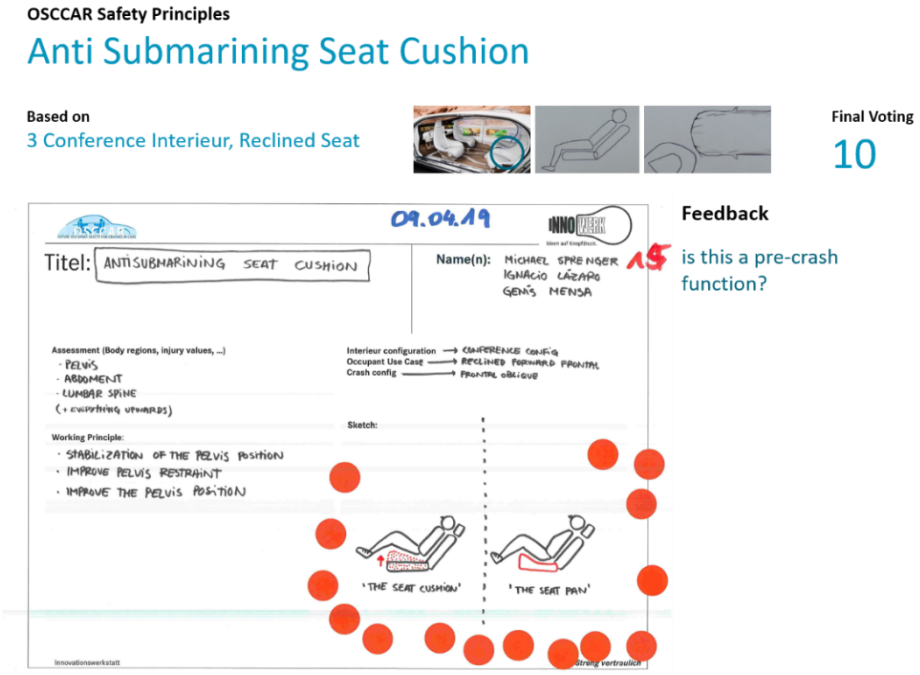

Figure 63 Original Protection Principle defined in deliverable D2.3 [4]

3.3.2 Research Questions

It is assumed that when the seat is positioned away from the instrument panel or in a living room layout, the risk of submarining will increase especially in the reclined occupant position, and even if submarining is avoided the consequences will be increased loading to the pelvis from the lap belt, and increased lumbar spine loading due to unfavourable kinematics, with the upper body loading the lumbar spine when pitching forward.

Therefore, the following research questions for Protection Principle 3 were generated:

- What are the challenges when restraining a forward-facing occupant sitting in the ‘face 2 face’ position in a frontal oblique crash?
- What influence on occupant safety does a reclined seat have? Are there specific challenges related to obesity and / or small females?
- Is it possible to reduce occupant loading with seat-integrated countermeasures? (crush element, energy absorption in x / xz direction)
- Are there trade-offs between different restraints / protection principles like seat load limiter, forward positioned seat belt anchor points, lap belt pretensioning etc.? (submarining / spine load / belt load)
- Are there specific challenges related to oblique load cases and related occupant kinematics?
- How will pre-crash manoeuvres (braking) affect occupant pelvis restraint in forward-facing reclined positions?
- How different are the results using passive and reactive HBM (after pre-crash phase / after in-crash phase)?

In addition, with a special focus on lap-belt interaction and its influence of varieties of lower extremity postures and impact directions, one study investigated variations of occupant postures, providing input on HBM sensitivity for postural changes.

3.3.3 Simulation Studies

Several simulation studies were performed by Autoliv, Volkswagen, Toyota, Mercedes and Volvo Cars, see Table 21. Each simulation study is presented separately, including aim, method, result and conclusion, in the following Chapters 3.3.3.1 - 3.3.3.5.

Partner	Mercedes	Autoliv	Toyota	Volvo Cars	Volkswagen
Chapter	3.3.3.4	3.3.3.1	3.3.3.3	3.3.3.5	3.3.3.2
Seating direction	Forward facing	Forward facing	Forward facing	Forward facing	Forward facing
Braking	No braking	No braking	No braking	No braking	Pre-braking
Crash scenario	Frontal, SCP & LTAP OD	Frontal, SCP & LTAP OD	Frontal, SCP & LTAP OD	Frontal, SCP & LTAP OD	Frontal
Interior model	Generic, no steering w. & bolster	Semi-rigid seat with foot support	Semi-rigid seat with foot support	In-house models	Semi-rigid seat with foot support
HBM	THUMS-TUC	SAFER HBM	THUMS v 4	SAFER HBM	THUMS TUC VW AHMB
Occupant anthro-pometry variation	THUMS-V4-D-Obese THUMS-V4-D-Asian-Female	No (50%-ile only)	No (50%-ile only)	No (50%-ile only)	No (50%-ile only)
Solver	LS-Dyna	LS-Dyna	LS-Dyna	LS-Dyna	VPS
Initial seat back angle	25°, 48° & 60°	25° & 48°	25° & 48°	25°	25° & 48°
Seat pan angle	entire seat rotated	15°	15°	15°	15° & 20°

Protection principle	Energy absorption in seat structure	Double lap belt PT, seat track LL, seat pan LL, seat back LL and pelvis lap belt LL	Replicate test loop1 at BASt with SOTA seat belt and double lap belt PT	Variety of sitting postures; including torso, head & extremities	Seat pan angle & stiffn., Lap belt geometry, pre-tensioning & load limiting

Table 21 Overview of Protection Principle 3 simulation studies

3.3.3.1 Influence of seat and lap belt load limiting

The aim with this study performed by Autoliv is to investigate the influence of seat track, seat pan and lap belt (anchor & buckle sides) load limiting on the kinematics and loading of the SAFER HBM in selected worst-cases, intersection crash types for both upright and reclined occupant postures [6].

Method:

The study was carried out for a belted occupant in a generic environment consisting of a semi-rigid seat [30] and a seat-integrated, triple-pretensioned, 3.5 kN load-limited conceptual three-point belt system with a crash locking tongue, that mitigates webbing transfer from the shoulder belt to the lap belt [31]. The conceptual belt system was designed to improve pelvis restraint in order to avoid submarining in reclined occupant postures. No footwell was used. This set-up was chosen to represent a seat away from frontal airbags and knee bolsters and / or a rear seat of a living room interior layout. In this simulation study the SAFER human body model (HBM) version 9 was used. It is a mathematical model of an adult mid-sized male which was developed to improve the understanding of impact response and injury mechanisms in humans. The SAFER HBM, originally developed from the Total Human Model for Safety (THUMS) version 3 [32], has been updated with new head, neck, and rib cage models [33]. The lumbar spine was also modified, with updated geometric modelling of the vertebrae and the material properties of the intervertebral ligaments and discs, as well as new contact definitions to improve biofidelity [34][35]. Further, the SAFER HBM was evaluated to newly-released reclined PMHS test data from 2020 [36][37]. The mathematical simulations were performed using the finite element (FE) solver LS-DYNA version 971 R9.3.1.

The SAFER HBM model was positioned in an approximately 20° upright posture, as measured on the sternum with respect to the vertical using a male driver posture-prediction model [28], and in an approximately 50° reclined posture using target positioning data from 3D position measurements on PMHS [36][39]. Pelvis angle, as measured between ASIS and pubic symphysis to the vertical, was 43° for the upright and 72° for the reclined posture.

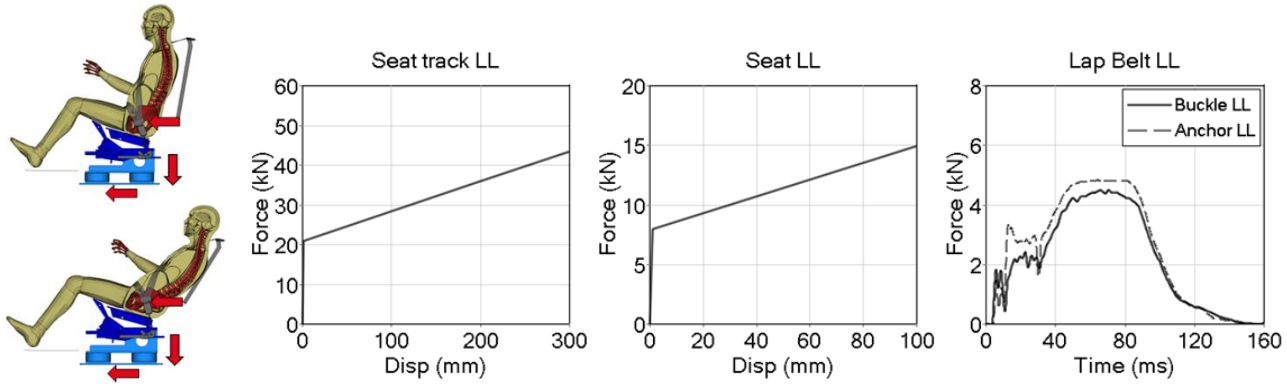

Figure 64 SAFER HBM in upright and reclined postures (left). Load limiting characteristics in the seat track (frontal direction), seat (vertical direction) & lap belt (anchor and buckle sides) (right)

The semi-rigid seat, seat belt, and SAFER HBM were subjected to four crash pulses: the two intersection crashes SCP (Straight Crossing Path) and LTAP OD2 (Left Turn Across Path - Opposite Direction), and the full frontal 40 km/h and 56 km/h crashes [6], Figure 65. For the SCP crash, the SAFER HBM was positioned on the driver side with a driver-side belt geometry. For the LTAP OD2 and the full-frontal crashes, the passenger side with a passenger-side belt geometry was used. The selected positions and belt geometries were identified as being worst-case conditions for occupant loading [6]. The lower body of the occupant is restrained by the seat and the seat belt system, which stiffnesses control the amount of loading to the occupant. Three protection principles were evaluated in order to reduce the loading to the lower body, i.e. pelvis and lumbar spine: seat-track load limiting (21 kN) in frontal direction (SeatTrack_LLx), seat and submarining pan load limiting (8 kN) in vertical direction (Seat_LLz) and lap belt load limiting on both anchor (4.4 kN) and buckle (4.8 kN) sides (Lap_LL), Figure 64. Head excursions relative to the seat and loading on the head, neck, chest, lumbar spine and pelvis (ASIS) were measured in the HBM to evaluate the effect of seat and lap belt load limiting. Lumbar spine forces and moments were measured in the L1 to L5 vertebrae and the maximum values from all five vertebrae were used as the result parameters.

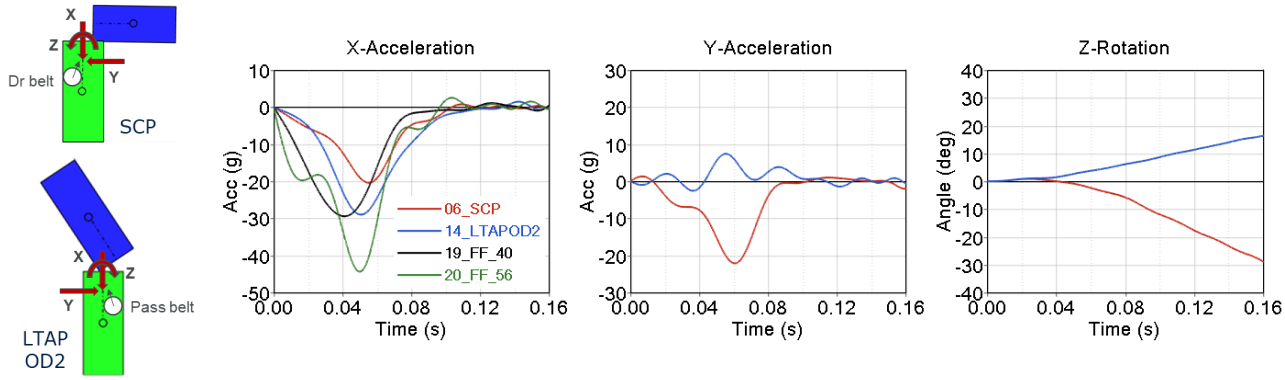

Figure 65 SAFER HBM positions & intersection crash pulses for the evaluated SCP, LTAP OD2 & full frontal crashes

Results:

For both upright and reclined postures, the largest head excursion was obtained in the FF 56 km/h crash, intermediate excursions for both the FF 40 km/h and LTAP OD2 crashes and the smallest, but in an oblique direction, for the SCP crash, Figure 66.

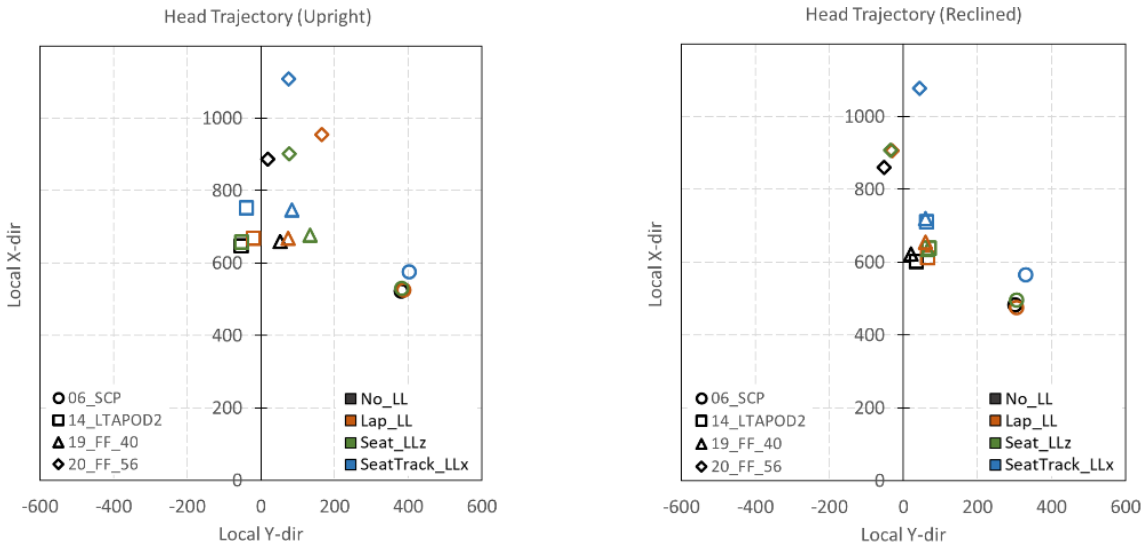

Figure 66 Head COG trajectories for SAFER HBM in upright and reclined postures

The largest increase in head x-excursions was obtained from using the seat track LL, for which the excursions increased by 53 - 222 mm in upright posture and 83 - 218 mm in reclined posture. The largest reduction in head- and neck loading was obtained from the seat track load limiting, especially in the FF 56 km/h crash, Figure 67 and Figure 68. For the lumbar spine loading, the largest reductions were obtained using seat- and seat-track load limiting. Maximum loading in the lumbar spine was measured in either the L1 or L2 vertebra.

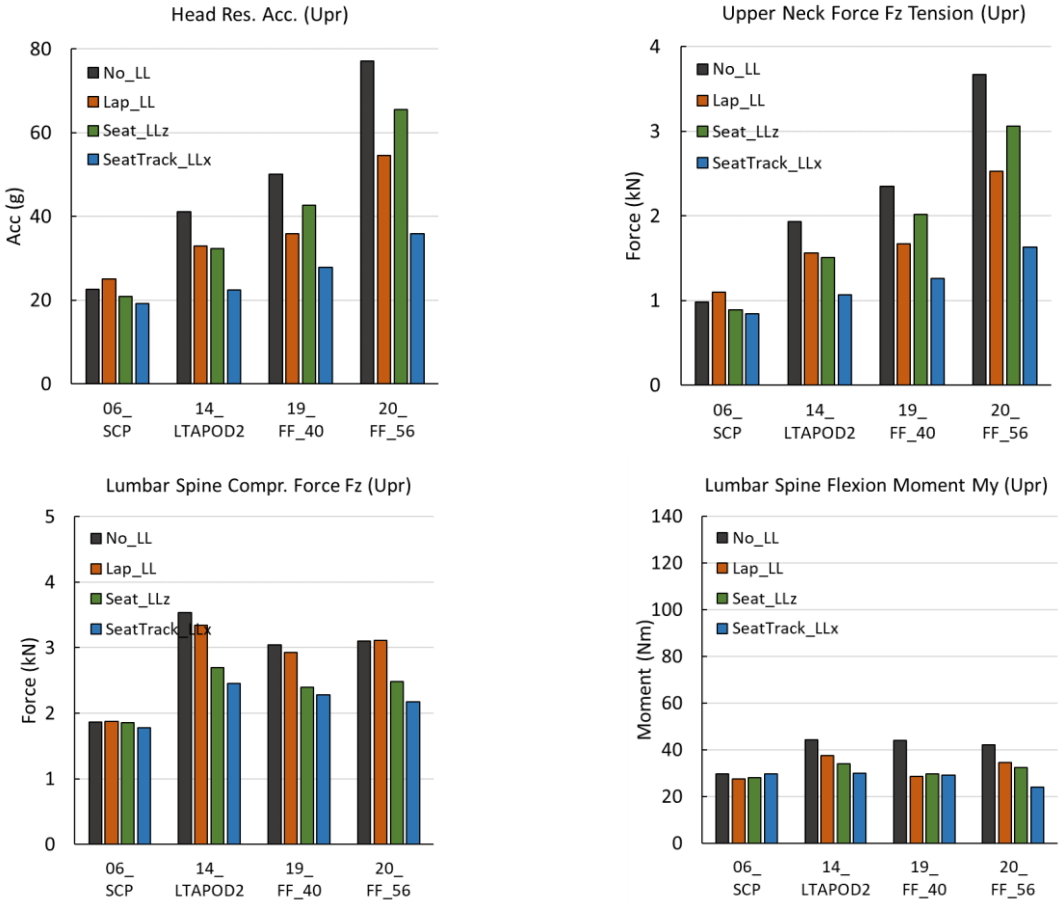

Figure 67 Head, upper neck & lumbar spine loading for SAFER HBM in upright posture

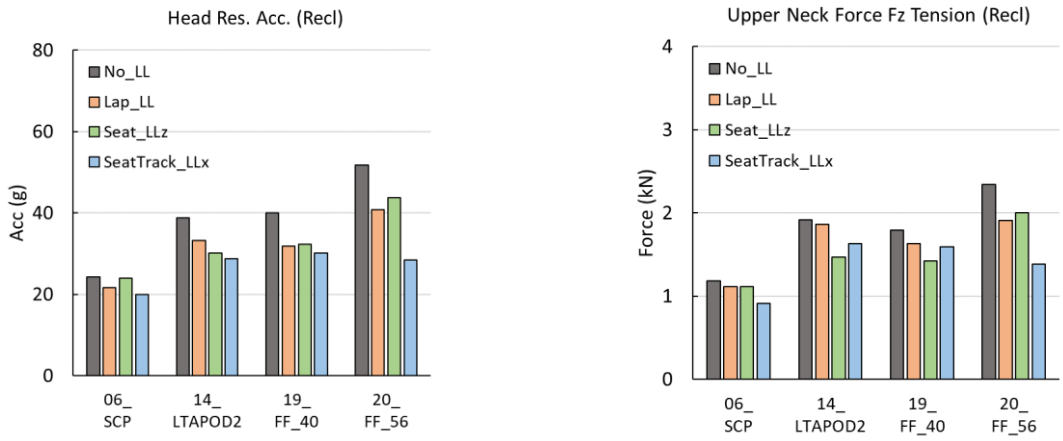

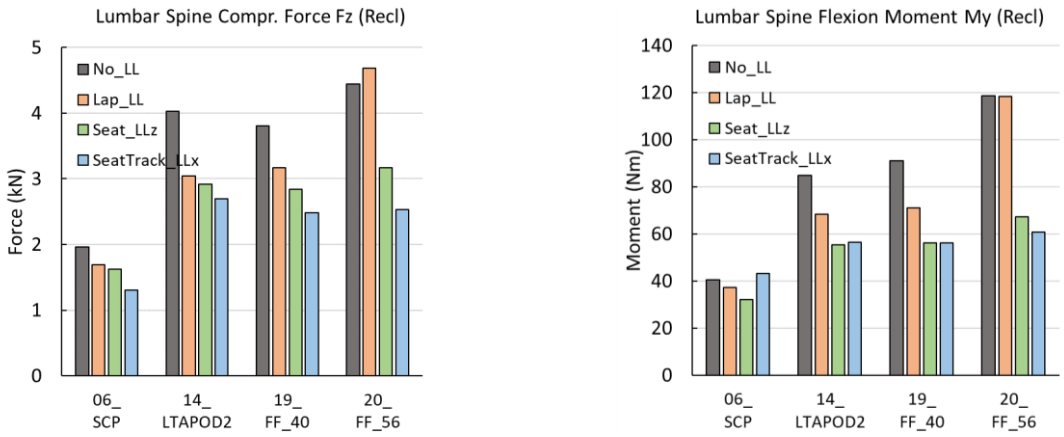

Figure 68 Head, upper neck & lumbar spine loading for SAFER HBM in reclined posture

The largest reduction in pelvis ASIS loading was obtained from the lap belt load limiting followed by seat-track load limiting, Figure 69. The reductions were larger for the reclined compared to the upright posture. For the upright posture in the SCP crash, increased rib fracture risk due to belt slip-off was observed for the seat and seat-track load limiting, Figure 69. For the upright posture in the 56 km/h crash, a reduced rib fracture risk was obtained for all protection principles investigated within the framework of PP3 and with the largest reduction for lap belt load limiting. For the reclined posture, the 16% risk of number of fractured ribs (NFR) 2+ rib fractures for the FF 56 km/h crash was reduced almost fully using any of the protection principles related to PP3.

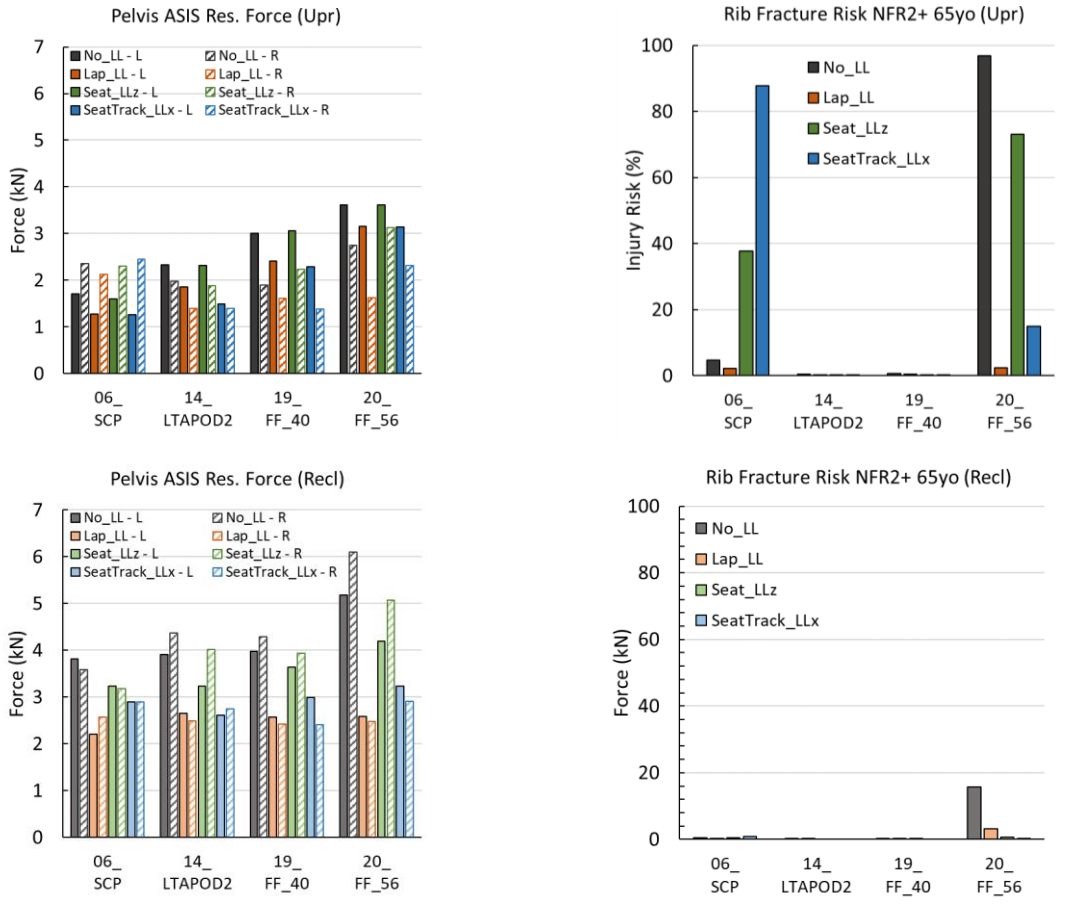

Figure 69 Pelvis ASIS forces & risk of 2+ fractured ribs for a 65 yo, SAFER HBM in upright (upper) & reclined (lower) postures

A delayed loading of the shoulder belt was obtained for the intersection compared to the full frontal crashes due to the pulse differences, Figure 70. In general, higher lap belt forces were obtained for the reclined compared to the upright posture. A reduced lap belt force was obtained for all protection principles within the framework of PP3, but mostly for seat track and lap belt load limiting.

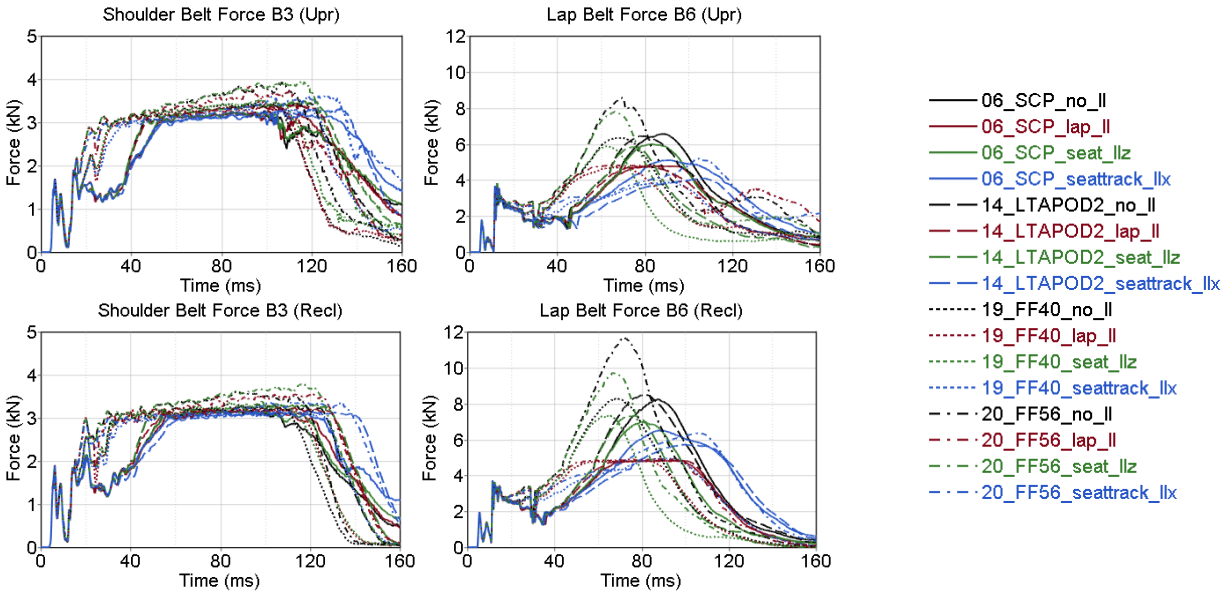

Figure 70 Shoulder (B3) & lap (B6) belt forces for all crashes & both postures

Discussion:

Despite the angled vehicle-to-vehicle impacts for the intersection crashes, an oblique occupant trajectory was obtained only in the SCP crash, which led to a belt slip-off and thus an increased risk of rib fractures. For these reasons, the SCP crash is an impact configuration to consider in the development of countermeasures, and potentially in future legislation. For the LTAP OD2 crash, similar excursions and occupant loading were obtained as for the full-frontal 40 km/h impact, and smaller compared to the currently used full-frontal 56 km/h load case.

For the seat-track load limiting in the full frontal 56 km/h crash, peak seat displacements of 321 - 337 mm, and increased peak head excursions by approximately 222 mm, were obtained depending on the occupant posture. Sufficient space should be provided in future vehicle interiors to allow for these increased displacements. If sufficient space is not available, the load limiting setting for this protection principle needs to be increased considering the 56 km/h crash severity.

The primary loading on the lumbar spine was determined by the structure supporting the pelvis, as indicated by the large effects from load limiting of the seat and seat track. For pelvis ASIS, the primary loading was from the lap belt. Lap belt load limiting thus reduces the pelvis loading directly, while seat-track load limiting reduces it indirectly through decreased lap belt forces.

Conclusion:

Seat-track and seat load limiting were most effective at reducing lumbar spine loading. Seat pan load limiting in z-direction was less effective in reducing lumbar and pelvis loads. For the SCP crash, increased risk of belt slip-off and risk of rib fractures was observed. The LTAP OD2 crash was less severe than the full frontal 56 km/h crash.

3.3.3.2 Avoidance of submarining in a reclined seating position and reduction of pelvis and lumbar spine loads

In this study performed by Volkswagen, the aim was to analyse the effects of different belt system and seat-related countermeasures in a reclined occupant position. Submarining and an increase of pelvis and lumbar spine loadings must be avoided in this position. Therefore, different restraint countermeasures were added to the baseline restraint system, which initially provided a belt system with triple pretensioning.

Method:

For the simulation study the semi-rigid seat model, foot rest and belt geometry in VPS code already described in [1] and [3] were used.

To be able to investigate the basic protection principle combined with additional countermeasures, the belt system included in the original model was replaced with an internal Volkswagen belt system while keeping the original belt fixation points. This belt system provided more possible variations of its parameters. An overview of the adjustable belt parameters is shown in Table 22.

Belt Component	Buckle	Anchor	Retractor
Pre-Pretensioner		X	X
Pretensioner	X	X	X
Load Limiter		X	X
Locking Tongue	X		

Table 22 Belt system parameterisation used by Volkswagen

Some further modifications to the original seat model had to be adapted, considering the defined boundary conditions used in the study. Since all simulations in this study included pre-crash braking, a simplified generic backrest was added to the seat model and fixed in space. This was necessary to support the occupant in the reclined position during the pre-crash phase. Therefore, a rigid surface was generated based on the HBM's back surface and then placed in contact-thickness distance to it (Figure 71).

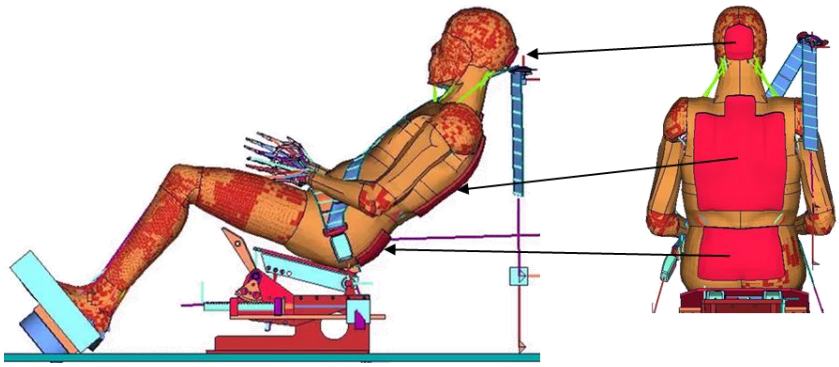

Figure 71 Added back support for pre-crash phase

The active HBM used by Volkswagen is the same as already described in Chapter 3.1.3.1 of this report. The active HBM was used during the entire simulation, however, the muscle controller was deactivated during the in-crash phase.

To evaluate the forces and moments on each vertebrae of the lumbar spine the HBM was extended with section definitions. In order to evaluate the loadings for each section, the rigid body definitions

were removed from the lumbar vertebrae. Also, the ASIS section [36] force calculation used for submarining assessment was integrated into the HBM model (Figure 72).

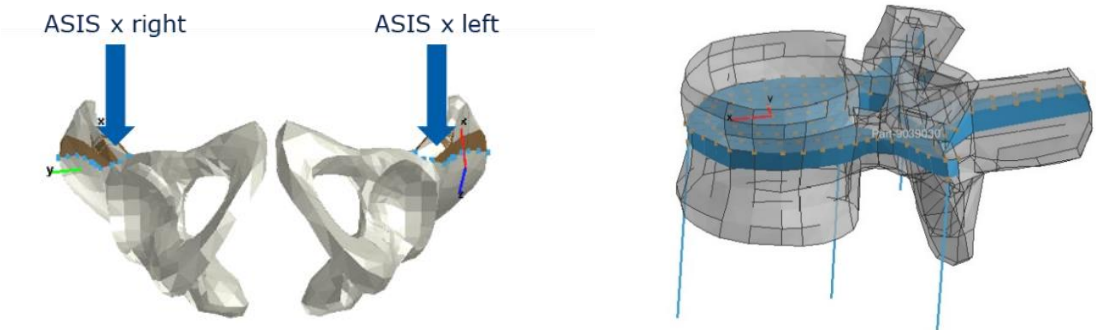

Figure 72 Section definitions on ASIS (left) & on the lumbar vertebrae, shown for L2 (right)

The pre-positioning of the HBM to the 48° reclined position was done following the method shown in Figure 73. In the first step the new PIPER-based OSCCAR positioning tool provided by TU GRAZ was used together with the landmark positions taken from UVA test data [41]. The hands and arms of the HBM, originally in a driver position, were then positioned so that the hands rest on the thighs. Finally, the pre-positioned HBM was settled onto the seat by applying gravity forces to the HBM while keeping its posture by applying a rigid body definition to the skeleton.

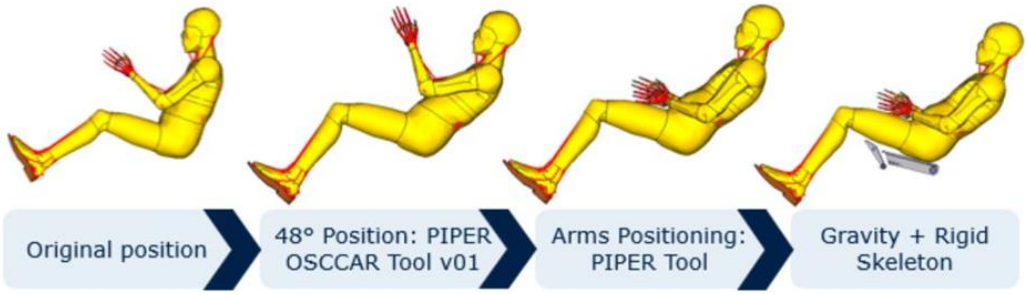

Figure 73 Positioning method for the reclined occupant

After the HBM positioning and belting was completed, it was realised that the use of the original buckle position resulted in an unrealistic lap belt routing. To improve the lap belt routing the buckle was rotated 10° forward around the fixation point (Figure 74).

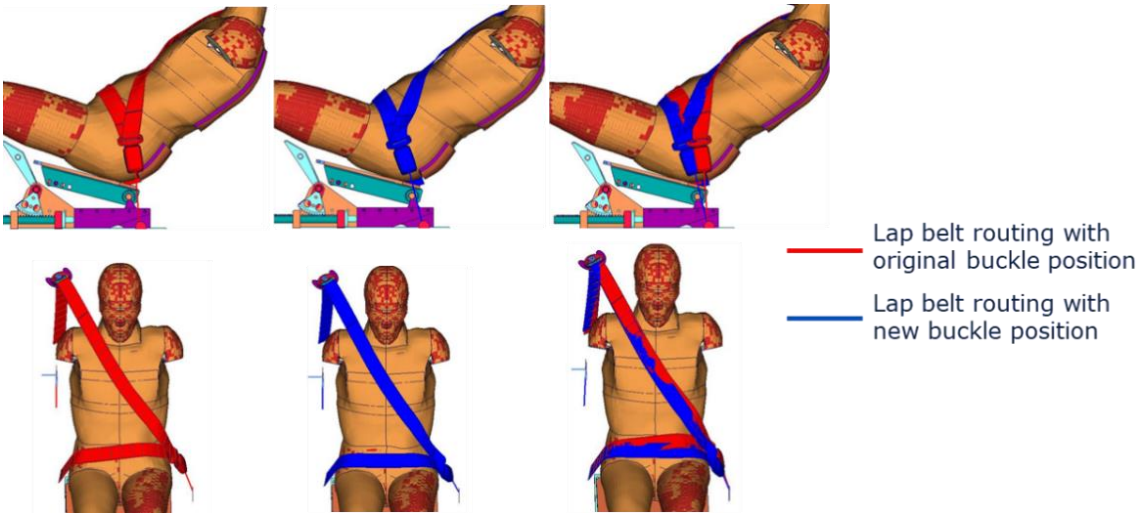

Figure 74 Adapted lap belt routing in the reclined position

Focus of the Volkswagen study was a so-called highway scenario, defined by WP1 [28]. Therefore, in all simulations, the generic acceleration-based crash pulse for a full frontal impact with 40 km/h was used. This crash pulse was combined with a pre-crash braking pulse also recommended by WP1 [28]. To compare the effect of the different restraint countermeasures, the same combination of pre-crash and crash pulse was used for all the simulations.

The overall timeline used in all Volkswagen simulations, including all triggering points of the active measures, is shown in Figure 75.

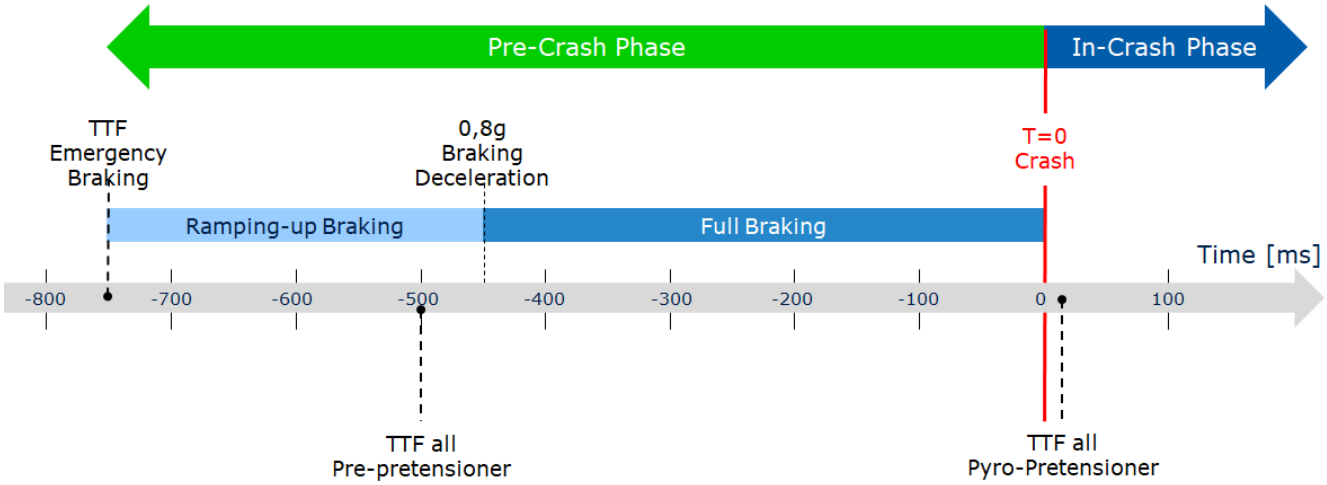

Figure 75 Overall simulation timeline used in Protection Principle 3 study

First of all, a baseline simulation was performed with the 48° reclined seat using pre-pretensioning of the shoulder belt, triple pretensioning on all belt fixation points, load limiting of the shoulder belt and a locking tongue.

In all other simulations, different countermeasures were added to the baseline setup to investigate the effect of those belt system- and seat-related countermeasures regarding submarining avoidance and reduction of pelvis and lumbar spine loadings.

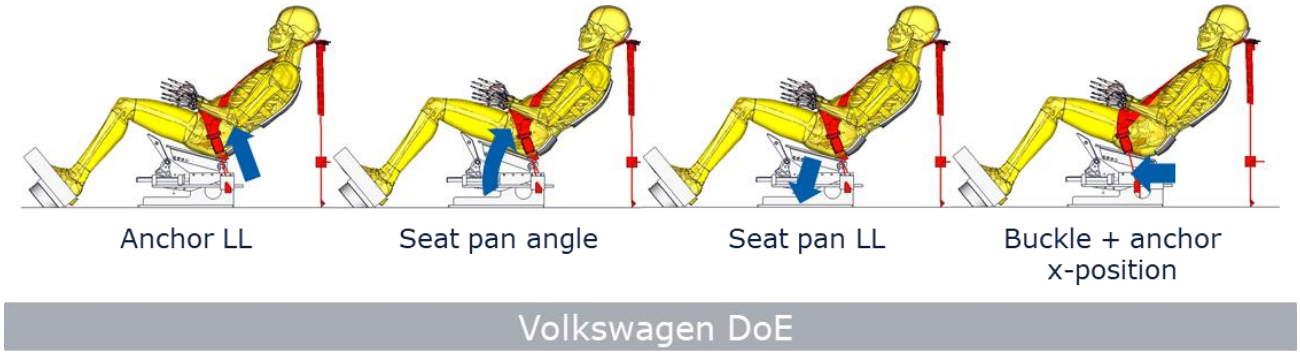

Figure 76 Countermeasures evaluated and compared in the Volkswagen DOE

As an additional countermeasure an anchor load limiter, an increased seat pan angle, a seat pan load limiter and a forward shifted anchor and buckle fixation point were investigated.

To define suitable ranges for the individual restraint countermeasures, some pre-simulations with variations of the parameters were performed. The decided parameter settings finally used in the DOE are listed in Table 23.

Countermeasure	Parameter settings Var0	Parameter settings Var1
Anchor load limiter (LL)	0 kN	4.5 kN
Seat pan load limiter (LL)	Baseline 130 N/mm	Seat pan -30% Seat ramp -15%
Seat pan angle	15°	20°
Buckle & anchor position in x	Baseline	~100 mm (forward)

Table 23 Parameter settings of the investigated countermeasures

The main simulation study considered not only the potential benefit of each individual countermeasure, but also all possible combinations of the different countermeasures were analysed. This approach led to a full DOE matrix with 16 simulation runs in total, of which all were performed within this study.

Results:

The first objective was the avoidance of submarining in the reclined position. As an indicator if submarining occurred in a simulation run or not, an ASIS force-related approach was used (Figure 77). Therefore, the left and right pelvis ASIS forces in the x-direction (Figure 72) were assessed. A sudden drop of the force is an indication for submarining. In addition, a visual assessment of the according animations was done.

In Figure 77, two examples taken from the DOE, one with submarining and one without, are shown. In the red example submarining occurred on the left iliac wing, which is the buckle side.

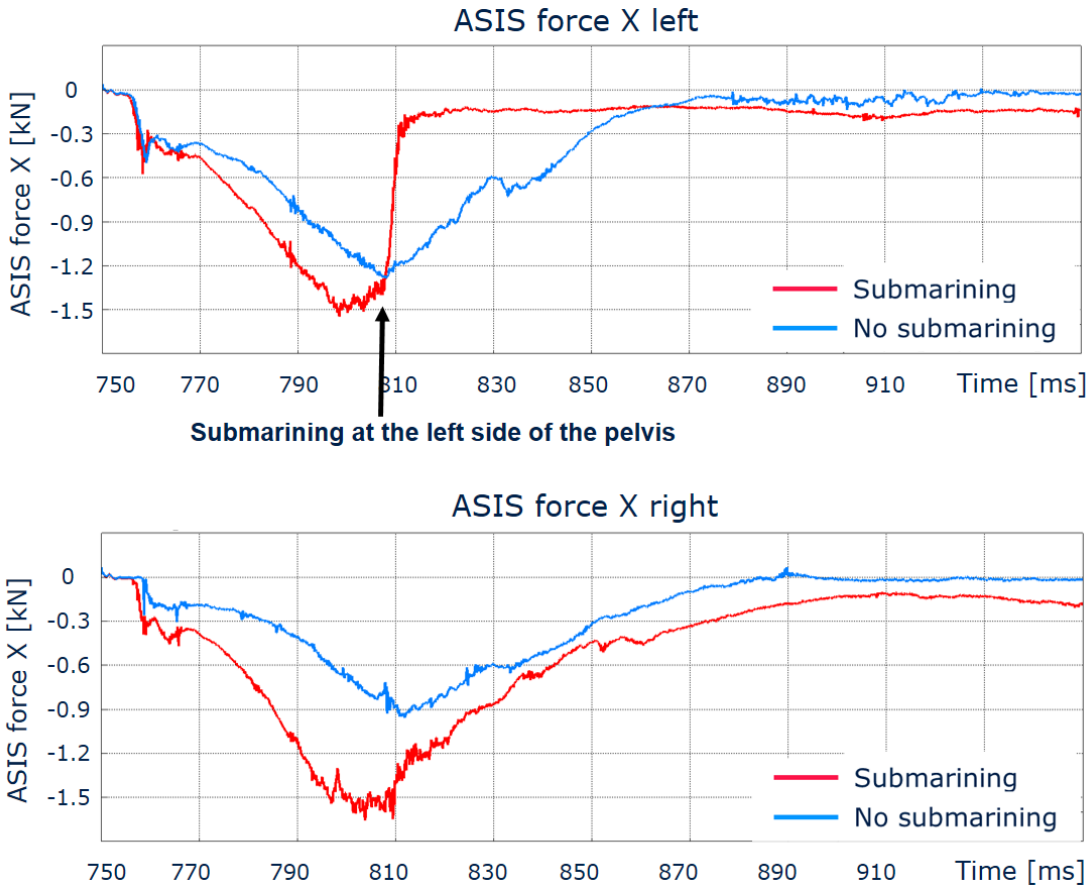

Figure 77 Approach used for submarining evaluation

This approach of submarining evaluation was performed for all simulations. The results of this submarining evaluation are illustrated in Table 24.

Considered countermeasures	Submarining	Spine & pelvis loadings
Baseline (triple pretensioner)	YES	
Seat pan LL	YES	
Anchor LL	YES	
Seat pan LL + anchor LL	YES	
Seat pan angle	NO	Evaluated
Buckle & anchor position	NO	
Seat pan angle + anchor LL	NO	Evaluated
Seat pan angle + seat pan LL	NO	Evaluated
Seat pan angle + buckle & anchor position	NO	
Buckle & anchor position + seat pan LL	NO	
Buckle & anchor position + anchor LL	NO	Reference
Seat pan angle + seat pan LL + anchor LL	NO	Evaluated
Seat pan angle + anchor LL + buckle & anchor position	NO	
Seat pan angle + seat pan LL + buckle & anchor position	NO	
Buckle & anchor position + anchor LL + seat pan LL	NO	
Seat pan angle + buckle & anchor position + seat pan LL + anchor LL	NO	

Table 24 Simulations with submarining and without

Although the triple pretensioner was already included in the baseline simulation, submarining was observed at the buckle side. The simulations with additional load limiting countermeasures also showed submarining on the buckle side. One possible explanation for this submarining observation could be the pre-pretensioning function of the shoulder belt triggered in the pre-crash phase. This pre-pretensioning pulls the buckle in a more upward position due to the flexible fixation of the buckle. This effect would be interesting for further studies outside of OSCCAR. A buckle load limiter, not considered in this study, could also have a positive effect regarding submarining avoidance on the buckle side.

The two countermeasures “seat pan angle” and “buckle & anchor position” have the highest effect regarding the avoidance of submarining. Since submarining avoidance was a main objective, all simulations where submarining occurred were excluded from further in-depth evaluation. Besides submarining avoidance, loading of the lumbar spine and pelvis was the focus of this study.

In a first assessment of lumbar spine forces in the simulations without submarining, it was identified that in all DOE simulations with the countermeasures “buckle & anchor position” included, high lumbar spine compression forces were found. This countermeasure avoids submarining by hindering the pelvis rotation, though resulting in high compression forces of the spine. However, the maximum forward pelvis displacement is larger than for the other countermeasure combinations.

The highest values were found in L5 vertebra with absolute values of approximately 4.5 kN. In order to investigate the potential reduction of the compression forces using other countermeasure combinations, no results of the DOE runs with the countermeasure “buckle & anchor position” are reported in detail. Only one of them was taken as a reference case to compare the effect of the other

countermeasures regarding spine and pelvis loadings. The results for the five DOE runs marked in the right column in Table 24 are presented on the next pages.

The simulations were done without a frontal airbag, which has normally a big influence on head, neck and thorax kinematics and loadings. Therefore, the results for the head, neck and thorax loadings are not shown in detail here. As an example, the AIS3+ rib fracture risk was equally close to 100% in all of the simulations, based on [43].

The comparison of the lumbar spine compression forces is shown in Figure 78 for each vertebra. Overall, the highest lumbar spine forces were found in L5, whereas the lowest occurred in L4. Compared to the reference case, lumbar spine forces could be reduced by the seat pan angle in combination with the investigated load-limiting countermeasures. Between those countermeasure combinations no big differences could be observed and the force levels are similar.

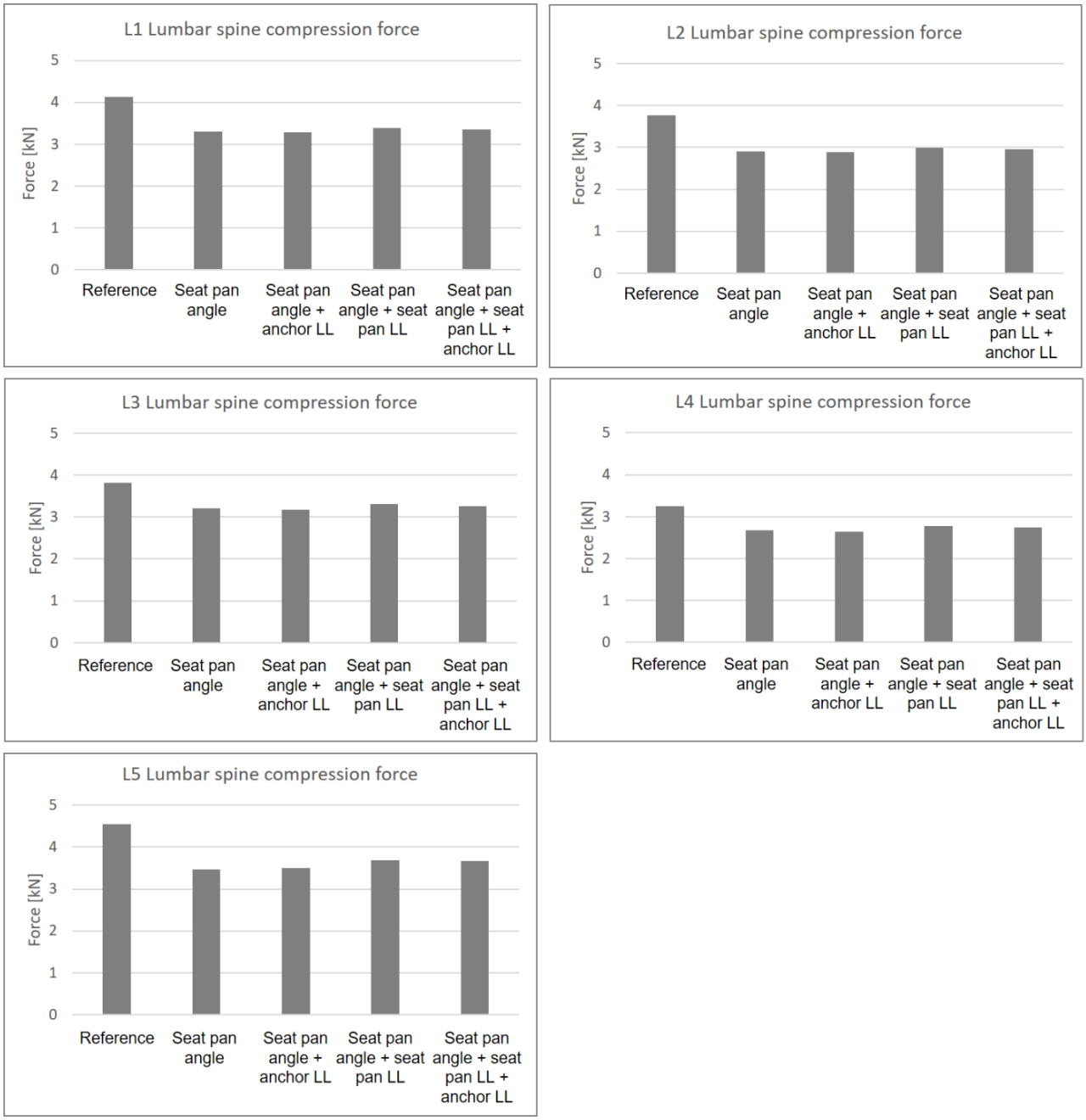

Figure 78 Lumbar spine compression forces

Beside the lumbar spine forces, the lumbar spine flexion moments were also considered. The results for the flexion moment are shown in Figure 79. The lowest moments were received in L4 and L5. In the other vertebrae the flexion moments are twice as high as in L4 and L5. Compared to the reference case no positive effect of the seat pan angle and the load limiting countermeasures could be observed. In most of the lumbar vertebrae the flexion moment was slightly increased relative to the reference.

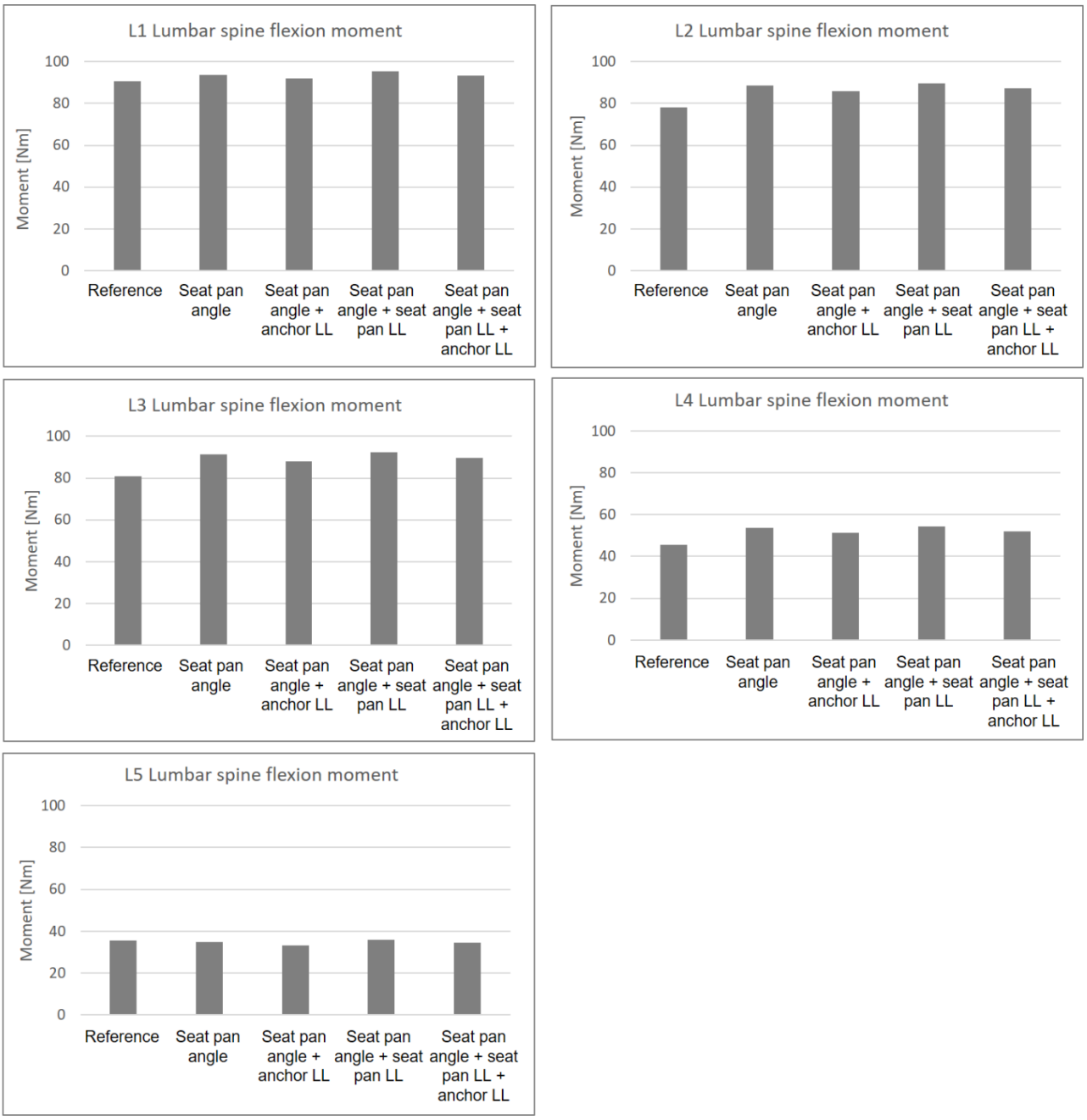

Figure 79 Lumbar spine flexion moments

ASIS forces in the x-direction were analysed as evaluation criteria for the pelvis loading. The forces were determined for the defined sections on the left and right side of the pelvis (Figure 80).

In the reference case, the lowest ASIS forces were received. The reason is the different lap belt routing caused by the further forward-located lap belt fixation points. This lap belt geometry also resulted in a larger forward displacement of the pelvis relative to the seat. For the other

countermeasure combinations higher ASIS forces were received compared to the reference. The difference between the combinations is very small. It also can be seen in Figure 80 that the ASIS forces on the left and on the right are nearly at the same level for each countermeasure combination.

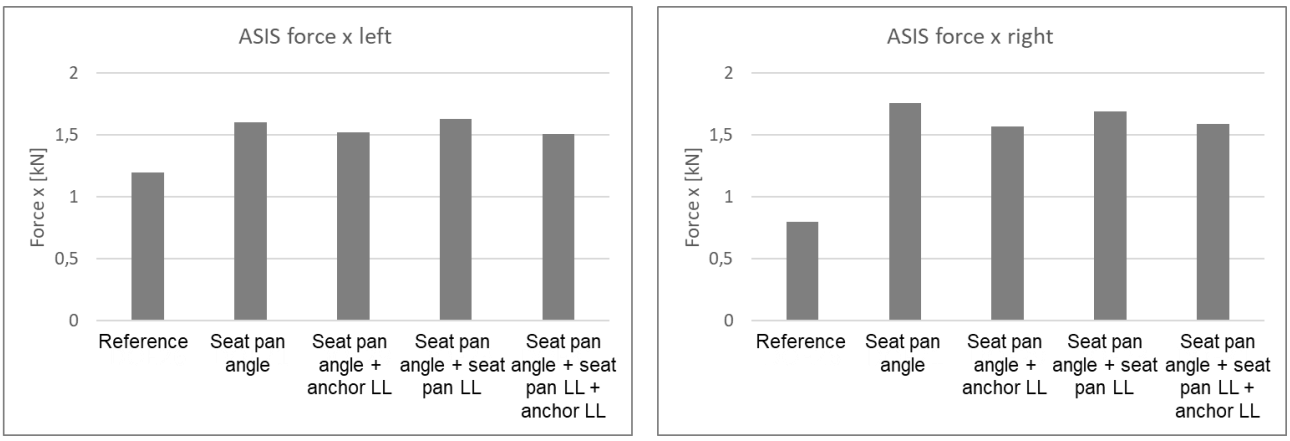

Figure 80 Pelvis ASIS forces x left & right

Discussion & Conclusion:

In this study, performed by Volkswagen, considering specific boundary conditions and applying the THUMS TUC-VW AHBM, submarining was observed at least on the buckle side in the reclined position. The triple pretensioner alone was not sufficient to prevent this partial submarining and therefore additional countermeasure combinations were considered. Countermeasure combinations including a steeper seat pan angle and / or further forward located lap belt fixation points were most effective to avoid the submarining, however these also led to increased lumbar spine compression forces. Using seat- and belt-related load limiting countermeasures, the lumbar spine forces could be reduced. For a further reduction of the lumbar spine forces, other load limiting countermeasures not considered in this limited study, e.g. a buckle load limiter, could be options for further improvement. Lumbar spine forces seem to be very sensitive to the pelvis rotation during the crash.

Overall, a broader range of parameter variation is necessary to find a well-balanced solution considering all loading relevant for the reclined occupant. An airbag, also influencing the whole occupant kinematics in the crash phase, should be included for an assessment of the head, neck and thorax loadings.

3.3.3.3 Double lap belt pretensioning

In this study performed by Toyota, the THOR sled tests performed in Task 2.4 (deliverable D2.5 [1]) were simulated using THUMS model v4.1. The objective was to evaluate the effect of the double lap belt pretensioning for an occupant seated with a 48° reclined seat back. External load measurements and THUMS kinematics were compared to THOR simulations performed by BASt [1]. Furthermore, the THUMS injury predictions with regard to a reclined seat back were analysed. More precisely, submarining occurrence, pelvis, lumbar spine and rib cage injuries were studied.

Method:

The simulations used the virtual environment of the sled tests performed in Task 2.4. The seat Finite Element Model (FEM) was initially developed in [30] and was further validated by Autoliv to simulate the hardware used in the sled tests.

The belt assembly model and anchorage point geometry were provided by Autoliv. Only the belt webbing material properties were changed to internal Toyota belt material properties. The State Of

The Art (SOTA) belt consisted of a seat-mounted belt composed of a shoulder retractor with a load limiter and a pretensioner, a Crash Locking Tongue (CLT) at the buckle. The CLT prevents webbing transport between the shoulder belt and the lap belt. The double lap belt pretensioning was based on the SOTA belt with the addition of two lap pretensioners: one at the external anchorage point and one at the buckle.

The Total Human Model for Safety (THUMS) 50th percentile male was used to simulate the car occupant. The THUMS human finite element model was jointly developed by Toyota Motor Corporation and Toyota Central R&D Labs (TCRDL) in 2010. It represents an average-sized adult male occupant (39 YO, 175 cm and 77 kg). The model is fully deformable and consists of around 2,000,000 elements [36]. The THUMS v4.1 has an updated geometry for its pelvis and lumbar spine to represent more closely the available frontal impact PMHS kinematics. The THUMS v4.1 has also a more accurate definition of its rib cortical bone thicknesses to improve rib fracture prediction.

The THUMS model was positioned in the semi-rigid seat trying to match the THOR dummy position measured in the sled tests and replicated with the THOR FEM model developed by NHTSA and UVa. The THUMS H-point (middle of the two acetabulum centres) and the THUMS Antero-Superior Iliac Spine (ASIS) were aligned with those of the THOR dummy. Gravity was applied on the THUMS model to set the final posture. Figure 81 shows the THUMS postures in upright and reclined seat back superimposed with the THOR FEM model.

The contact between THUMS and belt was defined with a static friction coefficient of 0.4 and a dynamic friction coefficient of 0.25.

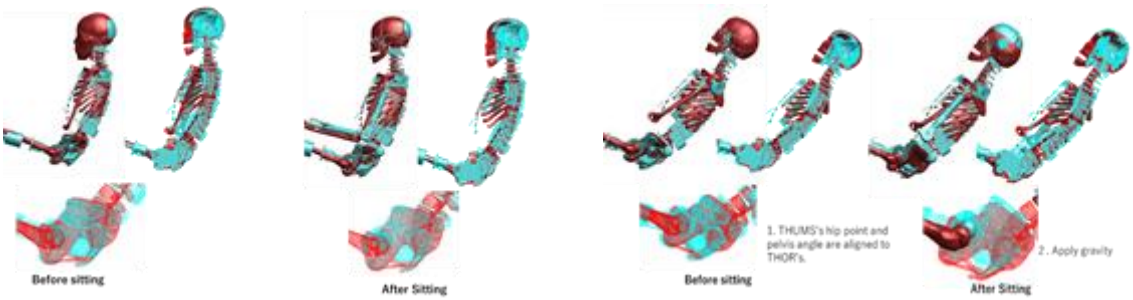

THUMS positioning: Upright seat back THUMS positioning: Reclined seat back

Figure 81 THUMS (in red) & THOR FEM (in blue) initial positions

The model was run on 128 CPUs using LS-DYNA MPP version LS971R7 with a minimum time step of 2.7 E-7 s.

The model was subject to three different crash pulses identical to the ones used in the THOR sled tests:

- 50 km/h Full-Width Rigid Barrier (FWRB) pulse, as used in the Euro NCAP FW protocol
- 38.5 km/h SCP1 and 23.3 km/h LTAP OD2 pulses, as defined in OSCCAR WP1. These pulses represent the most frequent accident configurations for intersection accident scenarios and are the most severe ones as shown in OSCCAR deliverable D1.3 [6].

The simulation matrix is shown in Table 25. Seat deformations (seat pan and anti-submarining pan displacements), seat belt forces and THUMS measurements were compared to the THOR measurements. The prediction of bone fractures for the THUMS model was analysed by looking at the cortical bone strains. A first principal strain above 2% in an element was defined as a fracture.

ID	Pulse	Velocity [km/h]	Sled angle [°]	Seat back angle	Restraint system
1	FWRB	50	0	Upright	SOTA belt
2	FWRB	50	0	Reclined (48°)	SOTA belt
3	FWRB	50	0	Reclined (48°)	Double lap belt pretensioning
4	SCP1	38.5	15	Reclined (48°)	Double lap belt pretensioning
5	LTAP OD2	23.3	15	Reclined (48°)	Double lap belt pretensioning

Table 25 THUMS simulation matrix

Results:

The THOR and THUMS simulations were in good agreement (Table 26). As expected, no submarining was observed in the upright seat-back configuration whereas it was observed on the buckle side in the reclined seat-back configuration with the SOTA belt. However, the introduction of the double lap belt pretensioning allowed to avoid submarining. Additional curves are displayed in Appendix 2.1, Table 36.

Upright seat back & SOTA belt (no submarining)	Reclined seat back & SOTA belt (submarining @ 72 ms)	Reclined seat back & double lap belt pretensioning (no submarining)
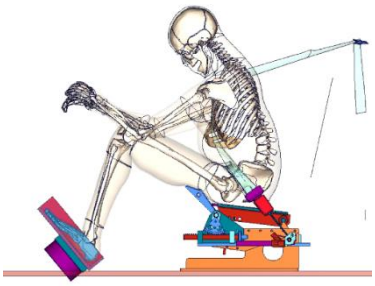	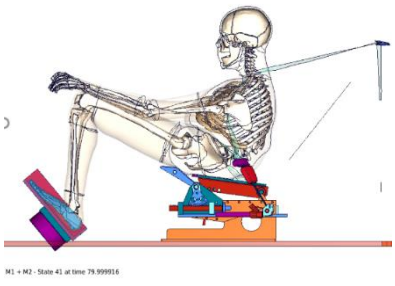	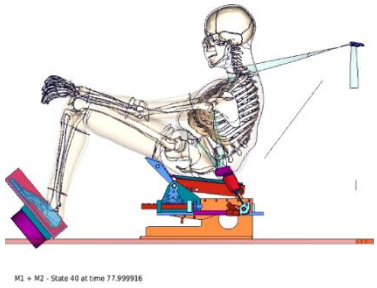
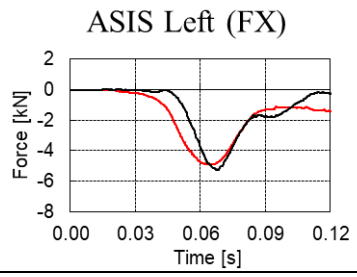	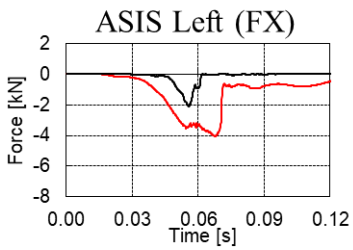	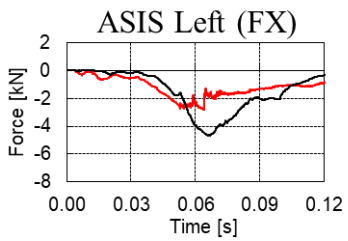
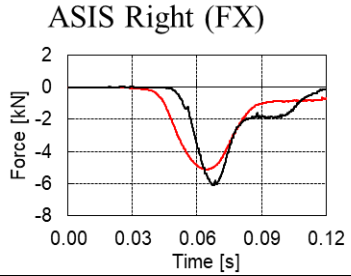	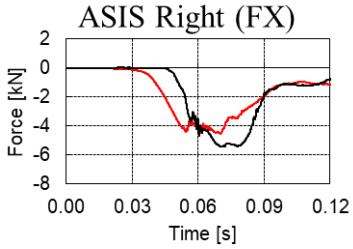	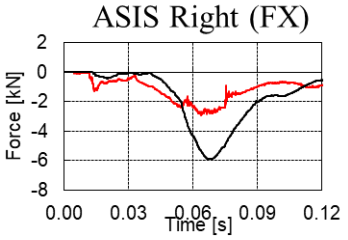

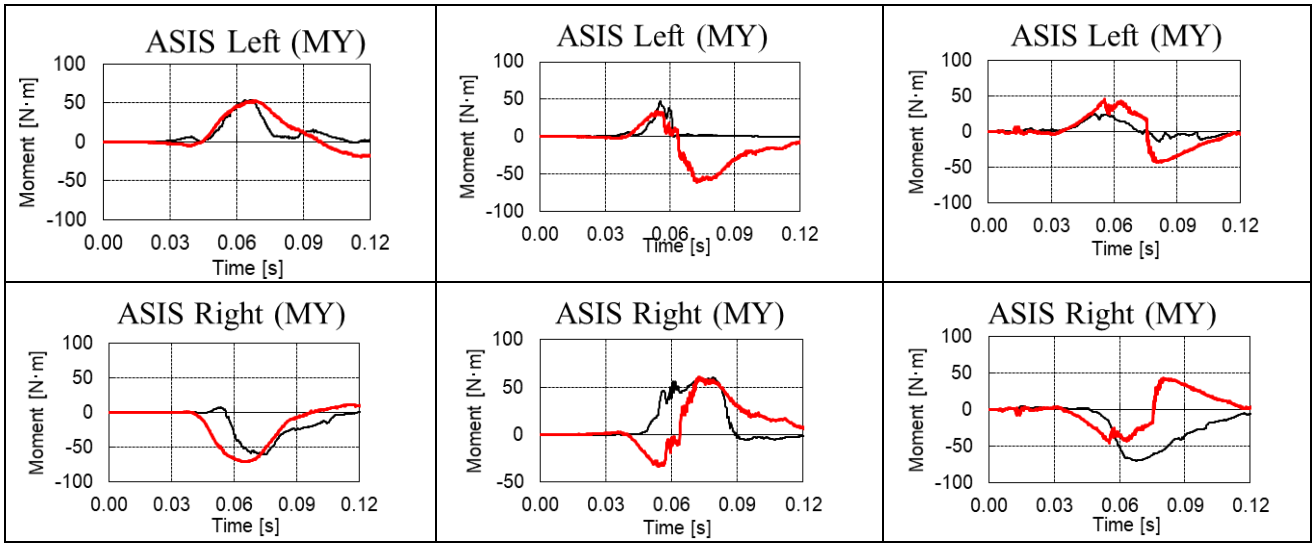

Table 26 Effects on submarining (Black: THOR, Red: THUMS)

The double lap belt pretensioning also helped to reduce some of the strains measured in the spine and in the ribs. Mainly, T1, T11 to T12 and L1 to L4 bone strains were reduced in simulation n°3 compared to simulation n°2 (Figure 82).

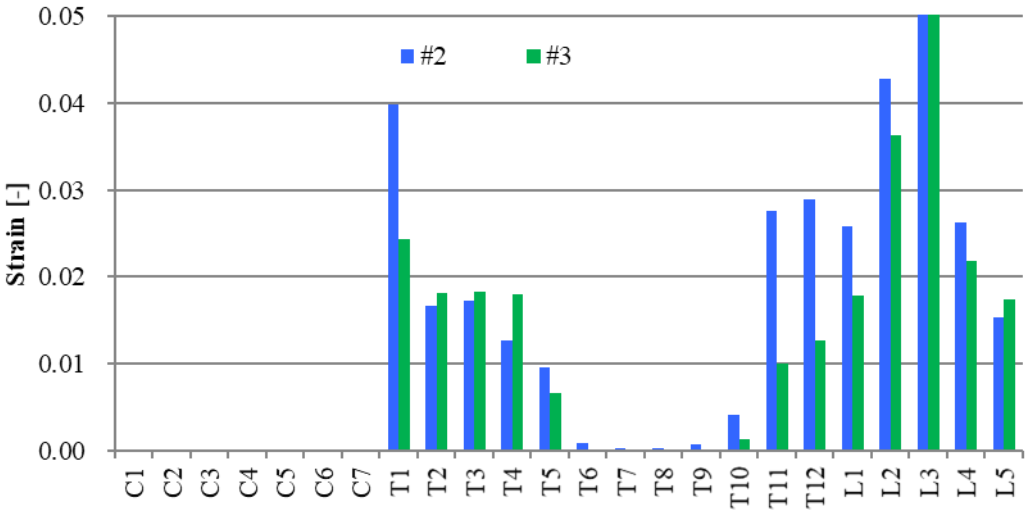

Figure 82 Strain value in spine vertebrae. Blue for simulation n°2 (Reclined seat back with SOTA belt), Green for simulation n°3 (Reclined seat back with double lap belt pretensioning)

Similarly, a reduction of right rib strains was observed (Figure 83). The pelvis strain values were identical between simulation n°2 and simulation n°3 and predicted in both cases a pelvic bone fracture at the right and left ASIS locations (Figure 84). Table 27 summarises the main results for the overall simulation matrix.

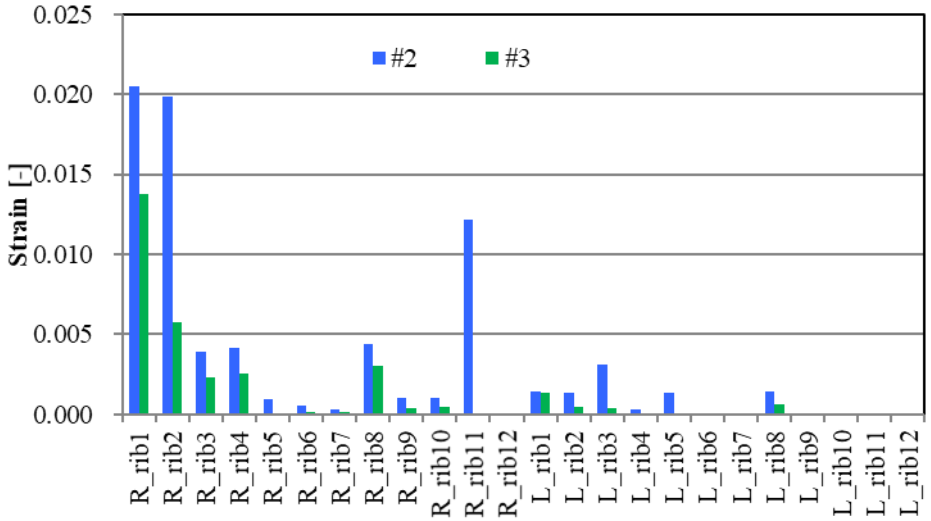

Figure 83 Strain value in ribs. Simulation n°2 in blue, simulation n°3 in green

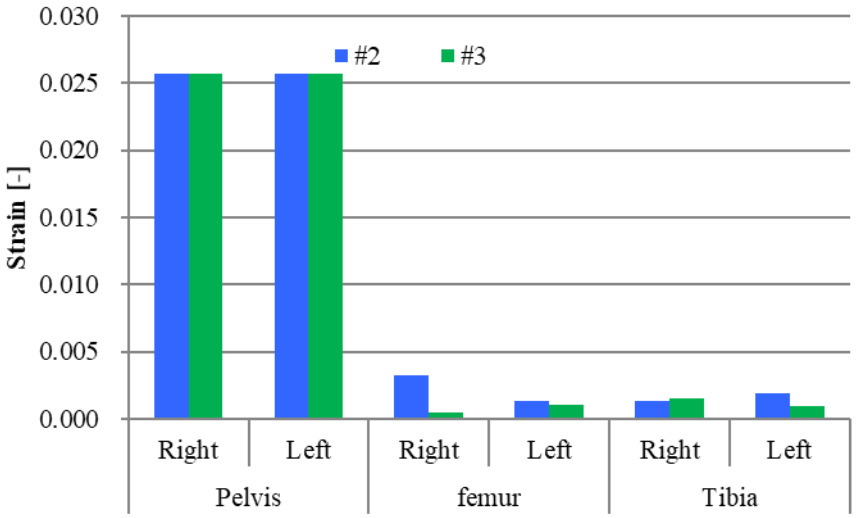

Figure 84 Strain value in pelvis, femurs & tibias. Simulation n°2 in blue, simulation n°3 in green

ID	Pulse	Velocity [km/h]	Sled Angle [°]	Seat back angle	Restraint system	Pelvis stroke [mm]	Sub-marin-ing	Bone fracture
1	FWRB	50	0	Upright	SOTA	159	No	Right Rib 1
2	FWRB	50	0	Reclined	SOTA	227	Yes	T1, T11, T12 L1, L2, L3, L4 Right Rib 1 Left & Right ASIS
3	FWRB	50	0	Reclined	Double lap belt pretensioning	164	No	T1, L2, L3, L4 Left & Right ASIS

4	SCP1	38.5	15	Reclined	Double lap belt pretensioning	76	No	No
5	LTAP OD2	23.3	15	Reclined	Double lap belt pretensioning	105	No	No

Table 27 Pelvis stroke, submarining occurrence & bone fractures in the different simulations

Discussion:

The full-width crash was the most severe and the only one where submarining and bone fractures were observed. The submarining occurrence was visible from the animation files, but little difference was observed in ASIS forces and moments between simulations n°2 and n°3. Further investigation was performed on the belt model by adding some shell elements on the external end of the lap belt. This resulted in no submarining in simulation n°2 and thus revealed some uncertainties in the submarining prediction that could be affected by the restraint system modelling choice.

Conclusion:

The double lap belt pretensioning was effective in reducing pelvis stroke and submarining for the defined simulation conditions. The double lap belt pretensioning also reduced the number of fractures predicted in the spine and chest areas. The strains in the pelvis bones were not increased with the double lap belt pretensioning but ASIS fractures were predicted.

The seat belt webbing behaviour was sensitive and the choice of modelling may lead to slightly different kinematics of the HBM, leading to a different prediction of submarining for configurations close to submarining. A probabilistic approach for submarining prediction using ASIS force and moment of HBMs may quantify in a more robust way the risk of submarining than any single analysis of the animation files.

3.3.3.4 Energy absorbing seat structure

Current restraint systems available in vehicles running on the road provide adequate safety for the 50th percentile anthropometric population in standard seating postures. However, the benefit of these restraint systems needs to be evaluated from two perspectives: population heterogeneity and advanced seating postures. In the baseline studies conducted in deliverable D2.1 [2] these two perspectives are discussed in Case 3, which comprises an obese occupant in a reclined seating posture. It is observed that in such a seating configuration, high loading on the thorax and lumbar spine is one of the major concerns for obese occupants. Therefore, the aim of this study performed by Mercedes is to develop a concept to reduce loads in the thoracic and lumbar regions by the introduction of a seat track load limiting system based on the generic vehicle environment developed in deliverable D2.1 [2] for both 50th percentile male and obese occupants.

Method:

The seat track load limiter (Seat LL) is a concept that incorporates the integration of a crush element into the seat track. The characteristics of the crush element are illustrated in Figure 85. These characteristics (nature of curve) are formulated based on previous research [45] and serve as illustration. Final threshold values are derived based on the optimisation study done during the course of this study.

The seat track load limiting function was incorporated in the OSCCAR generic seat system [3] by modelling it as simplified one-dimensional elements. The characteristics of these one dimensional

elements are intended to represent a mechanical device which dissipates energy by shearing action in the metallic structure. The seat track LL was represented by two systems in left and right seat track proximity. The seat was then integrated into the sled environment developed and discussed in deliverable 2.1 [2]. Seat pan and backrest were rotated by 60° relative to the floor of the generic vehicle. The generic full-frontal crash pulse defined in WP1 was used to evaluate the seat track load limiting characteristics as illustrated in Figure 86. The collision velocity was 40 km/h (FF40). No airbag systems were deployed in the seat track LL optimisation study for the full frontal pulse and contact settings regarding the instrumentation panel were deactivated.

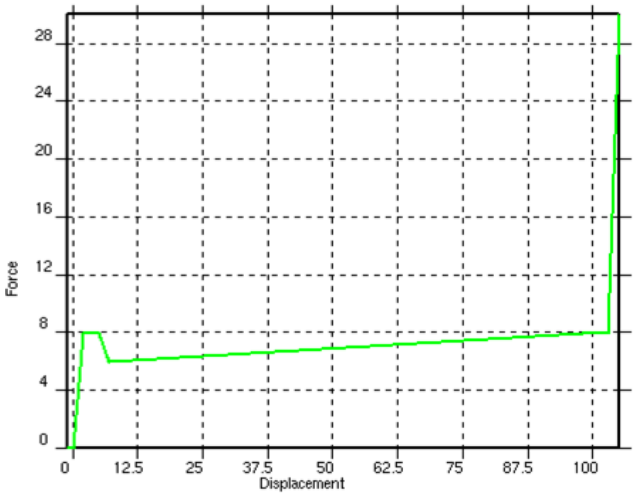

Figure 85 Crush element stiffness function

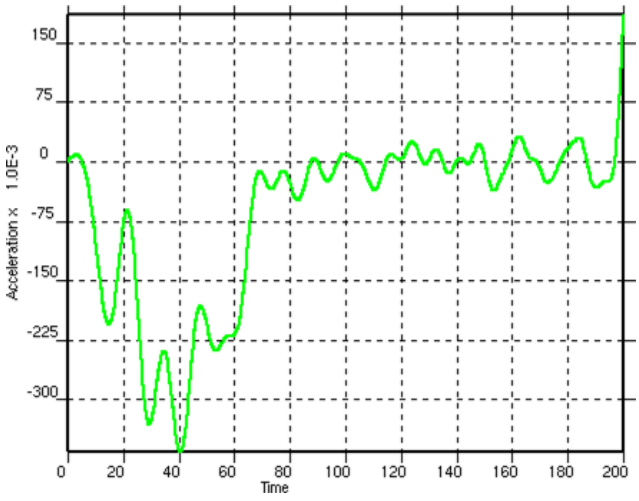

Figure 86 Generic full frontal pulse

A seat-integrated belt system with a belt load limiting of 2.1 kN was used for the 50th percentile male occupant and 4 kN for the 50th percentile obese occupant. Figure 87 (a) shows the sled set-up with the 50th percentile occupant in the reclined seating posture. Belt forces and lumbar forces were monitored to determine the benefit of the system. Furthermore, Figure 87 shows the location of section forces on the belt (a), and lumbar section forces (b) used for monitoring. A local coordinate system was defined for each of the lumbar vertebrae, and z-forces (longitudinal human body axis) formed the primary evaluation parameter.

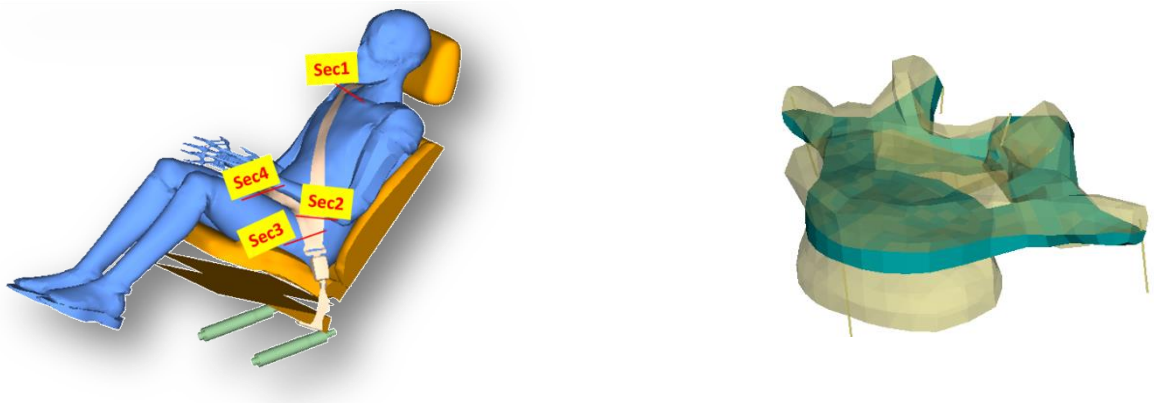

(a.) (b.)

Figure 87: Section forces on the belt (a) & lumbar vertebra (b)

The simulation matrix is shown in Table 28 below. The performance of the seat track LL was first evaluated in the reclined seating posture with a standard 50th percentile male occupant Human Body Model (THUMS-TUC 2020). The threshold value for the actuation of the system was the varied

parameter, as represented in ID 1 to 4 in the following table. The lumbar section forces, the seat belt section forces and the seat displacement were taken as parameters for setting a system threshold value that could also be aligned to the requirements of the 50th percentile obese model.

ID	Pulse	Velocity [km/h]	HBM Model	Activation Threshold
Pre-study				
1	FF40	40	THUMS-TUC 50th %ile male	No Activation
2	FF40	40	THUMS-TUC 50th %ile male	12 kN
3	FF40	40	THUMS-TUC 50th %ile male	16 kN
4	FF40	40	THUMS-TUC 50th %ile male	20 kN
5	FF40	40	THUMSv4 Daimler 50th %ile obese male	16 kN
Main Study				
6	SCP06	63	THUMS-TUC 50th %ile male	7 kN
7	SCP06	63	THUMSv4 Daimler 50th %ile obese male	7 kN

Table 28 Simulation Matrix

Results & discussion:

Figure 88 illustrates the response of the aforementioned parameters. The results suggest that the belt forces (shoulder region) are reduced with a lowering of the system activation threshold. This indicates that an activation of the system reduces the loads experienced in the torso.

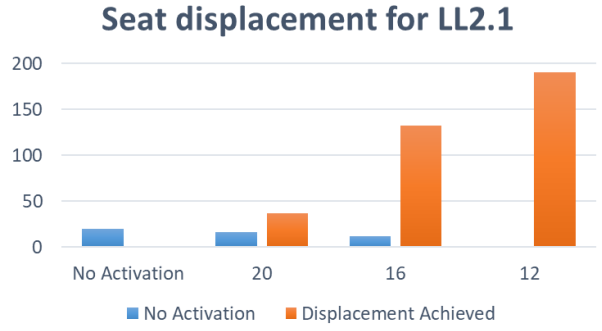

a.

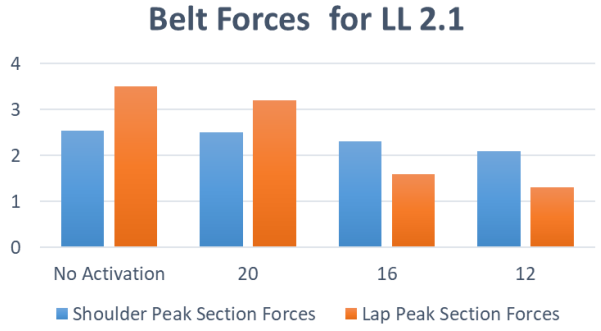

b.

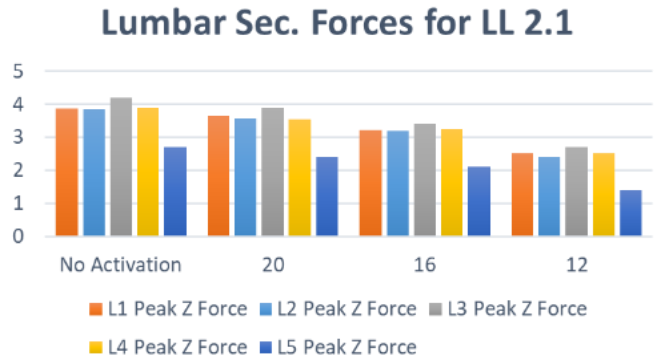

c.

Figure 88 Results of parameter variation

The reduction in lumbar forces (longitudinal to the human body) indicates that system activation had a positive effect on the injury risk to this body region. The 3rd lumbar vertebra experienced the maximum force in this reclined seating posture. The results from the 50th percentile male model suggest that a system activation threshold of 12 kN is appropriate for load reductions in the thoracic and lumbar region. However, as the system also needs to fulfil the requirements of a 50th percentile obese model, a 16 kN activation value is used for further study. A Seat track LL with a 16 kN activation was then applied to the 50th percentile obese male model and similar findings were observed. Figure 89 illustrates the kinematics of both occupant variants for a system activation threshold value of 16 kN.

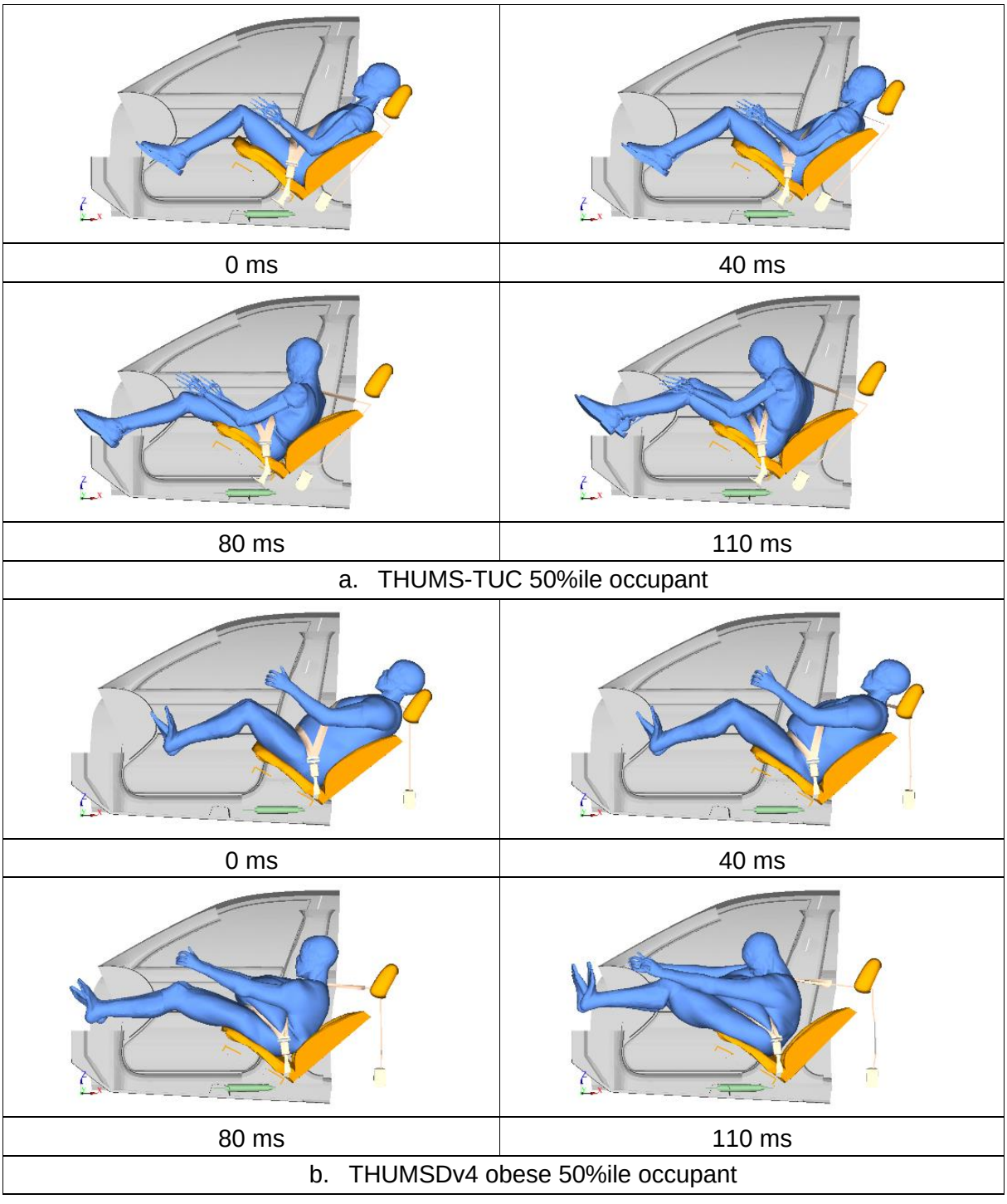

Figure 89 Results of parameter variation

The system response for the 50th percentile obese male model is illustrated in Figure 90. A general reduction in lumbar loads was observed due to inclusion of the seat track LL, however, some model-dependent effects were also observed. The flexing of the spine was predominant for the obese 50th percentile male model (basis THUMSv4) compared to the 50th percentile male occupant model (THUMS-TUC basis THUMSv3), which led to reduced lumbar section forces in the spine.

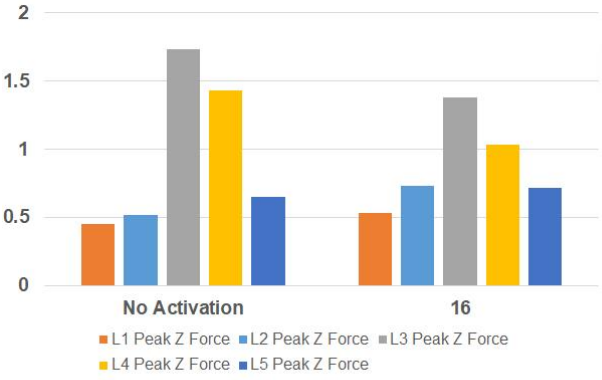

a. Lumbar section forces for Obese occupant for different system thresholds

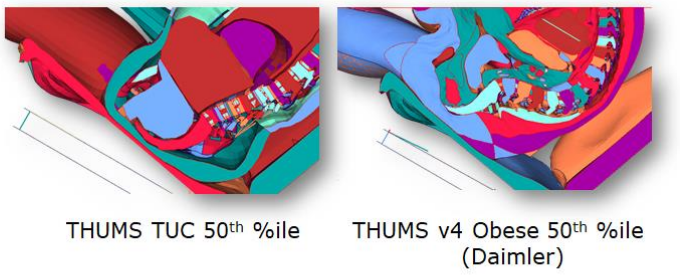

b. Flexion of Lumbar Spine

Figure 90 Influence of system activation on lumbar forces

The Seat track LL with a 16 kN activation threshold is further evaluated for the SCP06 crash configuration. This SCP pulse has high deceleration components in both longitudinal and lateral directions. The expectation is therefore that new system thresholds would be required to reduce the loads on the lumbar and thoracic region. A simulation of a Seat track LL with a 16 kN activation threshold and a 50th percentile male occupant model suggested that the maximum force experienced in the track sections are 8 kN. Therefore, a seat track LL activation threshold force of 7 kN was considered for further evaluation. Figure 91 (a & b) shows the kinematics of the 50th percentile occupant male in this collision scenario for a system threshold of 7 kN. The occupant in this scenario was observed to move towards the door trims and the B-pillar. Head contact with the B-pillar was observed for both standard and obese 50th percentile male occupant.

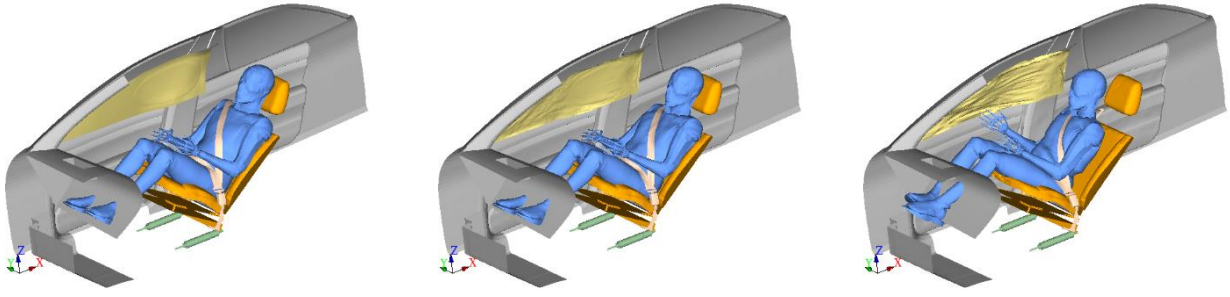

0 ms 40 ms 80 ms

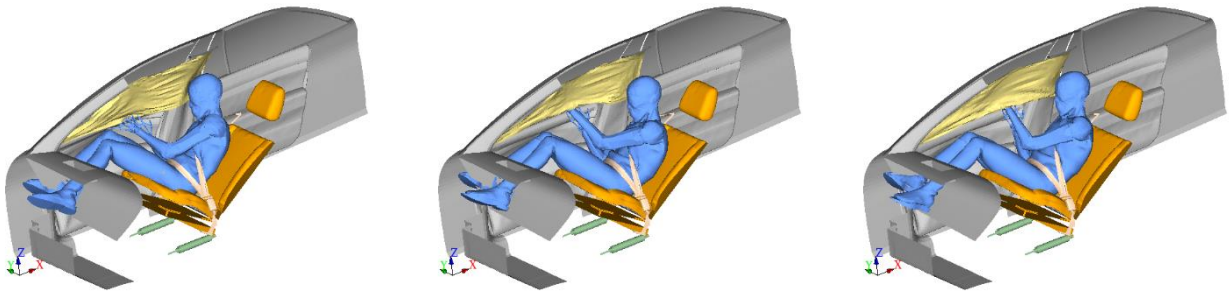

120 ms 160 ms 200 ms

a. Occupant kinematics for 50%ile male model

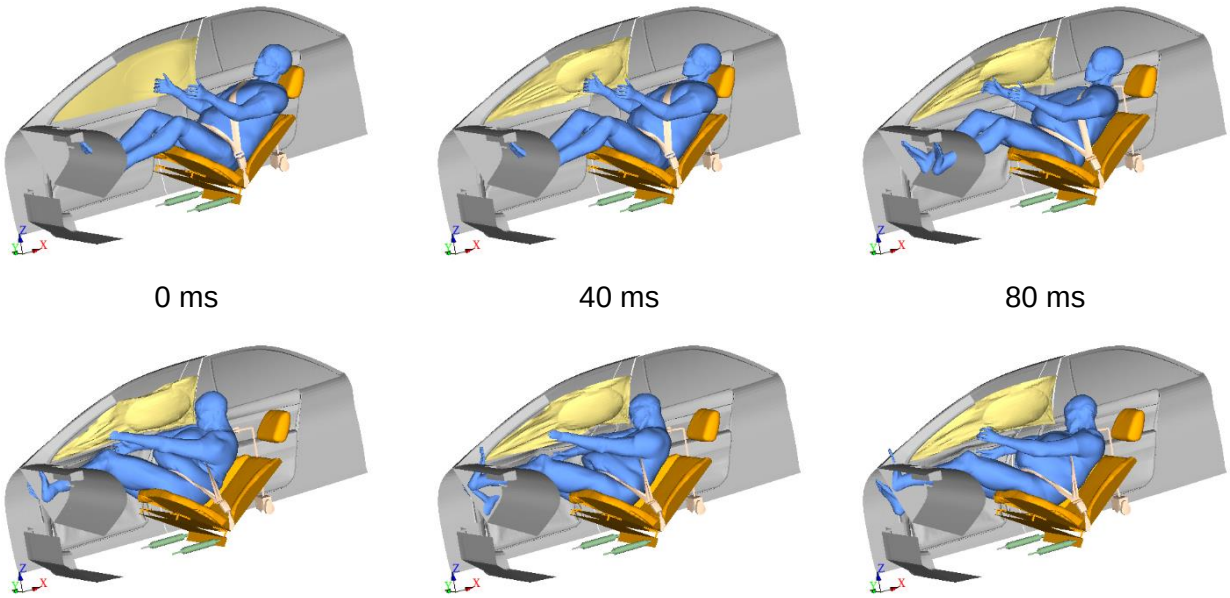

b. Occupant kinematics for 50%ile obese male model

Figure 91 Occupant kinematics for 50th percentile male models (SCP06)

The coverage of the existing curtain airbag modelled in the current generic vehicle environment was not sufficient to prevent the head contact. Another observation was the significant lateral movement of the neck and slipping of the belt inwards towards the neck, which could be a potential injury source. The benefit of the Seat track LL in this collision scenario is assessed based on the lumbar forces and seatbelt forces as shown in Figure 92 for the standard 50th percentile occupant. A reduction in both lumbar and seatbelt forces was observed, however, the reduction is not very significant in the belt section forces. Similar findings were also observed for the obese occupant.

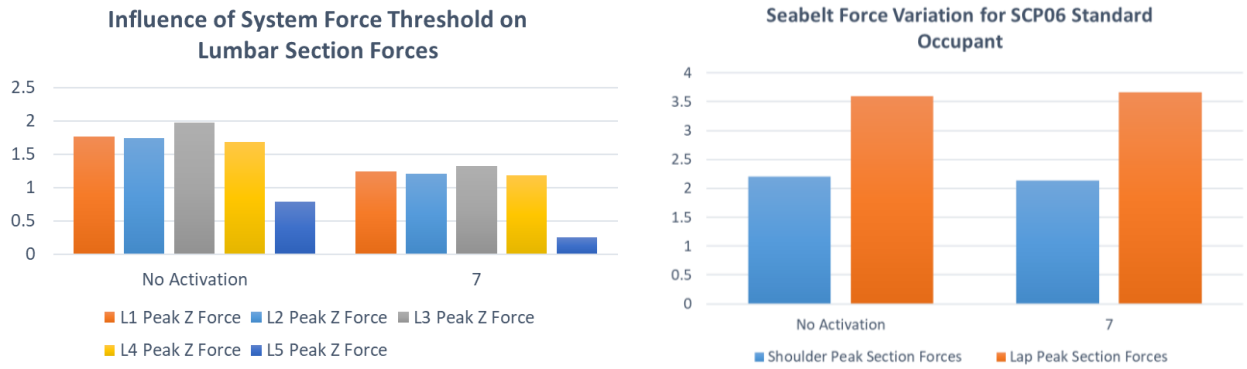

a. Lumbar forces b. Belt forces

Figure 92 Lumbar & belt forces for THUMS-TUC model regarding SCP06

Figure 93 illustrates the injury risk analysis for the standard 50th percentile male occupant for the SCP06 crash configuration. The Dynasaur tool was used for the post-processing of the results.

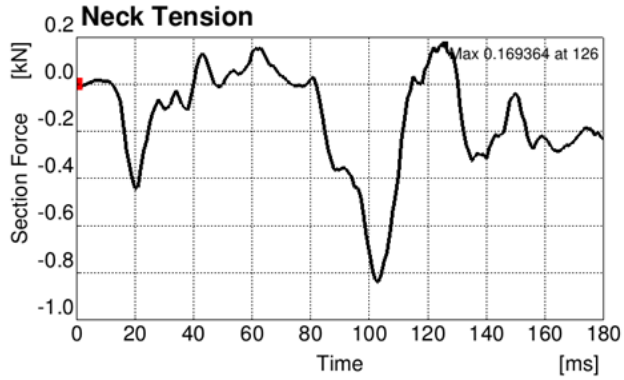

a. Neck Tension Force

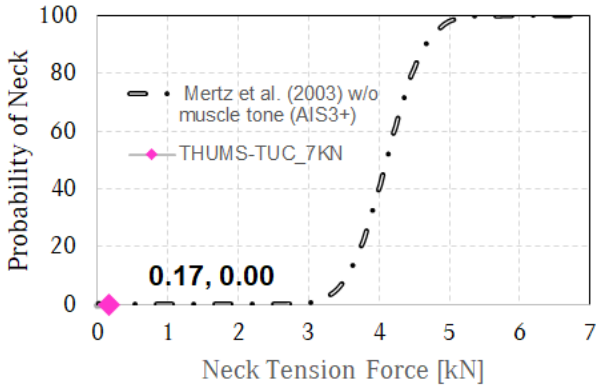

b. Neck Tension Force (IRC – AIS3+)

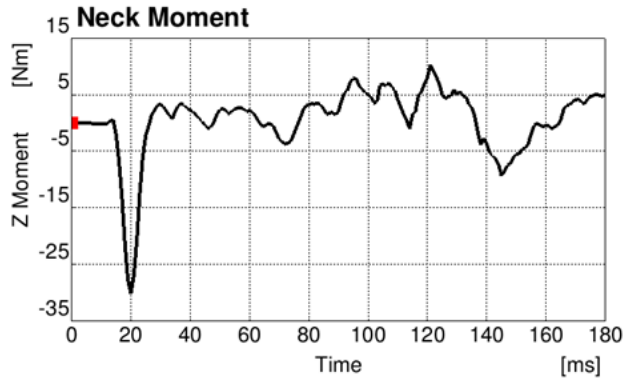

c. Neck Y Moment

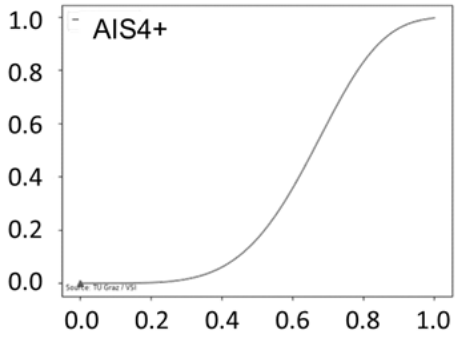

d. Head Injury Risk

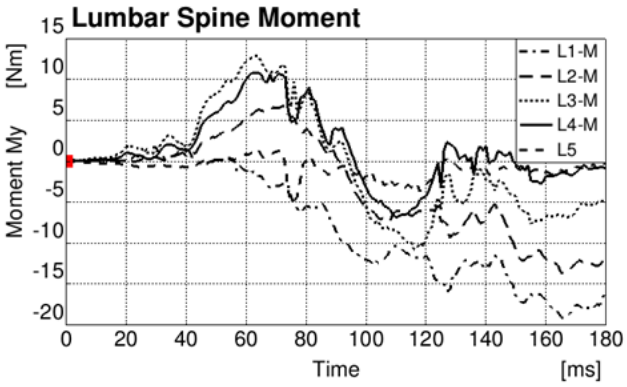

e. Lumbar Spine Moment

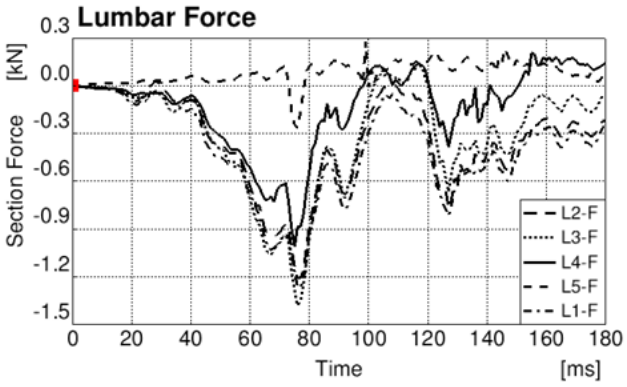

f. Lumbar Forces

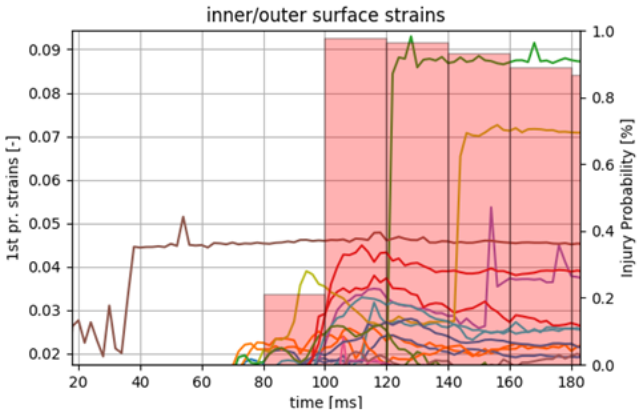

g. Rib fracture risk

Figure 93 Injury risk for 50th percentile male model (SCP06)

1. No head injury risk was observed for the crash configuration. This could be due to the use of an AIS4+ injury evaluation scale; a reduction in AIS scaling may lead to injuries being observed. Moreover, the head touches the B-pillar in this scenario and some level of protection is provided by the deployed curtain airbag.
2. No risk of neck injury was observed based on the Mertz injury risk (IR) curve.
3. A high rib fracture risk was observed for a 45 YO occupant, with 7+ fractured ribs. The fractures in the left thoracic region were due to loading from the belt, whereas on the right they were due to interaction with the seat structure.
4. The lumbar forces were lower than in the full-frontal load case, due to a lateral movement of the occupant. However, a benefit of the system could be observed.

Figure 94 illustrates the injury analysis for the obese 50th percentile male occupant in the SCP06 crash configuration.

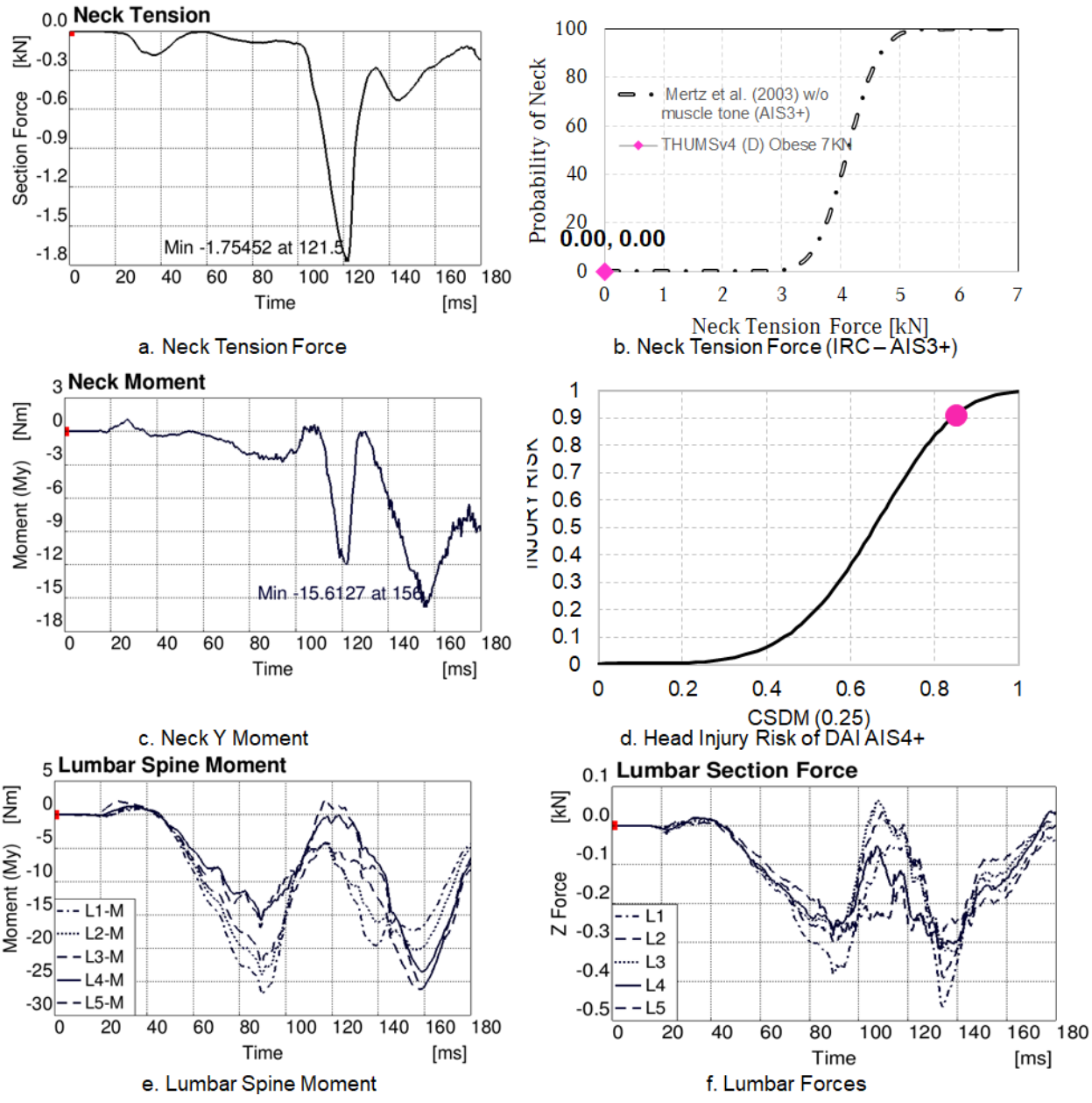

a. Neck Tension Force
b. Neck Tension Force (IRC – AIS3+)
c. Neck Y Moment
d. Head Injury Risk of DAI AIS4+
e. Lumbar Spine Moment
f. Lumbar Forces

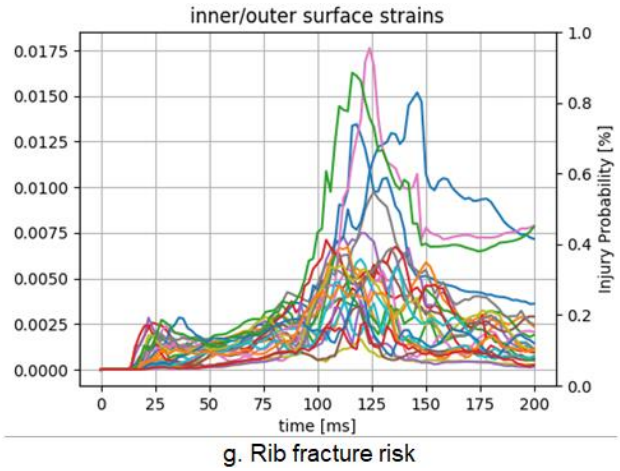

Figure 94 Injury risk for 50th percentile obese male model (SCP06)

1. A head injury risk of around 90% was observed for the obese occupant in this crash configuration. The hard contact with the B-Pillar and the inertia of the moving occupant could be possible reasons for such a high injury risk.
2. No risk of neck injury was observed based on the Mertz injury risk (IR) curve. Peak neck moments of 17 Nm were experienced by the 50th percentile obese occupant.
3. A high rib fracture risk was observed for a 45 YO Occupant with 7+ fractured ribs. The fractures in the left thoracic region were due to loading from the belt, whereas on the right due to interaction with the seat structure.
4. The lumbar forces were lower than in the full-frontal load case due to a lateral movement of the occupant. Furthermore, the lumbar forces were lower than for the standard 50th percentile male occupant due to flexion of the lumbar spine, as in the full-frontal crash configuration.

Conclusion:

The Seat track LL protection principle investigated in this study seems to provide reasonable benefit for the lumbar loads and associated injury risk of occupants travelling in reclined positions. Such a system needs to be adaptive in nature to respond to different types of pulses and population heterogeneity. In this study, a common threshold was achieved for 50th percentile normal weight and 50th percentile obese occupants for both full-frontal and SCP pulses. However, adaptive system characteristics are required if such a system also has to protect occupants with small statures like a 5th percentile female. Currently, with the use of both 50th percentile normal and obese male occupant, the benefit of this system could be demonstrated and the models could be used to also assess the potential injury risks. Model-dependent effects were observed when using the THUMS-TUC 50th percentile male model and the THUMSv4 Daimler 50th percentile obese model with regard to spine flexion. However, there is a need to further develop an injury risk curve for the evaluation of lumbar injuries.

3.3.3.5 Influence of different postures on occupant loading and kinematics

With the purpose of reflecting real-world crashes in present-day and future cars, the objective of this study performed by Volvo Cars was to investigate the effect of sitting postures on kinetic and kinematic responses. Specifically, the research questions addressed variations of occupant postures when exposed to three different real-world intersection crashes, representative of predicted future

crashes. Special focus was given to the lap-belt interaction and its influence on varieties of lower-extremity postures and impact direction.

Method:

A simulation series using a mid-sized male HBM in the front passenger seat of a midsize SUV was performed; investigating posture variations of the lower extremities, the torso, the upper extremities and the head (Figure 95). In total, the simulation matrix included 35 posture combinations in three different crash configurations. Details on the study set-up are presented in [46].

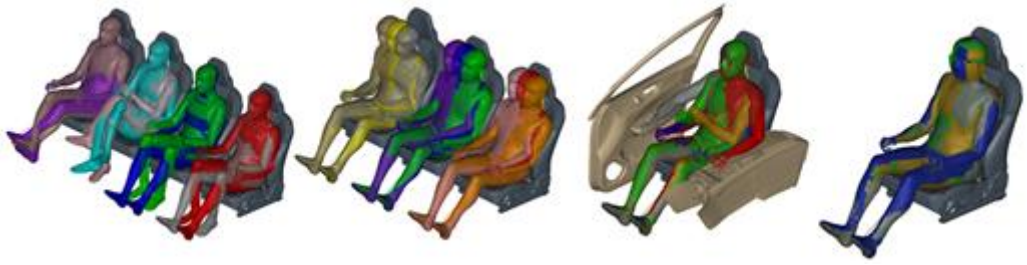

Figure 95 The posture variants investigated. From left to right: lower extremities, torso (nominal / leaning forward / semi-reclined), upper extremities & head postures

Figure 96 shows the mid-sized male HBM (SAFER HBM v9.0.1) in its simulation environment, positioned as a front seat passenger. The HBM was restrained using a three-point pyrotechnically pretensioned load-limited seatbelt. The frontal passenger airbag was activated in all crash configurations, while the seat-mounted side airbag and the Inflatable Curtain were activated in the side impact crash configurations only. The seatback angle was set to 25 degrees for all postures, except to 30 degrees when the occupant was semi-reclined.

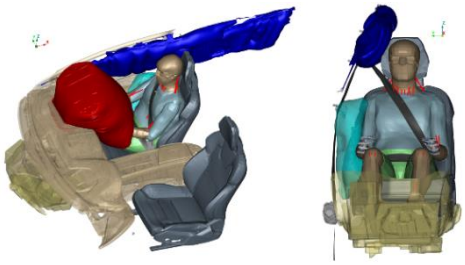

Figure 96 Simulation set-up

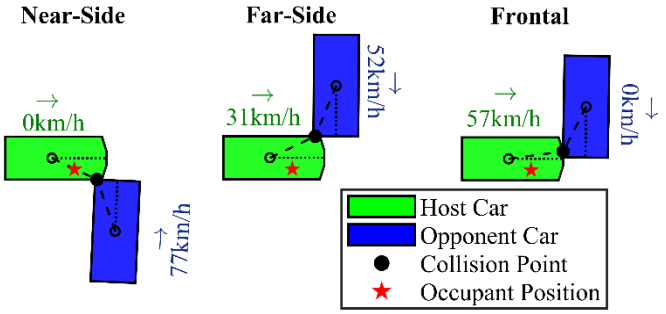

Figure 97 Visualisation of crash configurations

The three crash configurations (Figure 97) were derived from studies in OSCCAR WP1 [47], based on data from Swedish crash databases. The near-side configuration represents a lateral impact to the front right corner when at rest, by another car travelling at 77 km/h. The far-side configuration is a lateral impact to the front left corner, when traveling at 31 km/h, by another car at 52 km/h. The frontal configuration is an impact with almost 50% left-side overlap when traveling at 57 km/h into another car's right front side. The crash pulses were derived from car-to-car simulations and applied to a sled model with deformable interior using 6-DOF.

The simulations were performed using the explicit finite-element solver LS-DYNA MPP s R9.3.0. As part of the study, a method using CORA (Correlation and Analysis Method) was used to systematically investigate which postures have the largest influence on occupant kinematics. This is further described, as well as the complete test matrix, in [46].

Results:

Overall, it was found that the lower extremity positions were those with the largest posture influence on the whole-body kinematics for all tested crash configurations, followed by the torso position. In all simulations the lap-belt stayed on the pelvis and no submarining was observed.

In the frontal crash configuration, crossing the knees resulted in up to 7.5 degrees increase in maximum pelvic angle, as compared to nominal. This also resulted in the highest pelvis excursion among the lower extremity variants (Figure 98) and among the lowest for lumbar loads (Figure 99). The lumbar resultant load, measured at L5, was reduced by up to 60% when the knees were crossed.

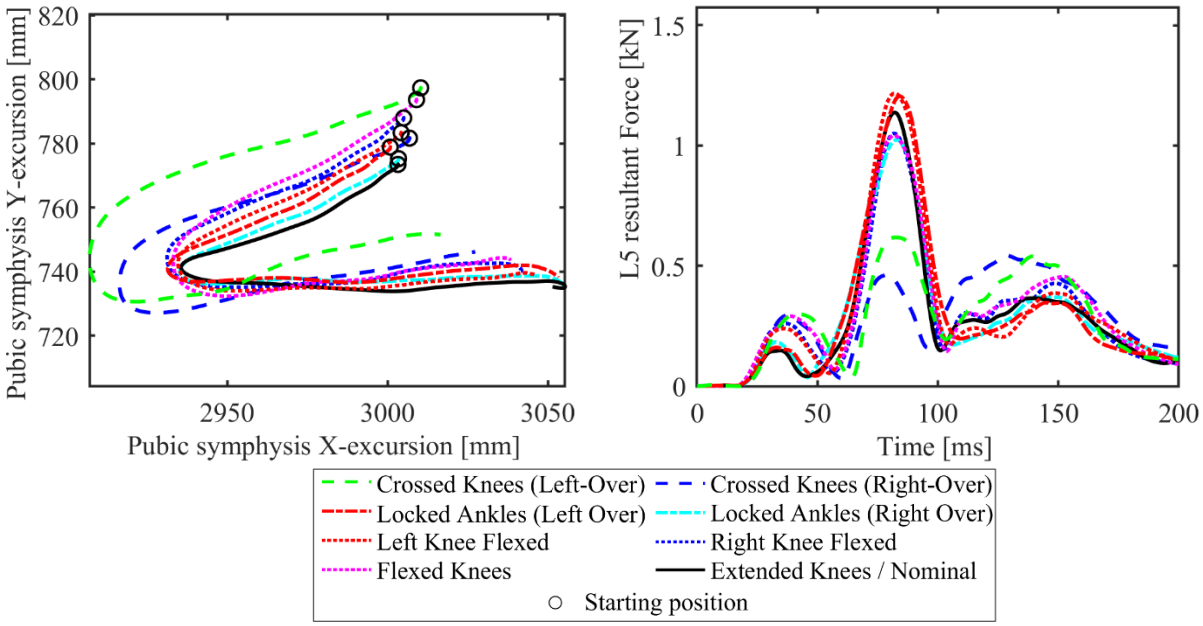

Figure 98 Pelvis excursion, measured at pubic symphysis, for lower extremity posture variants in frontal crash configuration

Figure 99 Lumbar load (L5) for lower extremity posture variants in frontal crash configuration

The semi-reclined posture in the frontal crash configuration resulted in increased sternum excursions of 28 mm, as compared to the nominal posture (Figure 100). In addition, a 7° larger torso rotation around the z-axis was observed and the lumbar load was increased from 1.1 kN to 1.3 kN (Figure 101). While, for the occupants leaning forward, a relative decrease in load (0.9 kN) was seen.

In the near-side configuration, the torso posture affected the interaction with the Inflatable Curtain and consequently affected the head rotations, resulting in higher rotational velocities (28 rad/s compared to 12 rad/s) for the occupant leaning outboard. In both side-impact configurations, leaning the torso in the coronal plane affected the torso and head kinematics by changing the interaction with the vehicle's interior. Additionally, in the far-side configuration supporting the upper extremity on the centre console resulted in increased torso excursions. Moreover, the response of the upper extremities was consistently sensitive to posture variations of all body regions. Further results from the study are available in [46].

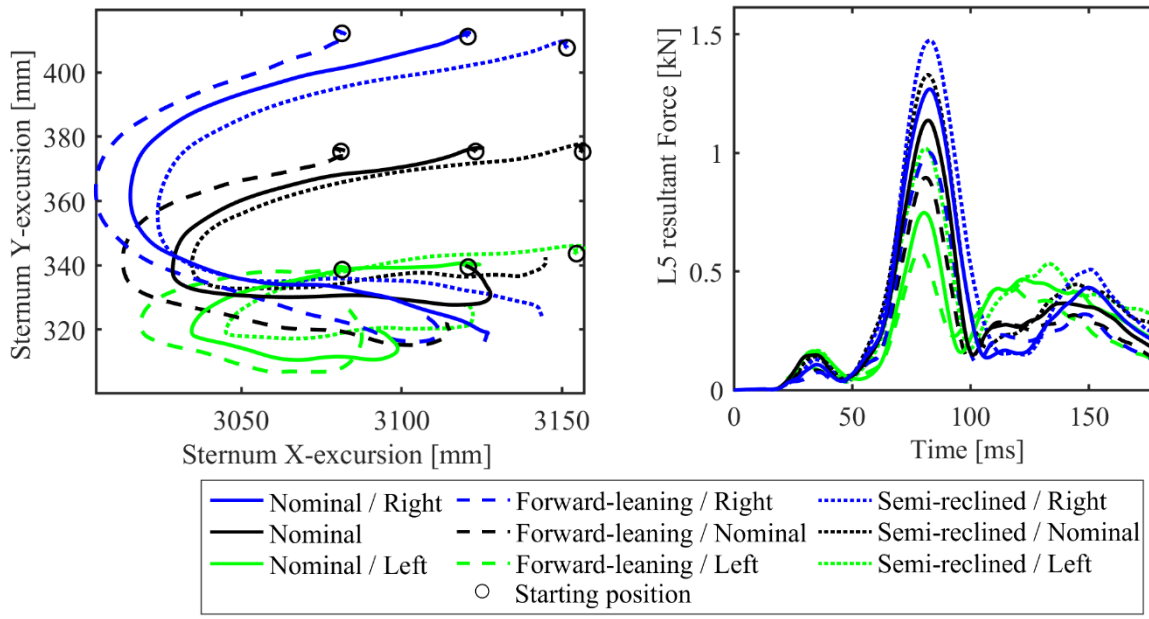

Figure 100 Sternum excursion for torso posture variants in frontal crash configuration

Figure 101 Lumbar load (L5) for torso posture variants in frontal crash configuration

Discussion:

In real-world traffic, passenger sitting postures are varied and, in many cases, deviate from the nominal posture used in standardised crash tests. This study showed that crossing the legs affected pelvis rotation and movement, which consequently also affected the rest of the occupant's body kinematics. It was found that changing the lower extremity posture can have a larger effect on the lumbar forces than changing the torso posture, within the degree of this study (Figure 99 and Figure 101). Crossing the knees of the HBM affected the initial pelvic angle as well as the interaction with the vehicle's dashboard. This overall behaviour is expected to be similar to a human, however, further studies are required to validate the relationship between lower extremity posture and pelvis. Considering that the interaction with the dashboard influenced the excursion of the occupant, variations in anthropometry and seat positions could have affected the pelvis kinematics as well.

The HBM was an enabler for performing this study. It was capable of adjusting postures that would not have been possible, nor likely relevant, to achieve with an ATD. Using omnidirectional models allows the assessment of oblique crash configurations, which can bridge the gap between regulatory testing and real-world crashes.

Although none of the combinations included in this test series are likely to be of injurious level, mainly due to the relatively low severity of the impacts, the trends with respect to influence on kinematics are important to understand. The trends will likely remain at higher severity crashes.

When designing protection principles to be used for the development of future vehicles, it is essential to understand the influence and potentially increased injury risks in real world situations, where the variations of sitting postures cannot be neglected. The trends in this study can contribute to identifying the most challenging combinations, which can help in the development of restraint systems based on the principles of protection.

Conclusion:

Variations in sitting posture are shown to influence occupant loading and kinematics. Especially, it was seen that lower extremity postures influence pelvis kinematics and lumbar spine loading. In the

frontal crash configuration, crossing the knees increased the maximum pelvic angle by up to 7.5° and the pubic symphysis excursion by up to 29 mm.

The torso posture had a considerable influence on the whole-body kinematics. In the frontal crash configuration, the torso posture in the sagittal plane affected torso excursion and rotations, with forward-leaning occupants showing smaller excursion but still reaching closer to the dashboard (Figure 100) in comparison to the baseline.

The FE-HBM is a tool capable of recreating a large variety of sitting postures as well as the variety in crash configurations ranging from near-side and frontal to far-side impacts. This capability is an important complement in the design of protection systems addressing real-world situations.

3.3.4 Conclusion

Different HBMs were successfully used to evaluate a novel occupant sitting position i.e. the reclined position. Although none of the HBMs were validated for such load cases, the outcome from the investigation gave interesting insights in many different areas such as:

- Importance of initial seat belt position when evaluating submarining of the lap belt.
- Pre-pretensioning of the seat belt might move the initial position of the buckle and thereby induce submarining.
- Risk of submarining is reduced with a tilted seat pan and forward-positioned lap belt anchorage points.
- Using seat- and belt-related load limiting countermeasures, the lumbar spine and pelvis forces could be reduced.
- Oblique impact like the SCP might lead to belt slip-off from the shoulder and thus increased risk of rib fractures.

However, the above-listed areas should be re-evaluated when HBMs validated for reclined seating positions become available to ensure that those are valid.

Additionally, one of the studies investigated the effect of sitting posture on occupant loadings and kinematics. The FE-HBM was shown to be capable of representing a large variety of sitting postures and providing insightful results for the varied responses of 35 different sitting postures in a variety of non-standardised impact scenarios. This capability and the understanding of posture variation influence are important complements when understanding the real-world safety impact by different protection principles.

3.4 Protection Principle 4 - Mushroom Airbag

Protection Principle 4 deals with an advanced airbag design for new seating configurations in automated vehicles. The corresponding working group consists of Mercedes, supported by Autoliv.

3.4.1 Motivation and Background

This protection principle focusses on analysing a novel restraint concept named “Mushroom Airbag”. The use case for this airbag is primarily related to a “Living Room Environment” for advanced seating configurations in autonomous cars. The living room environment is represented in the simulation environment with the typical front seat of a car rotated 180° backwards to face the rear occupants of the vehicle. This allows direct face-to-face interaction between the occupants while the vehicle is driven autonomously. In the living room environment, much more free space is available between the occupants, which can be used for a range of applications.

The free and open space between the occupants raise the question of the utilisation of traditional airbag solutions and their applicability in the given environment, as they rely on a supporting structure to be present to mitigate the occupant movement during a crash scenario (e.g. steering wheel for a traditional driver airbag). The absence of such a structure led to the evaluation of a novel concept as shown in Figure 102. The airbag in this study is deployed from the roof of the vehicle and is designed to fill the space in between the occupants to mitigate any possible physical interaction between them in case of a crash, and potentially reduce head, neck and thoracic loads.

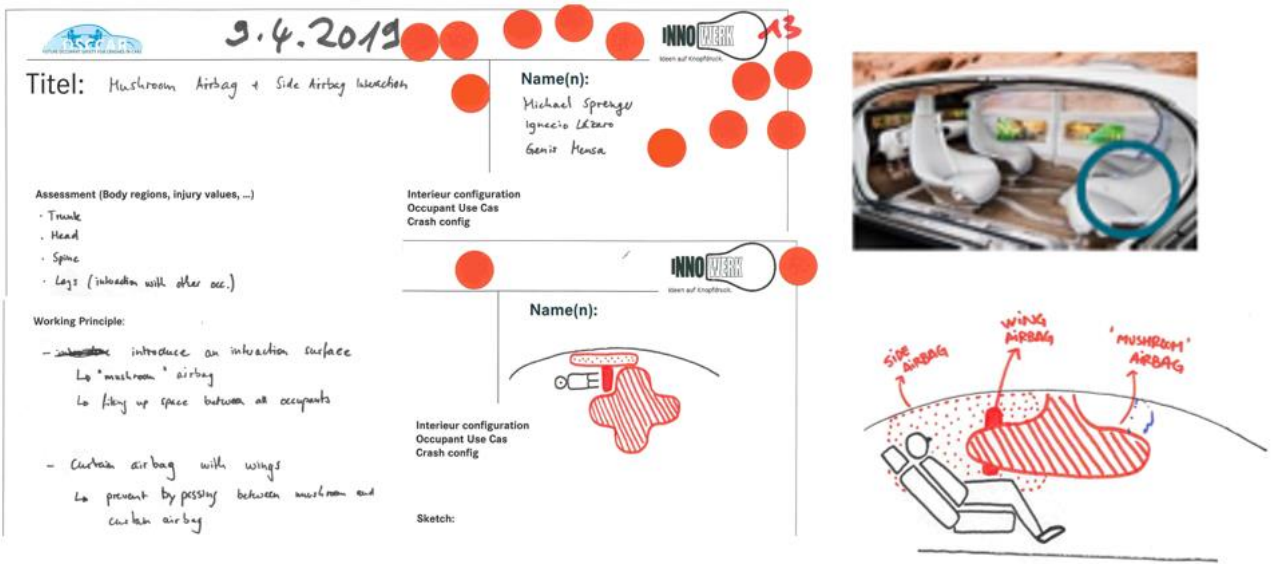

Figure 102 Mushroom Airbag concept proposal (ideation workshop) [4]

3.4.2 Research Questions

The following research questions were identified to be answered by this study:

- What is the protection potential of the Mushroom Airbag in frontal oblique collisions?
- Can the Mushroom Airbag “fill the space” between the occupants?
- Is the Mushroom Airbag concept suitable for different seating positions?
- Is the Mushroom Airbag concept suitable for different occupant types?
- Can the Mushroom Airbag avoid interactions between the occupants?

3.4.3 Simulation Studies

The novel airbag concept was studied based on crash pulses from WP1: LTAP OD1, SCP and Full frontal [28]. The cases were chosen based on the highway and urban crash scenarios with full frontal, oblique frontal and oblique impacts to the vehicle at different speeds. A 50th percentile male and CNIS 5th percentile female anthropometry were chosen to study the variation in airbag performance with different anthropometry. Seating position 1, 3 and 4 were chosen to study occupant interactions during the event of a crash. Table 29 describes the simulation matrix which was defined for this study.

Parameter	Variation 1	Variation 2	Variation 3
Crash Pulse variation	LTAP OD1 (Urban scenario)	SCP	Full frontal 40 km/h (Highway pilot)
Seating Position	Position 3 & 4 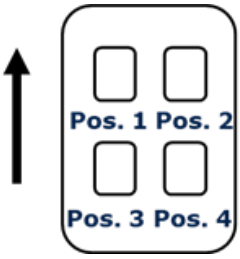	Position 3 & 4 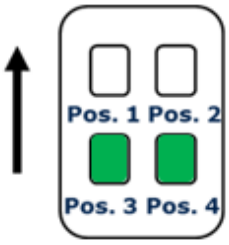	Position 3 & 4 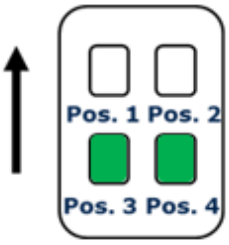	Position 1 & 3 (FF40 Pulse) 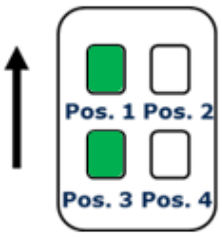
HBM Anthropometry	THUMS TUC M50	THUMSD F05 CNIS	-
Generic Airbag design	Dual OHA (Pre-study)	Single Volume Design (Mercedes-Benz)	Stitched OHA design (Autoliv)

Table 29 Simulation matrix for the Mushroom Airbag concept

3.4.3.1 Pre-Study considering a dual bag design

The concept assessment for the preliminary study was based on a previously developed Over-Head Airbag (OHA) with focus on HBM kinematics. This airbag design provided by Autoliv is a roof mounted airbag system, which was implemented in a generic environment with a living room seating configuration in order to provide support to occupants in a frontal oblique crash scenario.

The kinematics analysis of the HBMs in the simulations with the Dual OHA (Figure 103) revealed that the airbag design offers support to the head and neck complex in frontal crash scenarios. However, it failed to provide any support for lateral occupant movement. This led to an interaction between the occupants in side / oblique crash scenarios when occupants were seated in position 3 and 4 of the living room environment setup, as illustrated in Figure 104.

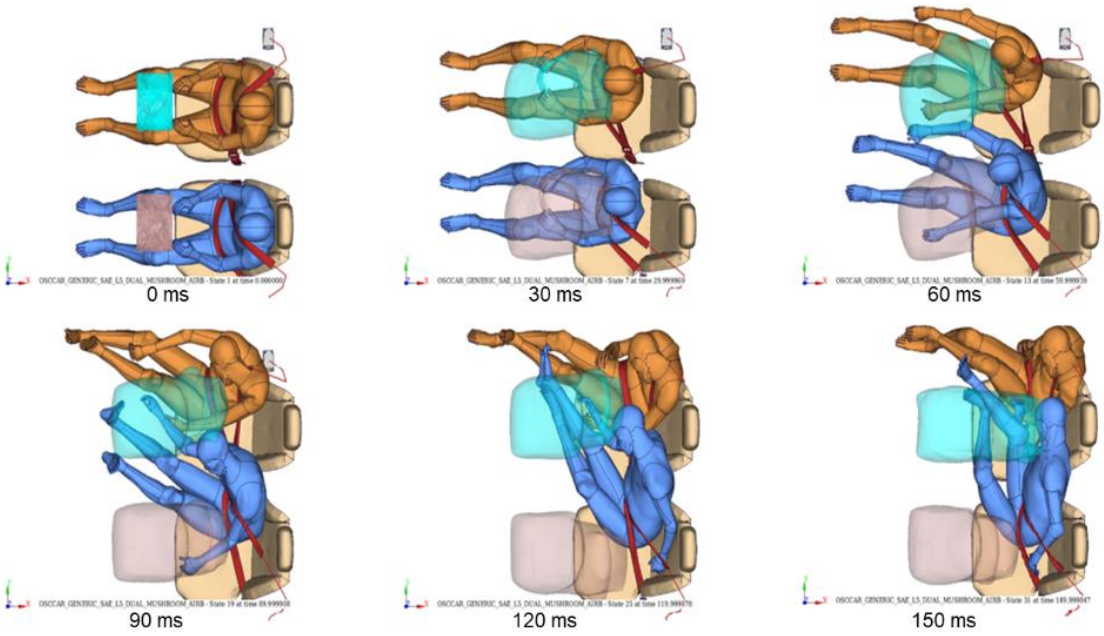

Figure 103 THUMS v4 M50 in oblique frontal crash scenario with Dual OHA

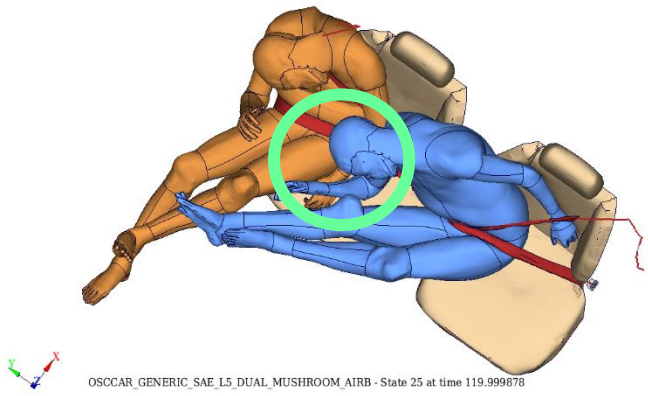

Figure 104 Dual OHA solution fails to provide support for lateral occupant movement

3.4.3.2 Main study considering a one volume design

The limited lateral support offered by the Dual OHA concept discussed in the previous section led to modifications in the existing airbag design through the introduction of an additional volume. Two airbag designs were proposed to achieve the same:

1) Single airbag volume to fill the space between the occupant
2) Stitching multiple OHA airbags into one shared volume to fill the space between the occupants

This section of the study focuses on the design process and the performance analysis of both approaches.

Single volume Mushroom Airbag

The airbag was designed from ground up at Mercedes to achieve the desired result of avoiding occupant interaction in frontal as well as oblique crash scenarios.

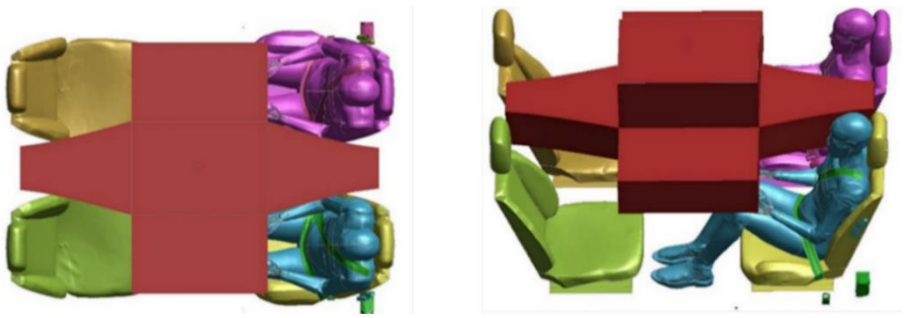

Figure 105 Single volume Mushroom Airbag Concept

The concept was simulated considering the scenarios as illustrated in the simulation matrix (Table 29) to analyse the occupant kinematics in frontal and oblique crash scenarios. Figure 106 to Figure 108 show the kinematic behaviour of the THUMS TUC 50th percentile male in previously-discussed crash scenarios. The corresponding behaviour of the THUMSD 5th percentile CNIS female model is illustrated in Figure 164, Figure 165 and Figure 166 of Appendix 3.1.

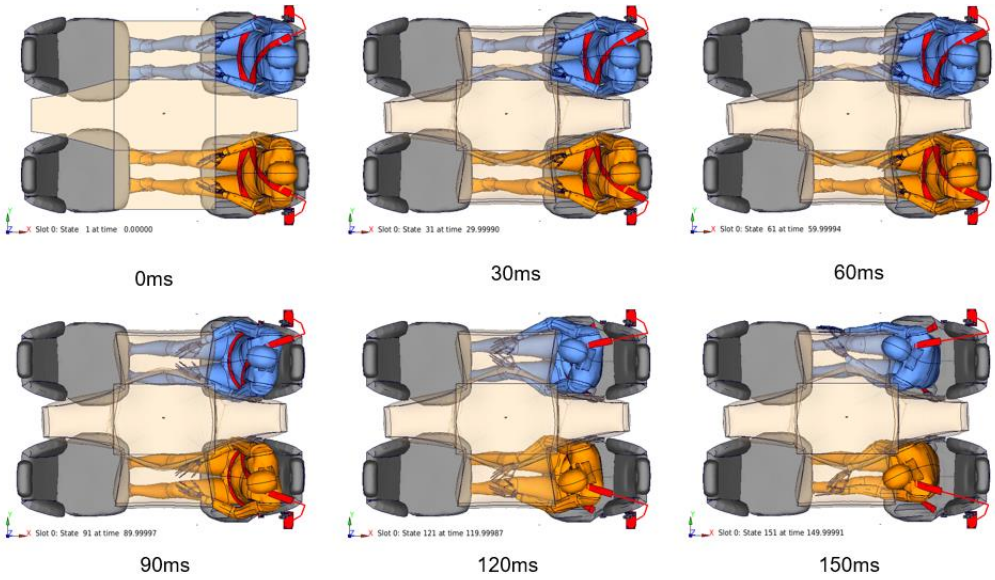

Figure 106 THUMS TUC M50: LTAP OD1 Pulse

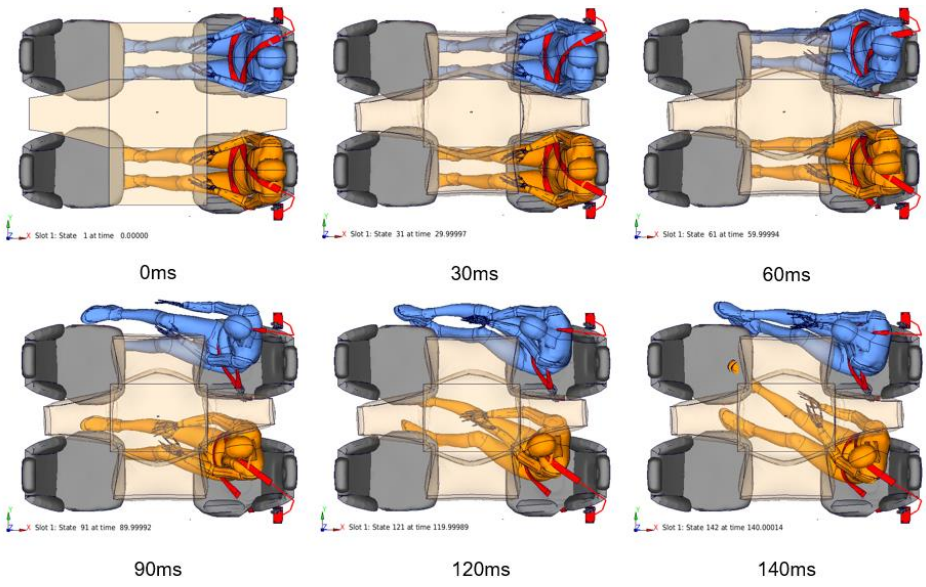

Figure 107 THUMS TUC M50: SCP Pulse

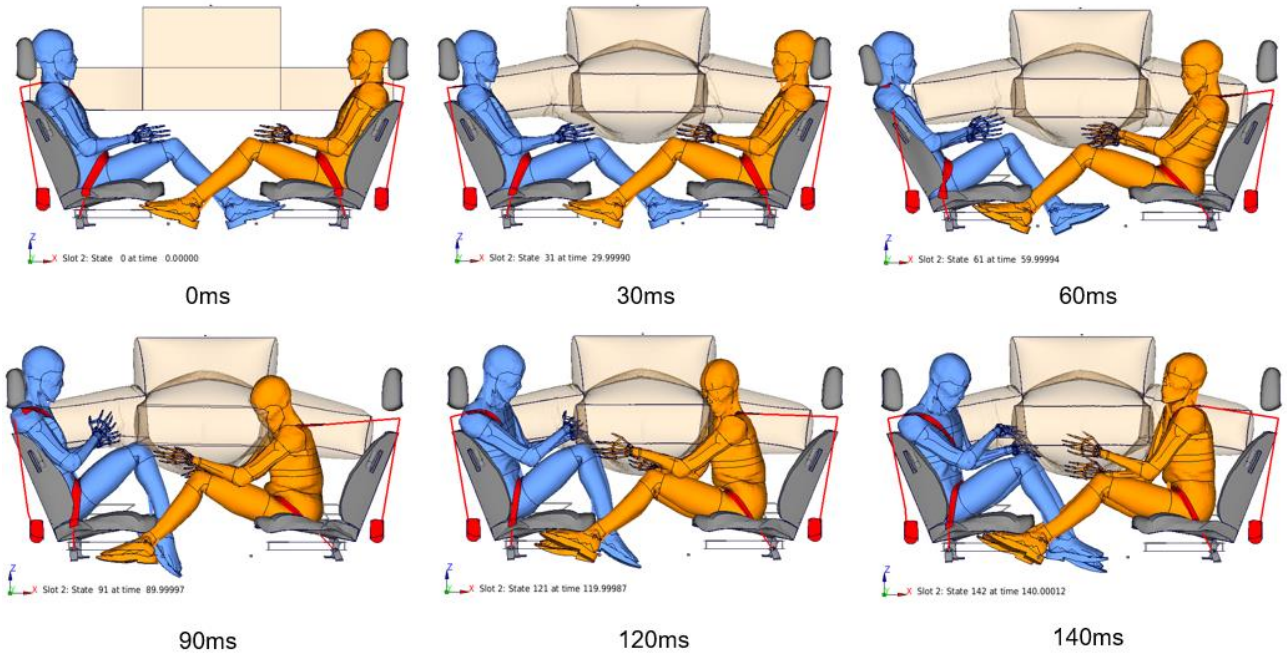

Figure 108 THUMS TUC M50: FF40 Pulse

Injury Risk Analysis:

An injury risk analysis was conducted to assess the performance of the Mushroom Airbag in relation to the full-frontal 40 km/h crash scenario, and to compare it with the performance without Mushroom Airbag. The kinematics of the 50th percentile male occupant shown in Figure 109 suggested that the single-volume Mushroom Airbag was able to provide benefits by avoiding occupant interaction in this crash scenario.

The support provided to head and neck was observed as beneficial based on the neck section forces experienced during the interaction with the airbag. Incorporation of the Mushroom Airbag shows 50% lower neck section forces when compared to a scenario where the Mushroom Airbag was absent. The section forces in the neck (Figure 110) were 2.1 kN without Mushroom Airbag and 1.15 kN with Mushroom Airbag.

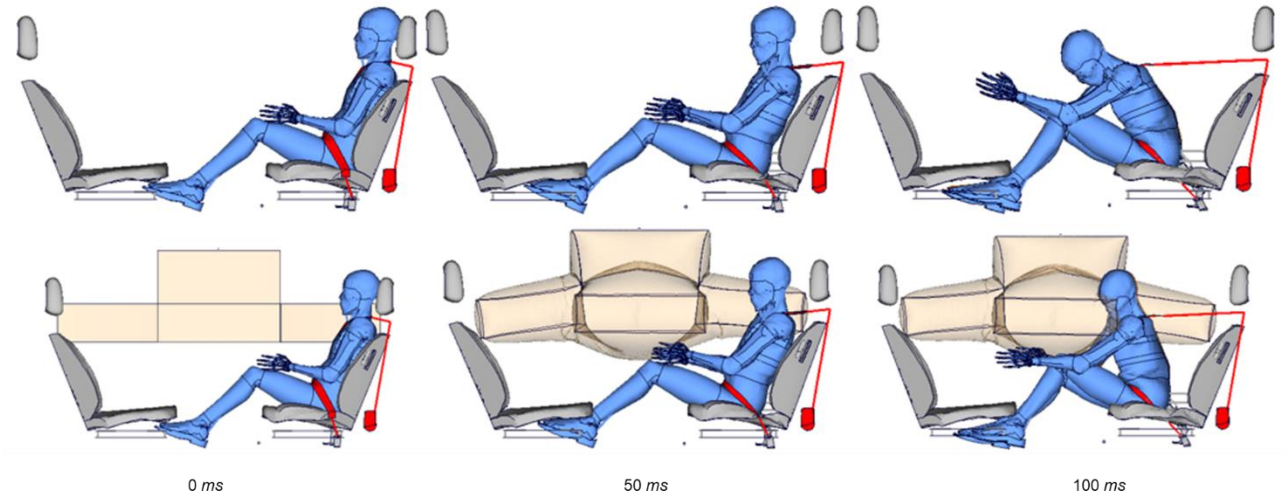

Figure 109 Occupant kinematics: Without Mushroom Airbag v/s with Mushroom Airbag

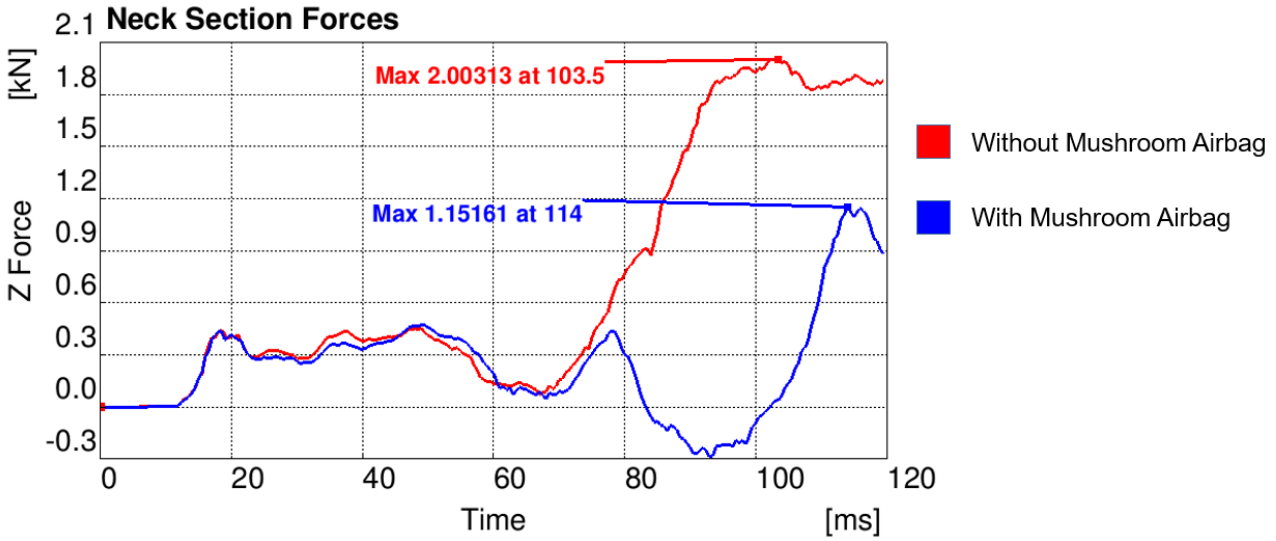

Figure 110 Comparison of cross section forces in the neck

A significant reduction in neck section forces was observed due to the incorporation of the Mushroom Airbag. However, the neck injury risk remains low in both the cases (~0.02%), as shown in Figure 111.

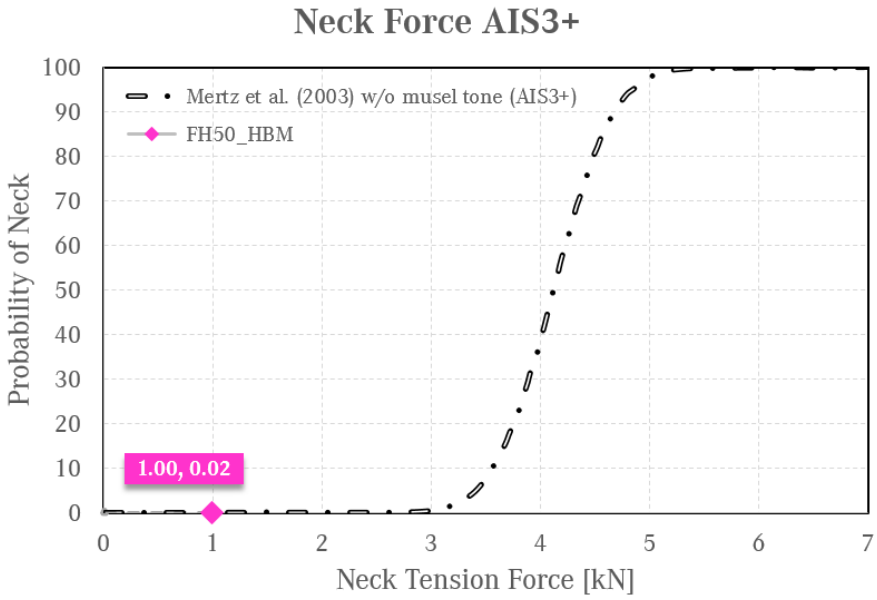

Figure 111 Neck injury prediction based on the cross-section forces

The brain injury evaluation suggested a slight increase in injury risk with the use of the Mushroom Airbag. This could be possibly due to interaction of the Mushroom Airbag with the occupant head, as opposed to no part coming into contact with the head for the configuration without Mushroom Airbag. Figure 112 illustrates that in both cases a virtually no risk of injury (0.0% probability in AIS2+ level) was observed for the head, due to the absence of any hard parts.

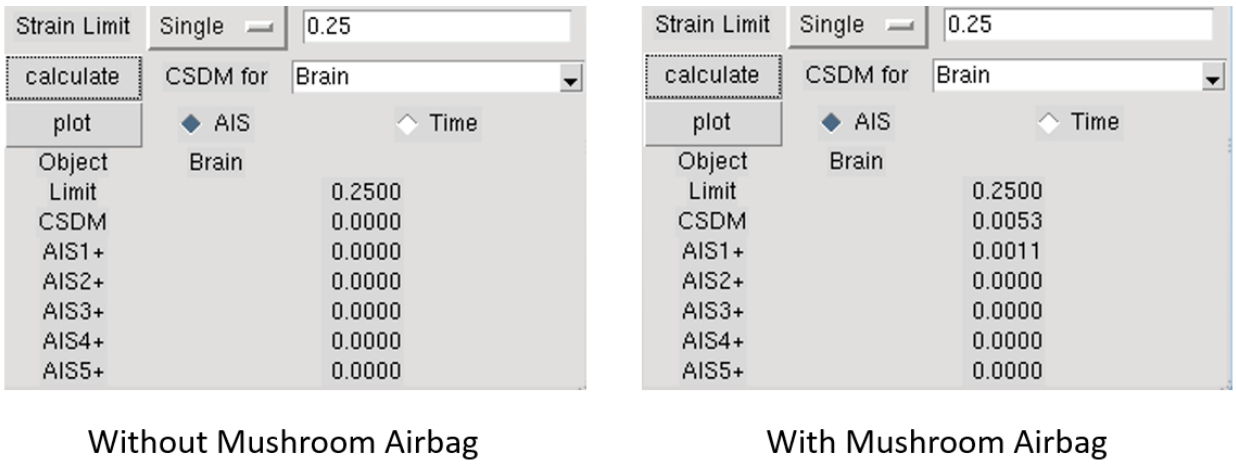

Figure 112 Comparison of brain CSDM injury risk prediction

An additional analysis on rib fracture injury risk was also conducted in this comparative study. The current Mushroom Airbag concept shows a slight reduction of injury risk in the initial stages of the simulation (0 ms - 60 ms). Figure 113 shows the injury risk analysis conducted by the TUC rib injury assessment tool showing the AIS3+ injury risk probability with more than three rib fractures for an occupant aged 45 years. The curves in the plot below illustrate the principal strain development in each rib which is used for prediction of the overall injury probability.

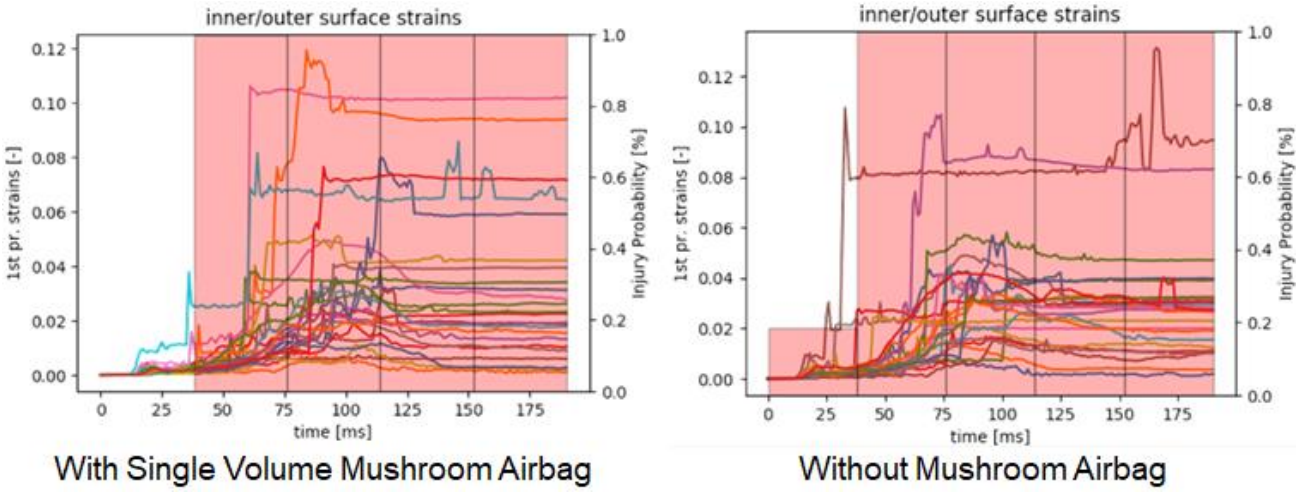

Figure 113 Rib fracture injury risk analysis

Stitched OHA concept (Autoliv):

The stitched Over-Head Airbag (OHA) concept is an extension of the single Over-Head Airbag concept by Autoliv and Mercedes-Benz Cars which was designed and tested in real life some years ago. The nature of roof-mounted airbag deployment of the OHA was the motivation to combine multiple OHAs into a single volume and to form a Mushroom Airbag model. Due the fact that this was a carline-related product development as shown in Figure 114, no further details can be given and published in this report.

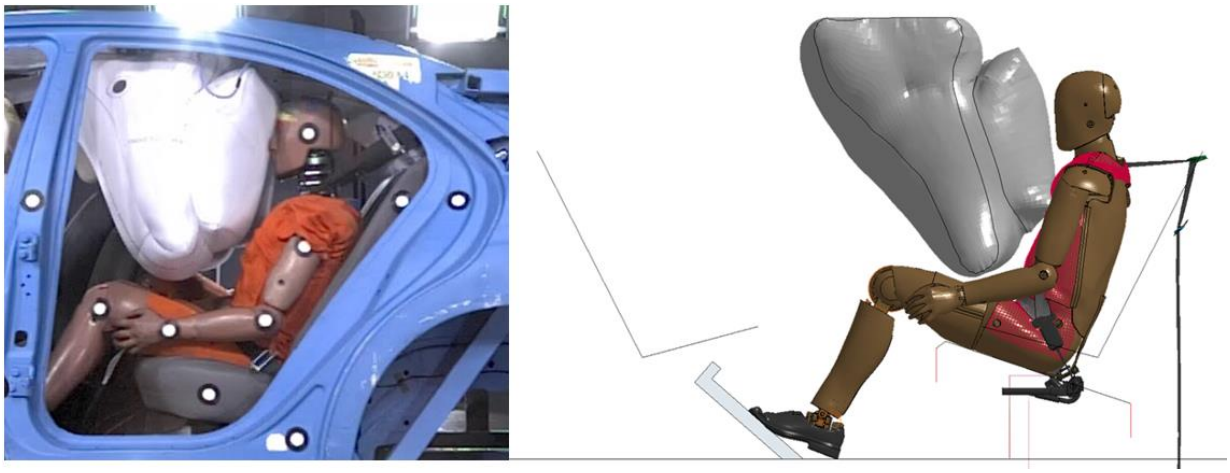

Figure 114 OHA concept testing simulation

To increase the protection performance of the previously developed Over-Head Airbag concept, six of them were stitched together to create one large overhead airbag. Two double overhead airbags and two single overhead airbags were positioned between four occupants, see Figure 115. To be able to stitch the airbags together, the upper part of the single bags needed to be elongated in the x-direction. The stitched airbag consists of six airbag chambers, meaning that there are fabric parts between all connected chambers. This version of the Mushroom Airbag is not validated to any hardware test regarding airbag pressure, leakage or inflation process. However, it is constructed from validated base elements such as validated airbag fabric and inflator data. The static analysis of the stitched OHA Mushroom Airbag concept is shown in Figure 116.

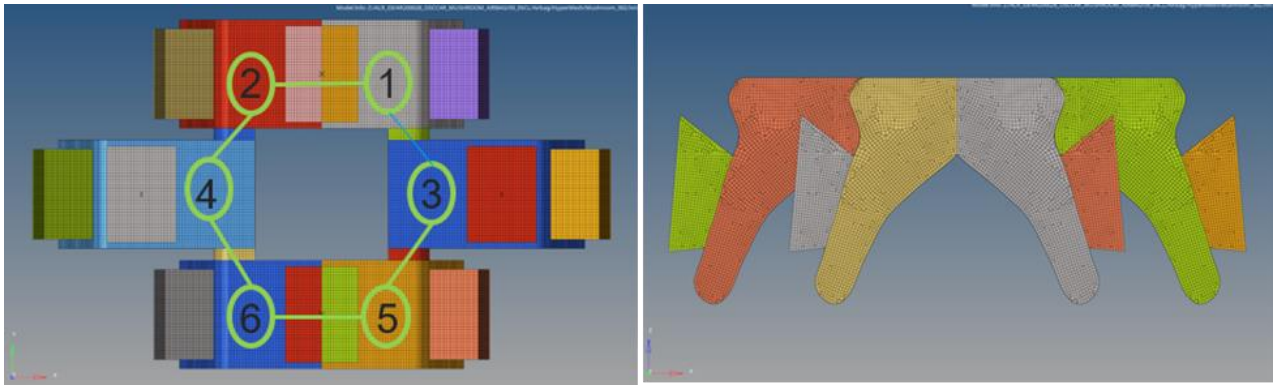

Figure 115 Mushroom Airbag model developed by stitching 6 single OHAs together

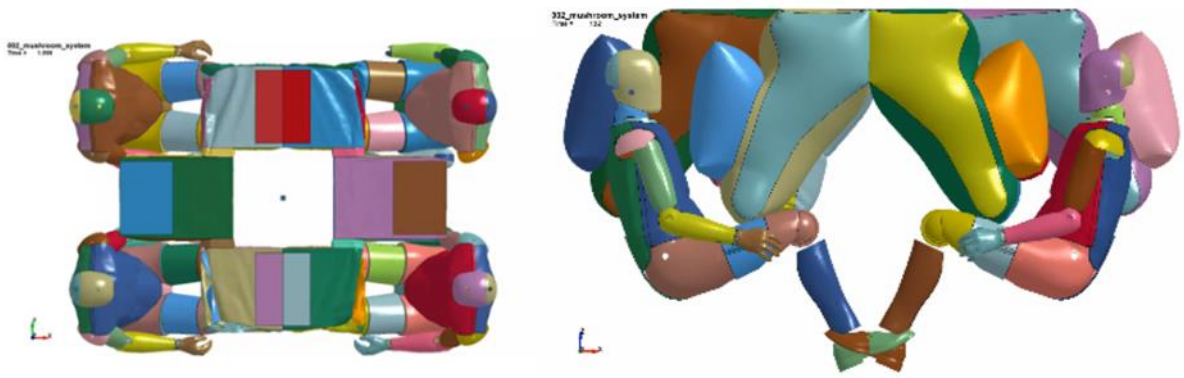

Figure 116 Static analysis of stitched OHA concept (Autoliv)

Figure 117 shows the kinematics of the occupants sitting in position 1 and 3 of the living room seating configuration when subjected to a full frontal 40 km/h crash pulse. The stitched OHA Mushroom Airbag provides better support to the head, neck and thorax of the THUMS TUC HBM compared to the single volume airbag. The occupant sitting in position 1 is also supported as the large volume of the stitched OHA concept provides support in the rebound phase of the crash scenario.

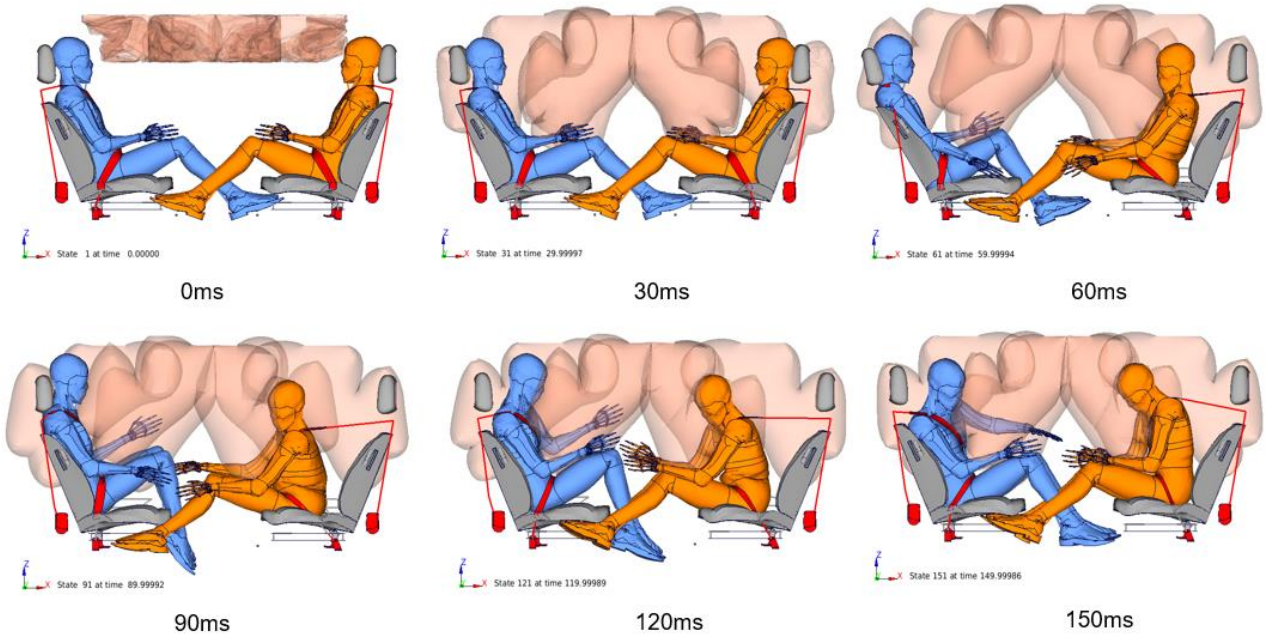

Figure 117 Stitched OHA Mushroom Airbag with THUMS TUC M50 HBM: FF40 Pulse

To assess the performance of the stitched OHA Mushroom Airbag, the THUMS TUC M50 HBM was subjected to a full-frontal 40 km/h pulse as previously with the single volume Mushroom Airbag concept.

The support provided by the new stitched airbag concept shows improvement regarding the neck section forces experienced by the THUMS TUC HBM as well. Figure 118 shows a neck section force comparison between the case where no Mushroom Airbag is implemented, the single volume Mushroom Airbag and the stitched OHA Mushroom Airbag concept.

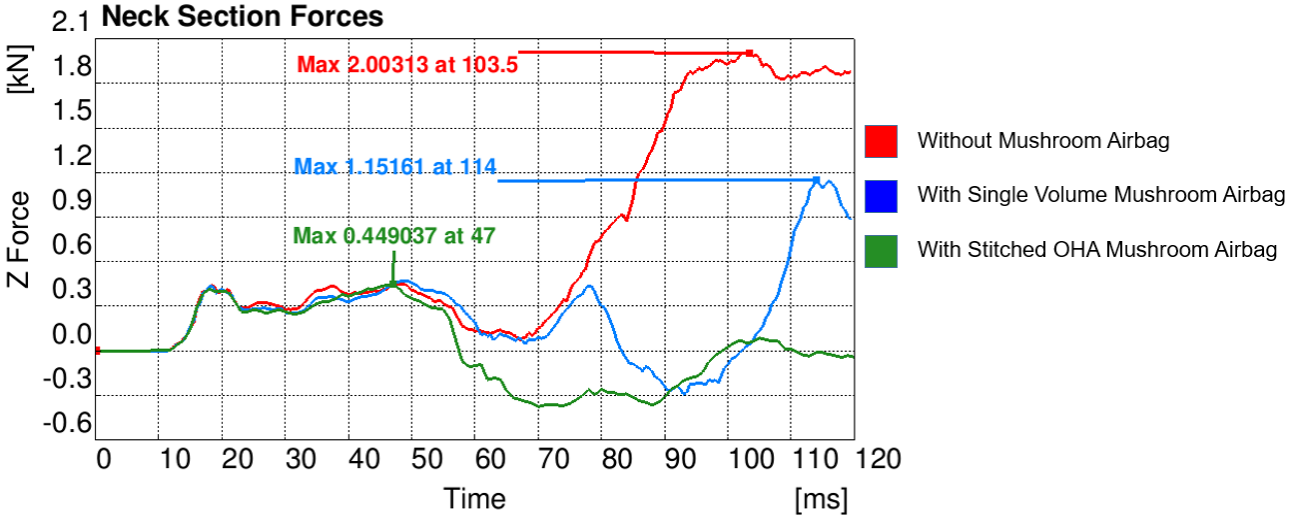

Figure 118 Neck section force comparison

While the case without Mushroom Airbag shows a maximum force of 2 kN, the simulation with the stitched OHA Mushroom Airbag shows a maximum force of 0.45 kN. As already shown in Figure 111, the predicted risk of Neck injury remains very low. The stitched OHA Mushroom Airbag provides a better support for the head compared to the single volume Mushroom Airbag concept. The injury prediction by Brain CSDM analysis shows that the injury risk is lowered to 0% probability at any AIS level, as illustrated in Figure 119.

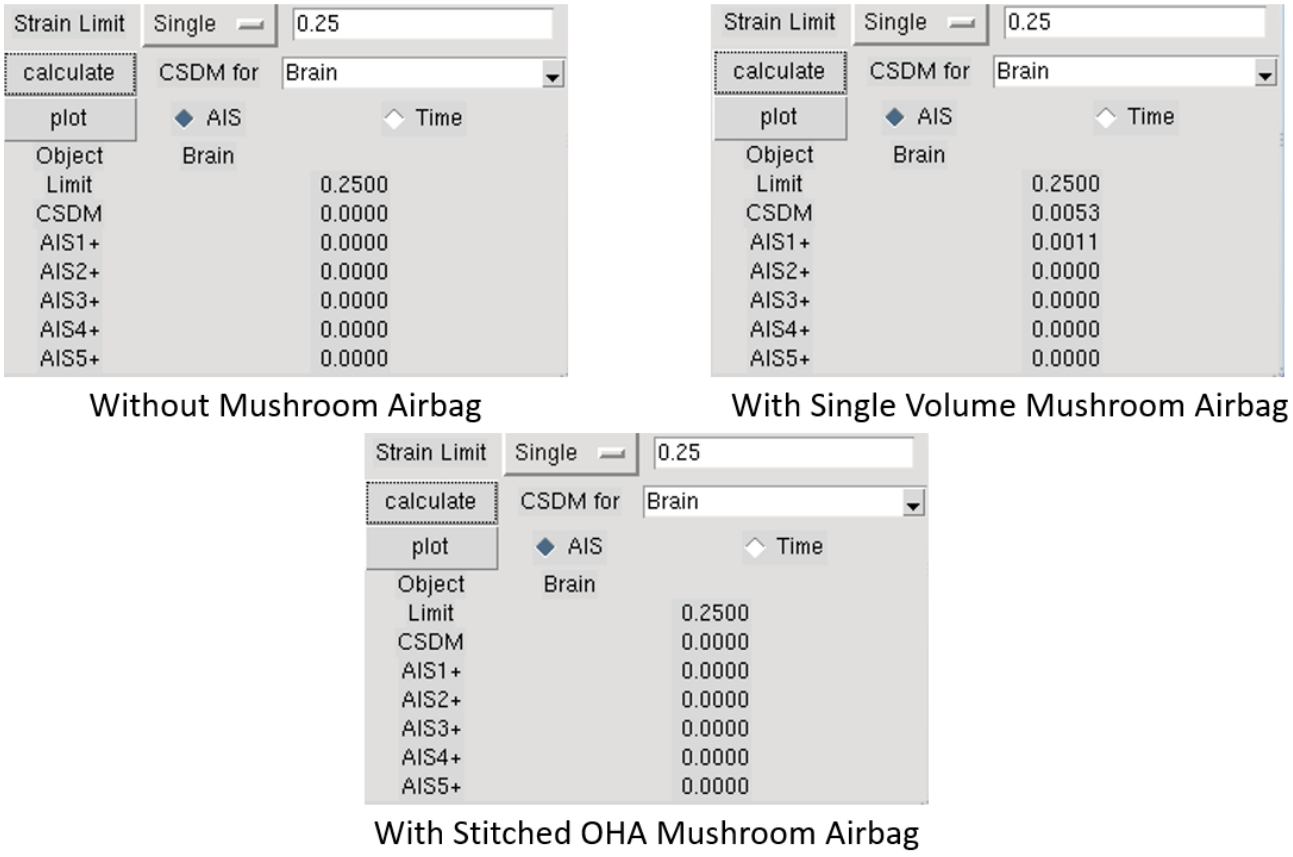

Figure 119 Comparison of brain CSDM injury risk prediction

The rib injury analysis by the RibFX tool is shown in Figure 120. The stitched OHA Mushroom Airbag provides further improvement regarding the rib injury risk in the 0 - 75 ms time range. After 75 ms all cases show a high rib injury risk according to the RibFx tool; this needs to be addressed in the future by further refining the vehicle environment and the Mushroom Airbag.

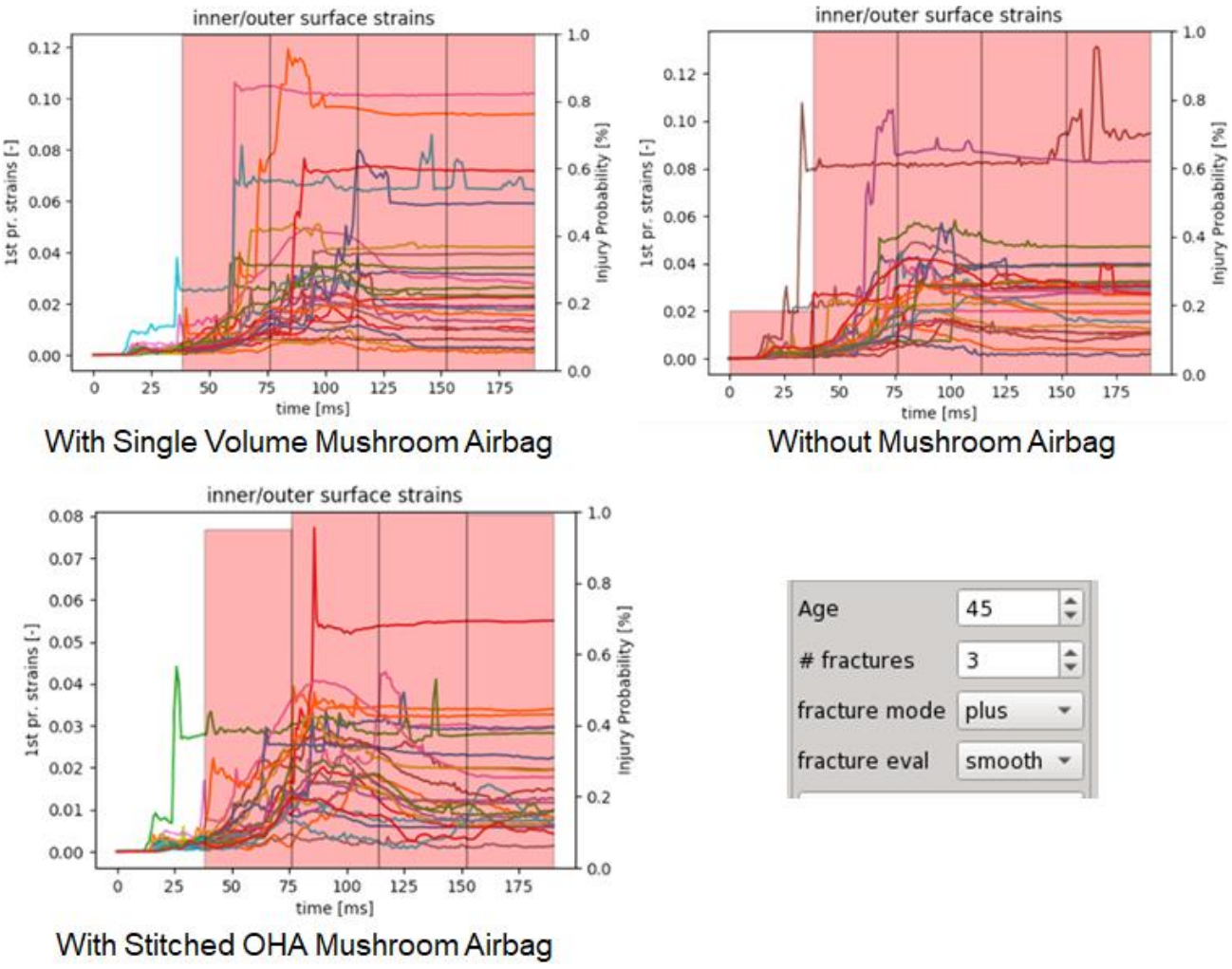

Figure 120 Rib fracture injury risk analysis comparison

3.4.4 Conclusion

The Mushroom Airbag concept, as defined by the initial proposal, successfully answers the research questions that were set at the beginning of this study. The need for volume between the occupants in a living room environment setup, which is to be filled in case of highway and urban crash scenarios, was fulfilled by the proposed Mushroom Airbag concepts. The single-volume airbag gives a good baseline in establishing the benefits of the Mushroom Airbag concept, whereas the stitched OHA Mushroom Airbag showcases the benefits of a more mature airbag design.

The living room environment analysed under oblique crash scenarios (LTAP OD1 and SCP) shows that the use of a Mushroom Airbag provides good protection against interaction of occupants seated in positions 3 and 4. An analysis of the setup in a full-frontal crash scenario shows that the Mushroom Airbag provides good support for the head and neck of the occupant in a crash, especially the stitched OHA concept, due to the higher overall airbag volume and the additional head and thorax support volumes incorporated here. The single volume Mushroom Airbag provided a 50% reduction in neck section forces whereas the stitched OHA Mushroom Airbag reduced the section forces by more than 50%. Both airbag designs provided better support for the thorax. This resulted in a reduction of the rib fracture injury risk in the initial stages of the analysis, as shown by the RibFX tool. There is however still a high rib injury risk shown by the RibFx tool for the later stages, which needs to be addressed in the future by further refining the vehicle environment and the Mushroom Airbag.

3.5 Protection Principle 5 - Active Seat Backrest

This chapter summarises the results related to Protection Principle 5 (PP5), which were generated within the working group of ika / fka, Volvo Cars, Bosch, ZF and Siemens, led by ika and fka.

3.5.1 Motivation and Background

Based on the outcomes of the ideation workshop, documented in deliverable D2.3 [4], PP5 addresses raising of the occupant from a reclined- to an upright seating position prior to a crash situation (see Figure 121).

As future interiors and automated driving functions may enable relaxed seating positions, the restraint of the occupant in a reclined position might become necessary. Increased submarining tendency due to the reclined occupant posture, and an increased distance to airbag and support structures make occupant restraint challenging in the novel situation (assuming a forward-facing seat and a frontal crash) [48], [49]. For rearward-facing and reclined positions, occupant ramping and a reduction of the effective seat back restraint area due to the seat back inclination could lead to increased occupant displacement during the crash [50]. To address these challenges and to ensure safety for reclined positions, raising the occupant to an upright seating position, which can then be restrained with conventional systems, might be a solution. The effectiveness and the boundary conditions that need to be considered in terms of a pre-crash seat back rotation are part of the following investigations.

The investigations are separated into two different use cases, a forward-facing (standard interior or rear passenger in a living room configuration) and a rearward-facing seating position (frontal passenger in a living room configuration) (see Figure 121). As the restraint concept after repositioning depends on the principal direction of force, this general distinction of use cases was introduced.

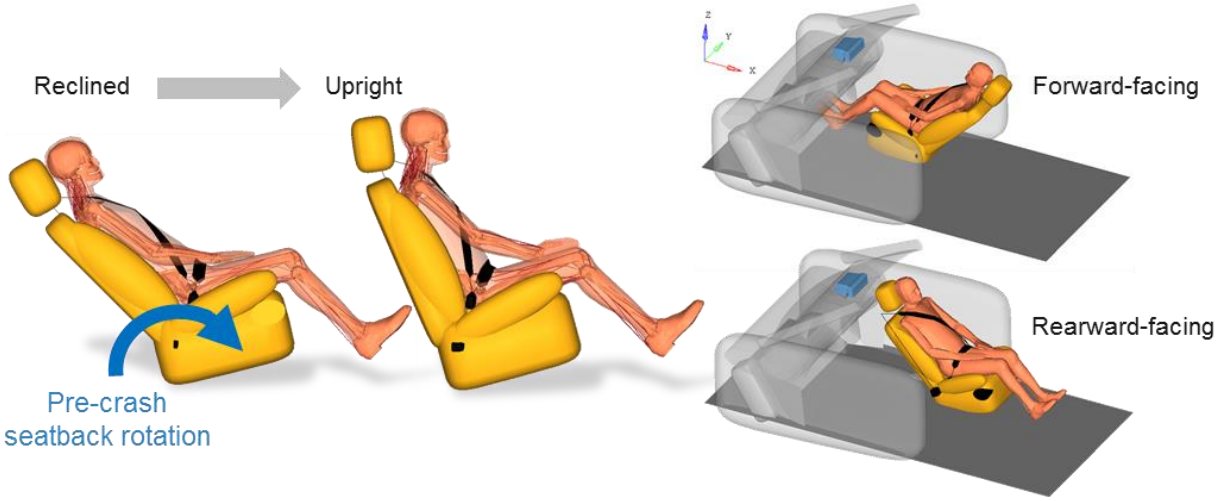

Figure 121 Mechanism of Protection Principle 5 & investigated occupant orientations

3.5.2 Research Questions

Within the working group of PP5, several research questions were addressed by the different simulation studies. The various research approaches and focusses of the individual studies were refined during the work process and can be summarised in the following three main research questions:

I. How does repositioning from a reclined to an upright sitting posture prior to a crash affect the occupant kinematics?

II. Which boundary conditions need to be taken into account when repositioning an occupant from a reclined to an upright sitting posture?

III. How does repositioning from a reclined to an upright sitting posture prior to a crash affect the occupant restraint interaction and safety during the crash phase?

The first two questions focus on the occupant repositioning and general functionality of the principle during the pre-crash phase. Related research addressed the overall applicability (rotational velocity and necessary pre-crash timeframe) of the principle and the occupant kinematics during the repositioning. Effects of pre-crash Automated Emergency Braking (AEB), additional belt system features like an Electrical Reversible Restraint (ERR), and HBM settings and characteristics were taken into account when the repositioning effects were investigated.

For the third research question, the focus is on the effect of the repositioning on the occupant kinematics and safety during the in-crash phase. Here, the transfer of pre-crash repositioning to in-crash occupant safety is addressed.

3.5.3 Simulation Studies

A detailed overview of the simulation studies and related settings that were performed in the working group of PP5 is given in Table 37 and Table 38 of Appendix 4.1. The overview is separated into the two different occupant use cases (forward and rearward facing reclined seat) and summarises the settings and characteristics of the performed simulation studies partner specifically.

In total, four different simulation studies were performed in the context of PP5, whose results are documented in a condensed form in the following chapters:

- Occupant repositioning in a forward-facing seating position (Volvo Cars)
- Effect of seat back rotation velocities on the pelvis angle (Bosch)
- Effects of pre-crash retractor belt pretensioning (ZF)
- Occupant repositioning in a rearward-facing seating position (ika and fka)

3.5.3.1 Occupant repositioning in a forward-facing seating position

Using an active HBM, the study evaluates combinations of repositioning and other possible pre-crash interventions, such as pre-crash braking and the activation of an Electrical Reversible Restraint (ERR), to answer research questions on how repositioning a driver from a reclined to an upright sitting posture prior to a frontal impact would affect kinematics and restraint interaction during the crash. Simulations with the HBM without activated muscles were included to contrast the influence of active musculature on the model response in these situations.

This chapter summarises the study published at IRCOBI 2020 [35]. See publication for further details.

Methods

A simulation series considering an FE vehicle sled model with the 50th percentile male SAFER HBM v9.0.1 [51] was performed, Figure 122. In the reclined position, the seat back and torso of the HBM were reclined 20° compared with the upright reference position (27.5° seat-back angle), Figure 123. The impact simulated was a Full-Frontal Rigid Barrier impact at 56 km/h.

Figure 122 The interior model with the SAFER HBM. Adapted from [35]

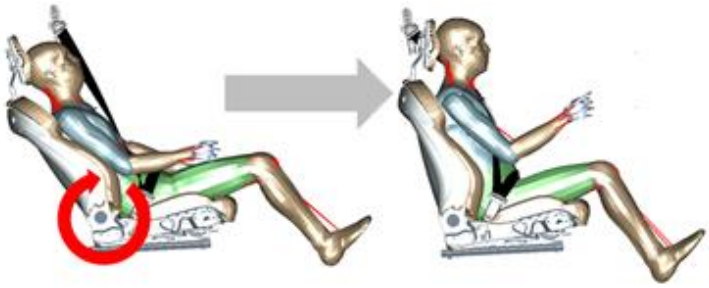

Figure 123 Repositioning; from reclined occupant position (left) to upright position (right)

In total, 27 simulations were performed with combinations of the following parameters. For the simulations in a reclined position, three repositioning conditions were investigated: no intervention, and a 20° rotation of the seat back to the upright position over 250 ms (80°/s) or 125 ms (160°/s), respectively, at the start of the pre-crash phase. Two pre-crash scenarios were simulated; without vehicle dynamics intervention, i.e. at a constant velocity, and braking (11 m/s^2 achieved after a 100 ms delay and then a ramp-up over 200 ms). The retractor response during the pre-crash phase was varied between a locked state and 180 N ERR activation. For ten simulations the seat belt anchor and buckle location were varied to a position 50 mm forward and downward of the nominal positions.

Results

In the reclined position with the nominal buckle and anchor attachment points, the HBM submarined at the buckle side of the lap-belt, irrespective of seat-back repositioning, while this was avoided when the seat belt anchor and buckle location was moved 50 mm more forward and downward. This means that repositioning of the seat back to upright at 80°/s or 160°/s and in combination with ERR was not successful in preventing submarining. However, the submarining occurred later with the repositioning and more so with the faster repositioning rate.

When the HBM was repositioned during the pre-crash phase by the seat back, the rotation of the pelvis forced by the repositioning was not enough to recover the upright HBM pelvic angle. The pelvic angle, measured as the inclination of a vector between the mid-point of the ASIS to the pubic symphysis, relative to the vertical axis, increased 17° after repositioning to reclined (Figure 124). For the strongest repositioning strategy (160°/s seat back repositioning), the pelvis was almost back in the upright position at 250 ms (peak rotation of -15°), but then rebounded so that it was -7° from its starting position in the reclined position when the crash phase started (Figure 125).

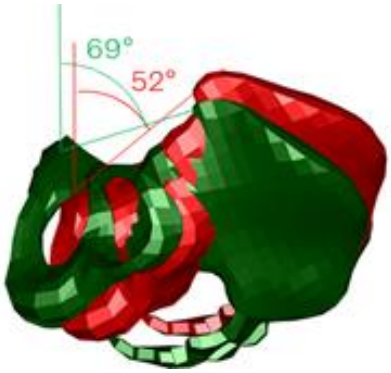

Figure 124 Initial pelvic angle in upright position (red) & reclined position (green)

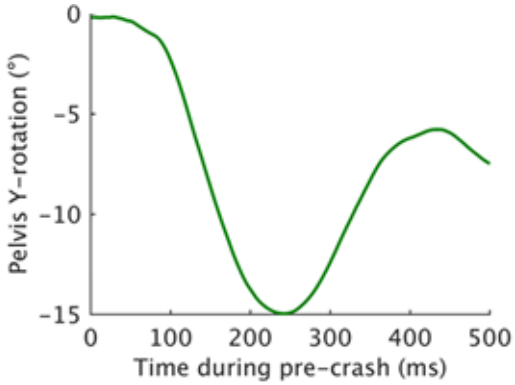

Figure 125 Pelvis Y-rotation during pre-crash phase during simulation with 160°/s seat back repositioning

Pre-crash repositioning back to upright reduces the head impact velocity to the airbag by reducing the distance to the restraints (belt and airbag), Figure 126. The combination of repositioning the seat back and applying the 180 N ERR led to a similar initial crash position after the pre-crash phase of 500 ms. With the 160°/s seat back repositioning, the head of the occupant was maximally 140 mm more forward during the repositioning phase than after 500 ms. With the ERR activation, this was reduced to 95 mm, as the combination of tightening the belt and pushing the seat back upwards led to a shoulder belt force of 250 N at the end of the pre-crash phase in both simulations with ERR.

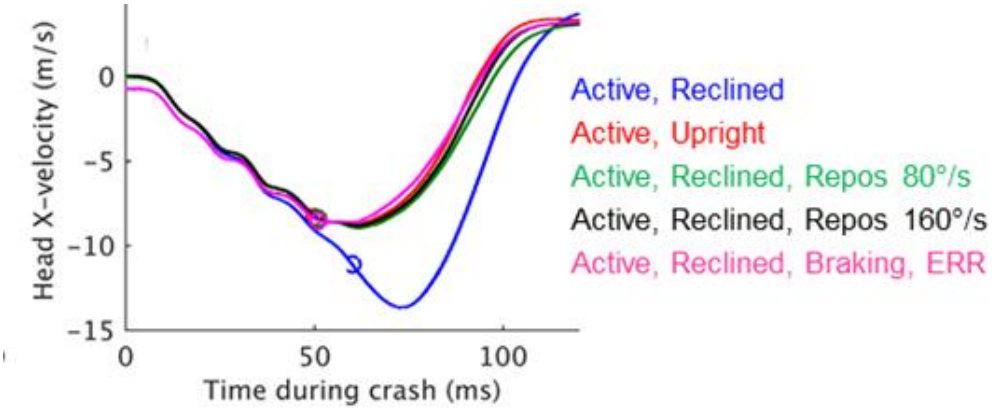

Figure 126 Head X-velocity during the crash phase for different repositioning strategies. The circle indicates the head contact time with the airbag in the simulations

Analysis of the head and sternum positions after the pre-crash phase, indicated that there was no large difference in initial position at the start of the in-crash phase for simulations with either a repositioning or braking intervention during the pre-crash phase. This led to similar kinematics during the in-crash phase.

A comparison of the injury predictors between the passive HBM and the active HBM in the upright position revealed lower values for the active model, except for the lumbar spine values which were slightly increased, while the in-crash kinematics were largely the same as indicated by the similar head trajectories, see further details in [35].

Discussion

Repositioning the occupant prior to the crash by raising the seat back showed that while the occupant position and spinal curvature were quite similar to those in the upright position after repositioning, the orientation of the pelvis was not completely restored. As a result, submarining was not avoided in the repositioning with the nominal lap-belt anchor and buckle locations. The orientation of the pelvis relative to the lap-belt line of action has been shown to be central for the risk of submarining [52], but pushing the torso upward by the seat back was not sufficient to reposition the pelvis as the lumbar spine of the HBM is flexible and bends into flexion.

The different strategies of repositioning the occupant to an upright seat position resulted in reduced loading to head and chest compared to when reclined, since the restraint systems (airbag and seat belt) used in this study are designed for an upright position. If the occupant is in the reclined position at the start of the crash, the current restraint system needs further development to reduce the delays before starting to interact with the occupant.

Conclusion

In the reclined position, the model submarined under the lap-belt and a higher head impact velocity was achieved due to the greater distance to the airbag and seat belt compared with an upright position. When the HBM was repositioned prior to crash by moving the seat back, the higher head

impact velocity was avoided due to a reduced head-to-airbag distance in the in-crash phase. However, submarining was not avoided as the pelvis did not fully return to the upright position due to flexibility in the lumbar spine of the HBM. Pre-tensioning the seat belt prior to crash reduced the forward displacement of the occupant during the pre-crash phase, but also restrained the pelvis during repositioning. The study also revealed that repositioning could be achieved by the occupant's own torso inertia during pre-crash braking as well as by moving the seat back. Comparison of simulations with both active and passive HBM showed that the active muscles could potentially influence the crash consequence predictions from the HBM.

3.5.3.2 Effect of seat back rotation velocities on the pelvis angle

There are two possible strategies for protecting occupants in new seating positions. The first strategy is on-the-spot occupant protection, i.e. protect the occupant in his actual position and adapt the restraint systems to it. The second strategy implies to "move" the occupant from a "new" seating position like a reclined seat back by 45° (w.r.t the state-of-the-art position) to a "standard" seating position, as typically tested in legal and consumer tests.

Protection Principle 5 follows the second strategy: During the pre-crash phase the occupant is repositioned from a reclined to an upright seating position (compare Figure 127 left). In this study the influence of seat rotation velocity on pelvis rotation in an USNCAP full front crash, with and without pre-crash braking, was analysed (see Appendix 1.2 - Siemens USNCAP Pulse). The Simcenter Madymo AHM was used. The seat back was rotated by 23° from a reclined position of 45° to an upright seating position of 22°. The start of the seat rotation was varied from -0.05 s to -0.4 s corresponding to rotation velocities between 57.5°/s and 460°/s. Figure 127 shows a 23° rotation curve which starts at -0.3 s and ends at t = 0 s, with spline_5 interpolation. The activation of a pre-crash belt pretensioner (motorised seat belt - MSB) was considered as well.

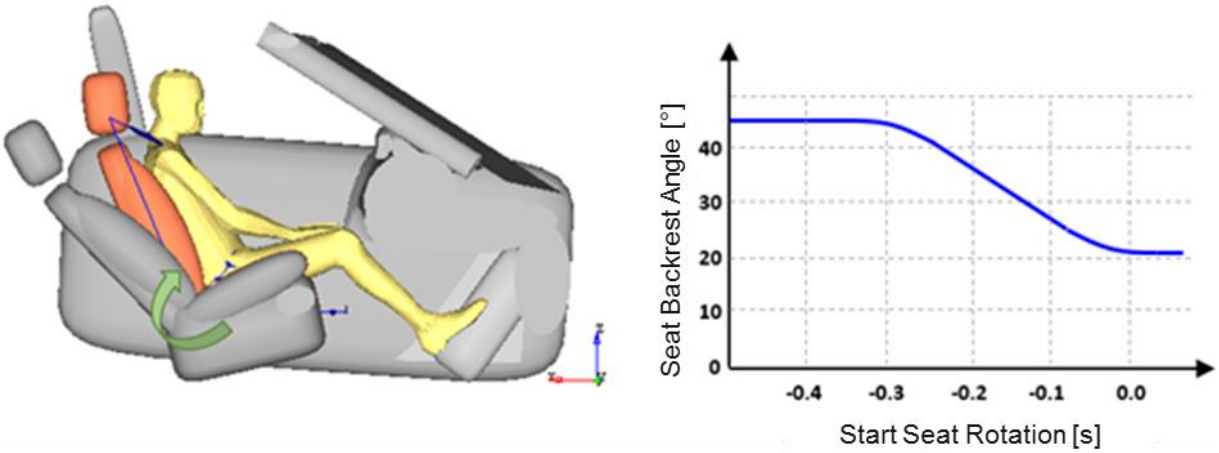

Figure 127 Principle of PP5: grey seat represents initial stadium & orange one the final before crash starts (left) & example for seat rotation curve with Madymo spline_5 interpolation (right)

The simulation DoE included variations of pre-crash braking, pretensioner activation, and start of seat rotation and finally yielded four curves, which are displayed in Figure 128. The y-axis represents the relative angles between a situation where the pelvis is in an upright position and the pelvis after repositioning. Negative rotation means the pelvis is rotated further than the upright position due to repositioning. Positive rotation means the pelvis is rotated less than the upright position due to repositioning and remains in a reclined position compared to the upright position.

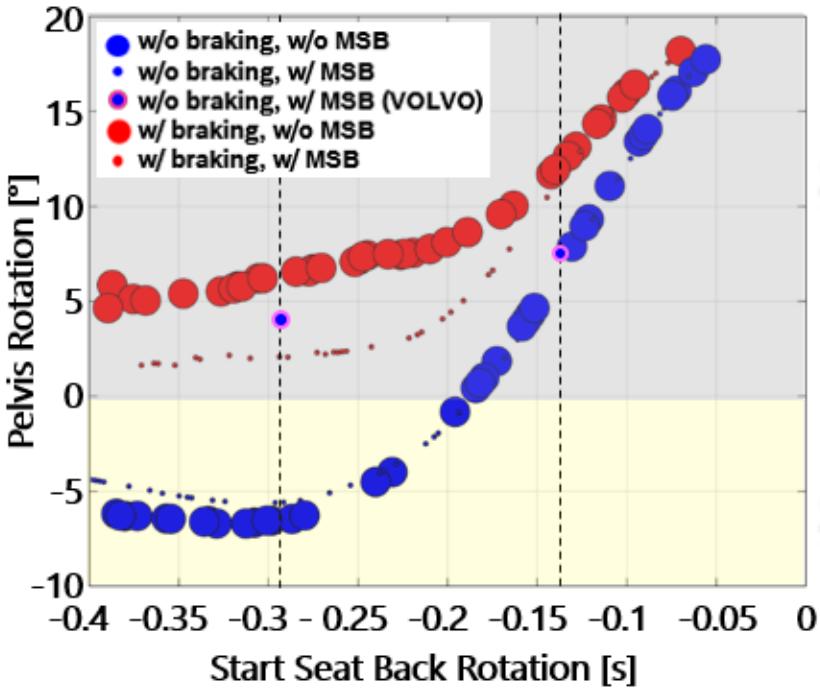

Figure 128 Difference of pelvis rotation after repositioning compared to upright sitting position

With pre-crash braking (red dots) the pelvis remained in a reclined position after repositioning. The relative angle of pelvis inclination increased with a later start of seat rotation, induced by the higher seat rotation velocity. Activation of belt pretensioner (MSB) during the pre-crash braking (small red dots in Figure 128) decreased the relative inclination of the pelvis, which means with pre-crash braking and belt-pretensioner the pelvis regained almost the whole 23° of seat raising, for a start time of seat back rotation earlier than -0.25 s. Without pre-crash braking the pelvis is rotated further than the upright position (blue dots in Figure 128) if seat back rotation started earlier than -0.2 s. Activation of seat belt pretensioning did not have any influence on the pelvis repositioning (compare small and large blue dots in Figure 128). Despite using different HBMs and simulation codes, comparison of Bosch results (Madymo AHM) with two selected Volvo Cars' cases (THUMS) shows a good match for faster rotation velocities (compare blue dot with pink edge to small blue dots at approx. -0.14 s). For the slower rotation velocity, the pelvis of the THUMS model remained slightly reclined after repositioning and the pelvis in the Madymo AHM rotated further than the upright position (compare blue dot with pink edge to small blue dots at approx. -0.28 s). Furthermore, no submarining was visible in any of the simulations of the complete DoE.

To analyse the reason for the difference, the two models (AHM and THUMS) have been aligned w.r.t. model landmarks. As shown in Figure 129, the THUMS pelvis in the upright position is more reclined than the pelvis in the AHM model. Thus, in the reclined position the THUMS model is also more reclined than the AHM. In the following study the pitch angle of 35.74° was increased to reach a higher pelvis inclination angle than in the first study. Afterwards a DoE with the same parameter settings and variations was conducted. Figure 129 right shows the results with a more reclined AHM pelvis. As a result, a higher initial inclination of the pelvis also yielded a positive pelvis rotation after repositioning compared to the upright position. Contrary to the first simulation study reported above, these results match the dedicated Volvo Cars' case for the slower seat back rotation velocity but not for the fast rotation. Therefore, an additional, not yet identified parameter must cause the difference in the models, which will be analysed in the following section.

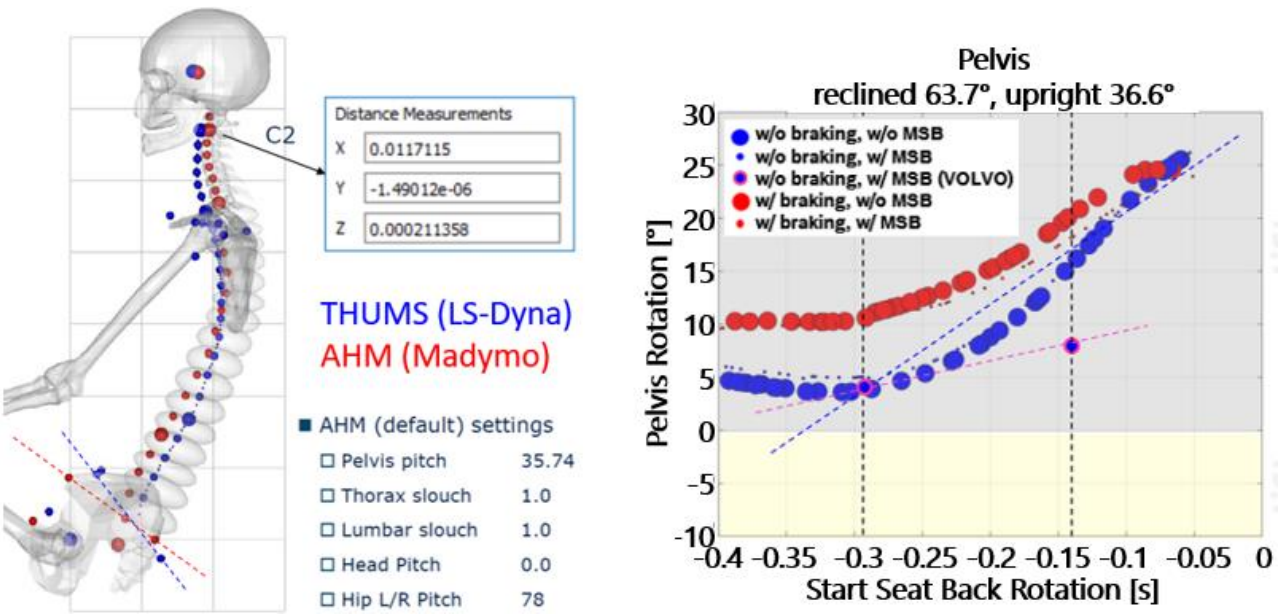

Figure 129 Comparison of THUMS & Madymo AHM model landmarks (left), pelvis rotation after repositioning for a higher initial pelvis inclination

In Figure 130 (left), the seat back rotation curves for rotation velocities of 80°/s and 160°/s are displayed. For the definition of the simulation input curve, the initial (45°) and target (22°) angles are given and between these points the curve was interpolated by a linear spline and spline_5 method. In Figure 130 the solid line shows the spline_5 interpolation, which was chosen for the above simulation studies. The dashed curves show the spline interpolation. The difference of these two interpolation methods is visible in the right graphs in Figure 130, where the first derivative of the seat rotation curve is shown. With the spline interpolation method, the rotation velocity is constant during the whole rotation (80°/s, 160°/s). The curves with the spline_5 interpolation method represent the same average rotation as with the spline interpolation method, but the characteristic of the curve is much different. If a typical electrical drive is considered as actuator for the seat back rotation, a curve such as the derivative of the curve with spline_5 interpolation could be expected.

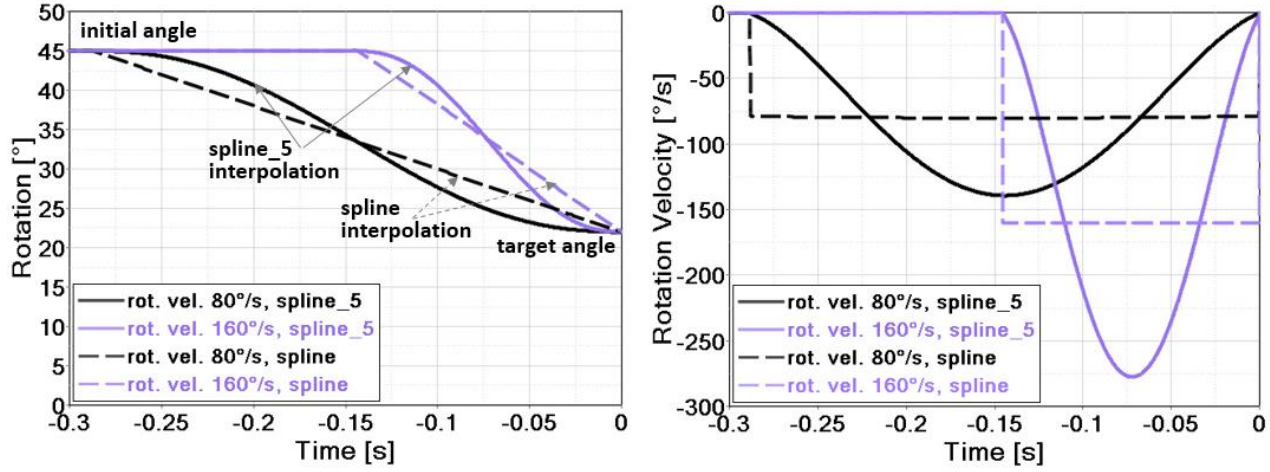

Figure 130 Interpolation of seat back rotation curve (left) & 1st derivative of seat back rotation (right) for rotation velocities of 80°/s & 160°/s

To analyse the influence of the rotation curve characteristics on the pelvis rotation, an additional simulation study was carried out. The corresponding DoE from the previous study was altered by

using a spline interpolation method for the seat rotation curve instead of the spline_5 method. The results of the DoE are shown in Figure 131. All four curves are more flattened compared to the results from the previous study. Also, the area where the rotation angle is almost constant is larger and has increased from approximately 0.1 s (-0.4 s to -0.3 s, compare Figure 129) to 0.2 s (-0.4 s to -0.2 s, compare Figure 131).

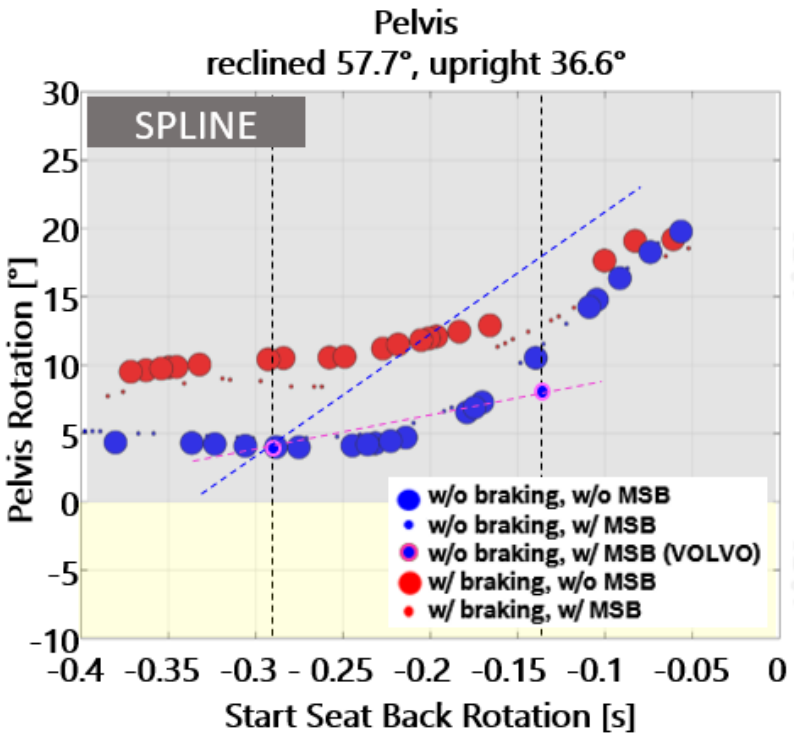

Figure 131 Difference of pelvis rotation after repositioning compared to upright sitting position for a seat rotation curve with spline interpolation method (instead of spline_5 method)

It is clear that seat-back rotation with a constant velocity has a favourable effect on the pelvis rotation. Furthermore, the results with the Simcenter Madymo AHM now match Volvo Cars' results for both defined rotational velocities. This could be expected since Volvo Cars used constant velocity curves as shown in Figure 130 (dashed lines in right graph). Now the question remains: which of these two rotation curves is the "right" one? Although an electric drive would provide a curve characteristic such as shown by the solid line in the right graph in Figure 130, the seat back itself represents a transfer path between electric motor and occupant. Which of the two curve interpolation methods should be used depends on an alignment of the electric drive characteristics with the stiffness of the seat back.

3.5.3.3 Effects of pre-crash retractor belt pretensioning

ZF's contribution is based on the same basic model as used in the previous Chapter 3.5.3.2, but applied to the rear seat positions. Since left and right position are fully symmetrical with regard to PP5, only P4 (right outboard rear occupant) is considered. Furthermore, a more realistic pre-pretensioning model (ACR) is introduced, see Chapter 3.1.3.10 for more details.

Focus and research question

The study focuses on the reversible pre-pretensioner attached to the retractor, which can be activated during the pre-crash phase. The aim of the study is to investigate the effect of a pre-pretensioner (PPT) with regard to PP5 in general and the effect of different characteristics of the more realistic ACR in particular.

Parameter variation

For this study, reversible pre-pretensioning was only considered at the retractor. The triggering time, the power output (i.e. belt force) of the ACR model and the seat back up-rise velocity are varied and compared. Furthermore, two crash pulses (generic full-frontal and SCP06, see Figure 42) are used in this study to analyse the impact of different pre-pretensioning characteristics on the restraint function and HBM values. An overview of the simulation model set-up can be found in Table 30.

Parameter	PP5
Occupant position	(P3), P4
Pre-crash pulse **Crash pulse**	Figure 4 Madymo's generic 56 FF, SCP06
Initial z-seat orientation **Z-seat rotation** **Z-seat rotation start** **Seat rotation velocity**	0° - - -
Initial seatback rotation **Seatback rotation velocity**	50° prescr. motion: 80, 120, 160°/s
Occupant model type **Excitation**	AHM v3.1 Soft
Airbag	None
Pre-pretensioning at retractor **Seat belt system type**	None / gen. PPT / ACR Fully seat integrated
Retractor pyro pretensioner TTF	10 ms
Load limiter type **Shoulder force**	Constant 3 kN
Anchor pyro pretensioner **Anchor pyro pretensioner TTF**	None -
Buckle pyro pretensioner **Buckle pyro pretensioner TTF**	None -
Generic PPT TTF **ACR TTF**	-200 ms -900, -750, -500 ms
Generic PPT belt force **ACR belt force**	250 N 175, 250, 425 N
Simulation solver	Madymo 7.8
OSCCAR model	Generic interior

Table 30 Simulation model set-up

Results

For the considered load case, a good coupling between occupant upper body and seat back is already induced by the pre-crash upward inclination of the seat back. However, there is still potential for a better coupling, especially in the pelvis area. Analysing the simulation results, a small improvement for the pelvis coupling can be observed for the ACR activation, which can be further improved by an earlier activation and higher electrical power. Furthermore, using the ACR model could also slightly improve the belt routing, i.e. the distance between belt and neck can be optimised. Figure 132 shows the occupant position at the end of the pre-crash motion for one exemplary parameter set. Looking on the colouring of the figures it can be concluded that the golden coloured occupant (ACR activated) is slightly more backward positioned for the whole body from pelvis to

head. However, differences are small compared to the studies for other protection principles, see Chapter 3.1.3.10 and 3.2.3.4.

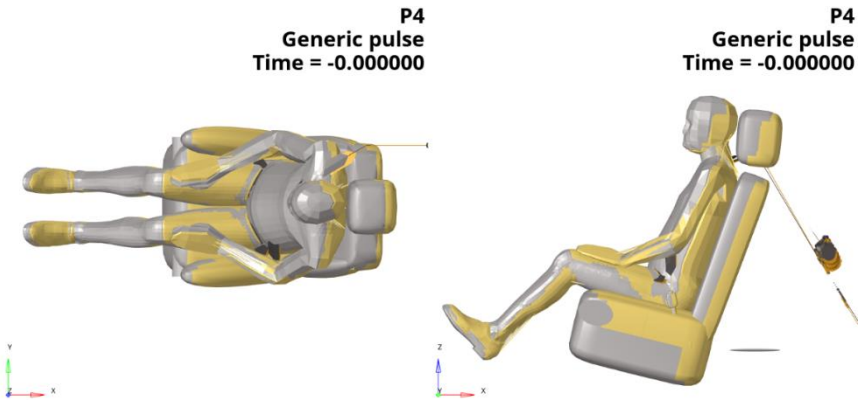

Figure 132 Occupant position at 0 ms for no PPT (grey) and ACR (gold)

Looking into the in-crash phase, for the two given crash pulses, the differences for no PPT and ACR are also quite small. However, a slightly better initial position for the pelvis can also slightly improve the overall kinematics, especially for hard pulses like the generic full-frontal pulse used here. Figure 133 shows the occupant position and forward displacement for SCP06 (left) and the generic full-frontal pulse (right). For both crash pulses a slightly better initial position due to ACR activation leads to a slightly reduced forward displacement, as can be seen by the colour distribution. However, the differences are small and for an adequate restraint function in the generic full-frontal pulse a frontal airbag would have to be added, which was not the focus here.

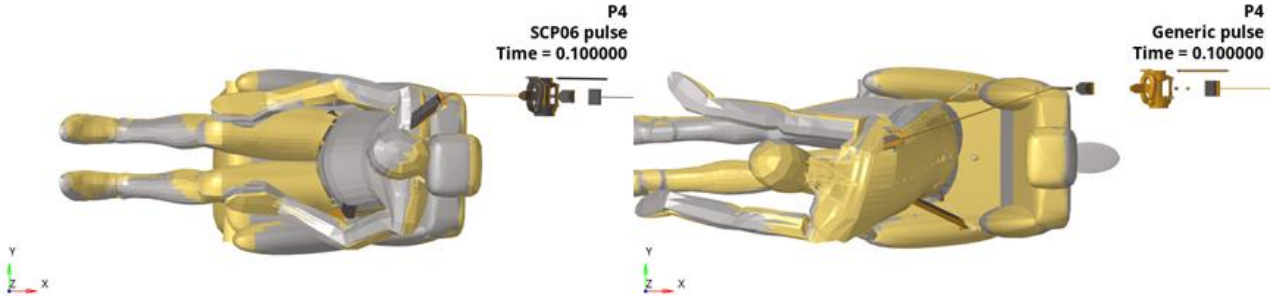

Figure 133 Occupant position at 100 ms for SCP06 (left) & generic full-scale crash pulse (right), comparing no PPT (grey) to ACR (gold)

Discussion

Activating the ACR seat belt pre-pretensioning model can also slightly improve the seat-occupant coupling for PP5, but to a lower degree than for PP1 and PP2. As a result, also the restraint function in the in-crash phase can be slightly improved. Earlier activation and higher electrical power can further enhance this effect, but still on a small scale compared to other protection principles. In general, as also stated for the studies in PP1 and PP2, an additional frontal airbag should be considered for adequate restraint function in case of hard frontal crash pulses.

3.5.3.4 Occupant repositioning in a rearward-facing seating position

In this chapter, the results generated by ika and fka for the repositioning of an occupant according to PP5 in a rearward-facing and reclined occupant use case considering a frontal crash scenario will be summarised.

The study investigated the effect of different seat back and seat base repositioning settings on a rearward facing occupant in a living room interior configuration prior to a frontal crash. Combinations of different seat back rotation as well as seat translation velocities were investigated to assess the effects of the repositioning on the occupant. The main goals of the repositioning within this study were: (a) to increase the space between occupant and dashboard to gain additional deceleration-space; (b) to bring the occupant to an upright seating position in order to avoid severe contacts between head and interior structures during the crash event; (c) to provide a reasonable effective restraint area of the seat back by rotating the seat back to an upright angle.

Methods

Two simulation studies were conducted. Both studies investigated a rearward-facing occupant in a living room interior within a frontal crash situation. The reclined seating position is defined as 45° reclined seat back angle, measured from the vertical axis of the recliner joint, whereas the upright position has an angle of 22°. The curves for repositioning in the studies were always modelled with a spline interpolation function (allowing smooth rotational velocity transitions). The recliner stiffness of the seat is modelled according to state-of-the-art production seats.

For the first study the multi-body solver Madymo was used to run a simulation study on the effects of different reposition velocities on the occupant kinematics in the pre-crash phase, using an active 50th percentile male HBM (Madymo Simcenter AHM v3.1) in a generic front interior environment, which was adapted to the previous described occupant use case (see Figure 134 (left)). Muscle activity was applied for the head and neck within this simulation study. The average seat back rotation velocity was varied from 33°/s (23° in 700 ms) to 460°/s (23° in 100 ms). The average seat translation velocity was varied from 0.21 m/s (0.15 m in 700 ms) to 3 m/s (0.15 m in 100 ms). The angle for rotation was defined as 23° and the distance for translation as 0.15 m. Two pre-crash situations with and without Automated Emergency Braking (AEB), starting at 750 ms before the crash, were investigated.

In the second study the finite element (FE) solver LS-Dyna was used to simulate the repositioning effects on a passive 50th percentile male HBM (THUMS v4.0.2) in a generic living room interior during the crash (see Figure 134 (right)). No HBM muscle activity was simulated in this second setup. The effects of four different repositioning velocities (23° and 0.15 m in 250 ms, 500 ms, 750 ms and 1000 ms) and three crash pulses (medium and high whiplash according to Euro NCAP and a generic 40 km/h full frontal crash pulse) on the occupant were assessed in this study. The crash cases were simulated without AEB being applied before the impact.

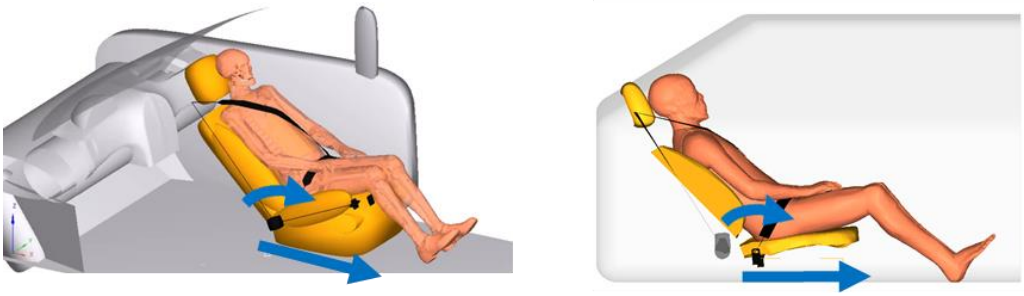

Figure 134 Madymo model setup, including Simcenter Madymo AHM v3.1 (left). LS-Dyna model setup, including THUMS v4.0.2 (right)

The seat model which is used in this study, is based on the generic model, described in Deliverable D2.2 [3]. To represent the seat back behaviour of a production seat under rear loading conditions, a recliner rotational stiffness was derived from [68] and transferred to the recliner joint of the generic

seat model. The rotational recliner stiffness curve can be found in Appendix 4.2. During the in-crash phase a linear translational stiffness of 54 kN/m is defined for the seat base, to allow a controlled seat shift into the principal direction of force during the crash. The value was defined based on the maximum acceleration of the 40 km/h FF crash pulse, the mass of the occupant and the available translation distance of 0.15 m. The feature was introduced, to use the gained space from the pre-crash phase for a controlled deceleration of the occupant during the in-crash phase.

Results (Multi-body pre-study)

When the occupant is repositioned from a reclined to an upright seating position the distance between occupant and dashboard increases and additional space for deceleration can be gained. Depending on the rotation velocity of the repositioning, the occupant may be pushed out of the seat, especially the unrestrained body parts (head, neck). Therefore, in the rearward-facing occupant use case, the assessment focus for evaluating the effectiveness of the PP during the pre-crash phase was put on the backset, which was defined as the smallest distance between back of the head and the centre of the head restraint (see Figure 135). This indicator was introduced with reference to [53] and indicates that a minimisation of whiplash injuries may be accomplished by limiting the head restraint backset to less than 60 mm. In this study the backset represents a limiting factor, under which reasonable repositioning can be conducted.

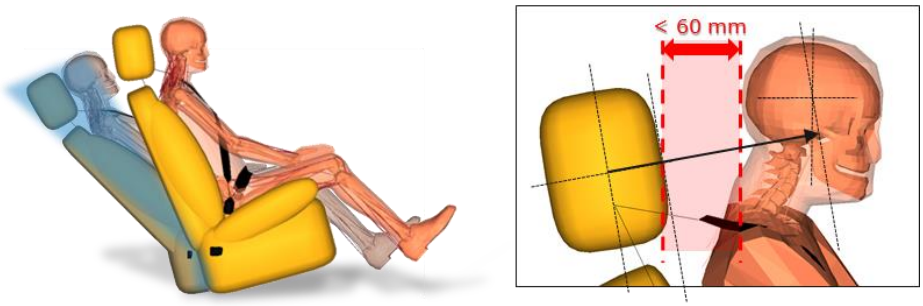

Figure 135 Definition of backset after repositioning the occupant

Figure 136 and Figure 137 show the backset at the end of the repositioning for different combinations of seat back rotation, as well as seat base translation velocities with and without AEB. At the end of the repositioning the start of the in-crash phase is initiated.

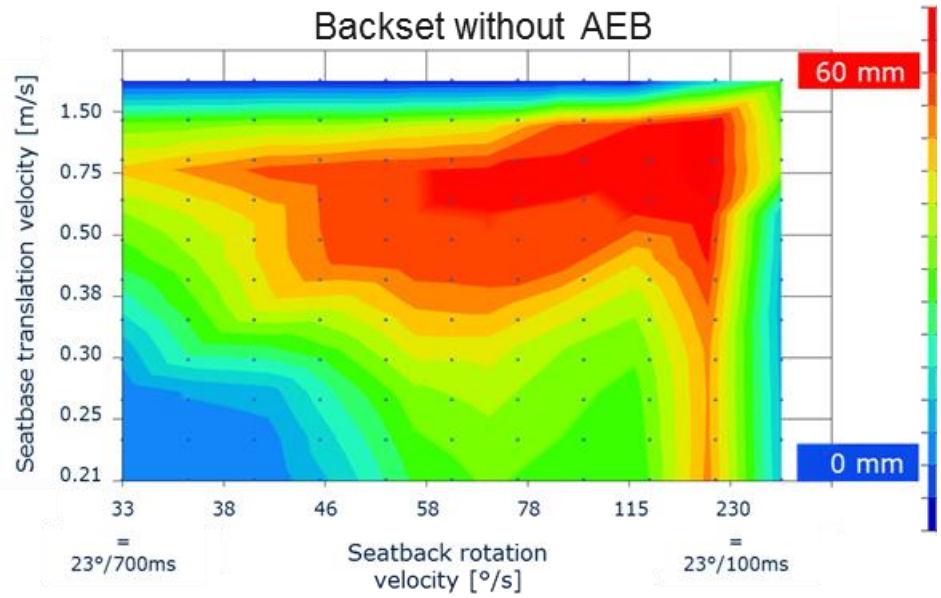

Figure 136 Backset assessment without AEB

The results therefore show the backset after repositioning, i.e. at the start of the in-crash phase. Due to the inertia of the head, the backset increases with an increase of the repositioning velocity. AEB reduces the backset, as the braking acceleration keeps the occupant closer to seat and head restraint.

For cases where the AEB-induced acceleration is higher than the repositioning-induced acceleration, the backset can be eliminated (see deep blue area in Figure 137).

Backset values below 60 mm can be achieved in cases without AEB for an average rotation velocity of 100°/s (23° in 230 ms) and a translation velocity of 0.35 m/s (0.15 m in 429 ms). When AEB is applied before the crash, an average rotation velocity of 120°/s (23° in 192 ms) with a translation velocity of 0.7 m/s (0.15 m in 214 ms) seems feasible in terms of the 60 mm backset threshold defined in [53].

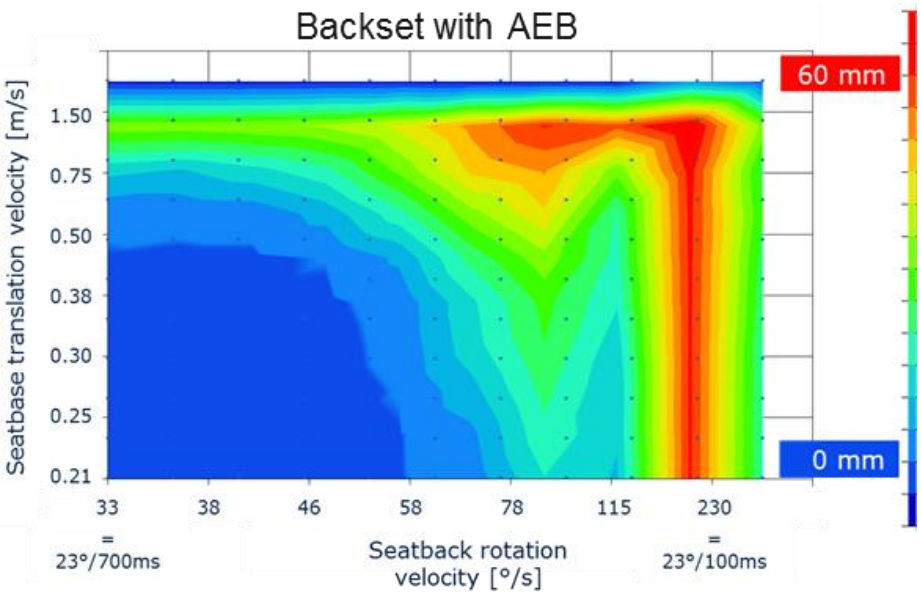

Figure 137 Backset assessment with AEB

Results (Finite element study)

The passive THUMS model shows backset values above 60 mm for the two highest repositioning velocities (23° and 0.15 m in 250 ms and 500 ms). As in this study no muscle activation is supported by the HBM, the inertia when being repositioned has a higher effect on the head and neck displacement compared to the previous study. For repositioning times of 750 ms and 1000 ms the backset values remain below the critical boundary of 60 mm (within these cases the occupant kinematics is comparable to the AHM in the first study). The occupant pre-crash kinematics are shown in Table 39 in Appendix 4.3 for a repositioning time of 750 ms.

The kinematic trajectories of the model with regard to the three different crash pulses are exemplarily shown for a repositioning time of 750 ms in Figure 138 and Figure 139. For reference, the baseline cases in an upright (22° seat back) and a reclined (45° seat back angle) position are shown as well. The initial occupant positions at the start of the crash are highlighted as cut sections in the graphs. The detailed occupant kinematics can be found exemplarily for the high whiplash and the 40 km/h FF pulse in the Appendix 4.3 (Table 40 and Table 41).

During the in-crash phase, it can be seen that the reclined seating position shows higher occupant ramping due to the seat back inclination. Moreover, the occupant in the reclined seat is more prone to contact the interior structure behind the seat (higher relative x-displacement of the head). PP5 maintains a higher distance between the occupant and the interior while reducing both longitudinal

and vertical displacement for the whiplash crash scenarios. The seat back is the main occupant restraint in the shown loading condition. However, the recliner stiffness used in this study cannot withstand the occupant load in the higher severity frontal crash scenario (40 km/h), which leads to excessive excursions of the occupant, as shown in Figure 139. The higher displacement in the reclined case is an indicator for an insufficient restraint of the occupant in the reclined case, which could lead to severe contacts between occupant and interior.

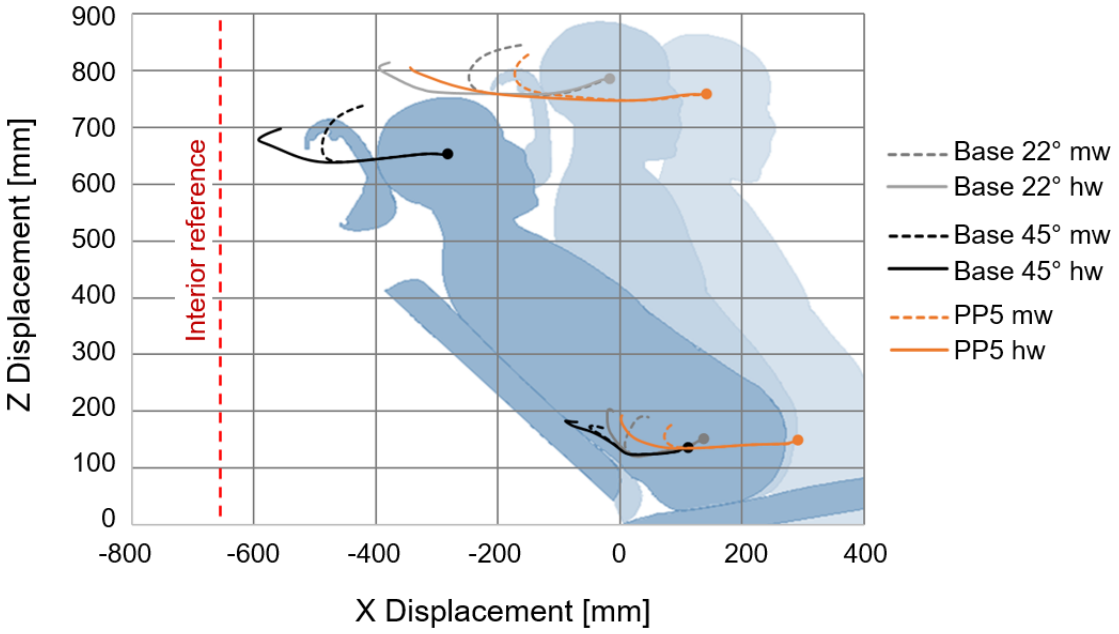

Figure 138 Medium & high whiplash crash: Trajectory for baseline (grey, black) & PP5 (orange)

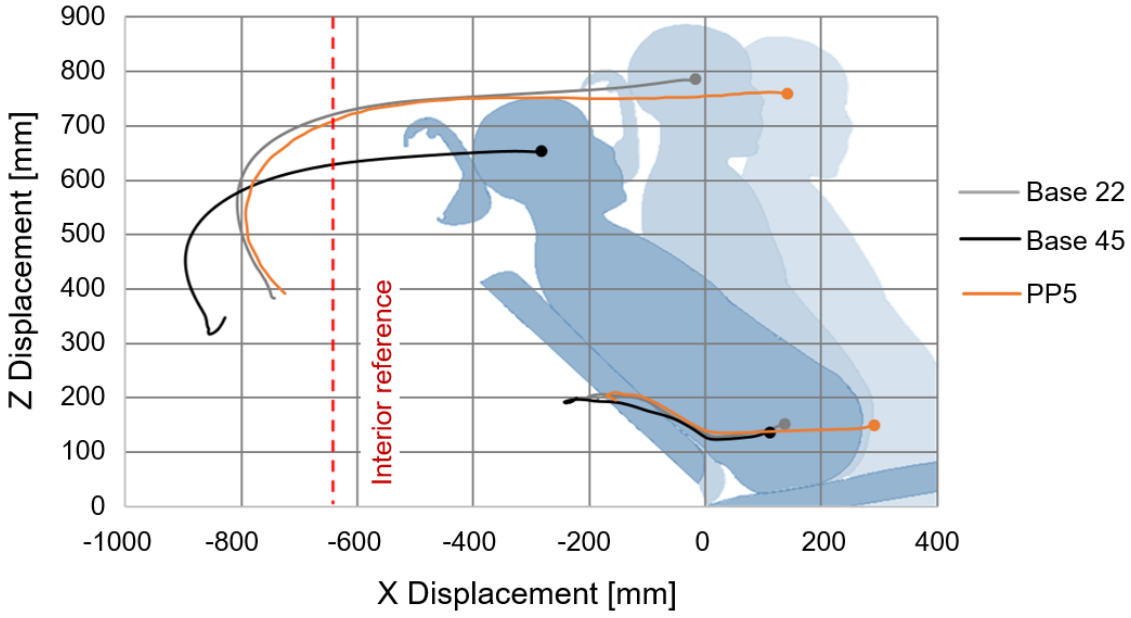

Figure 139 40 km/h full-frontal crash: Trajectory for baseline (grey, black) & PP5 (orange)

Discussion

When the occupant is repositioned by a seat base translation in combination with a seat back rotation, the occupant position at the end of the repositioning is highly affected by the applied repositioning velocity. Especially the distance between head and head restraint tends to increase

and can be a limiting factor. A state-of-the-art seat-integrated three-point belt system could not prevent an increase of the backset in the simulated multi-body and FE environments.

Sufficient repositioning is based on the initial situation (delta of seat back angle and / or seat translation as well as pre-crash timeframe for repositioning). The multi-body pre-crash study gives a reasonable repositioning velocity recommendation, for cases with and without AEB, to keep the backset below 60 mm. It has to be noted, that all findings are limited to the investigated environment.

The comparison of active and passive HBMs in Madymo and LS-Dyna showed that the measured backset highly differs between the two models, whereby the active model shows generally smaller backset values up to a repositioning time of 750 ms (for a repositioning delta of the seat back angle of 23° and a seat base translation distance of 0.15 m). This may be due to the muscle activity settings, or may be based on differences in occupant modelling and solver specific characteristics.

The repositioning increases the space behind the seat and brings the occupant to an upright position. During the crash event, the additional space can be used for controlled deceleration of the occupant when a sufficiently small seat back reclination angle can be realised. Such a sufficient angle must still be determined, to prevent the seat from causing a more dangerous ramp for the occupant. The effectiveness of the repositioning was analysed for three different crash acceleration pulses. The results for the medium and high whiplash acceleration pulse show that the upright position and the extra deceleration space in translatory direction reduce the absolute displacement and ramping tendency of the occupant. In the 40 km/h crash scenario, the advantages of PP5 compared to the reclined situation are less convincing, as the seat cannot keep the occupant in place, resulting in excessive ramping and high occupant displacements. Further development and investigations of seat structures for frontal crashes in rearward-facing occupant positions are needed. The seat model, which was used in this study represents the seat back stiffness only in a limited way with a recliner joint stiffness curve. Therefore, the generic seat back model does not show any structural deformation, which has to be taken into account when generalising the results.

Conclusion

A total number of 242 multi-body as well as 12 FE simulations were run in terms of the two presented studies. Seat repositioning increased the space between occupant and dashboard and brought the occupant to an upright position. The repositioning to an upright occupant posture caused an increase in backset, depending on the repositioning velocity and the HBM muscle activity. AEB generally lowers the backset for the rearward-facing use case.

During the crash event, the upright and translated seating position reduced the ramping tendency as well as the distance between occupant and dashboard for low acceleration pulses, which can be favourable when contact between occupant and vehicle structures must be avoided in the deceleration phase. The effectiveness of the principle was shown for medium and high whiplash acceleration pulses. For higher acceleration pulses (40 km/h FF), the seat back recliner stiffness as well as the generic seat model definition highly limited the results. Nevertheless, also in these cases the principle reduced the maximum displacement of the occupant compared to the reclined baseline case.

3.5.4 Conclusion

Referring to the initially-raised research questions for PP5 (see Chapter 3.5.2), the conclusion focuses on the one hand on occupant repositioning and general functionality of the protection principle, and on the other hand on the effect of the repositioning of the occupant model with regard to safety and overall kinematics. The conclusions are based on the simulation studies presented in Chapters 3.5.3.1, 3.5.3.2, 3.5.3.3 and 3.5.3.4.

The repositioning of a forwards-facing occupant by seat back rotation was not able to fully restore the pelvis rotation compared to an upright seating position, due to flexibility in the lumbar spine of the HBM. It was found that a constant repositioning velocity curve has a favourable effect on the pelvis angle restoration. The upright occupant position provided a shorter distance between head and airbag, which reduces the head impact velocity in the in-crash phase. Despite this, submarining was not avoided by repositioning the occupant. A belt PPT reduced the forward displacement of the occupant during the pre-crash phase, but also restrained the pelvis during repositioning. A study on the advanced PPT system ACR showed that an optimisation of the belt pre-pretensioner can reduce the reaction time as well as increase the belt force and pull-in. In combination with seat back repositioning, a more robust coupling between occupant and airbag could be achieved in frontal collisions. Additional to the active repositioning of the occupant by backrest rotation, it was found that AEB prior to a crash can be used to reposition the occupant similarly, based on the torso inertia and without rotating the backrest.

For a rearward-facing occupant, a critical increase of the backset during the repositioning was observed in the simulations. The backset increased with an increase of repositioning velocity. The effect was reduced when AEB was applied during the repositioning, leading to a lower distance between head and head restraint at the beginning of the crash phase. An upright rearward-facing occupant position reduced ramping effects, and the additional space between occupant and dashboard due to the translatory movement could be used to lower the risk of interactions between occupant and interior structures. In addition, the newly gained space can be used for a controlled deceleration of the occupant, when a sufficiently small seat back reclination angle can be realised. This angle must still be determined and could be considered in the development of future seat structures to protect occupants in the best possible way within the rearward-facing use case.

Several human body models (SAFER HBM v9.0.1, Madymo Simcenter AHM v3.1 and THUMS v4.0.2) were used in the studies. Despite the model differences, similar kinematic trends were shown. Nevertheless, muscle activity settings affect the overall kinematics of the occupant during the repositioning and lead to different simulation outcomes during the pre-crash and in-crash phase. When defining the repositioning velocity, the seatback stiffness as well as the characteristics of the electrical motor become important, as it was found that the characteristics of the repositioning velocity curve, applied to the human body, highly affect the outcome of the simulations and the repositioning. All presented results are only applicable for the investigated simulation environment, as well as the applied vehicle interior and occupant models.

3.6 Protection Principle 6 - Far-side Load Case

The overall objective of Protection Principle 6 (PP6) is to evaluate countermeasures, i.e. protection principles, for the far-side load case. In this case, the challenge is to restrain the occupant mainly through seat-mounted protective measures in order to allow maximum freedom for seat positioning in AD vehicle interiors. The corresponding working group consists of TME and IDIADA.

3.6.1 Motivation and Background

OSCCAR deliverable D1.1 [28] highlighted collisions at intersections in urban or rural areas. These results were obtained by filtering out accidents which an AD car would not cause, and running pre-crash simulations of the remaining accidents with emergency manoeuvre. Further description of this accident scenario from the Swedish accident dataset showed that side impact collisions where the AD car would be struck from the side represented 20% of the remaining intersection collisions (Figure 140). It was therefore thought important to investigate new protection principles for this load case as well.

	Visualisation	Cluster share	CA host [°]	CA opp [°]	yaw [°]	Cluster share	V host [km/h]	V opp [km/h]
#1		7%	65	37	-92	2%	0	31
						5%	31	9
#2		24%	-48	41	92	14%	3	32
						4%	4	57
						6%	21	14
#3		16%	-3	-51	-92	4%	14	30
						12%	34	12
#4		7%	-61	-43	98	4%	14	13
						3%	15	30
#5		14%	-6	54	90	7%	36	17
						7%	9	24
#6		6%	-90	42	79	3%	11	56
						3%	17	19
#7		19%	48	-42	-92	10%	14	33
						9%	30	13
#8		2%	-34	-116	-108	1%	18	50
						1%	21	27
#9		4%	21	-95	-78	1%	50	18
						2%	19	51
						1%	17	14
#10		1%	6	132	90	1%	23	34

Figure 140 Representative cases of Swedish intersection collisions (green car: ego AD car, blue car: opponent car). Adopted from Figure 41 in ref. [28]

One of the challenges for occupant protection in an AD car under this load case was identified as being the protection of the occupants sitting on the far-side where the main occupant retention might be done through the seat design and the seat-mounted belt system without the supporting effect of a centre console. Indeed, it is foreseeable that in an AD car no centre console will be used in order to free up space in the cabin and allow for new seating configurations (e.g. “living room” or “fire camp” use case configuration) as those identified in OSCCAR deliverable D2.1 [2].

Several protective measures were investigated for a test case combining the far-side load case and the rear-seat use case shown in Figure 141. Therefore, the double lap belt pretensioning studied in Working Group 3 was combined with a seat side-support designed to reduce the excursion of the occupant in case of side loading conditions. The effects of an inverted belt were also investigated in this study, similarly to [54].

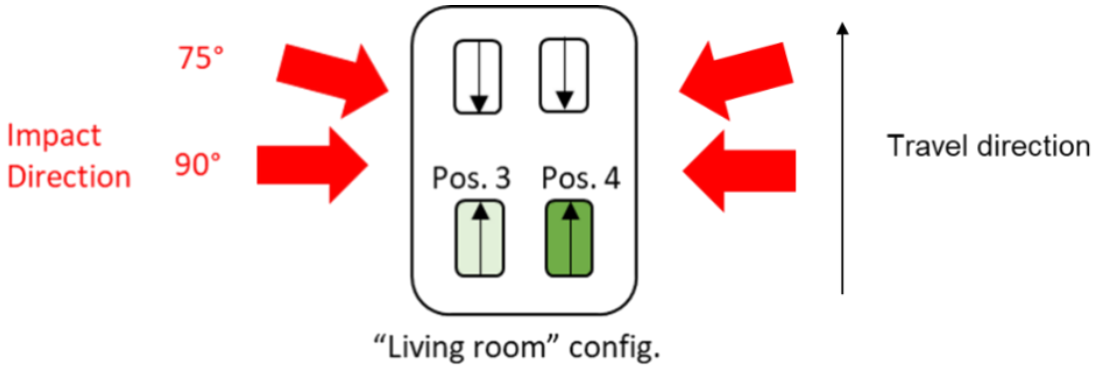

Figure 141 Far-side test case

3.6.2 Research Questions

On the far-side, the limitation of the occupant's head excursion and the prevention of the occupant's impact with the opposite intruding structures are the main safety concerns. This question is currently addressed by the far-side protocol recently added by Euro NCAP [55]**.**

Petit at al. (2019) [56] demonstrated that the WorldSID crash test dummy allows a fair estimation of the occupant head excursion but points out some differences with Post Mortem Human Subjects (PMHSs) regarding the relative head-to-chest angle and thoracic spine curvature (Figure 142). These differences were attributed to the WorldSID dummy spine design, rigid in its thoracic area and concentrating the flexibility in the neck and lumbar spine only. This can lead to a different interaction between the WorldSID and the car interior parts than for a car occupant. This may also affect WorldSID injury prediction.

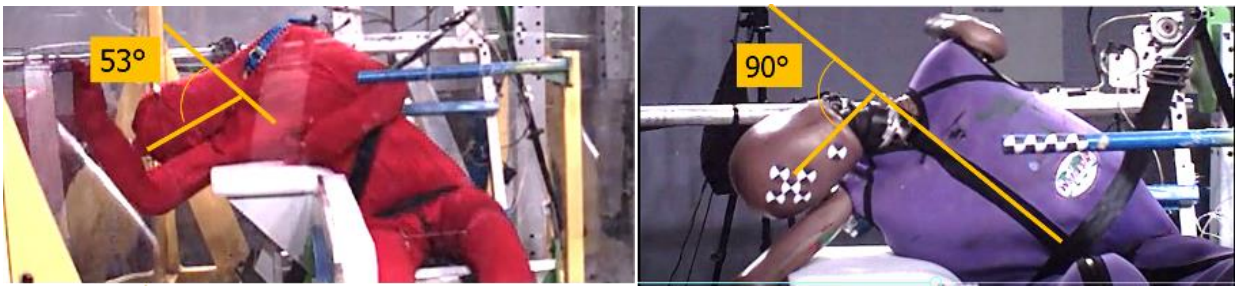

Figure 142 PMHS & WorldSID far-side test in generic car environment with centre console [56]

Through the study of PP6, the following research questions are investigated:

- How to protect occupants in AD L4/L5 cars in a far-side load case? How to restrain the occupant pelvis and thorax on the far-side when no centre console is available and therefore limit occupant interaction?
- Is the WorldSID dummy biofidelic enough to assess occupant protection on the far-side? What are the dummy limitations and can the WorldSID predict injuries accurately enough?

- What can HBMs bring in addition to the dummy for this load case? Due to its rib cage and spine design, the WorldSID dummy kinematics might be different to the HBM kinematics when interacting with the countermeasures related to PP6. This may affect the loads transmitted to the neck, lumbar spine and pelvis, as well as the rib fracture prediction.

3.6.3 Simulation Studies

Three main protective measures were evaluated by this working group using the THUMS v4.1 Human Body Model. The double lap belt pretensioning, also used in PP3 with regard to a frontal-oblique load case, was used as baseline and combined with two other protective measures.

At first, WorldSID dummy simulations were performed to confirm the feasibility of a PP6 hardware demonstration by sled tests. This pre-study is reported in 3.6.3.1. The corresponding physical evaluation of PP6 will be documented in OSCCAR deliverable D2.5 [1]. Finally, THUMS simulations were carried out under the same conditions as the sled tests.

3.6.3.1 Pre-study using a WorldSID 50M dummy model

The test conditions described in [56] were simulated. The restraint system (3-point belt mounted on B-pillar and centre console) was modified gradually to check the effect of each parameter and simulate the different protective measures studied under PP6:

I. Double lap belt pretensioning

II. Inboard-mounted double lap belt pretensioning

III. Seat side supports in addition to the inboard-mounted double lap belt pretensioning

The FEM environment consists of a rigid inclined seat pan, a rigid seatback, a rigid footrest and two rigid centre consoles (one for the legs and one for the pelvis) covered by 50 mm thick Ethafoam sheets (Figure 143). The double lap belt pre-tensioner FEM model was provided by Autoliv. It is the same as the one used in the PP3 simulations. The additional seat side supports (III) are modelled as rigid and are also covered by Ethafoam material. The seat side support geometry simulates the shape of a racing seat (Figure 144).

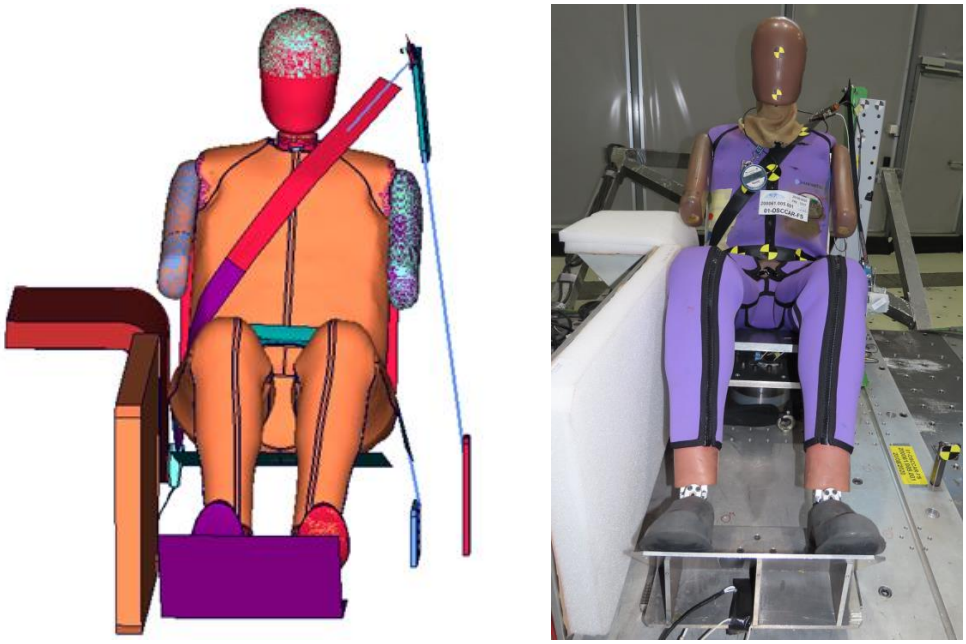

Figure 143 Simplified PP6 environment (left: FEM, right: FAR-SIDE test set-up)

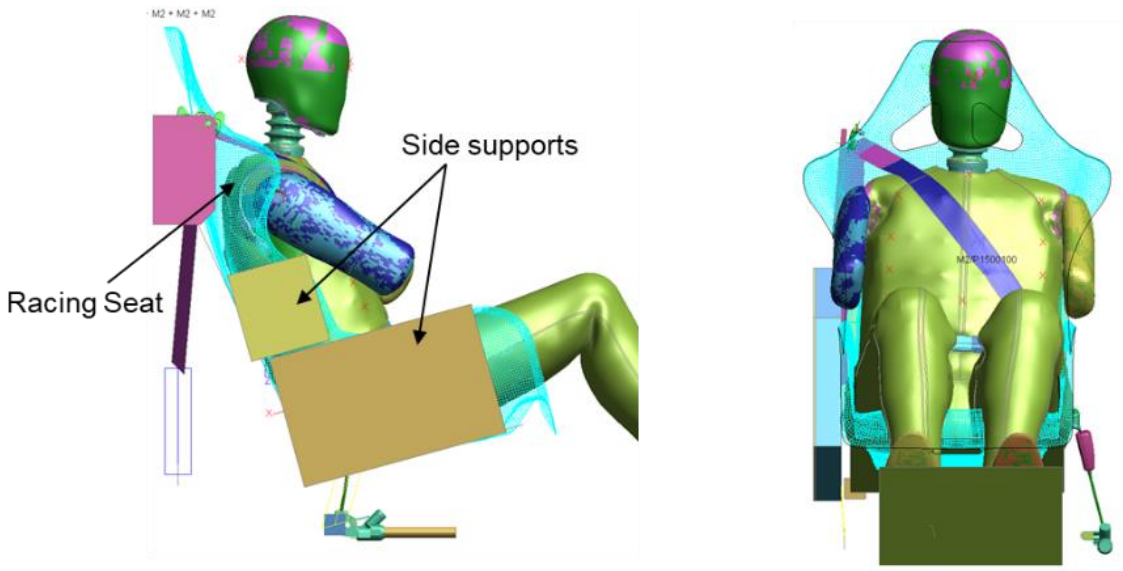

Figure 144 Seat side support design (torso support: 155×171×50 mm, pelvis support: 400×255×50 mm) & in-board shoulder belt routing

The WorldSID FEM model used is a TMC internally-developed dummy model. The model was validated at component level considering the correlation between FEM and test results under ISO 15830 head, neck, shoulder, thorax, abdomen and pelvis side impacts, but also considering additional component tests on neck and lumbar spine relevant for the far-side load case. The WorldSID FEM head excursion was validated using [56] and is shown in Figure 147.

The environment centre line was angled by 75° with respect to the pulse direction (Figure 145). The pulse from [56] was applied to the simulated environment (Figure 146).

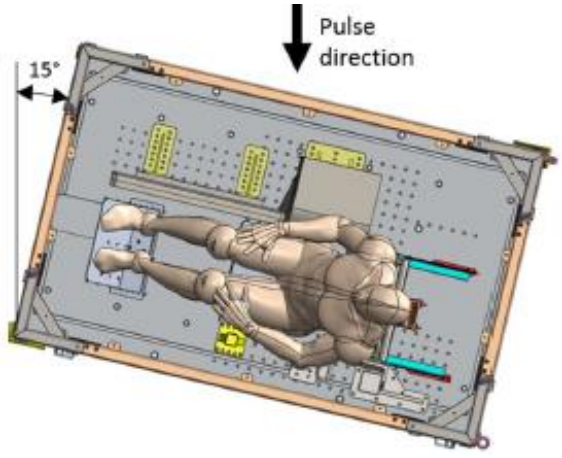

Figure 145 Test set-up [56]

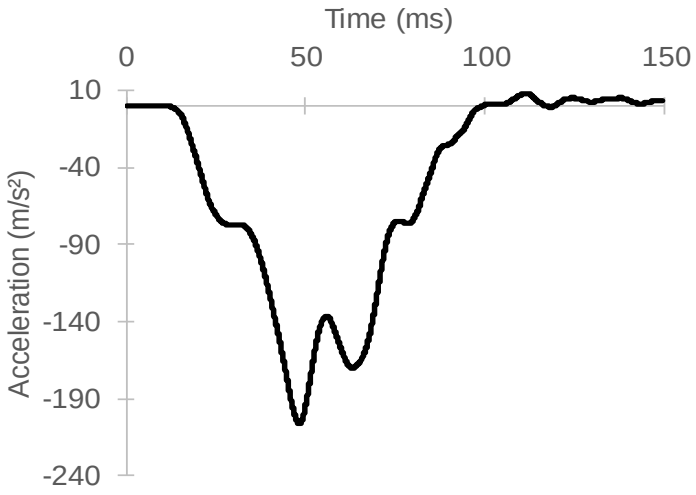

Figure 146 Pulse at 8 m/s [56]

The simulation matrix defined for this pre-study is presented in Table 31. In total five different configurations were considered.

ID	Centre console	Belt anchorages	Belt type	Seat side supports
W1_1	Yes	B-Pillar	3-point belt with static pre-tension (200 N)	No
W4_1	No	Seat mounted	3-point belt with shoulder retractor	No
W5_1	No	Seat mounted	Double lap belt pretensioning	No
W6_1	No	Seat mounted Inboard shoulder belt	Double lap belt pretensioning	No
W8_1	No	Seat mounted Inboard shoulder belt	Double lap belt pretensioning	Yes

Table 31 WorldSID simulation matrix

The simulation run W1_1 conducted in order to validate the simulation environment shows a good correlation with the test data of [56], as illustrated in Figure 147 to Figure 152.

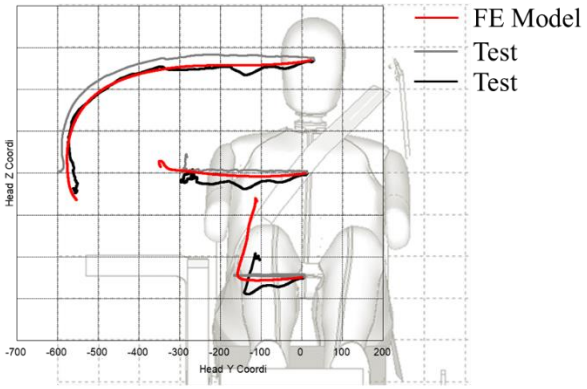

Figure 147 WorldSID kinematics

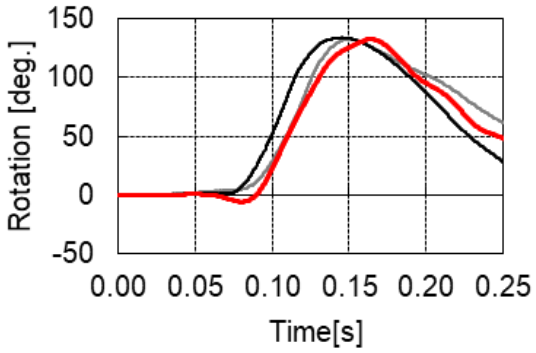

Figure 148 WorldSID head rotation

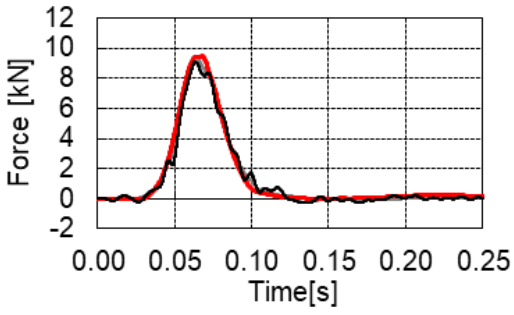

Figure 149 Fy contact force between WorldSID & centre console

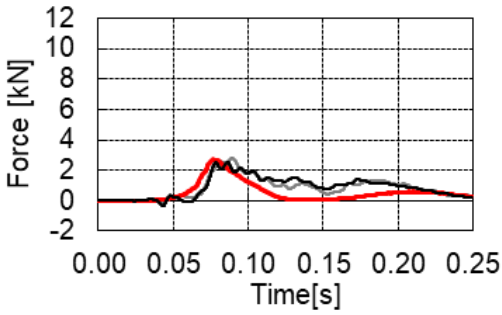

Figure 150 Fz contact force between WorldSID & centre console

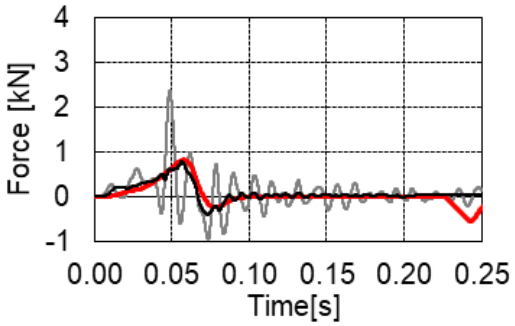

Figure 151 Fy contact force between WorldSID & seat

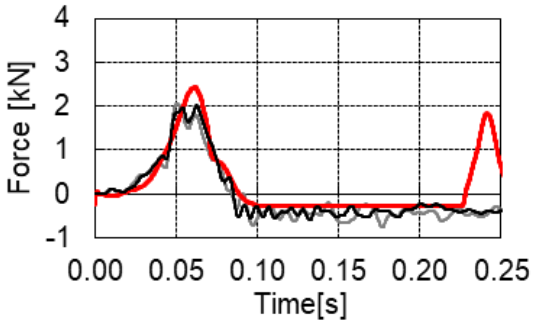

Figure 152 Fz contact force between WorldSID & seat

The effects of the different protective measures considered (double lap belt pretensioning, inboard shoulder belt and seat side supports) on the dummy kinematics and the dummy-belt interaction are visualised in Table 42 of Appendix 5.1.

The WorldSID head excursion could be decreased by 357 mm between simulation W4_1 (dummy restrained by a standard 3-point belt) and simulation W8_1 (dummy restrained with the inboard shoulder belt with double lap belt pretensioning and seat side supports) (Figure 153).

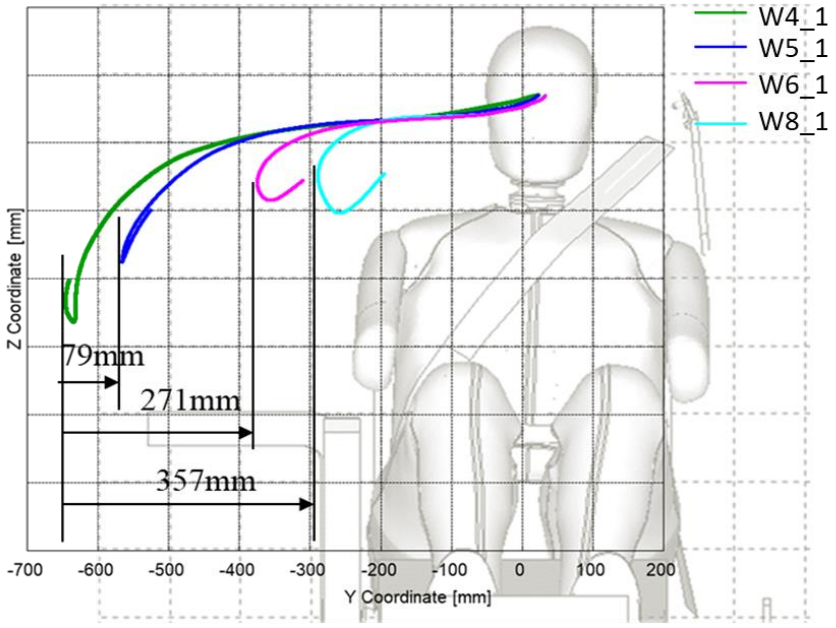

Figure 153 WorldSID head excursions

In summary, the considered protective measures had the following effects on WorldSID head excursions in a far-side load case:

- An increase of 30 mm when the shoulder belt anchorage points were changed from a B-pillar mounted belt to a seat-mounted belt.
- A reduction of 79 mm when the double lap belt pretensioning was used instead of the standard 3-point belt mounted on the seat.
- An additional reduction of 192 mm compared to the previous case when the double lap belt pretensioning was mounted inboard.

- A further reduction of 96 mm compared to the previous configuration when the seat side supports were added.

The WorldSID measurements showed an increase of rib deflections for the addition of the seat side supports. However, the rib deflection peaks (20 mm) were within the rib IR-TRACC capacity with no damage expected for the dummy during hardware tests. Neck forces and moments were also acceptable considering dummy thresholds as defined in the Euro NCAP far-side protocol [55]. It was therefore judged feasible to perform corresponding hardware demonstrator sled tests at CTAG-IDIADA in order to gain further validation data. As mentioned above, this test series is reported in OSCCAR deliverable D2.5 [1]. Additional THUMS simulations repeating the test matrix were performed in the main study for a more detailed investigation of PP6.

3.6.3.2 Main Study using THUMS human body model

The Total Human Model for Safety (THUMS) v4.1 50th percentile male was used for the main study. Compared to THUMS v4.0, THUMS v4.1 has updated pelvis and lumbar spine geometries and also a more accurate definition of the rib cortical bone thicknesses to improve rib fracture prediction.

THUMS head COG excursion (Y-displacement in sled direction, Figure 145), rib deflections (Figure 154) and section forces at upper / lower neck (Figure 155) and at 5th lumbar spine vertebra (Figure 156) were extracted from the THUMS simulations. Skeleton fractures were predicted in THUMS when first principal plastic strains were above 2% in the cortical bones.

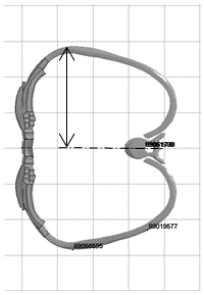

Figure 154 THUMS rib deflection measurement

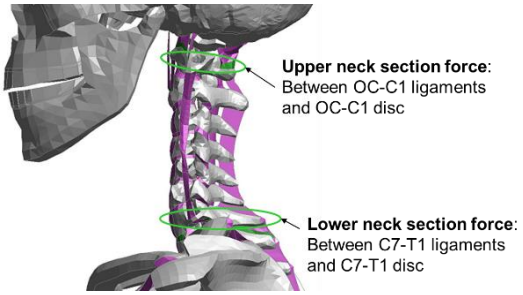

Figure 155 THUMS upper and lower neck section forces

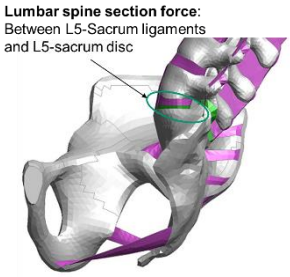

Figure 156 THUMS lumbar spine section force

Table 32 shows the simulations performed with the THUMS model. All simulations used the 8 m/s pulse from [56]. Identical simulations were run with the WorldSID FEM model (W1_2 to W5_2), which also correspond to the hardware tests performed at CTAG-IDIADA.

ID	Centre console	Belt anchorages	Belt type	Seat side supports	WorldSID simulation ID	WorldSID test ID [1]
T1	Yes	B-Pillar	3-point belt with static pre-tension (200 N)	No	W1_2	01-OSCCAR-FS 02-OSCCAR-FS
T2	No	Seat mounted	Double lap belt pretensioning	No	W2_2	09-OSCCAR-FS 10-OSCCAR-FS

T3	No	Seat mounted	Double lap belt pretensioning	Yes	W3_2	03-OSCCAR-FS 04-OSCCAR-FS
T4	No	Seat mounted - Inboard shoulder belt	3-point belt with shoulder retractor	No	W4_2	07-OSCCAR-FS 08-OSCCAR-FS
T5	No	Seat mounted - Inboard shoulder belt	Double lap belt pretensioning	Yes	W5_2	05-OSCCAR-FS 06-OSCCAR-FS

Table 32 THUMS v4.1 simulation matrix

The THUMS head excursions are shown in Figure 157. The highest head excursion was observed in the T1 simulation, followed by T2, T4, T3 and T5. The in-board shoulder belt as well as the seat side supports were effective measures to reduce the head excursion. With the in-board shoulder belt alone (T4), the head excursion was less than 400 mm and with the seat side supports and the outboard shoulder belt (T3), the head excursion was less than 340 mm. When both in-board shoulder belt and seat side supports were combined, the head excursion was close to 300 mm (T5).

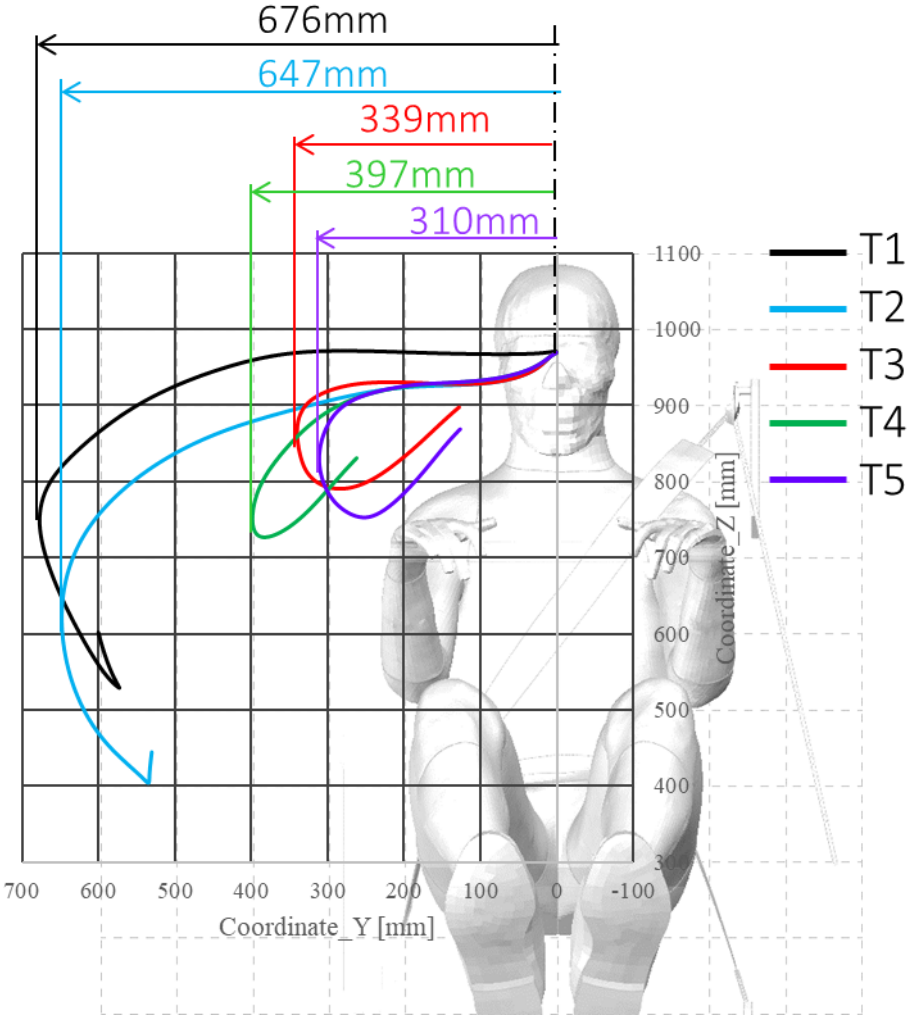

Figure 157 THUMS head COG excursions

The THUMS rib deflection peaks were generally higher at the lower chest (from rib 7 to 10) and around 30-40 mm in configurations T3 and T5 (Figure 158). Rib fractures were predicted in simulation T1 at the 10th rib and in T3 at the 5th and 6th ribs (Figure 159). The rib deflections were the lowest (below 15 mm) for the in-board shoulder belt (T4). The addition of the seat side supports, especially with the in-board shoulder belt (T5), increased the rib deflection.

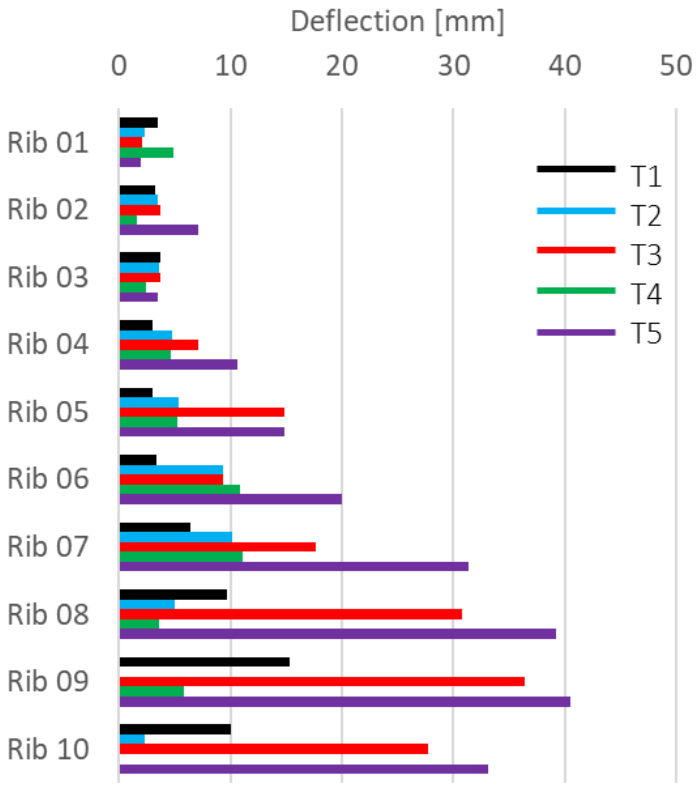

Figure 158 THUMS rib deflection peaks

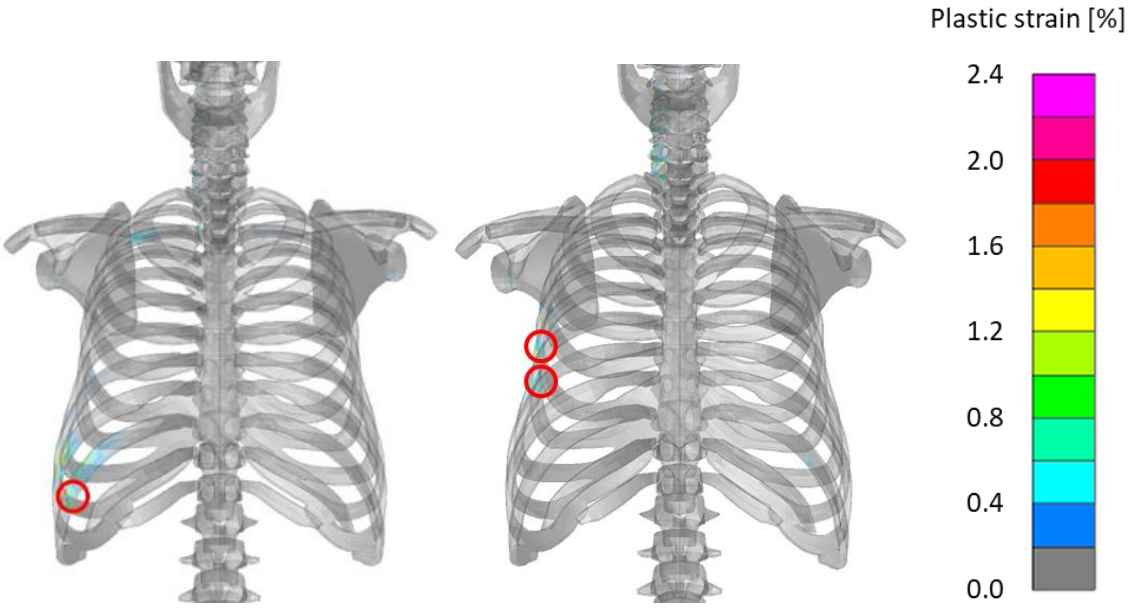

Figure 159 10th rib fractures in T1 (left) and 5th / 6th rib fractures in T3 (right)

Cervical spine fractures were predicted in simulations T1 (3rd and 7th cervical vertebrae), T2 (3rd, 5th 6th and 7th cervical vertebrae) and T5 (5th, 6th and 7th vertebrae) (Table 33). In simulation T2, two thoracic spine fractures were predicted in addition (1st and 2nd vertebrae).

No lumbar spine fracture was predicted in any of the configurations. The THUMS lumbar spine Mx was the highest in T2 and T4 (belt only configurations) (Table 48 in Appendix 5.1). A sacro-iliac fracture was predicted on the right side in simulation T4.

ID	Fractures
T1	3rd & 7th cervical spine vertebrae, Right side: 10th rib
T2	3rd, 5th, 6th & 7th cervical spine vertebrae, 1st & 2nd thoracic spine vertebrae
T3	Right side: 5th rib, 6th rib
T4	Right side: Pelvis
T5	5th, 6th & 7th cervical spine vertebrae

Table 33 THUMS skeleton fractures

THUMS & WorldSID FEM comparison:

The WorldSID head excursions showed a similar trend as the THUMS model. However, it has to be noted that the THUMS excursions were around 100 mm higher for the centre console configuration (simulation T1) and 165 mm higher with the double lap belt pretensioning alone (simulation T2) (Figure 160).

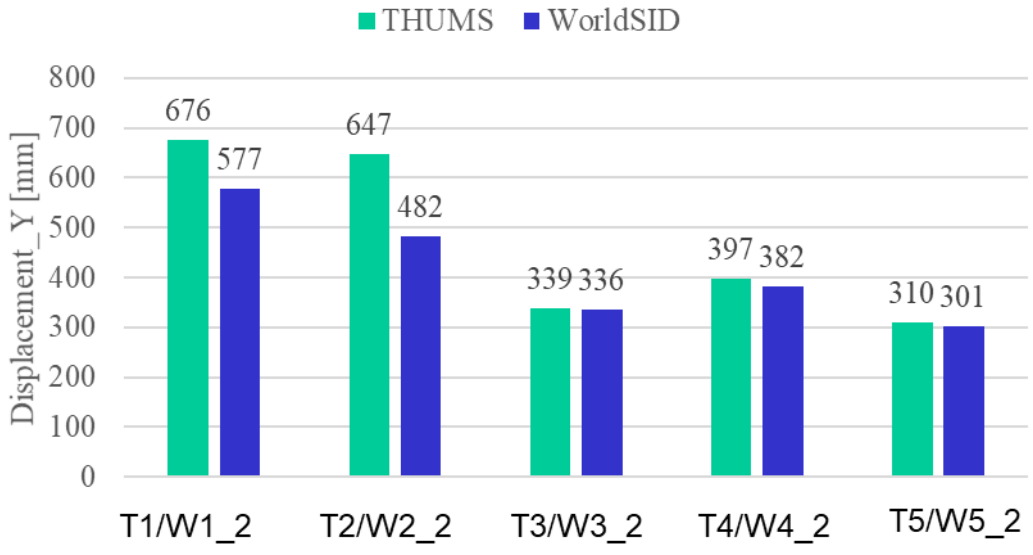

Figure 160 Comparison of THUMS & WorldSID FEM head COG excursion peaks

A comparison of THUMS and WorldSID kinematics at 0, 50, 100 and 150 ms can be found in Table 43 of Appendix 5.1. Shoulder interaction with the seat side supports was different between THUMS and WorldSID due to the fact that the WorldSID had only half arms (Figure 161).

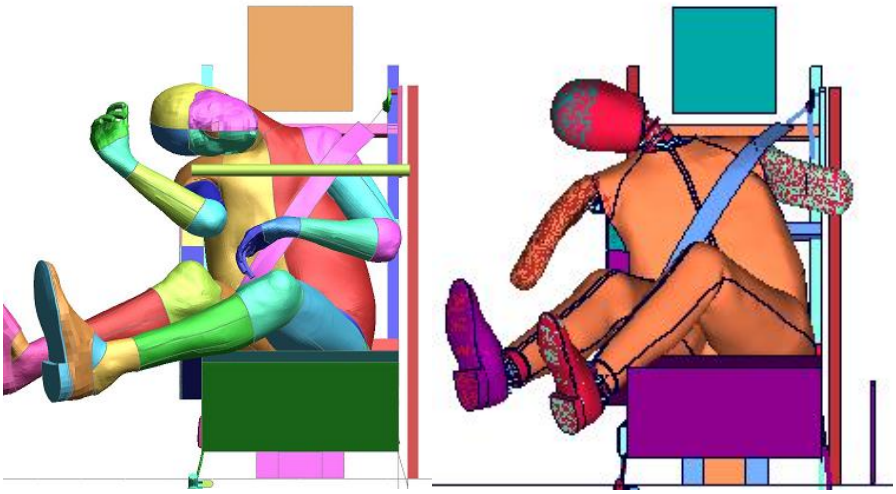

Figure 161 THUMS (left) & WorldSID (right) interaction with the seat side supports at 150 ms

Centre console and seat side support contact forces as well as seatbelt forces for both THUMS and WorldSID are illustrated in Table 44, Table 45 and Table 46 of Appendix 5.1.

Injury risk assessments given by THUMS and WorldSID can be compared in Table 33 and Figure 162 respectively. Additionally, injury risks related to Euro NCAP assessment limits are given in Table 47 of Appendix 5.1.

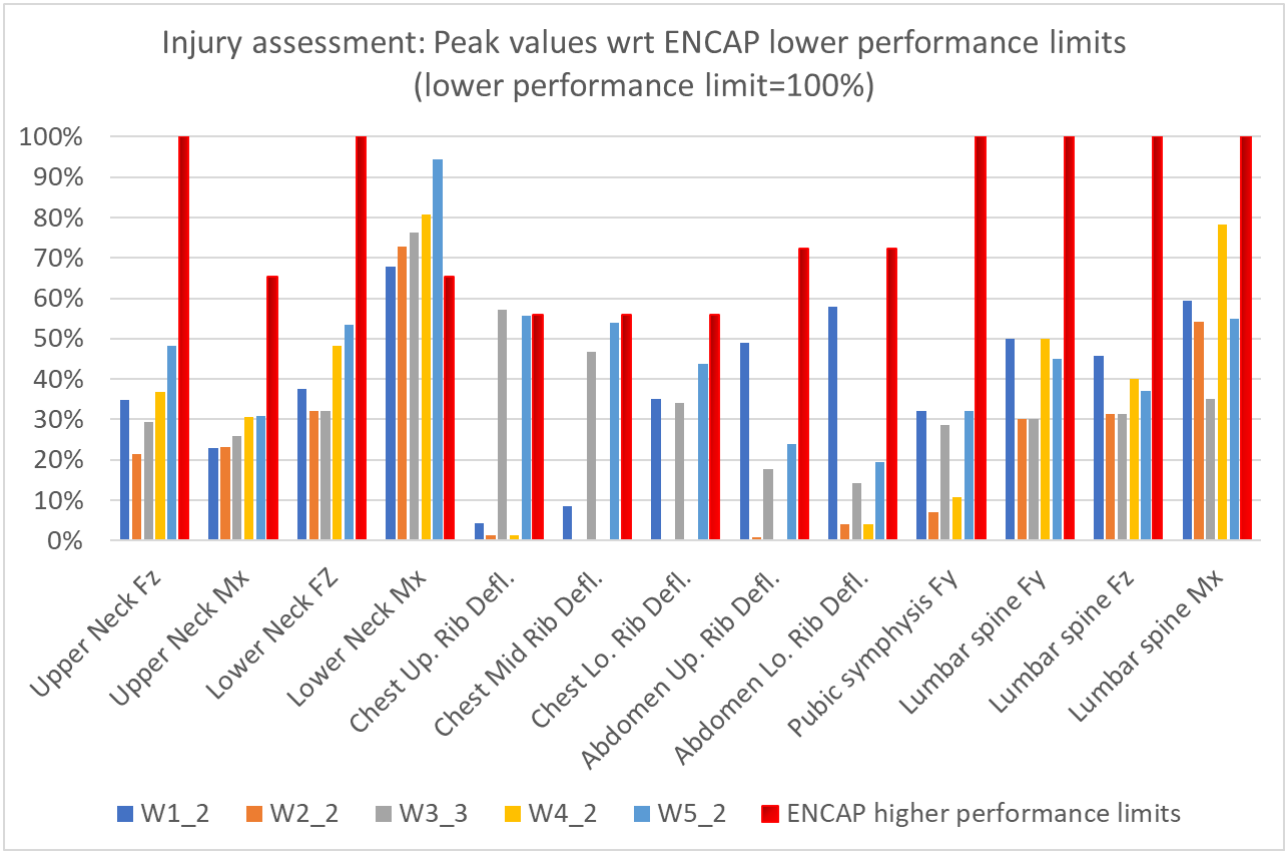

Figure 162 WorldSID injury assessment. Peak values in proportion of Euro NCAP lower performance limits

The WorldSID injury values were above the Euro NCAP higher performance limit for the lower neck Mx in all simulations and reached 95% of the lower performance limit in simulation T5 for which THUMS predicted three lower cervical spine vertebra fractures (from the 5th to the 7th vertebrae). The WorldSID upper neck measurements did not predict the risk for upper neck fractures shown by THUMS in simulations T1 and T2. Both THUMS and WorldSID predicted a higher risk of lower cervical spine fractures in simulation T5 (in-board shoulder belt with seat side supports).

The THUMS model predicted a 10th rib fracture in simulation T1 where the WorldSID had the highest abdominal rib deflection but still below the highest performance limit (between 68 and 80% of it). The THUMS model predicted 5th and 6th rib fractures in simulation T3 where the WorldSID had also the highest chest upper rib deflection (102% of the higher performance limit). The WorldSID chest upper rib deflection was of a similar value for simulations W3_2 and W5_2 (seat side support configuration) but the risk of a chest AIS3+ was predicted close to zero for a 45 years old occupant which was in line with the THUMS prediction (a chest AIS3 corresponds to at least three rib fractures). The WorldSID showed the highest lower neck Mx in simulation W5_2 and the highest lumbar spine Mx in simulation W4_2 whereas the THUMS model showed the highest lower neck Mx in simulation T4 and the highest lumbar spine Mx in belt only configurations T2 and T4 (Table 48).

3.6.4 Conclusion

Overall, the effects of the countermeasures related to Protection Principle 6 on injury assessment values and injury prediction correlated well between THUMS and WorldSID. The head excursion showed the highest discrepancy between THUMS and WorldSID when a standard 3-point belt with a centre console (T1 and W1_2 simulations) or only the double lap-belt pretensioning (T2 and W2_2 simulations) were considered. In the cases where more restraint was applied to surrogates (by an in-board shoulder belt or seat side supports), the excursions of THUMS and WorldSID were similar.

A combination of double lap belt pretensioning and seat side supports was the best compromise to control occupant kinematics while mitigating injury assessment values. The THUMS model predicted two rib fractures in this configuration that may be prevented by a softer seat side support. The lower neck bending moment might also be decreased by the integration of further countermeasures to support the head during the crash, such as a seat-mounted airbag.

4 OVERALL CONCLUSION

New seating positions as well as non-standard crash configurations (oblique crash scenarios like Straight Crossing Path = SCP) pose new challenges for occupant safety in automated vehicles. To ensure occupant safety even in new seating positions, a redesign or adaptation of standard restraint systems or even completely new restraint principles will be necessary. The six protection principles defined within the OSCCAR project were analysed individually, taking into account both the pre-crash and in-crash phase. All simulation-based studies within this report have shown that each protection principle has significant potential to increase occupant safety with regard to new seating configurations, and thus addresses the new challenges of automated vehicles. Furthermore, a combination of the presented protection principles may lead to additional benefits with respect to the single principles.

Protection Principle 1 (PP1) tackles the new occupant safety challenges by rotating the seat along the z-axis towards a more beneficial position, like the principal direction of force (PDOF) during the pre-crash phase. The rotation is not only possible towards the standard or driving direction but any given direction if the PDOF is known in advance (environmental sensing), the necessary time for the seat rotation is available and enough space within the passenger compartment is provided. Studies with regard to PP1 have shown that suitable seat rotation velocities and starting times for the seat rotation are a key for optimised protection. Furthermore, an adequate seat side support structure as well as a good coupling between occupant and seat belt is mandatory to ensure good occupant repositioning relative to the seat. An additional challenge for rotating seat concepts arises when the occupant is rotated towards the PDOF but is rearward-facing. In this case, the seat needs to act as primary restraint system. Here, a redesign of the seat as well as a rotatable footrest have the potential to increase the level of occupant safety. Furthermore, the PP2 studies showed that inertially-driven rotation of the seat is possible and beneficial as well, i.e. no actuator is needed to rotate seat and occupant to the direction of braking in the pre-crash phase. Without applying PP1 or PP2, the occupant would be exposed to different types of injuries caused by the interaction between occupant and seat structure, belt system and occupant compartment.

This observation was also made with regard to PP3 and PP4, where the SCP crash pulse was applied to reclined and living room seating configurations respectively. Especially the interaction between occupant and belt (neck, shoulder as well as pelvis area) shows that proper seat belt routing is necessary and must be ensured for good occupant restraint. A potential solution for this issue might be a sensor system which monitors and adapts the current belt positions. The study on different occupant sitting postures within PP3 showed the influence of lower extremity postures on overall occupant kinematics. This fact could potentially have an additional influence on occupant-to-seat coupling during the seat rotation by PP1 and PP2. An exemplary situation for this occurs if the contact between the seat side structure and the femur is missing due to a higher femur position with respect to the seat base, since the legs are crossed. Thus, when designing a seat rotation system different occupant postures must be considered and analysed, too.

The results of PP4 showed that a Mushroom Airbag with an additional airbag part between the occupants sitting next to each other (e.g. seat position 3 and 4) can prevent an interaction between them. However, the restraint effect of the Mushroom Airbag is limited if the occupant experiences a near-side oblique crash. In these situations, an additional inclusion of PP1 or also PP2 could serve to rotate the occupant inwards (in grey) and thus ensure lateral support by the Mushroom Airbag as shown in Figure 163.

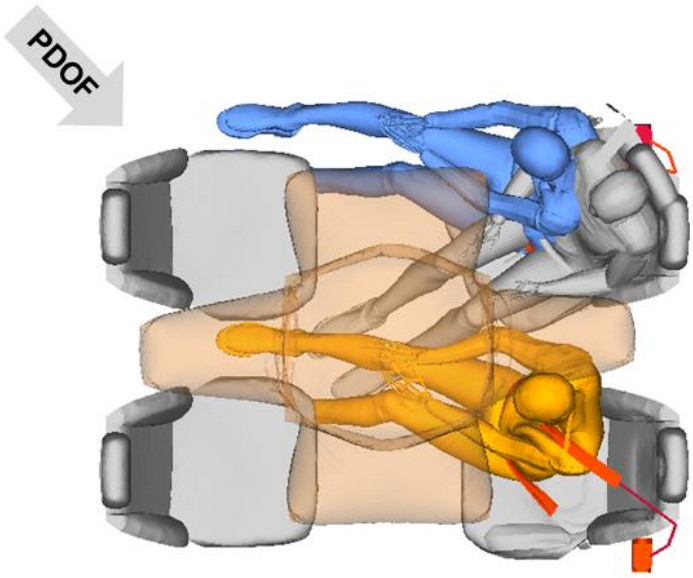

Figure 163 Combination of PP4 and PP1 / PP2

PP3 and PP5 both address reclined seating positions. While PP3 keeps the occupant in its reclined posture, PP5 repositions the occupant by an active seat back rotation. For both protection principles, the avoidance of submarining and the effect of pre-pretensioning the seat belt in this regard are important points. Different effects of pre-pretensioning have been observed, depending on the restraint strategies. On the one hand the pre-pretensioner reduces belt slack and the forward displacement of the occupant during the crash. On the other hand, pre-crash belt tensioning can increase the submarining tendency by restraining the pelvis while repositioning (PP5) or by shifting the buckle unfavourably (PP3). For PP5 especially, the characteristics of the repositioning velocity curve acting on the human body affect the kinematic response of the occupant model. Furthermore, with regard to a forward-facing occupant it was found that, in addition to an active repositioning of the occupant by a seat back rotation, AEB prior to a crash can be used to reposition the occupant similarly due to the torso inertia, i.e. without rotating the seat back.

While PP1 to PP5 dealt with frontal and oblique crashes, PP6 addressed occupant restraint with regard to a side crash in a future interior without centre console. Considering different restraint system layouts as well as seat side supports it was investigated how to limit the excursion of the far-side occupant in order to provide protection from a collision between two rear-seated occupants. The combination of double lap belt pretensioning and seat side supports was shown to be the best approach to control the occupant kinematics while mitigating the injury risk. An additional benefit in terms of avoiding occupant interactions and reducing the risk of injury would be expected if a Mushroom Airbag (PP4) were applied as well.

5 DISSEMINATION, EXPLOITATION AND STANDARDISATION

It could be shown that HBMs will allow the creation and assessment of pre-crash safety systems for future accidents, as well as helping to develop according restraint systems like airbags, seat belts and seat-based restraints. Exploitation in industry will depend on the different perspectives of the partners, i.e. OEM, Tier-1 restraint system, Tier-1 electronic supplier and simulation tool supplier.

OEMs and Tier-1 suppliers will exploit the results of the studies on advanced occupant protection principles internally for future vehicle safety development. The simulation tool providers will benefit from the results by identifying market intentions for these new use cases. The findings will be used to optimise the simulation toolchain and methodology for rapid prototyping and DoE analysis of new load cases and restraint concepts with regard to new seating configurations applicable to integrated assessments in the pre- and in-crash phase.

In summary the following exploitation is expected in the time frame 2025 - 2030:

- Valuable insights into advanced occupant protection principles to support the development of future car occupant protection technologies, including the impact of novel interior design on relevant safety means like airbags, seat belts and seats.
- Industry-internal usage and dissemination allows the development of methods, knowledge and tools that enable occupant protection in novel interiors. The implementation and transfer of these findings will start in generic studies and head over to internal development by individual partners.
- These results will be very helpful in designing pre-crash functions and the according logic within the safety control units of future vehicles as well as creating an according layout of the safety system itself. Furthermore, these findings will help industry to derive requirements for electric drives in order to allow the pre-crash actuation of seats in new interiors.

The work presented in this report is intended to be shared through all possible dissemination channels, including publications and presentations as well as academic use. Some details regarding the respective protection principles are given in the following chapters.

5.1 Protection Principle 1

Dissemination:

- Becker et al. (2020) / Occupant Safety in Highly Automated Vehicles – Challenges of Rotating Seats in Future Crash Scenarios / J Becker, GA D'Addetta, M Wolkenstein, F Bosma, R Verhoeve, S Schaub, M Sprenger, M Hamacher: / 2020 IRCOBI Conference Proceedings.
- Becker et al. (2020) / Application of Human Body Models to analyse the challenges of future occupant use cases in highly 4 automated vehicles / J Becker, M Hamacher, GA D'Addetta, M Wolkenstein, T Wohllebe, A Mishra, C Mayer, LV Nölle, OV. Martynenko, S Schmitt, F Bosma, R Verhoeve: / 8th International Symposium: Human Modeling and Simulation in Automotive Engineering, November 19 - 20, 2020.
- D'Addetta (2020) / Your Automated Driving trip – How we create a really safe trip using human body models / GA D'Addetta / Bosch Research Blog Post to be published 02/2021
- Mishra et al. (2021) / Development and Performance Evaluation of an Active 5th Percentile Female Human Body Model with Eastern Anthropometry for Integrated Safety Analysis / A

Mishra, P Ghosh, R Chitteti, C Mayer, S Yang, Q Zhou: / 2021 Frontiers in Bioengineering and Biotechnology (Manuscript Submitted & Waiting Reviewer Response)

Exploitation:

In summary, one can say that systems that aim to capture the functionality of Protection Principle 1, i.e. to rotate the seat prior to a crash to a more beneficial situation, may have a very positive effect on occupant safety in new interiors. In particular for SAE L4 and L5 vehicles rotated seats by 10°, 15° or even 30° may become reality.

Project transfer:

Transfer of simulation results and findings to EU Horizon 2020 project SAFE-UP (Grand Agreement No. 861570)

5.2 Protection Principle 2

Dissemination:

Peer-reviewed conference publications:

- Becker J., et al.; Occupant Safety in Highly Automated Vehicles - Challenges of Rotating Seats in Future Crash Scenarios. Proceedings of the IRCOBI Conference, Munich, 2020

Exploitation:

A knowledge transfer to education within the Master degree courses “Automotive Engineering M.Sc.” and “Fahrzeugtechnik und Transport M.Sc.” at RWTH Aachen University was done in terms of the research studies. This was accompanied by raising awareness for the topics of occupant safety and future restraint strategies in relation to the application of human body models.

Project transfer:

Transfer of simulation results and findings to EU Horizon 2020 project SAFE-UP (Grand Agreement No. 861570)

5.3 Protection Principle 3

Using the new pulses that represent possible future crashes that HAV will be exposed to in mixed traffic, in combination with new protection principles for new sitting positions, will form a knowledge base when moving into development of restraint system for new vehicles.

The following peer-reviewed publications from the PP3 studies have been published or are soon to be published:

- Leledakis, A., Östh, J., Davidsson, J., Jakobsson, L. 202X. The influence of car passenger’s sitting posture in intersection crashes. Submitted to Accid. Anal. Prev.
- Mroz, K., Ostling, M., Richardson, R., Kerrigan,J., Forman, J., Gepner, B., Lubbe, N., and Pipkorn B. (2020) Effect of Seat and Seat Belt characteristics on the Lumbar Spine and Pelvis Loading of the SAFER Human Body Model in reclined Postures, Proceedings of the IRCOBI Conference, 2020, Munich, Germany.

Project transfer:

- Transfer of simulation results and findings to EU Horizon 2020 project SAFE-UP (Grand Agreement No. 861570)

5.4 Protection Principle 4

Currently no disseminations are planned for the Mushroom Airbag concept. However, the concept will be further improved and will be used for internal application only. Results provided in this report can be used by the partners in any future use cases of fully autonomous vehicle designs.

5.5 Protection Principle 5

Dissemination:

Peer-reviewed conference publications:

- Östh J, Bohman K, Jakobsson L. Evaluation of kinematics and restraint interaction when repositioning a driver from a reclined to an upright position prior to frontal impact using active Human Body Model simulations, Proceedings of the IRCOBI Conference, IRC-20-50, 2020

Exploitation:

A knowledge transfer to education within the Master degree courses “Automotive Engineering M.Sc.” and “Fahrzeugtechnik und Transport M.Sc.” at RWTH Aachen University was done in terms of the research studies. Additionally, some parts of the presented contents were created in terms of student thesis projects (master and bachelor). This was accompanied by raising awareness for the topics of occupant safety and future restraint strategies in relation to the application of human body models.

Project transfer:

Transfer of simulation results and findings to EU Horizon 2020 project SAFE-UP (Grand Agreement No. 861570)

5.6 Protection Principle 6

Toyota and IDIADA plan to submit a paper to a conference or a journal on the THUMS simulations for Protection Principle 6 and the comparison carried out with the WorldSID tests.

Toyota hopes to contribute with the PP6 far-side simulations to Euro NCAP discussions on the introduction of Virtual Testing in its assessment.

6 SUMMARY AND OUTLOOK

The studies presented in this report deal with the virtual conception and investigation of six advanced occupant protection principles (PP) for variable sitting positions and postures related to automated driving. Both, an adaptation of restraint systems towards these new boundary conditions and a repositioning of the occupant into a conventional seating configuration prior to a crash are considered. The respective working groups investigated various research questions related to rotated seats, reclined seating positions, an advanced airbag design for a “living room” configuration (occupants facing each other) as well as occupant restraint in a future interior with regard to a side crash. Both pre-crash activation and adaptation as well as in-crash protection were considered. A general proof of functionality and effectiveness was provided for all protection principles.

By the use of human body models the kinematic boundary conditions, e.g. the risk of submarining, and the related injury mechanisms for selected test cases could be analysed qualitatively well. The findings increase the confidence in the models and thus in the simulation results. Muscle activity settings affect the overall kinematics of the occupant during a repositioning and may lead to different simulation outcomes during the pre- and in-crash phase. Whether an active pre-crash rotation of the occupant (for example) leads to additional minor injury risks needs to be analysed in more depth. The presented method for analysing muscle injuries during the pre-crash phase represents a good starting point. Further work on how the HBM settings and muscle representation influence the minor injury assessment will follow in other research projects. It could be shown that HBMs allow the development and assessment of pre-crash safety systems for future accident scenarios. This is helpful in designing pre-crash functions and the according logic within the safety control units of future vehicles, as well as in creating an according layout of the safety system itself. Furthermore, it allows requirement specifications for the pre-crash actuation of safety systems in new interiors. It was illustrated that HBMs are capable of representing a large variety of sitting postures and providing insightful results for varied responses in a variety of non-standardised impact scenarios. This capability, and the understanding of the influence of posture variation are important complements when understanding the real-world safety impact by different protection principles.

All presented results apply primarily to the investigated simulation environments as well as the considered vehicle interior, restraint system and occupant models. Although variations in size, weight, posture and gender were already considered in some studies, human diversity needs to be considered more comprehensively with regard to a holistic assessment. This inevitably involves a high simulation effort, which could not be taken into account in the presented studies since it was beyond the scope of work. Furthermore, the trigger time of the pre-crash systems was not the focus of the conducted studies. However, this will play an important role in advanced development studies. In particular, the impact of delayed triggering of a pre-crash function is of interest.

Different hardware test series have been performed in order to gain data for the validation of the respective simulation environments and to demonstrate the functionality of selected protection principles, but this is subject of deliverable D2.5 [1]. Two sled test series regarding the homologation demonstrator test case are illustrated therein, which combine both physical and virtual testing and provide a direct link to OSCCAR WP4 and WP5. The focus of this demonstrator test case is on a reclined seating position and also addresses aspects related to Protection Principle 3. In addition, sled test series on Protection Principle 2 and Protection Principle 6 are presented in deliverable D2.5. With regard to PP2 an inertia-driven seat rotation is demonstrated for different types of occupants, i.e. the rotation is initiated solely by an emergency braking of the sled. The defined rotation axles and the seat layout are based on the simulation studies shown in Chapter 3.2.3. The PP6 sled test series uses a WorldSID dummy in a far-side load case considering different restraint system layouts as well as seat side supports according to Chapter 3.6.3.

7 REFERENCES

[1] N. N.; Validation and demonstration of advanced passenger protection principles; Deliverable D2.5, OSCCAR Project; Grant Agreement No. 768947; 2021

[2] Jakobsson L., Fornells A., Köhler A. L., Mayer C.; Test Case Matrix and selecting Demonstrator Test Cases; Deliverable D2.1, OSCCAR Project; Grant Agreement No. 768947; 2018

[3] Becker J., Sprenger M., Schaub S.; Interior Models for Occupant Protection Simulations in OSCCAR; Deliverable D2.2, OSCCAR Project; Grant Agreement No. 768947; 2019

[4] Schaub S., Becker J., D'Addetta G. A., Mayer C.; Selection of viable advanced passenger protection principles for further investigation; Deliverable D2.3, OSCCAR Project; Grant Agreement No. 768947; 2019

[5] U. Wössner; openPASS framework for integrated safety assessment; Deliverable D1.2, OSCCAR Project; Grant Agreement No. 768947; 2019.

[6] Dobberstein J., Ostling M., Höschele P., Schmidt D., Bálint A.; Final results on detailed crash configurations from collisions expected to remain for automated vehicles; Deliverable D1.3; OSCCAR Project; Grant Agreement No. 768947; 2021

[7] A. Eggers, M. Putzer and S. Kramer, "Investigation of repeatability and reproducibility of the dummy THOR-M in sled and component tests," in crash.tech Conference, Munich, Germany, 2016.

[8] M. A. Edwards and C. E. Nash, "Inflatable shoulder belts and inboard upper anchor shoulder belt geometry in far-side oblique impacts," in IRCOBI Conference Proceeding, Antwerp, Belgium, 2017.

[9] M. Boin, "Occupant protection in alternative seating positions", LS-Dyna Forum Conference, Bamberg, Germany; 2018

[10] Y. Kitagawa, S. Hayashi, K. Yamada and M. Gotoh, "Occupant kinematics in simulated autonomous driving vehicle collisions: influence of seating position, direction and angle," Stapp Car Crash Journal, pp. 101-155, November 2017.

[11] Jin, X.; Hou, H.; Shen, M.; Wu, H.; King H.Y.; Occupant Kinematics and Biomechanics with Rotatable Seat in Autonomous Vehicle Collision: A Preliminary Concept and Strategy; International Research Council on Biomechanics of Injury (IRCOBI), Athens, Greece; 2018

[12] J. Zhao, M. Katagiri, S. Lee and J. Hu, "GHBMC M50-O-Occupant response in a frontal crash of automated vehicle," in Human Modeling and Simulation (carhs) Conference, Berlin, Germany, 2018

[13] E. T. Dickinson, "Neck & Neck: Seat belt sign on the neck is as serious a finding as on the abdomen," Journal of Emergency Medical Service, April 2010

[14] A. Öztürk, C. Mayer, H. Kumar, P. Ghosh, A. Mishra, R. Chitteti and D. Fressmann, "A step towards integrated safety simulation through pre-crash to in-crash data transfer," ESV conference 2019, paper number 19-0257

[15] H. Kumar, P. Ghosh, S. Rajakumaran, H. Kenkere, R. Chitteti, C. Mayer and D. Fressmann, "Ergonomics" based occupant-positioning approach for safety simulations; in CARHS - Human Modeling Symposium, 2020

[16] B. D. Goodwin, S. Chirvi and F. A. Pintar; Injury Mechanisms in Traffic Accidents, Handbook of Human Motion 2018, p. 2363–2398, 2018

[17] carhs.training gmbh, "Safety Companion 2020," 2020

[18] L. V. Nölle, S. Schmitt and O. V. Martynenko, "Defining Injury Criteria for the Muscle-Tendon-Unit," IRCOBI conference 2020, 2020

[19] T. Stauber, U. Blache and J. G. Snedeker, "Tendon tissue microdamage and the limits of intrinsic repair," Matrix biology: journal of the International Society for Matrix Biology, 2019

[20] T. J. Noonan, T. M. Best, A. V. Seaber and W. E. Garrett, "Identification of a threshold for skeletal muscle injury," The American journal of sports medicine, p. 257–261, 1994

[21] P. K. Nikolaou, B. L. Macdonald, R. R. Glisson, A. V. Seaber and W. E. Garrett, "Biomechanical and histological evaluation of muscle after controlled strain injury," The American journal of sports medicine, p. 9–14, 1987

[22] C. T. Hasselman, T. M. Best, A. V. Seaber and W. E. Garrett, "A threshold and continuum of injury during active stretch of rabbit skeletal muscle," The American journal of sports medicine, p. 65–73, 1995

[23] A.-L. Köhler, F. Prinz, L. Wang, J. Becker, G. M. I. Voß, S. Ladwig, L. Eckstein, T. Schulte and N. Depner, "How will we travel autonomously? User needs for interior concepts and requirements towards occupant safety," in 28th Aachen Colloquium Automobile and Engine Technology, Aachen, Germany, 2019

[24] TASS International BV, "Model manual, MADYMO Application Model for Integrated Safety (Version 3.0)," TASS International, Rijswijk, Netherlands, 2018

[25] J. Iraeus and M. Lindquist, "Development and validation of a generic finite element vehicle buck model for the analysis of driver rib fractures in real life nearside oblique frontal crashes," Accident Analysis & Prevention, vol. 95, pp. 42-56, 2016

[26] Becker J., et al.; Occupant Safety in Highly Automated Vehicles - Challenges of Rotating Seats in Future Crash Scenarios. Proceedings of the IRCOBI Conference, Munich, 2020

[27] Dickinson E. T.; Neck & Neck. Seat belt sign on the neck is as serious a finding as on the abdomen; Journal of Emergency Medical Service, Vol. 34, p.7-36.; 2010

[28] Dobberstein J., Lich T., Schmidt D.; Accident data analysis - remaining accidents and crash configurations of automated vehicles in mixed traffic; Deliverable 1.1, OSCCAR Project; Grant Agreement No 768947; 2018

[29] TASS International BV; OSCCAR Madymo Workshop. Active Human Model. TASS International BV; Rijswijk, Netherlands; 2019

[30] Uriot, J., Potier, P., Baudrit, P., Trosseille, X., Petit, P., Richard, O., Compigne, S., Masuda, M., Douard, R. (2015) Reference PMHS Sled Tests to Assess Submarining. Stapp Car Crash Journal. Vol 59

[31] Östling, M., Sunnevång, C., Svensson, C., Kock, H.-O. (2017) Potential future seating positions and the impact on injury risks in a Learning Intelligent Vehicle (LIV). How to avoid submarining in a reclined seating position in a frontal crash. Conference: 11. VDI-Tagung Fahrzeugsicherheit, 2017, Berlin, Germany

[32] Iwamoto, M., Kisanuki, Y., et al. (2002) Development of a Finite Element Model of the Total Human Model for Safety (THUMS) and Application to Injury Reconstruction. Proceedings of IRCOBI Conference, 2002, Munich, Germany

[33] Iraeus, J., Pipkorn, B. (2019) Development and Validation of a Generic Finite Element Ribcage to be used for Strain based Fracture Prediction. Proceedings of the IRCOBI Conference, 2019, Florence, Italy

[34] Afewerki, H. (2016) Biofidelity Evaluation of Thoracolumbar Spine Model in THUMS, Master's thesis in Biomedical Engineering. Chalmers University of Technology, Sweden

[35] Östh, J., Bohman, K., Jakobsson, L. (2020) Evaluation of Kinematics and Restraint Interaction when Repositioning a Driver from a Reclined to Upright Position Prior to Frontal Impact using Active Human Body Model Simulations. Proceedings of the IRCOBI Conference, 2020, Munich, Germany

[36] Mroz, K., Ostling, M., Richardson, R., Kerrigan,J., Forman, J., Gepner, B., Lubbe, N., and Pipkorn B. (2020) Effect of Seat and Seat Belt characteristics on the Lumbar Spine and Pelvis Loading of the SAFER Human Body Model in reclined Postures Proceedings of the IRCOBI Conference, 2020, Munich, Germany

[37] Richardson, R., Donlon, J.P., Jayathirtha, M., Forman, J., Shaw, G., Gepner, B., Kerrigan J., Ostling, M., Mroz, K. and Pipkorn, B. (2020) Kinematic and Injury Response of Reclined PMHS in Frontal Impacts. Stapp Car Crash Journal, Vol. 64 (November 2020)

[38] Park, J., Ebert, S., Reed M. and Hallman, J. (2016). Statistical Models for Predicting Automobile Driving Postures for Men and Women Including Effects of Age. Human Factors, Vol. 58, No. 2, March 2016, pp. 261–278, Human Factors and Ergonomics Society

[39] Kerrigan, J.R. "Positioning Data for Human Body Models in Reclined Seating, March 16, 2020", https://virginia.app.box.com/s/pm1g83555o7kiqie0xlpnyjp51kmg363, Center for Applied Biomechanics, University of Virginia, USA [Accessed March 30, 2020]

[40] Becker J., Sprenger M., Schaub S.; Interior Models for Occupant Protection Simulations in OSCCAR; Deliverable D2.2, OSCCAR Project; Grant Agreement No. 768947; 2019

[41] N. N.; Demonstrator for continuous integrated virtual assessment of complex crash simulation tasks incl. HBMs; Deliverable D4.2, OSCCAR Project; Grant Agreement No. 768947; 2021

[42] N. N.; Standardised validation procedure for qualifying the HBM to be used for assessing effectiveness of pilot protection principles; Deliverable D5.2, OSCCAR Project; Grant Agreement No. 768947; 2021

[43] Forman, J.L., Kent, R.W., Mroz, K., Pipkorn, B., Bostrom, O., Segui-Gomez, M. (2012) Predicting rib fracture risk with whole-body finite element models: development and preliminary evaluation of a probabilistic analytical framework. Annals of Advances in Automotive Medicine 56:109-124

[44] Toyota Motor Corporation (2011). THUMS AM50 Pedestrian/Occupant Model Version 4.0_20111103 documentation, 1-74

[45] Selcuk Himmetoglu, M. Acar, K. Bouazza-Marouf, A. J. Taylor , Energy-Absorbing Car Seat Designs for Reducing Whiplash. Traffic Injury Prevention, 9(6): 583-91, January 2009

[46] Leledakis, A., Östh, J., Davidsson, J., Jakobsson, L. (202X), The influence of car passenger's sitting posture in intersection crashes, submitted to Accid. Anal. Prev.

[47] Leledakis, A., Lindman, M., Östh, J., Wågström, L., Davidsson, J., Jakobsson, L. (2021) A method for predicting crash configurations using counterfactual simulations and real-world data. Accid. Anal. Prev. 150, 105932. doi:10.1016/j.aap.2020.105932

[48] Gepner B., Draper D., Mroz K., et al.; Comparison of Human Body Models in Frontal Crashes with Reclined Seatback; International Research Council on Biomechanics of Injury (IRCOBI), Florence, Italy; 2019

[49] Laakman F., et al.; Enabling Technologies for Future Vehicles - Integrated Safety; Airbag Symposium; 2018

[50] Kitagawa Y., Hayashi S., Yamada K., Gotoh M.; Occupant Kinematics in Simulated Autonomous Driving Vehicle Collisions: Influence of Seating Position, Direction and Angle; Stapp Car Crash Journal, Vol. 61, p. 101–155; 2017

[51] Pipkorn B., Iraeus J., Björklund M., Bunketorp, O., Jakobsson, L. (2019) Multi-Scale Validation of a Rib Fracture Prediction Method for Human Body Models; Proceedings of IRCOBI Conference, 2019, Florence, Italy

[52] Uriot J., Baudrit P., Potier P., et al.; Investigations on the Belt-to-Pelvis Interaction in the Case of Submarining; Stapp Car Crash Journal, Vol. 50, p. 53-73; 2006

[53] Stemper B.D., Yoganandan N., Pintar F.A.; Effect of head restraint backset on head-neck kinematics in whiplash; Accident Analysis & Prevention, Vol. 38 (2) , p. 317-323; 2006

[54] Edwards M. A., Nash C. E. (2017) Inflatable shoulder belts and inboard upper anchor shoulder-belt geometry in far-side oblique impacts, Proceeding of IRCOBI Conference 2017, IRC-17-56

[55] Euro NCAP; Far side occupant test & assessment procedure, Version 2.0.1, June 2020

[56] Petit P., Trosseille X., Uriot J. (2019) Far side impact injury threshold recommendations based on 6 paired WorldSID / Post Mortem Human Subjects tests, Stapp Car Crash Journal, Vol. 63, 19S-23, November 2019

[57] Yigit, E. Reaktives FE-Menschmodell im Insassenschutz. AutoUni-Schriftenreihe 114, Springer Fachmedien Wiesbaden GmbH 2018, https://doi.org/10.1007/978-3-658-21226_1-1

[58] Sugiyama, T., Weber, J., Bensler, H. P. Enhancement of HBM Active Muscle Modeling in VPS. Menschmodelle in der Fahrzeugsicherheit / Human Body Modelling in Automotive Safety, VDI Fachkonferenz 2017, Berlin, Germany

[59] Sugiyama, T., Weber, J., Sandoz, B., Bensler, H-P. Validation of a reactive Finite Element Human Body Model under moderate lateral loading. Human Modeling and Simulation in Automotive Engineering Conference (carhs) 2018, Berlin, Germany

[60] THUMS User Community (TUC) Project [Online]. Available at: https://www.tuc-project.org (Accessed: 15 December 2020)

[61] PIPER Project [Online]. Available at: http://www.piper-project.eu/ (Accessed: 15 December 2020)

[62] Grujičić, R. (2020) Kenhub, Anatomy [Online]. Available at: https://www.kenhub.com/ (Accessed: 15 December 2020)

[63] N.N.; Validated and computationally robust active HBMs; Deliverable D3.2, OSCCAR Project; Grant Agreement No. 768947; 2021

[64] J. Peres, S. Auer and N. Praxl, "Development and comparison of different injury risk functions predicting pelvic fractures in side impact for a Human Body Model," in IRCOBI, Malaga, 2016

[65] O. Martynenko, F. Neininger and S. Schmitt, "Development Of A Hybrid Muscle Controller For An Active Finite Element Human Body Model In Ls-Dyna Capable Of Occupant Kinematics Prediction In Frontal And Lateral Maneuvers", ESV, 2019

[66] Petitjean A., Trosseille X., Praxl N. (2012) Injury risk curves for the WorldSID 50th male dummy, Stapp Car Crash Conference, Savannah, Georgia, United States, October 29-31, 2012

[67] Internal ACEA report on Brain Rotational Response by Toyota, 2018

[68] M. Edwards, M. Brumbelow, R. Trempel, T. Gorjanc, “Seat Design Characteristics Affecting Occupant Safety in Low and High-Severity Rear-Impact”. IRCOBI Conference, Florence, Italy, 2019

A. APPENDIX

1 PP1

1.1 Settings for qualitative Comparison

In Chapter 3.1.3.7 a qualitative comparison study for a highway crash scenario is reported. System and simulation specific settings were aligned and are summarised below.

Partner	Volkswagen	Mercedes	Bosch
crash scenario	highway	highway	highway
crash pulse	generic FF 40 km/h	generic FF 40 km/h	generic FF 40 km/h
braking	yes	yes	yes / no
braking pulse	generic	generic	generic
pos. of seat	2	2	2
interior model	generic	generic	generic
sim. code	VPS	LS-Dyna	Madymo
HBM	THUMS-TUC-VW AHM	A-THUMS-D3.3.6, THUMS-TUC	HBM
activ. HBM	active	active	active
initial seat rot.	30°	30°	30°
target angle	0°	0°	0°
pos. rot. axis	H-point THUMS	H-point THUMS	H-point AHM
seat activation	-350 ms	-350 ms	-350 ms
end of seat rot	crash start	crash start	crash start
seat rot curve	spline inter.	spline inter.	spline inter.
belt anch. point	seat integrated	seat integrated	seat integrated
pre-pretensioner	retractor	retractor	retractor
pre-tensioner	retractor	retractor	retractor
PPT activation	-450 ms	-450 ms	-450 ms
PT activation	10 ms	10 ms	10 ms
force PPT	250 N	250 N	250N
force PT	2500 N	2500 N	2500 N
BLL	2100 N	2000 N	2000 N
gravity	applied	applied	applied
Friction HBM / seat / airbag / belt / floor / envr.	0.35 / 0.2 0.5 / 0.3 / 0.2	0.35 / 0.2 0.5 / 0.3 / 0.2	0.3 / 0.2 0.2 / 0.3 / 0.3

1.2 Siemens USNCAP Pulse

USNCAP crash pulse and pre-crash braking pulse provided with the Siemens Madymo model and used for first studies since no generic OSCCAR pules were available at the beginning of the task.

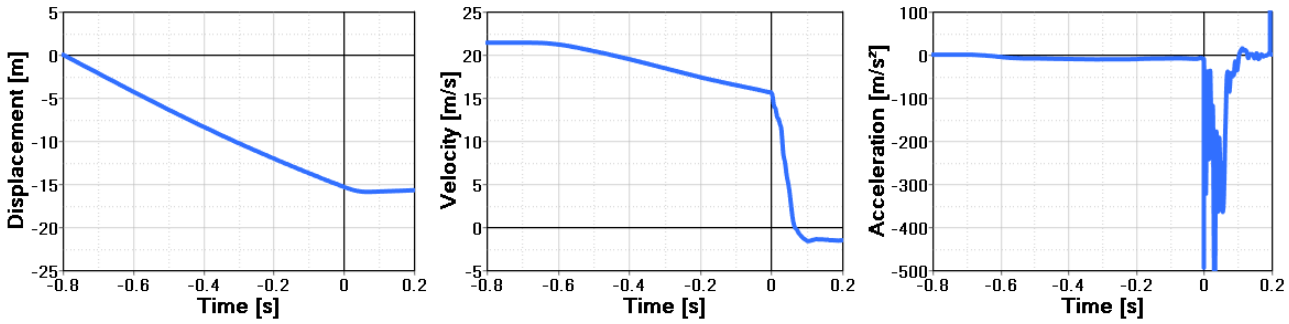

1.3 Benefit Assessment of pre-rotated Seat to non-rotated Seat

Time (ms)	Case 1	Case 2	Case 3
-500	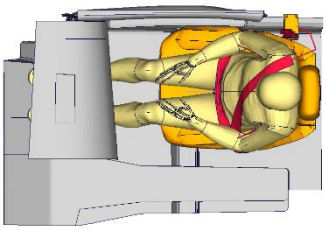	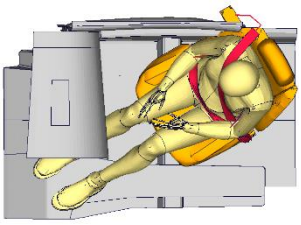	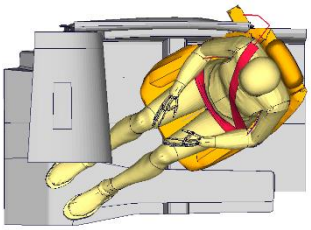
-400	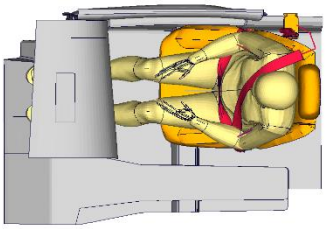	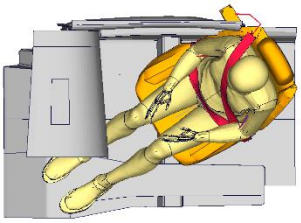	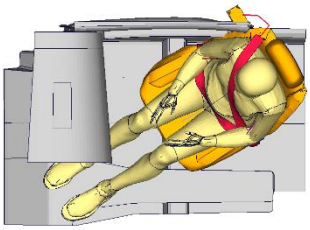
-300	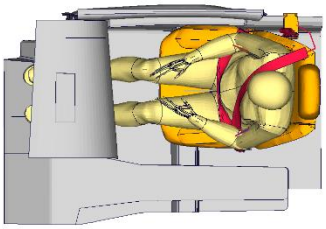	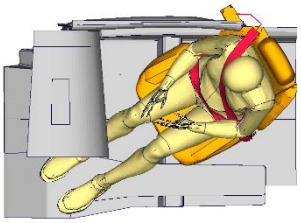	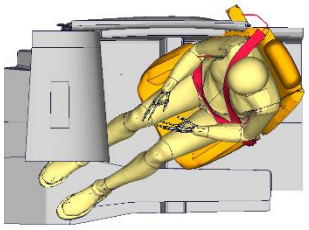
-200	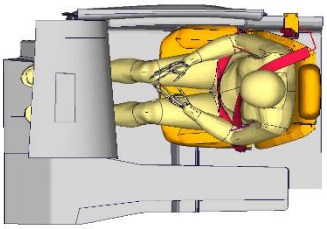	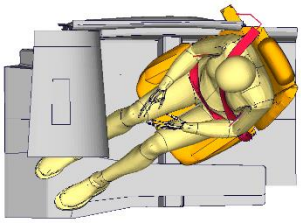	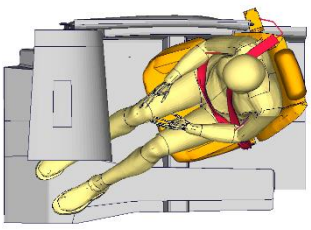

-100	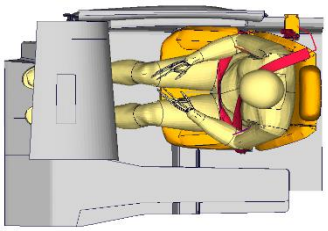	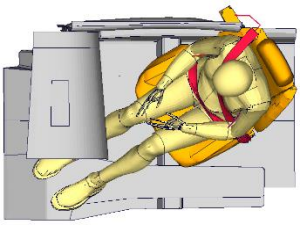	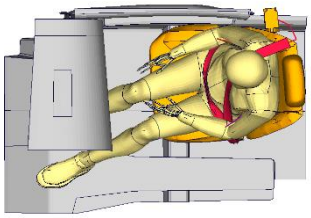
0	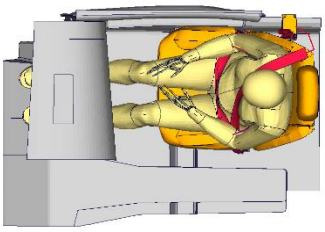	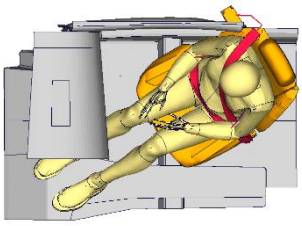	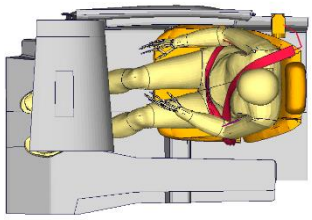
	end of pre-crash phase		
0	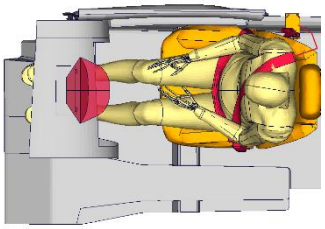	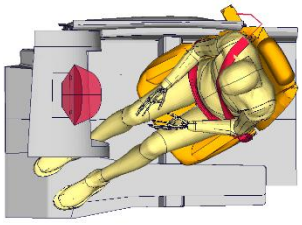	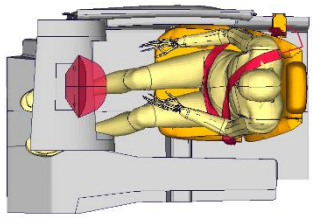
	data transferred to THUMS-TUC HBM		
20	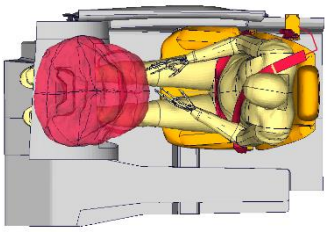	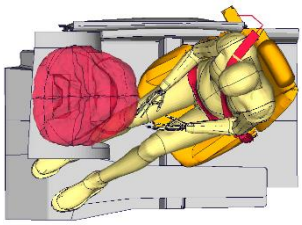	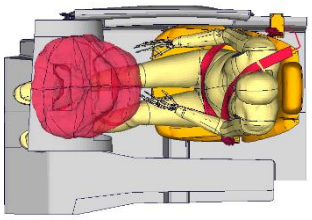
40	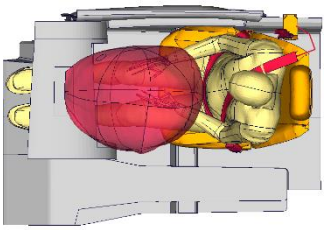	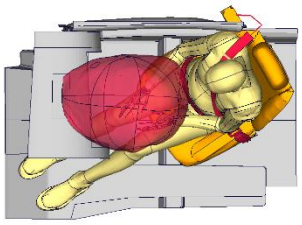	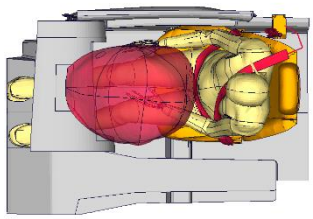
60	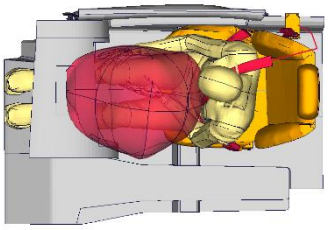	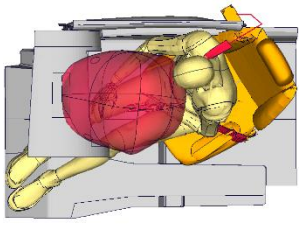	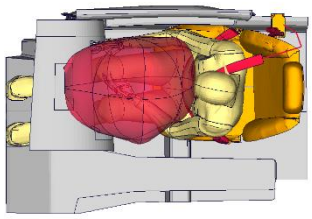
80	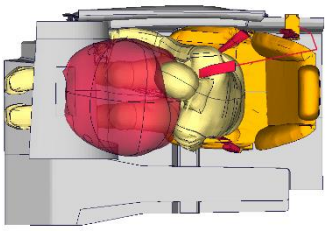	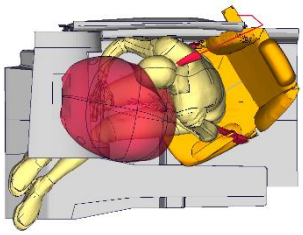	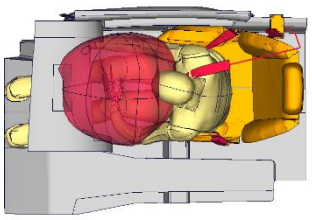

100	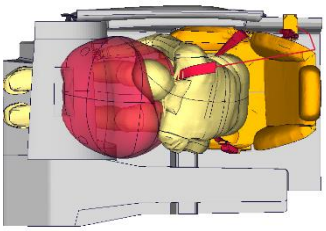	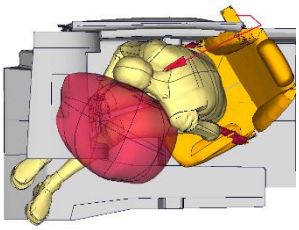	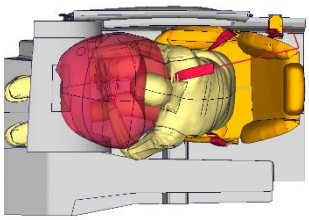
120	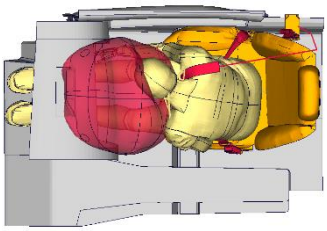	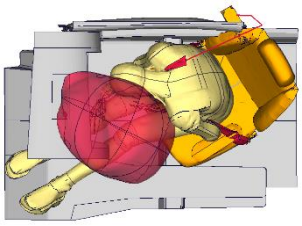	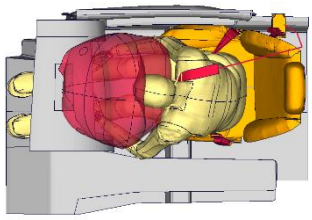
140	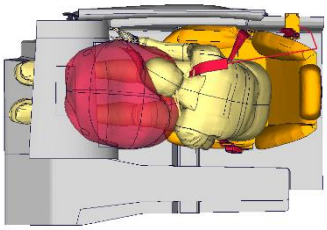	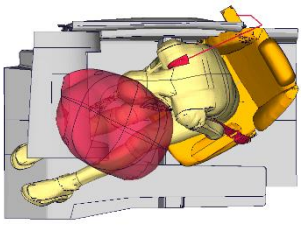	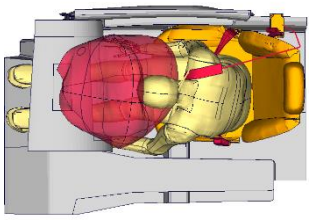
160	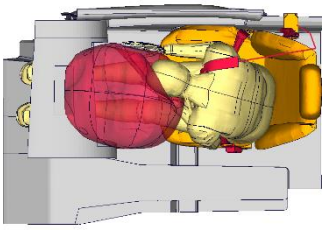	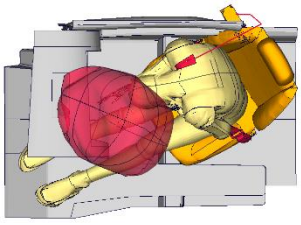	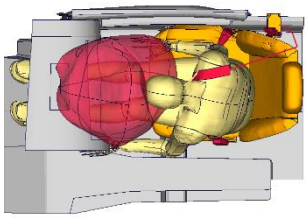
180	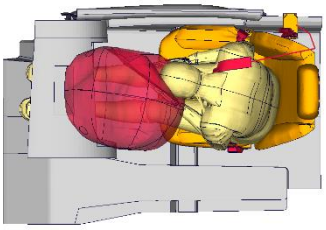	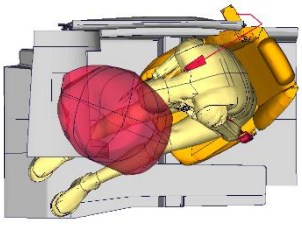	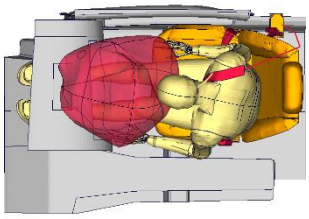

Table 34 Occupant kinematics for case 1, 2 and 3

1.4 Pre-rotated Seat in Rearward-Facing Use Case

Time (ms)	Case 1	Case 2
-500	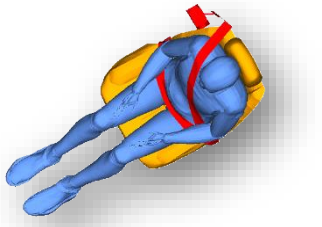	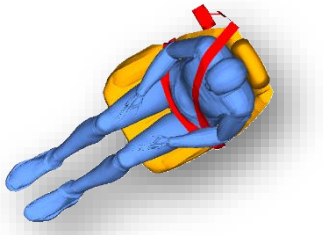

-400	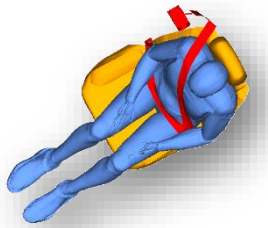	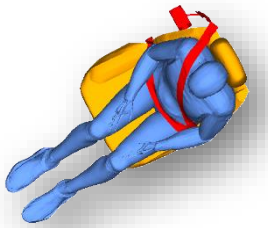
-300	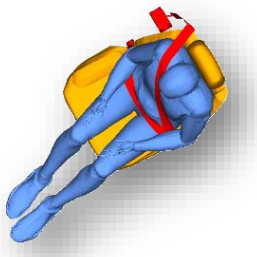	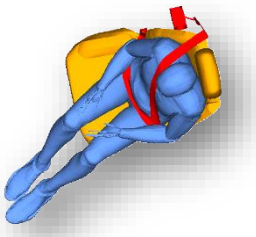
-200	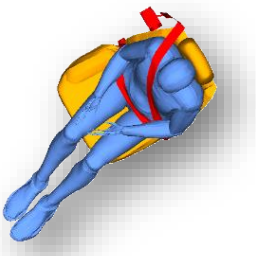	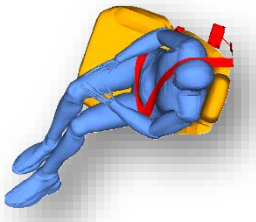
-100	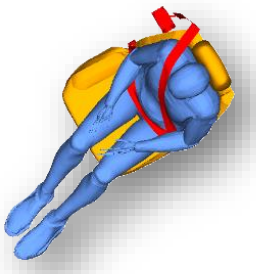	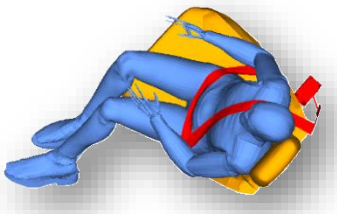
0	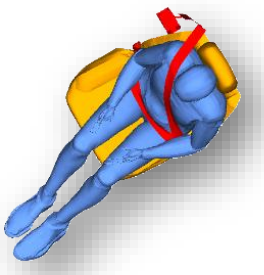	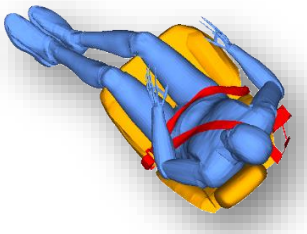
	end of pre-crash phase	

20	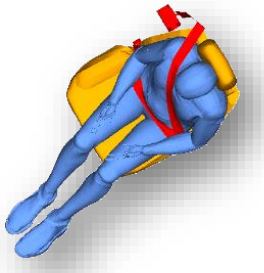	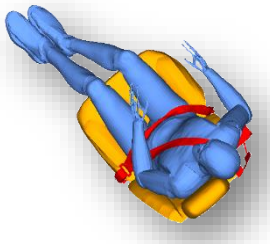
40	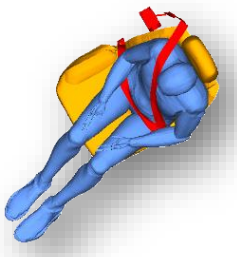	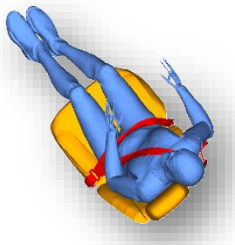
60	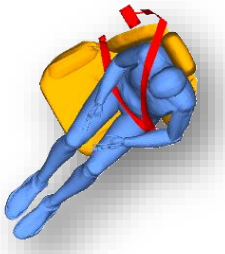	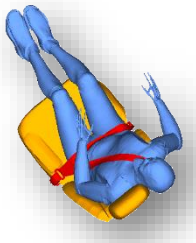
80	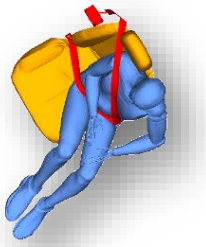	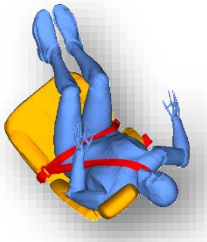
100	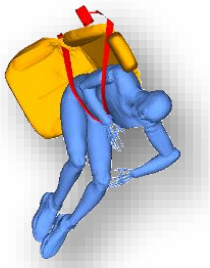	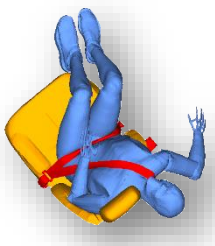

Table 35 Occupant kinematics for case 1 and 2

2 PP3

2.1 Double Lap Belt Pretensioning

Upright seat back and SOTA belt (No submarining)	Reclined seat back and SOTA belt (Submarining @ 72 ms)	Reclined seat back and double lap belt pretensioning (No Submarining)
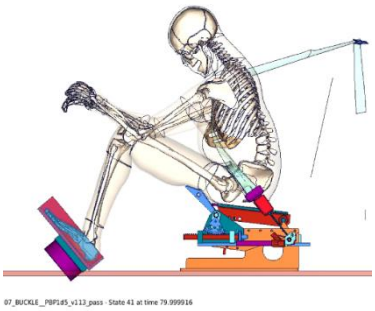	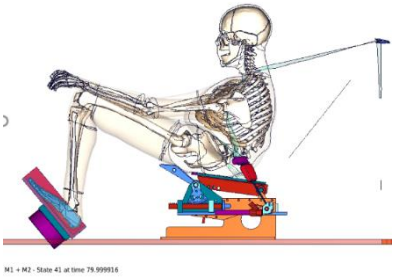	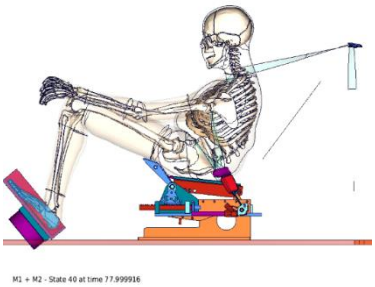
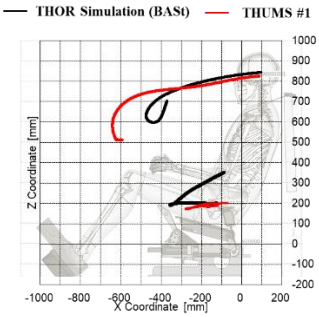	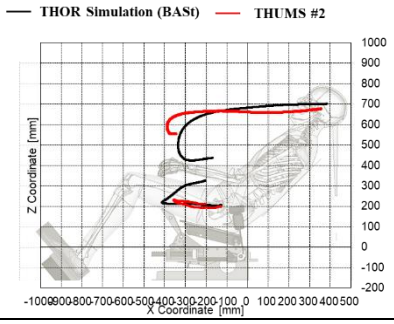	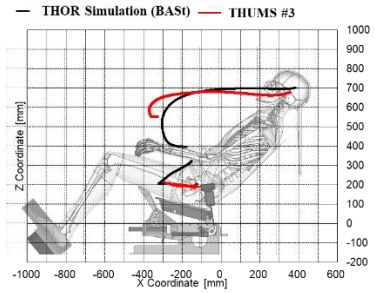
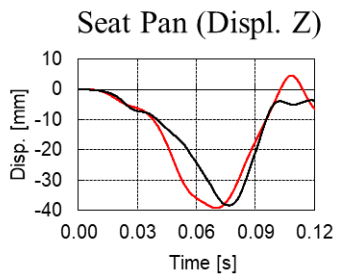	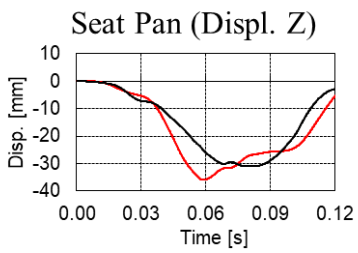	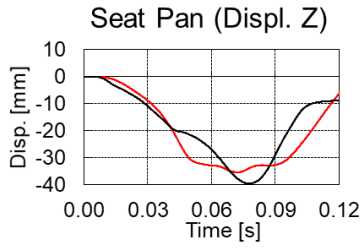
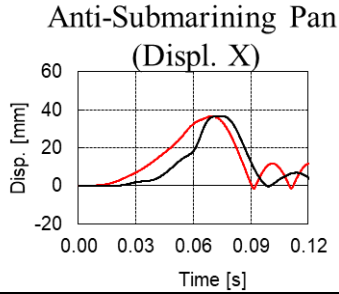	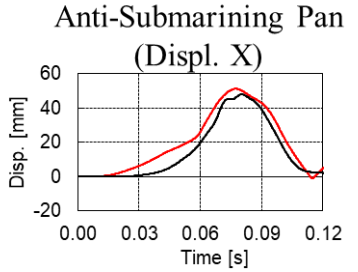	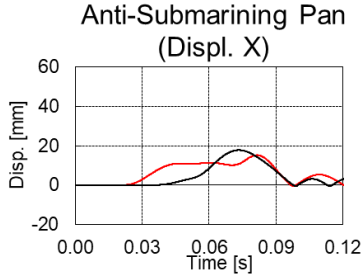
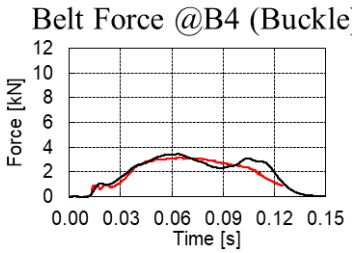	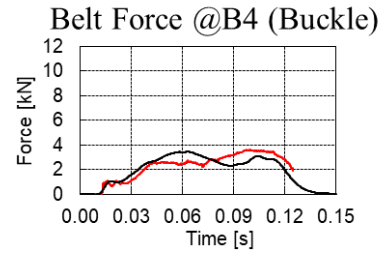	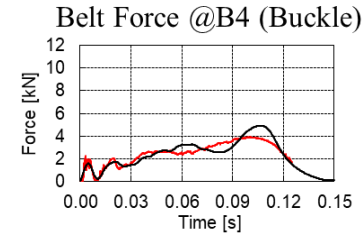

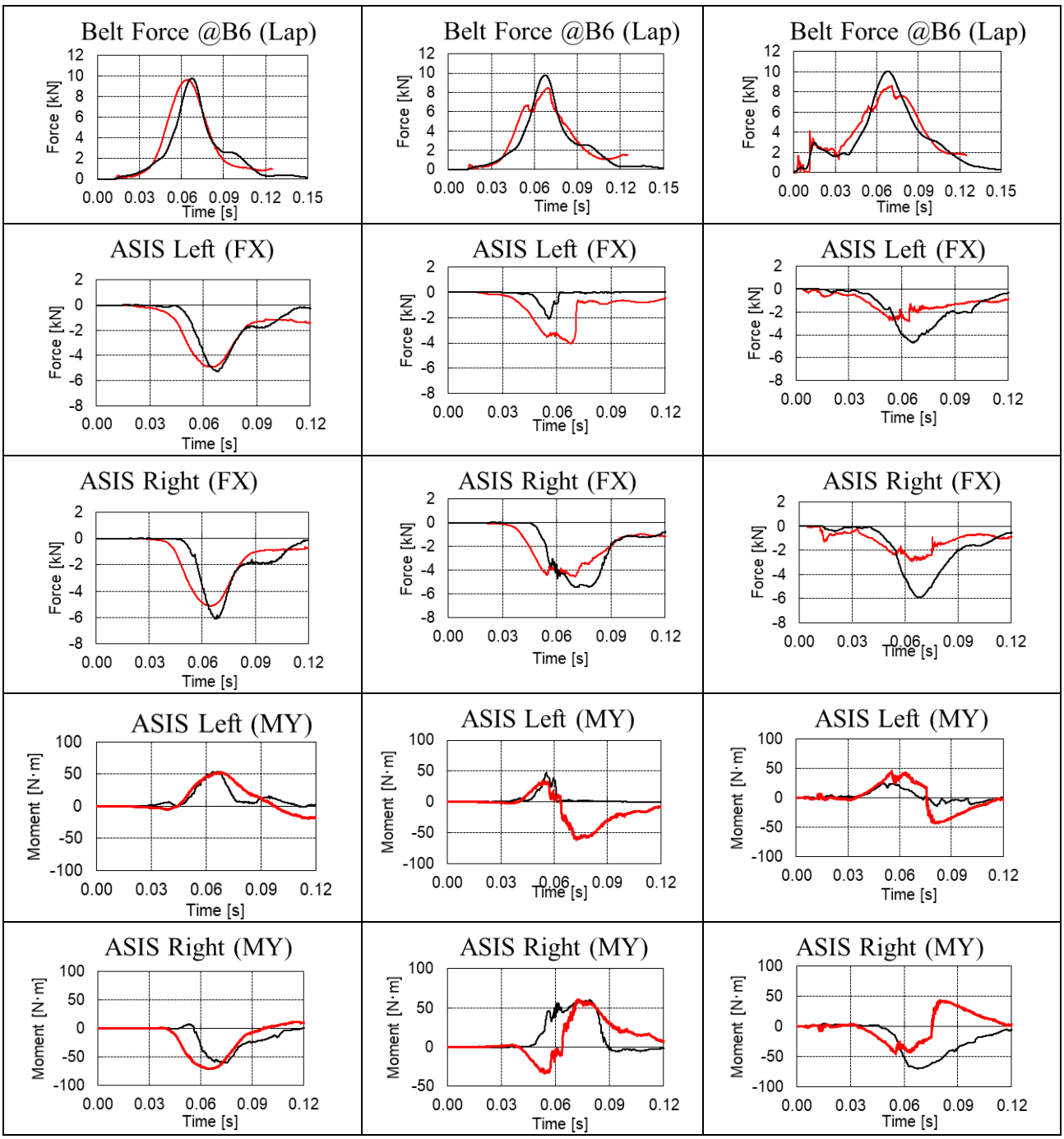

Table 36 Main simulation results (Black: THOR, Red: THUMS)

3 PP4

3.1 Kinematic Behaviour of THUMSD 5th percentile CNIS Female Model

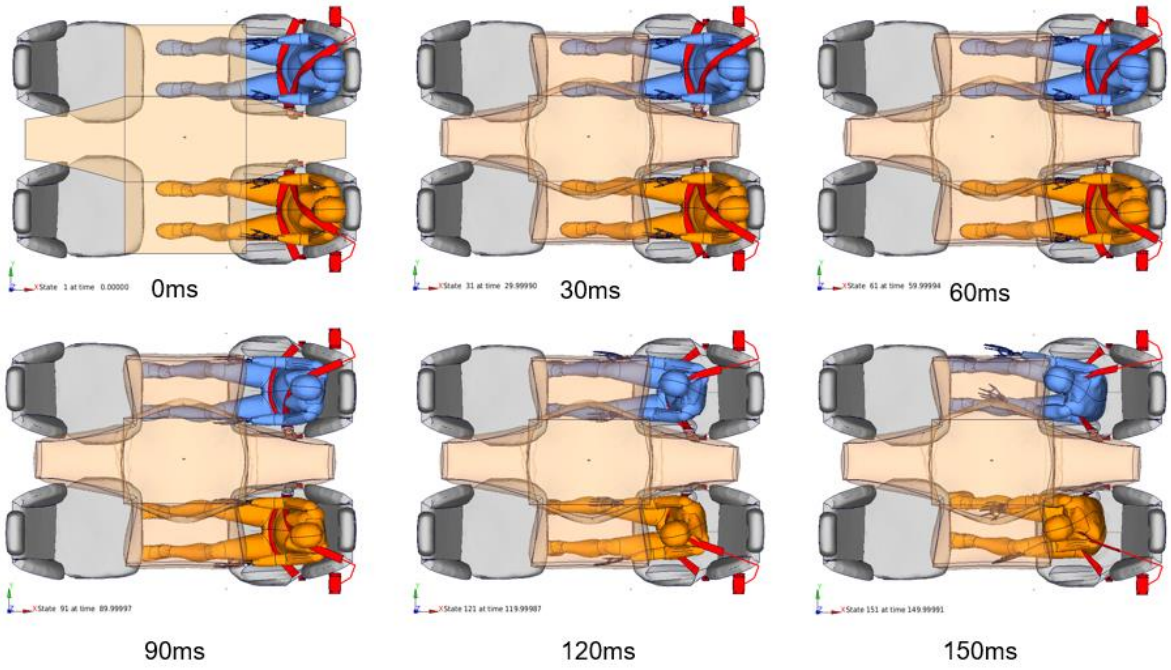

Figure 164 THUMSD F05 CNIS: LTAP OD1 Pulse

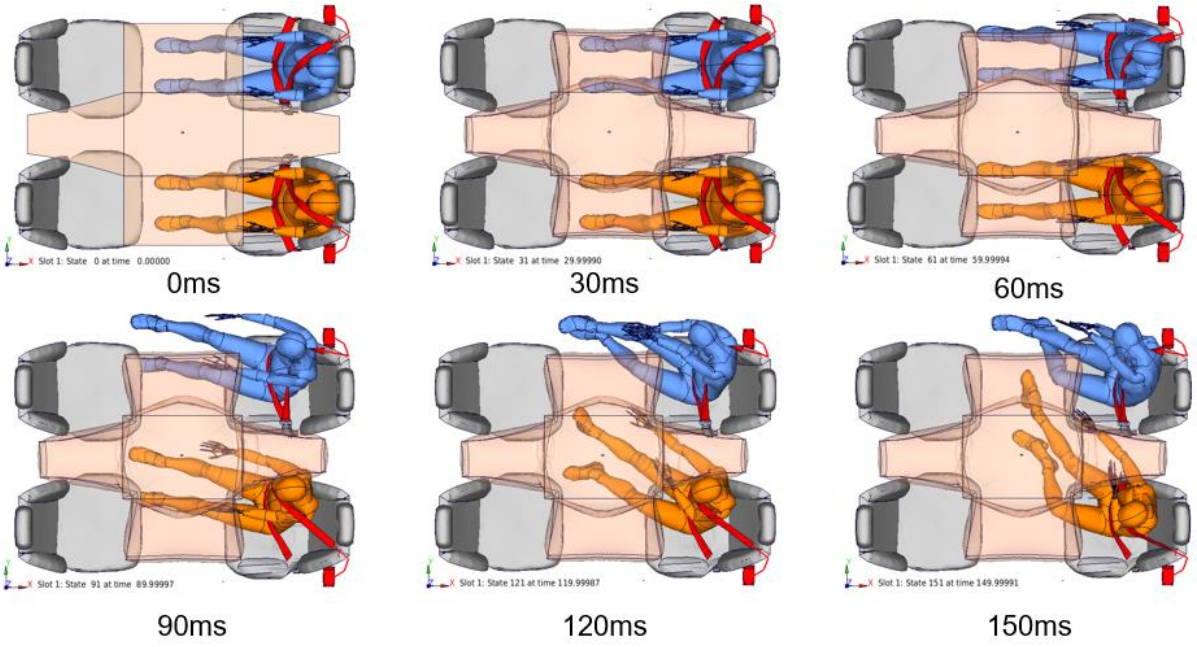

Figure 165 THUMSD F05 CNIS: SCP Pulse

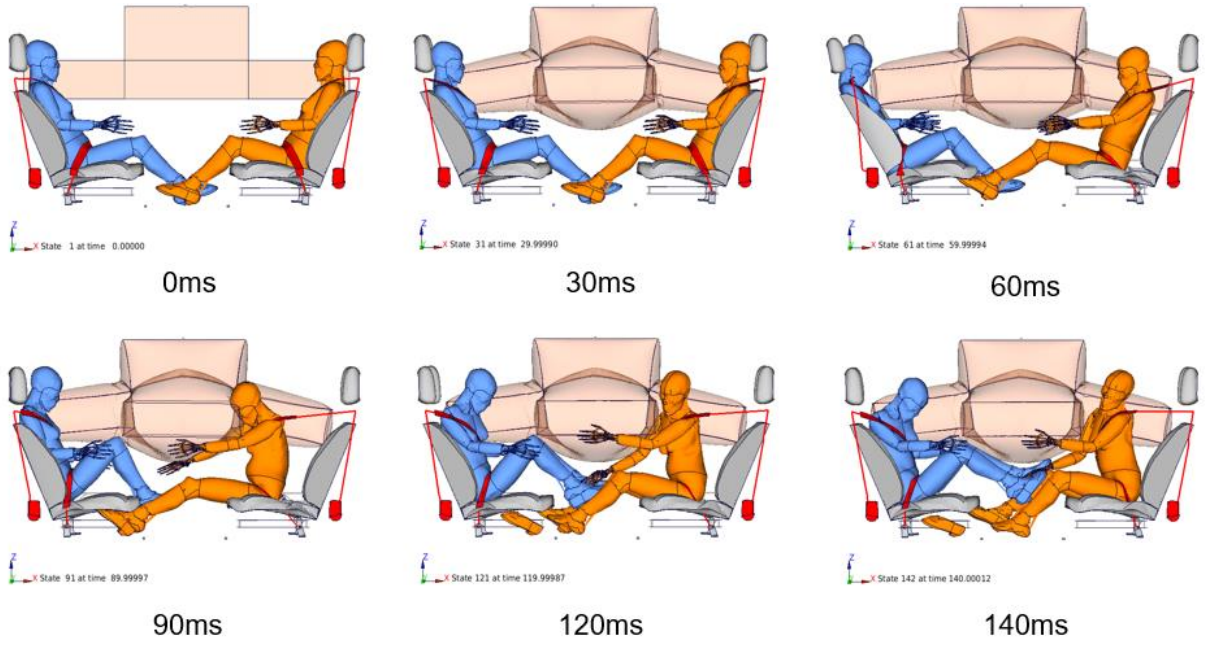

Figure 166 THUMSD F05 CNIS: FF40 Pulse

4 PP5

4.1 Simulation Overview

Seating direction	Forward facing									
Partner	**Volvo Cars**			**Bosch**				**ZF**		
Chapter	**3.5.3.1**			**3.5.3.2**				**3.5.3.3**		
Braking	CV (constant velocity)		11 m/s^2, a 100 ms delay and then a ramp-up over 200 ms (start @ -500 ms)	w/o			w/ Madymo Braking Pulse	Madymo Braking Pulse		
Crash scenario	56 km/h FF			56 km/h FF				56 km/h FF / SCP06		
Interior model	Volvo XC90 SUVdriver compartment			Madymo Generic Interior				Madymo Generic Interior		
Human Body Model	SAFER HBM v9.0.1			Madymo AHM v3.1				Madymo AHM v3.1		
Human Body Model activation	Passive		Active	Active				Active		
Solver	LS-Dyna			Madymo				Madymo		
Initial seat back Angle	27.5°		47.5°	45°				30°		
Delta seat back angle (if PP5 is applied)	20°			23°				20°		
Seat back rotation velocity	static	80°/s	160°/s	static	57.5°/s	…DoE…	460°/s	150°/s		
Seat base translation velocity	Static			Static				Static		
Pre-crash retractor PT	w/o		w/ ERR	w/o			w/ MSB	W (generic & ACR)		
Buckle and anchor position	Nominal		-50 mm X & Z	Nominal (Madymo Generic Interior)				Nominal (Madymo Generic Interior)		

Seat back / Seat base energy absorption (in-crash)	w/o	w/o	w/o	w/o

Table 37 Simulation overview: Forward facing use case

Seating direction	**Rearward facing**			
Partner	**ika (RWTH), fka**			
Chapter	**3.5.3.4**			
Braking	w/o		w/ Madymo Braking Pulse	
Crash scenario	Medium Whiplash, High Whiplash (Euro NCAP), 40 km/h FF			
Interior model	Madymo Generic Interior		LS-Dyna Generic SAE5 Interior	
Human Body Model	Madymo AHM v3.1		Thums v4.02	
Human Body Model activation	Active		Passive	
Solver	Madymo		LS-Dyna	
Initial seat back angle	45°			
Delta seat back angle (if PP5 is applied)	23°			
Seat back rotation velocity	static	33°/s	…DoE…	460°/s
Seat base translation velocity	static	0.21 m/s	…DoE…	3 m/s
Pre-crash retractor PT	w/o			
Buckle and anchor position	Nominal (Madymo Generic Interior / LS-Dyna Generic SAE5 Interior)			
Seat back/ seat base energy absorption (in-crash)	w/ (usage of 23° backrest rotation and 0.2 m seat base translation)			w/o

Table 38 Simulation overview: Rearward facing use case

4.2 Seat Recliner Stiffness for Rearward-Facing Use Case

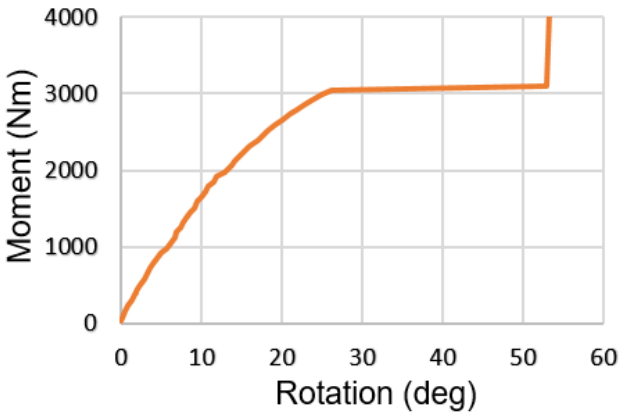

Figure 167 Seat recliner stiffness (rearward facing use case)

4.3 Occupant pre- and in-crash Kinematics in a Rearward-Facing Use Case

PP5 Pre-crash			
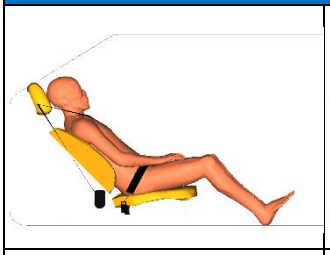	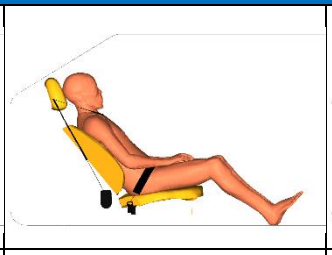	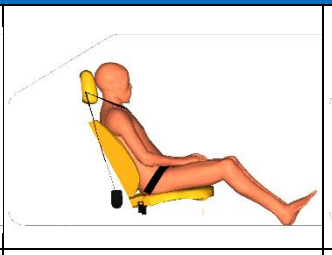	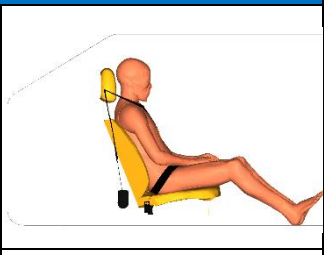
-750 ms	-500 ms	-250 ms	0 ms

Table 39 Pre-crash kinematics: PP5

Time [ms]	Upright	Reclined	PP5
0	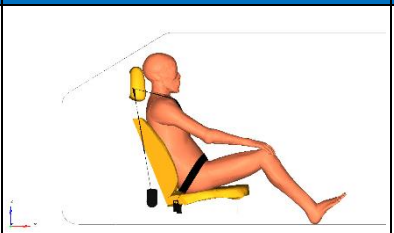	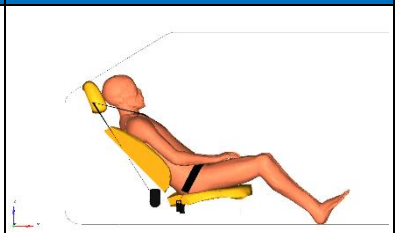	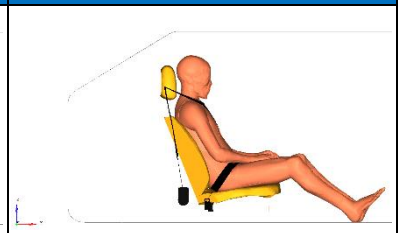
50	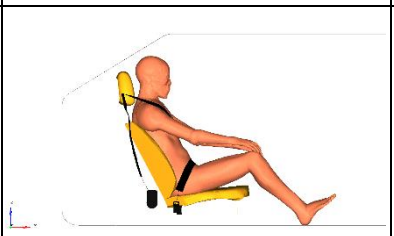	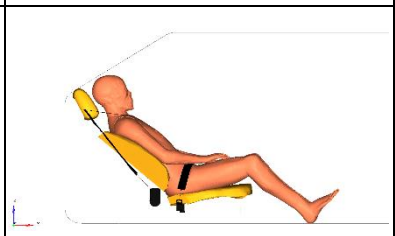	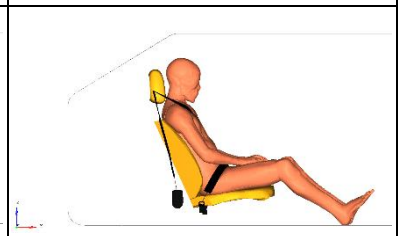
100	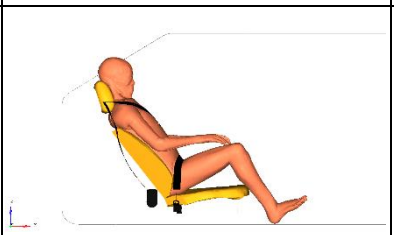	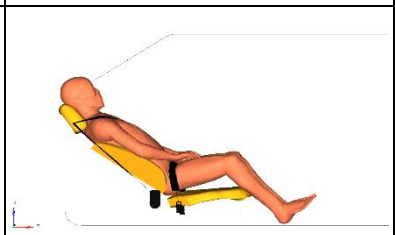	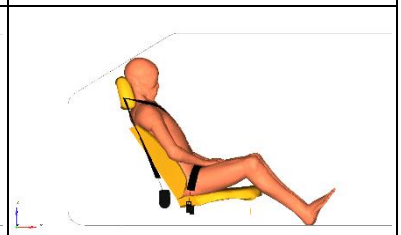
150	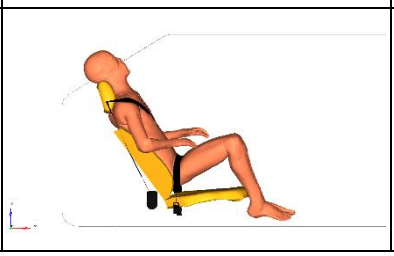	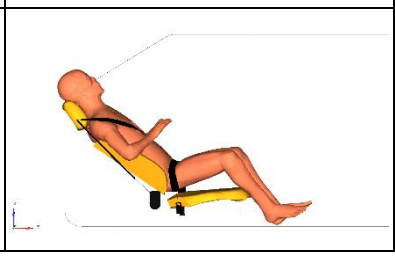	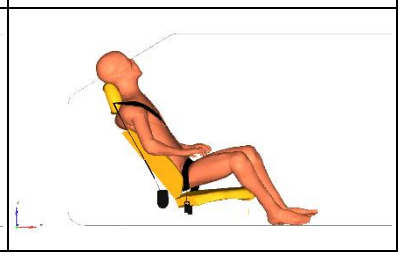

Table 40 In-crash kinematics: (Euro NCAP high whiplash pulse)

Time [ms]	Upright	Reclined	PP5
0	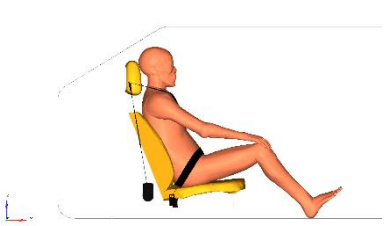	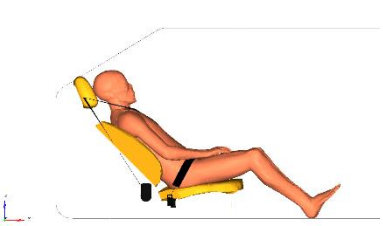	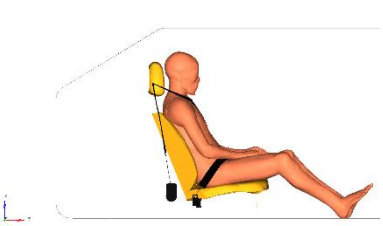
50		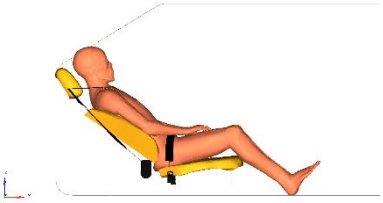	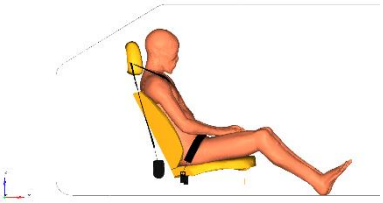
100	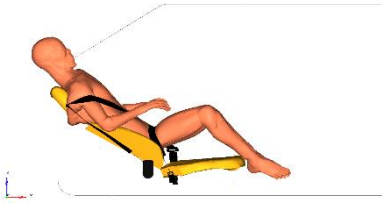	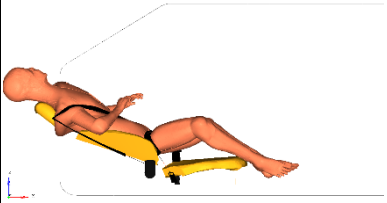	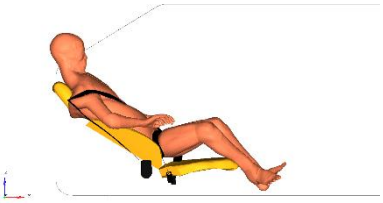
150	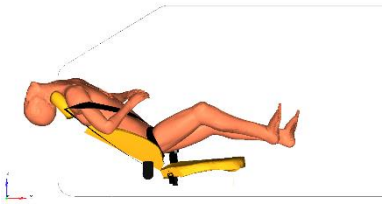	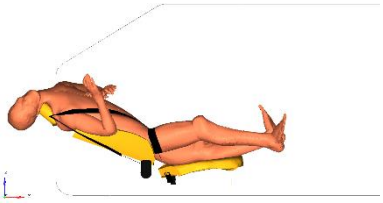	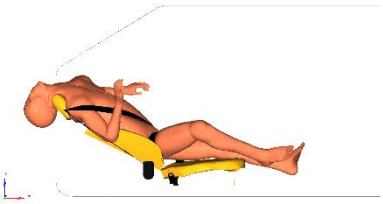

Table 41 In-crash kinematics: (40 km/h FF crash pulse)

5 PP6

5.1 Far-Side Load Case

ID	0 ms	50 ms	100 ms	150 ms
W4_1				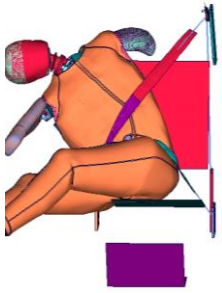
W5_1		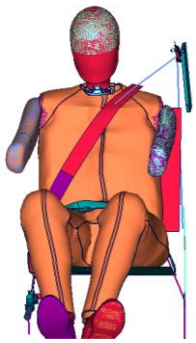	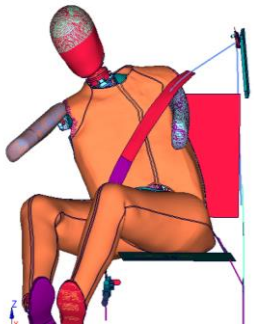	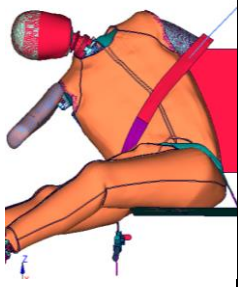
W6_1			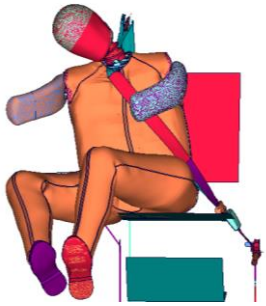	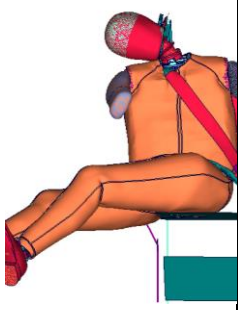
W8_1		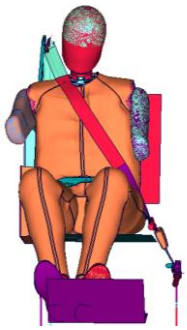	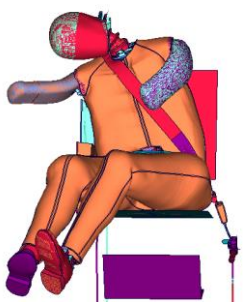	

Table 42 WorldSID kinematics & interaction with protection principles (pre-study simulations)

ID	0 ms	50 ms	100 ms	150 ms
T1	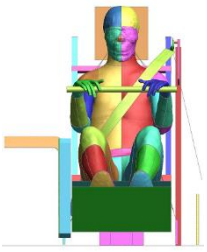	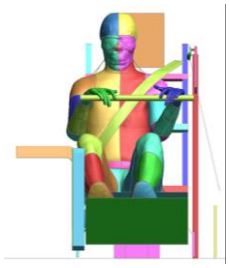	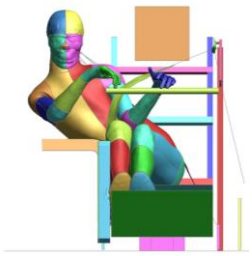	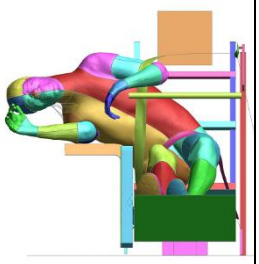
W1_2	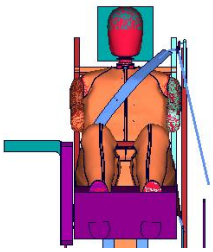	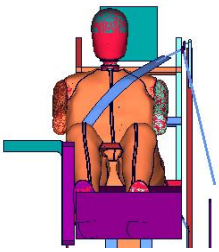	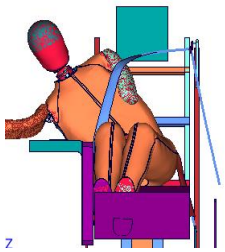	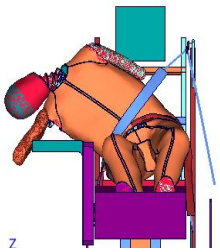
T2				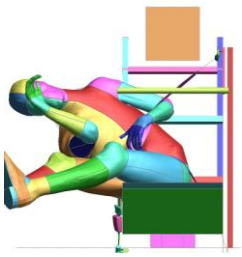
W2_2	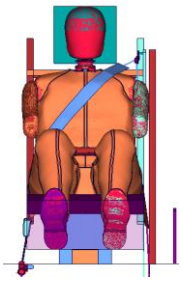	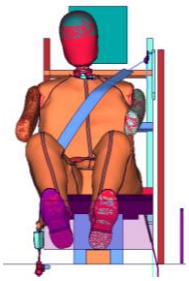	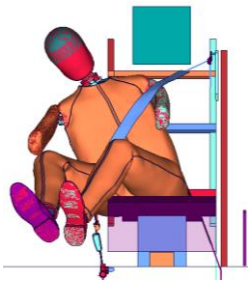	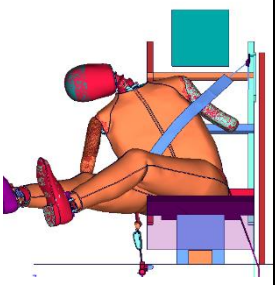
T3				

W3_2	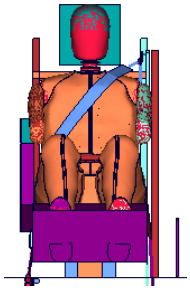	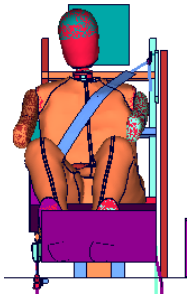	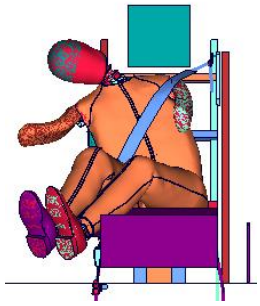	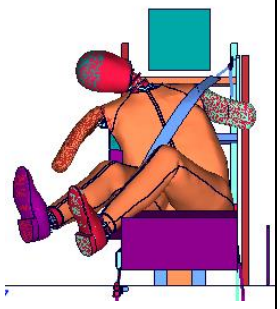
T4				
W4_2	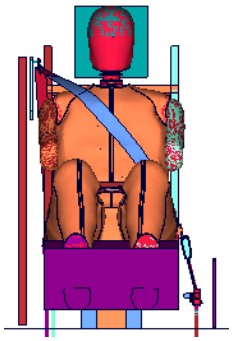	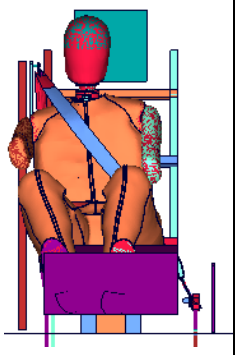	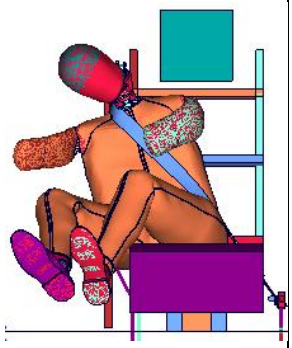	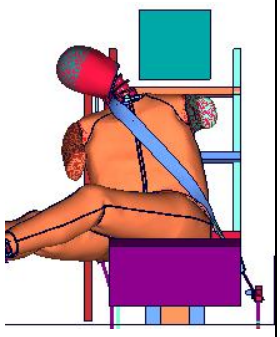
T5				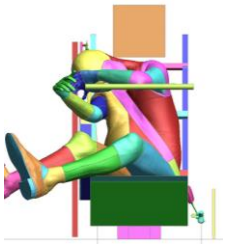
W5_2	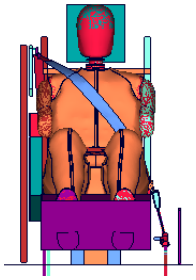	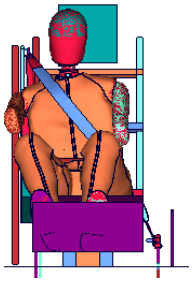	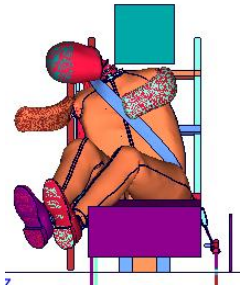	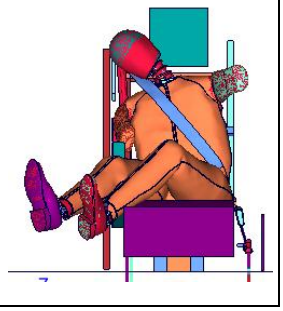

Table 43 Comparison of THUMS & WorldSID kinematics & belt interaction

ID	Console Fy [kN]	Console Fz [kN]
T1 W1_2	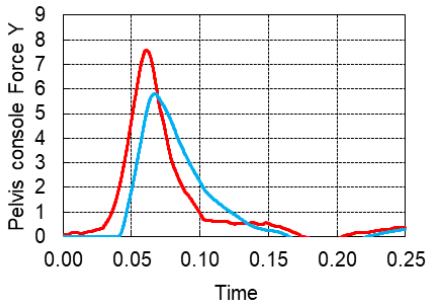	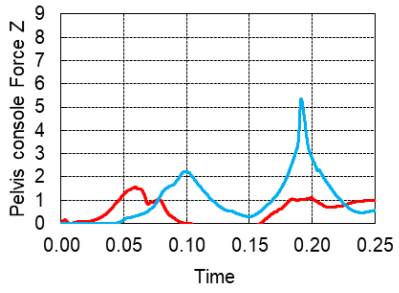

Table 44 Center console contact force. THUMS in blue & WorldSID FEM in red

ID	Thorax seat side support Fy [kN]	Pelvis seat side support Fy [kN]
T3 W3_2	Contact force with side support missing	Contact force with side support missing
T5 W5_2	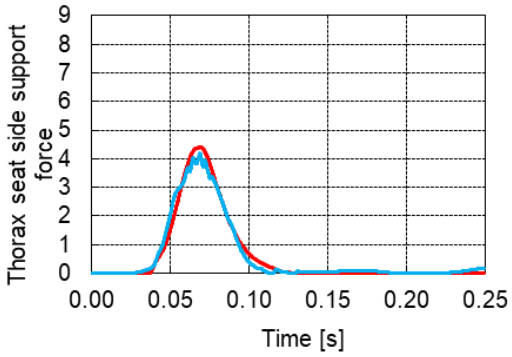	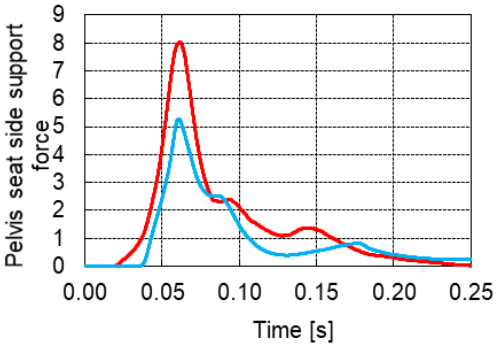

Table 45 Seat side support contact forces. THUMS in blue & WorldSID FEM in red

ID	Shoulder belt force (B3) [kN]	Lap belt force (B6) [kN]
T1 W1_2	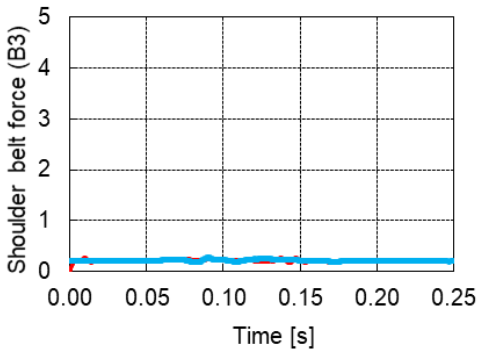	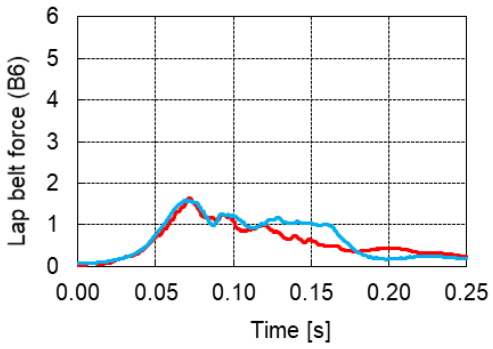
T2 W2_2	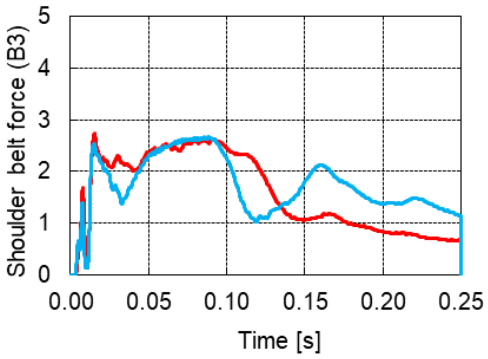	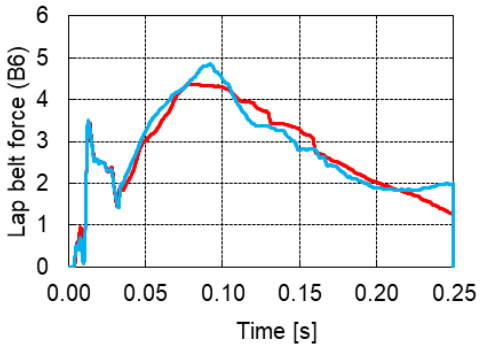
T3 W3_2	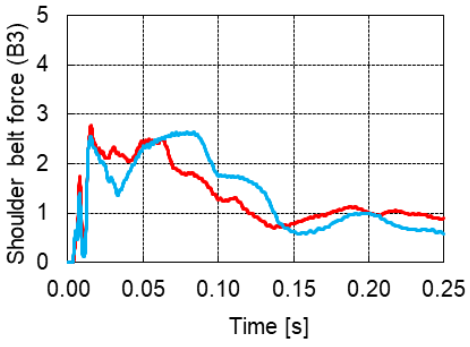	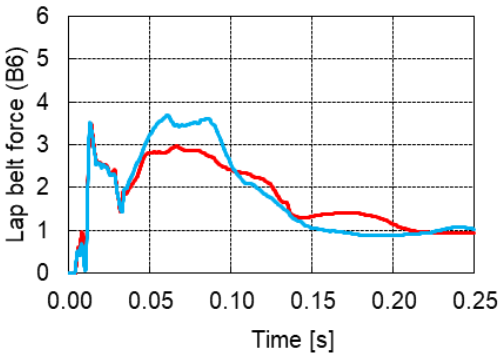
T4 W4_2	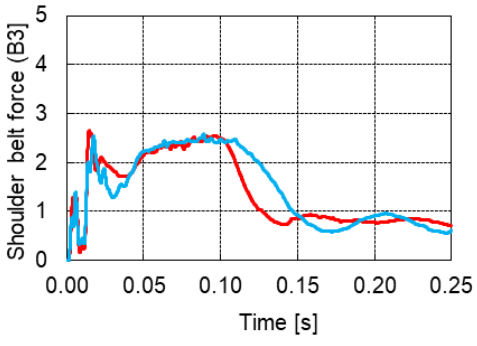	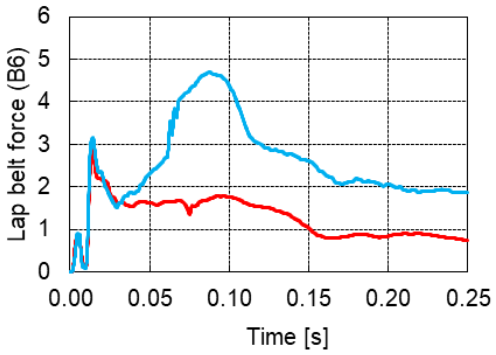

T5 W5_2	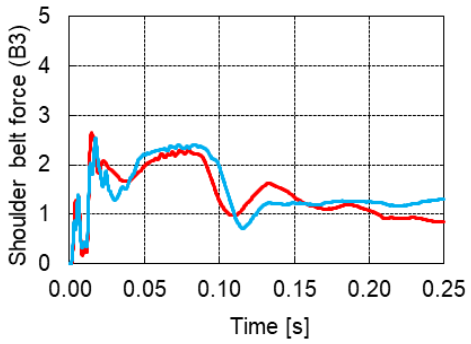	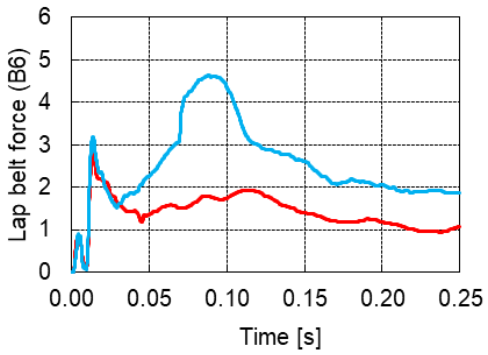

Table 46 Shoulder belt force (B3) & lap belt force (B6). THUMS in blue & WorldSID FEM in red

Euro NCAP limits	Lower performance limit	Lower performance injury risk	Higher performance limit	Higher performance injury risk
Upper/lower Neck Fz	3.74 kN	20% AIS3+	N/A	N/A
Upper Neck MxOC/Lower Neck Mx	162 Nm	5% AIS3+	248 Nm	50% AIS3+
Chest rib deflection	28 mm	0% AIS3+ (45 YO)	50 mm	21% AIS3+ (45 YO)
Abdomen rib deflection	47 mm	0% AIS2+ (45 YO)	65 mm	11% AIS2+ (45 YO)
Pubic symphysis Fy	2.8 kN	31% AIS2+ (45 YO)	N/A	N/A
Lumbar spine Fy	2 kN	N/A	N/A	N/A
Lumbar spine Fz	2.84 kN	N/A	N/A	N/A
Lumbar spine Mx	100 Nm	N/A	N/A	N/A

Table 47 Euro NCAP performance limits & associated risks [55] [66]

ID	Lower neck Mx [Nm]	Lumbar spine Mx [Nm]
T1 W1_2	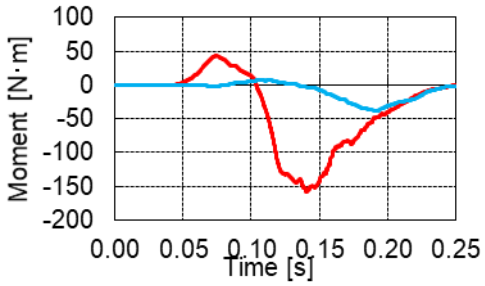	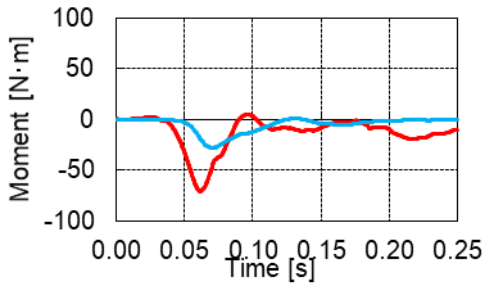
T2 W2_2	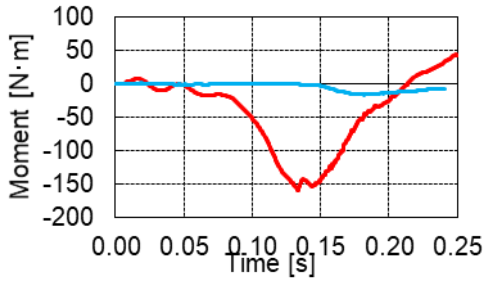	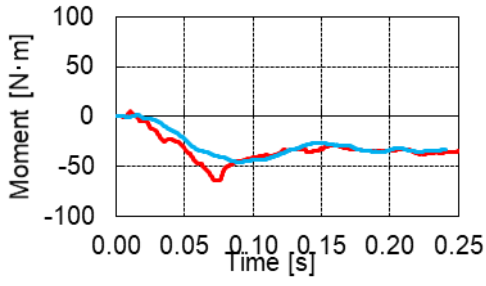
T3 W3_2	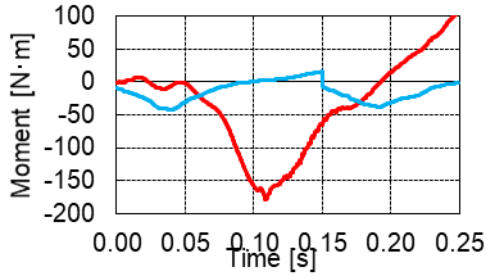	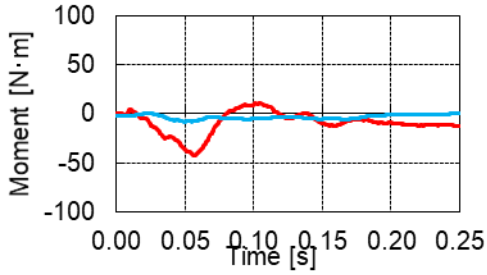
T4 W4_2	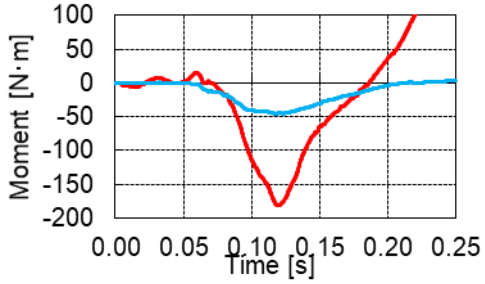	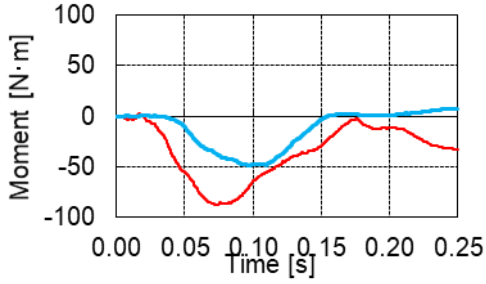
T5 W5_2	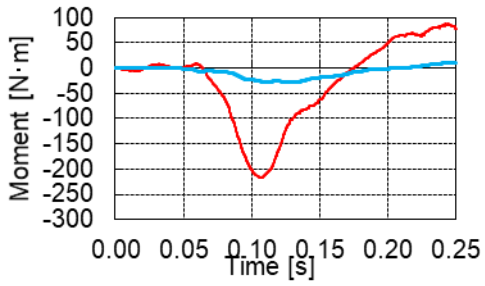	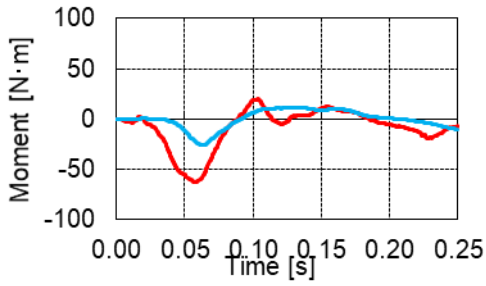

Table 48 Lower neck Mx & Lumbar spine Mx. THUMS in blue & WorldSID FEM in red